TECHNISCHE UNIVERSITÄT MÜNCHEN

Lehrstuhl für Anorganische Chemie

Polymer Brushes on Semiconductor Surfaces

Frank Michael Deubel

Vollständiger Abdruck der von der Fakultät für Chemie der Technischen Universität München zur Erlangung des akademischen Grades eines

Doktors der Naturwissenschaften

genehmigten Dissertation.

Vorsitzender:	Univ.- Prof. Dr. Klaus Köhler
Prüfer der Dissertation:	1. Univ.- Prof. Dr. Fritz E. Kühn
	2. Univ.- Prof. Dr. Rainer Jordan, Technische Universität Dresden
	3. Univ.- Prof. Dr. Tom Nilges

Die Dissertation wurde am 21.05.2013 bei der Technischen Universität München eingereicht und durch die Fakultät für Chemie am 16.07.2013 angenommen.

Danksagungen

An erster Stelle gilt mein besonderer Dank Prof. Dr. Rainer Jordan für die großartige Chance, dieses äußerst interessante Thema bearbeiten zu können und für seine Bereitschaft, mich auch nach seinem Ruf nach Dresden von dort aus weiter zu betreuen. Außerdem bedanke ich mich für das in mich gesetzte Vertrauen, was freie Gestaltung meiner Arbeit anging und die uneingeschränkte Unterstützung bei Fragen und Problemen.
Bei Prof. Dr. Fritz E. Kühn bedanke ich mich dafür, dass er es überhaupt möglich machte, diese Arbeit in dieser Art durchzuführen.
Prof. Dr. Martin Stutzmann und PD Dr. Jose Antonio Garrido danke ich für die Betreuung und Unterstützung bei physikalischen Fragestellungen.
Bei Prof. Dr. Oskar Nuyken möchte ich mich für die Hilfe bei der Planung und Auswertung der Versuche zur Thiol-Klick Polymerisation bedanken und für den umfangreichen Überblick über die Literatur zu diesem Thema.
Herrn Prof. Dr. Dr. h.c. Bernhard Rieger danke ich für die freundliche Aufnahme am Wacker-Lehrstuhl und die vielen anregenden Diskussionen im Laufe meiner Arbeit.
Bei Dr. Heinz Frey, Dr. Ian Sharp und Dr. Gary Moore bedanke ich mich für die äußerst produktive Zeit am Joint Center for Artificial Photosynthesis (JCAP) des Lawrence Berkeley National Lab in Berkeley, Kalifornien.
Prof. Dr. Jon Veinot danke ich vor allem für die anregenden Diskussionen und seinen Input bezüglich der Siliciumnanopartikel.
Meinen Betreuern seitens der Wacker Chemie AG und jetzigen Kollegen, Dr. Dennis Troegel, Dr. Jürgen Stohrer, Dr. Robert Maurer und Dr. Daniel Bräunling möchte ich für die Anregungen und Diskussionen und für das stete Interesse an meiner Arbeit danken. Im Übrigen danke ich der Wacker Chemie AG für die finanzielle Unterstützung im Rahmen eines Promotionsstipendiums am Institut für Siliciumchemie.
Außerdem danke ich allen meinen Mitstreitern, ohne die meine Arbeit wohl viel weniger fruchtbar gewesen wäre. Besonderer Dank gilt hier meinen ehemaligen Betreuer Dr. Marin Steenacker, meinen ehemaligen Kollegen Dr. Ning Zhang, Dr. Gerhard Richter, Dr. Naima Hutter, Timo Korfmann, meinen Masteranden Amelie Koch und Sebastian Schwaminger, meinen Bacheloranden und Praktikanten Tobias Lünskens, Sebastian Schächer, Alina Lyuleeva, Joachim Nagler, Zeyneb Karatas, Felix Flegiel, Richard Holzner und Tobias Helbich. Ohne euch hätte ich wahrscheinlich nur halb so viele Ergebnisse, wenn überhaupt.

Meinen zahlreichen Kooperationspartnern in der Makro, in Dresden und in der „Physik“, Victor Bretzler, Christian Anger, Stephan Salzinger, Ihsan Amin, Tao Zhang, Max Seifert, Lucas Hess, Matthias Sachsenhauser, Felix Buth, Andreas Reitinger, Roberta Caterino, Konrad Schönleber und Alexander Solovev danke ich für die tolle Zusammenarbeit.
Ich danke Dr. Carsten Troll und Dr. Sergej Vagin für die exzellente Organisation und Instandhaltung des ganzen Equipments. Was die Organisation angeht bedanke ich mich ebenfalls bei unseren Sekretärinnen Anette Bauer, Sabine Saul-Hubrich, Gabriele Uruk sowie bei unseren CTAs und Technikerinnen Sabine Martinetz-Große, Aleksandra Kuzmanovic und Katia Rodewald.
Dr. Marianne Hanzlik danke ich ganz herzlich für die TEM Messungen und die Hilfe bei deren Auswertung.
Außerdem danke ich meinen Laborkollegen Dr. Alexander Schöbel, Victor Bretzler und Andreas Eisele und allen übrigen Makros für die tolle Zeit am Lehrstuhl, in Freiburg, beim Skifahren, den Weihnachtsfeiern und Grillfesten sowie meinen Schreibraum-Kollegen Dr. Sanna Zimmer, Dr. Christian Anger, Konrad Hindelang, Dr. Carly Anderson und Victor Bretzler.
Sollte ich jetzt wirklich noch vergessen haben jemandem zu danken, tut mir das aufrichtig leid und ich hole das hiermit nach. Danke!

Ein riesengroßer Dank gebührt auch meinen Eltern für die Unterstützung und besonders dafür, dass sie mir während des Studiums finanziell den Rücken freigehalten haben.

Als letztes Danke ich noch meiner Freundin Rike für die moralische Unterstützung während meiner Promotion und vor allem für ihr Verständnis während der Zeit des Verfassens meiner Dissertation.

Es wurde zwar schon alles gesagt, nur noch nicht von jedem.

Karl Valentin

List of Abbreviations

4-BS	4-bromostyrene
4-VP	4-vinylpyridine
AA	allyl amine
AAc	acrylic acid
AFM	atomic force microscopy
APTMS	3-aminopropyl trimethoxysilane
ATR	attenuated total reflection
ATRP	atom-transfer radical polymerization
BDE	bond dissociation energy
BP	benzophenone
BPA	4-bromophenyl acetylene
CA	contact angle
ChemFET	chemically sensitive field-effect transistor
Đ	dispersity
DCM	dichloromethane
DEAEA	2,2-diethylaminoethyl acrylate
DMAEMA	2,2-dimethylaminoethyl methacrylate
DRIFT	diffuse reflection Fourier transform
EA	ethyl acrylate
EtOH	ethanol
EtOx	2-ethyl-2-oxazoline
FRP	free-radical polymerization
FRP	free-radical polymerization
FTIR	Fourier transform infrared
GATR	glazing angle attenuated total reflection
GHz	gigahertz
GMA	glycidyl methacrylate
GPC	gel permeation chromatography
H-Si	hydrogen-terminated silicon
HEA	2-hydroxyethyl acrylate
HEMA	2-hydroxyethyl methacrylate
HRTEM	high-resolution transmission electron microscope
iPOx	2-isopropenyl-2-oxazoline

IR	infrared
ITO	indium tin oxide
ITX	isopropyl thioxanthone
KCTP	Kumada catalyst-transfer polycondensation
LCROP	living cationic ring-opening polymerization
MEMS	microelectromechanical system
MeOH	methanol
MeOTf	methyl triflate
METAC	methacrylatoethyl trimethyl ammonium chloride
MMA	methyl methacrylate
M_n	number-average molar mass
M_w	weight-average molar mass
nc	nanocrystalline / nanocrystal
nc-Si	nanocrystalline silicon
Nd:YAG	neodymium-doped yttrium aluminum garnet
NEMS	nanoelectromechanical system
NEt_3	triethyl amine
nm	nanometer
P3HT	poly(3-hexylthiophene-2,5-diyl)
P4BS	poly(4-bromostyrene)
P4VP	poly(4-vinyl pyridine)
PAAc	poly(acrylic acid)
PAMS	poly(aminomethyl styrene)
PEA	poly(ethyl acrylate)
PGMA	poly(glycidyl methacrylate)
PHEA	poly(2-hydroxyethyl acrylate)
PHEMA	poly(2-hydroxyethyl methacrylate)
PiPOx	poly(isopropenyl oxazoline)
PMAAc	poly(methacrylic acid)
PMMA	poly(methyl methacrylate)
PNS	poly(nitrostyrene)
PS	polystyrene
PSSA	poly(styrenesfulfonic acid)
PtBMA	poly(tert.-butyl methacrylate)

PTFE	poly(tetrafluoro ethylene)
SAM	self-assembled monolayer
SEM	scanning electron microscopy
SI-ATRP	surface-initiated atom-transfer polymerization
SI-KCTP	surface-initiated Kumada catalyst-transfer polycondensation
SI-LCROP	surface-initiated living cationic ring-opening polymerization
Si-nc	silicon nanocrystals
SIP	surface-initiated polymerization
SIPGP	self-initiated photografting and photopolymerization
STM	scanning tunneling microscopy
tBMA	tert.-butyl methacrylate
TCO	transparent conductive oxide
TEM	transmission electron microscopy
TEMPO	(2,2,6,6-Tetramethyl-piperidin-1-yl)oxyl
TGA	thermogravimetric analysis
THF	tetrahydrofuran
UHV	ultrahigh vacuum
UV	ultraviolet
XPS	x-ray photoelectron spectroscopy

Table of Contents

1 Introduction

Materials science is a highly interdisciplinary field between chemistry, physics, engineering and biology and had a tremendous impact on technology. Materials science has driven, and at the same time was driven by the development of revolutionary technologies. These include plastics, semiconductors, and biomaterials together with the development of new analytical techniques. Progress of materials science in recent years has led to fundamental understanding of structure-property relationships on a macroscopic and nanoscopic scale. Materials properties can now be tailored to meet specific needs.

Surface science, one of the most prominent subdisciplines of materials science, helped in the understanding of many chemical processes in heterogeneous catalysis. Progress in coatings technology, such as the artificial Lotus effect, is based on fundamental understanding of interactions at a solid interface.

By definition, the surface of a crystalline material is just a defect of the crystal, because its infinite periodicity is interrupted. However, surface is where a solid interacts with its environment, whether liquid, gaseous or solid. Changes to a surface induce influence these interactions, e.g. by making a material more hydrophilic or hydrophobic. Modifying surfaces can also help to connect between to incompatible systems by introducing a “linker” between them. Such linkers can be inorganic or organic, depending on the projected use. Organic linkers for example, can be used to link redox-active complexes generating hybrid functional systems.

Surface chemistry is expected to become even more important with the rise of nanotechnology. The smaller a solid gets, the higher becomes the surface-to-volume ratio. This leads to interesting effects like quantum confinement, but also increases the surface property impact upon general materials properties of nanomaterials. Therefore, with knowledge about the modification of surface properties, material properties can also be easily tailored.

2 Background

2.1 Chemical Functionalization of Semiconductor Surfaces

No one can argue about the vast importance of semiconductors in today's world. Nearly all modern technologies make use of semiconductor devices, be it computing, microelectronic devices, microelectromechanical systems (MEMS)[1], memory chips or sensors, some of them even biocompatible. Perhaps the most important semiconductor material, silicon has received increasing attention since the 1980s with respect to surface modification. However, recently also other semiconductor materials, such as diamond, silicon carbide, insulators such as silicon nitride and conductors such as graphene, just to name a few, have come into focus of research. One of the main reasons for chemical modification of semiconductor surfaces is the possibility to tailor interfacial electronic properties. Especially for chemically sensitive field-effect transistors (ChemFETs), surface modification plays a crucial role. But not only there, also semiconductor nanomaterials, e.g. nanowires and nanocrystals, show a strong response to modification of their surfaces due to the high surface-to-volume ratio.

As every year semiconductor devices become smaller and smaller, their size reaches a regime where interface properties begin to have an actual impact on their performance. Moreover, by attaching functional molecules to semiconductor surfaces, functionality, such as sensitivity to certain substrates, temperatures, ion strength, and even chirality, can be introduced.

This makes organofunctionalization of semiconductor surfaces an interesting and also important field for future research with respect to semiconductor devices such as lab-on-chip systems, nanoelectromechanical systems (NEMS) or just miniaturized integrated circuits (ICs).

2.1.1 Functionalization of Silicon

Silicon is by far the most used semiconductor material for all kinds of electronic applications. Its bandgap energy of 1.12 eV is typical for a semiconductor and doping can be achieved by adding very small amounts of e.g. boron for p-type doping and arsenic or phosphorus for n-type doping.

One convenient possibility to modify the surface of silicon is by direct functionalization of the native oxide layer usually by condensation reactions of chloro- or alkoxysilanes.[2-6] However, this method has major disadvantages. The silicon oxide layer on silicon shortens minority charge carrier lifetimes compared to bare silicon. Furthermore, Si-O-C linked monolayers are

less stable against hydrolysis than directly Si-C linked layers and less suitable for long-term biomedical applications.[7] The schematic mechanism of this type of surface functionalization is depicted in Figure 1.

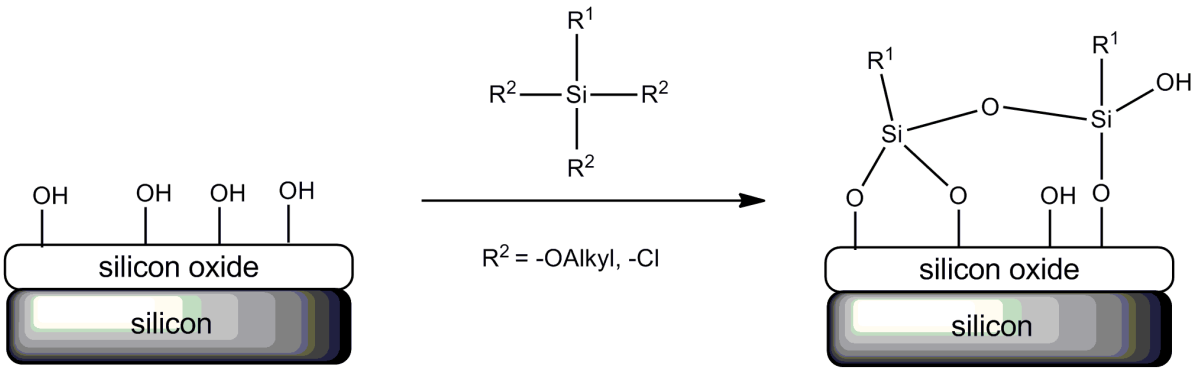

Figure 1: Schematic of functionalization of native oxide layer on silicon by condensation with chloro- or alkoxysilanes

For the reasons mentioned above, considerable effort has been given to the functionalization of oxide-free silicon surfaces. These surfaces can be generated by etching of an oxidized silicon surface with hydrofluoric acid and result a hydrogen-terminated silicon surface that is stable against oxidation in air for several hours.

In general, etching or 'stripping' of silicon oxide with hydrofluoric acid can be formulated as

$$SiO_2 + 4\ HF \rightarrow SiF_4 + 2\ H_2O$$

Due to the high fluorophilicity of silicon, it is expected that the silicon surface is fluorine-terminated after etching. Owed to its high complexity, the mechanism of hydrogen-passivation of silicon with hydrofluoric acid is not yet fully understood, although the mechanism postulated by Ubara (see Figure 2) is nowadays widely accepted and also proven in parts.[8] In this mechanism, an HF molecule is added to a polarized Si^{+}-Si^{-} bond, cleaving this bond and forming an Si-H and an Si-F bond, thus leading to a hydrogen-passivated silicon surface.

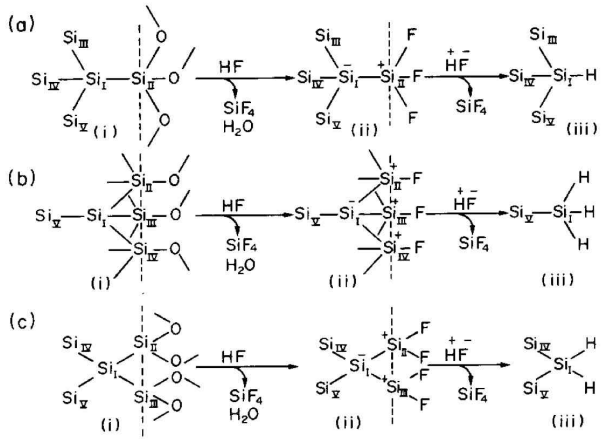

Figure 2: Possible mechanism of Si-H formation on silicon by HF etching[8]

The morphology of this surface strongly depends on the etching process and the orientation of the etched surface, as seen in Figure 3.

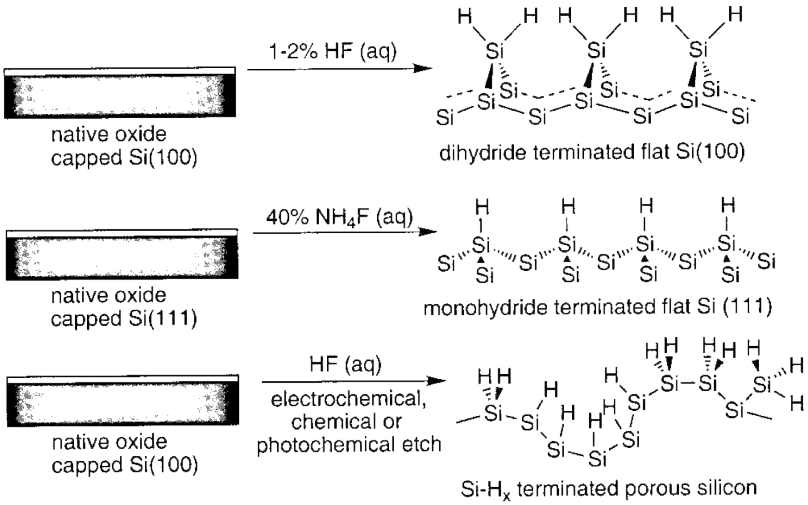

Figure 3: Fluoride-based etching conditions, leading to hydride-terminated flat and porous silicon surfaces[9]

In contrast to Si(111), which bears monohydride moieties on the surface, Si(100) bears silicon dihydride groups, when etched with dilute hydrofluoric acid or buffered oxide etch. Upon etching Si(100) with concentrated (~ 50 %) hydrofluoric acid, a porous surface containing mono-, di-, and trihydride species is formed. Since hydrogen-terminated silicon surfaces are prone to reoxidation, passivation is necessary to prevent a deterioration of electronic properties.

Besides ultrahigh vacuum (UHV) methods of silicon passivation being accompanied by high instrumental effort, wet chemical methods for generating Si-C bonded organic layers on

silicon have been established since the late 1990s. A straightforward method of functionalizing H-terminated silicon is the hydrosilylation reaction. Since the first report on hydrosilylation of unsaturated hydrocarbons onto H-terminated silicon by Linford and Chidsey in 1993 and 1995,[10,11] many groups have shown the functionalization of H-terminated Si with unsaturated organic compounds. Examples include, but are not limited to esters, carboxylic acids, aldehydes, alkyl halides, alcohols, olefins, amides and amines. Shows just a few examples of various moieties attached to H-terminated Si.

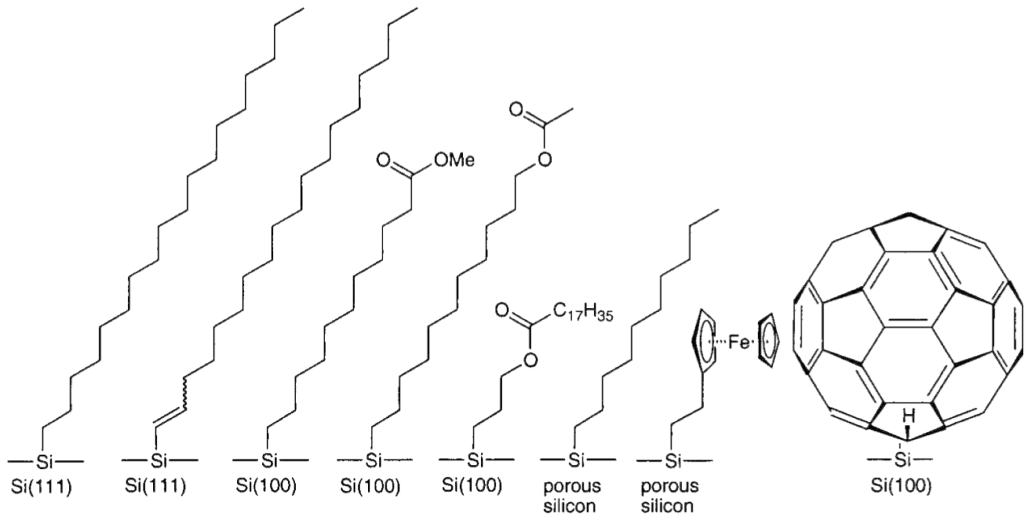

Figure 4: Examples of surface terminations produced by thermal hydrosilylation[9]

Moreover, also more and more unusual moieties have been attached to silicon surfaces, such as DNA[12-16], antibodies[17,18], nanoparticles[19,20], cyclodextrine[21], and even fullerenes[22]. There is hardly any functionality that has not been successfully attached to silicon nowadays.[9,23-25] This hydrosilylation reaction can be induced by temperature[10,11,26-28], UV light[12,29-31], electrochemistry[32], visible light[33,34], microwave[35], Lewis acids[36], radical starters[11] and even traces of oxygen[37]. Regarding the mechanism of this hydrosilylation reaction, Linford and Chidsey postulated a self-propagating surface chain-reaction that has proven to be valid. A scheme of the mechanism can be seen in Figure 5.

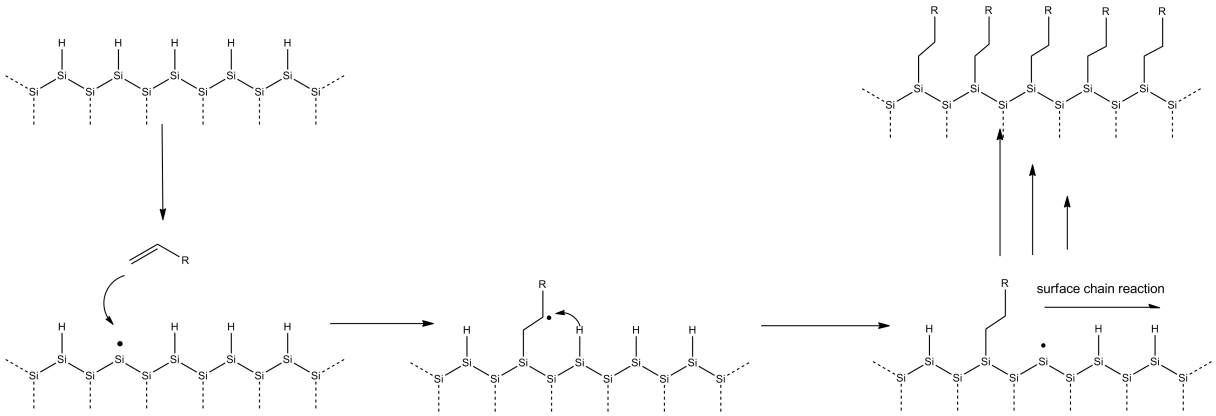

Figure 5: Mechanism of hydrosilylation *via* radical chain reaction on H-Si surface according to Linford and Chidsey[10,11]

In this radical mechanism, a radical is generated at the silicon surface, to which an unsaturated carbon-carbon bond is added, resulting in a surface-bonded alkyl radical, which will then abstract a hydrogen atom from a neighboring Si-H bond. This is made possible by the low energy needed for homolytic Si-H cleavage.[38,39] The abstraction of a hydrogen atom from a Si-H bond results in a surface silyl radical, to which an unsaturated compound can attach, starting the process again and leading to a radical surface chain-reaction. The mechanism of this reaction has been probed by STM experiments in UHV conditions, showing line-growth on Si(100)[40,41] and insular growth on Si(111)[42].

2.1.2 Nanocrystalline Silicon

Nanocrystalline silicon (nc-Si) is a relatively new material with intriguing properties. It can be synthesized *via* various routes,[43] including solution based reduction of chloro- or alkoysilanes,[44,45] decomposition of silane precursors by heat[46], laser irradiation[47,48] or microwave plasma,[49-51] or dispropartionation of silicon suboxides[52] or silsesquioxoanes.[53,54]

Due to quantum confinement effects, significant changes in electronic structure are taking place when the diameter of nc-Si is reduced below the exciton radius of bulk silicon (~ 5 nm).[50,55-58] While bulk silicon does not show strong optical absorption due to its indirect band gap, quantum-confined nc-Si shows much higher optical absorption owed to effective no-phonon transitions.[57] Additionally, nc-Si shows size-dependent visible photoluminescense (see Figure 6).[50,56]

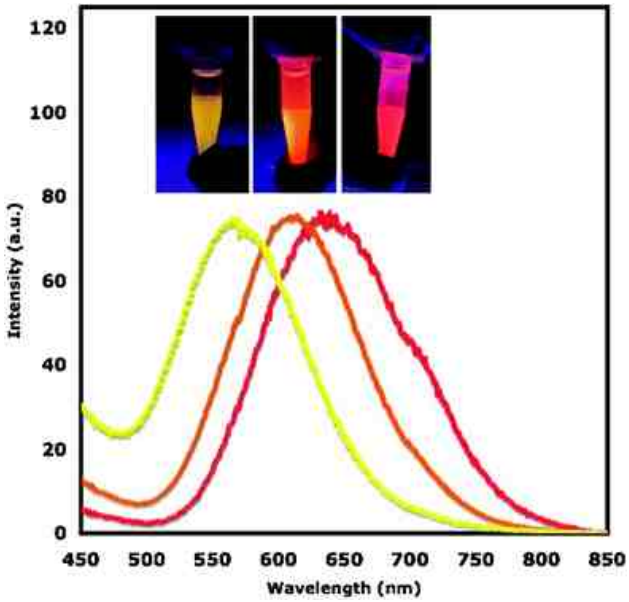

Figure 6: Normalized emission spectra of different sizes of hydride terminated silicon nanoparticles (λ_{ex} = 350 nm)[43]

With these intriguing optical and electronical properties it is not astonishing that there are many possible uses for quantum-confined nc-Si in optoelectronic applications, such as nc-Si lasers and LEDs.[59-61] Due to their luminescence, nc-Si also has attracted increased attention with regard to fluorescent labels for bioimaging[62] and chemosensors.[63,64] Especially in bioimaging, nc-Si is expected to have significant advantages over some other quantum dot materials such as CdSe, CdTe due to its low cytotoxicity.

Other effects occurring in nc-Si, such as MEG[58] or quantum cutting[65], have made them promising candidates for photovoltaic devices.[66-70] In MEG, photon absorption results in the generation of multiple electron-hole pairs, making energy conversion more efficient. Also applications as luminescent dyes in nanoimprint lithography are within reach.[51,71] Another important incentive for the use of nc-Si as a quantum dot material is its inherent compatibility with convential silicon-based microelectronics.

However, in order to harness these properties, one has to find ways to control both size and surface chemistry of nc-Si. Especially in quantum-confined nc-Si, chemistry of surface silicon atoms plays a dominant role due to their high surface/volume. As surface oxidation imposes strong changes on optical and electronical properties of nc-Si, ways to passivate the surface without compromising the electronic structure by the introduction of surface defects are paramount. Moreover, surface functionalization of nc-Si allows for tailoring the interface chemistry, making them compatible with different environments.[9,43,64]

2.1.3 Silicon Carbide and Silicon Nitride

As materials with many interesting properties, silicon carbide and silicon nitride have been organofunctionalized only recently. Their most important properties are high mechanically robustness, as well as chemical and thermal stability.

Silicon Carbide

Silicon carbide (SiC) is a semiconducting material with very high hardness (Mohs hardness ~ 9) and a wide band gap of 2.3 – 3.2 eV, depending on the polytype. Today, over 250 polytypes of SiC are known, the three most important polytypes can be seen in Figure 7.

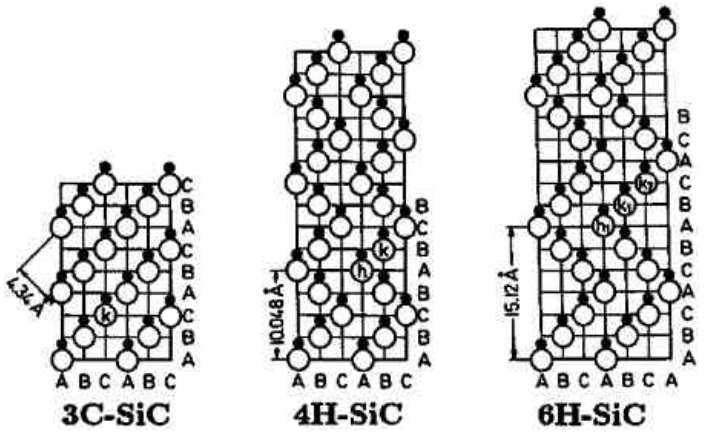

Figure 7: Schematic models of the three most common, also commercially available, SiC polytypes. h and k denote the hexagonal and cubic sites in the lattice, respectively. Open and full circles stand for the silicon and carbon atoms, respectively[72]

With regard to applications, SiC is used in high-power, high-voltage applications, high-temperature semiconductor devices and for sensing in harsh environments.[73-75] Additionally, it has found application in biosensing due to its inherent biocompatibility. Methods for functionalization of SiC also include silanization of the native oxide layer of SiC[76] as well as functionalization with alkenes, very much resembling the functionalization of silicon. Functionalization of SiC with alkenes has been carried out thermally[77] as well as photochemically[78]. Due to its polymorphism, SiC shows anisotropic reactivity of different crystal faces. In 6H-SiC for example, $000\bar{1}$ crystal faces are C-OH terminated upon etching, whereas 0001 facets are Si-OH terminated, leading to anisoptropic reactivity on different facets, as reported by Steenackers *et al.*[79] (see Figure 8)

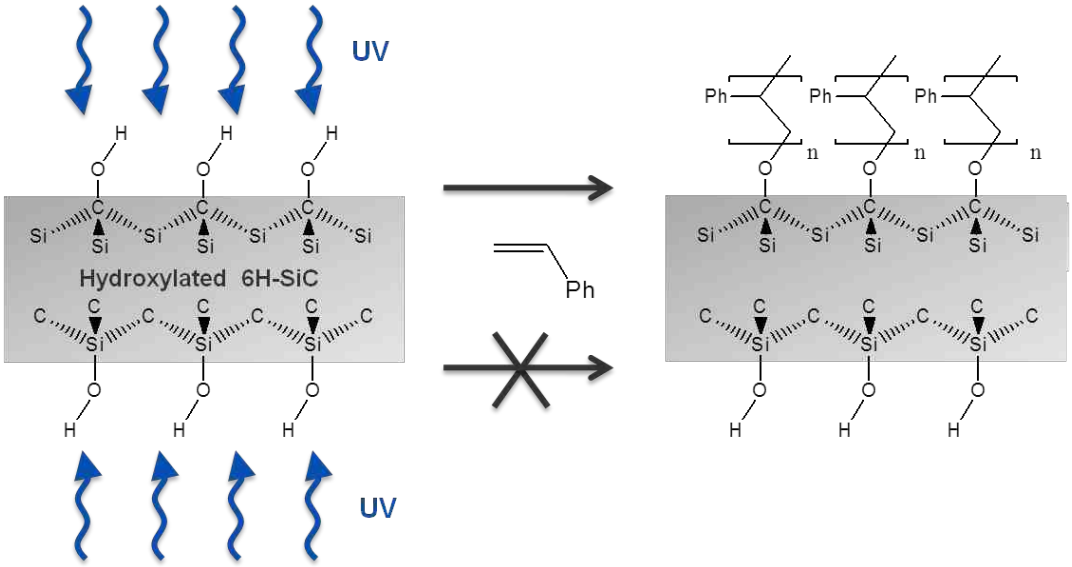

Figure 8: Reactivity difference of different crystal facets in 6H-SiC with photoactivated styrene as shown by Steenackers *et al.*[79]

Silicon Nitride

Although an insulator, silicon nitride, Si_3N_4, is among the materials most frequently used in semiconductor industry.[80] This is mainly due to its use as a passivation layer and diffusion barrier against oxygen, water, and ions. Functionalization of Si_3N_4 with organic molecules has recently been reported. Upon etching with hydrofluoric acid, Si_3N_4 surfaces are terminated with Si-H, N-H, and N-H_2 moieties as confirmed by XPS and contact angle studies.[81-83] This enables the surface to be functionalized with unsaturated hydrocarbons analogous to Si and SiC.[78,84]

2.1.4 Gallium Nitride

Gallium nitride, GaN, is a III-V semiconductor with a wide bandgap of 3.4 eV and shows high potential with respect to applications in short-wavelength optoelectronics.[85] This material exhibits high mechanical, thermal, and chemical stability[86] due to its strong ionic bonds, leading to high resistance towards degradation in harsh conditions, e.g. high electric current densities, intense irradiation, and high temperatures.[87] Moreover, GaN has been proven to be biocompatible[88] and sensitive to local pH changes,[89] which make it an ideal candidate for biosensing and bioelectronics applications.[90] Due to their inherent polarity, GaN surfaces are mainly Ga-terminated, leading to Ga-OH groups after plasma cleaning.[91-94]

2.1.5 Graphene

Graphene is a two-dimensional carbon allotrope material consisting of a single layer of sp^2-hybridized carbon atoms arranged in a honeycomb structure. It possesses fascinating properties structurally, chemically as well as electrically. Despite being only one atom thick, it has the highest tensile modulus ever measured (1 TPa), a breaking strength 100 greater than steel of the same thickness, its intrinsic charge carrier mobility is surprisingly high (up to 4000 $cm^2V^{-1}s^{-1}$), it can sustain much higher current densities than copper and it is impermeable to gases.[95] This makes graphene a promising option for chemical and biological sensing as well as for use in bioelectronics.[96] However, problems arise when graphene is to be chemically functionalized, since covalent functionalization of graphene usually leads to a change of hybridization from sp^2 to sp^3, inducing defects and leading to deterioration of electronic properties like electron transport and charge carrier mobilities. Yet, since chemical functionalization is a prerequisite for specificity in sensing applications a way of functionalizing graphene without compromising electronic properties is to be found. In order to circumvent these issues, routes for non-covalent functionalization are used. This is typically accomplished by π-π-stacking of aromatic compounds[97-99] or ionic interactions between end-functional molecules and edge-functional graphene.[100,101] Although these routes leave the electronic properties of graphene unchanged, the weakness of those interactions leads to less stable bonding to graphene than in covalent functionalization routes. While they have a broad range of applications in non-covalently bound composites containing graphene, these systems are not suitable for devices working in harsh conditions over an extended period of time, such as chemical or biological sensors, or for subsequent post-functionalization modifications.

Covalent functionalization significantly affects the electronic structure of graphene by converting sp^2-hybridized carbon atoms to sp^3-hybridization. This effect, however, is sometimes desired in order to generate a bandgap, which introduces a barrier for charge transport. One convenient method for covalent functionalization of graphene is reaction with aryl diazonium salts. The reaction of graphene with an aromatic diazo salt proceeds via electron-transfer from graphene to the positively charged aromatic ring.[102-104] A disadvantage of this method is the tendency of diazonium salts to form multilayers by grafting onto grafted aromatic rings, as shown in Figure 9. The generated bandgap can be detected by scanning tunneling microscopy (STM) and shows that grafting of aryldiazonium salts strongly affects

the electronic structure of graphene.[105] Further approaches for functionalization of graphene include photochemical reactions with radical starters[106] by photochemical excitation of graphene or 1,3-dipolar cycloaddition of azomethines analogous to the Prato reaction in fullerene chemistry.[107,108]

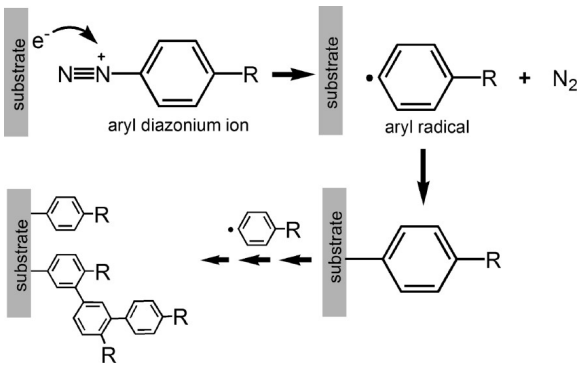

Figure 9: Schematic of the reaction of graphene substrate with diazonium salts (counter ions are omitted for clarity)

Although bandgap engineering can be quite useful for many applications, it is undesired for applications where good eletrical transport is needed, e.g. in sensing. Thus, functionalization of graphene without generating further defects is highly interesting. Some of the few results towards this kind of functionalization include selective reaction of diazonium salts with the graphene basal plane[109] or reactions of alkoxysilanes with the epoxy groups of graphene oxide, proceeding without further defect generation.[110]

Another way for tuning the electronic properties of graphene is hydrogenation. Hydrogenated graphene, also known as graphane, is generated from graphene by addition of hydrogen atoms to both sides of the basal plane to generate a 2-dimensional saturated hydrocarbon. Complete conversion of the sp^2-hybridized carbon atoms in graphene leads to sp^3-hybridized carbon and the resulting graphane is an insulator compared to the zero-bandgap semiconducting graphene.[111] Literature reports drastic changes in the electronic properties and atomic structure of graphene upon hydrogenation in a cold H_2 plasma.[112] While these hydrogen-terminated carbon atoms can be considered defects, this in turn is a possibility for covalent functionalization of the material. By tuning the defect density in the material, organic molecules could be selectively attached onto modified graphene while at the same time balancing degree of functionalization and electronic properties.

2.2 Polymers at Surfaces

The use of polymer coatings on surfaces has many advantages over conventional monolayers. Despite being less ordered, density of functional groups per surface area is much higher than for monolayers due to the three-dimensional structure. While the maximum number of functional groups for a monolayer is very limited due to the two-dimensional structure, polymer can drastically increase the number of functional groups close to the surface.

Moreover, polymers provide a less rigid linker material, being beneficial e.g. for biological applications such as binding of enzymes or DNA that could conformationally be changed by attachment to a rigid monolayer.[113] For semiconductor surfaces, this enables construction of sensors with high loading capacities and high sensitivities. Polymers also provide high variety in terms of chemistry and functionalization.

Depending on grafting densities, covalently grafted polymers at a surface can form structures ranging from pancake-like for very low grafting densities, over mushroom-like to brush-like structures for high grafting densities, as can be seen by the scheme in Figure 10.

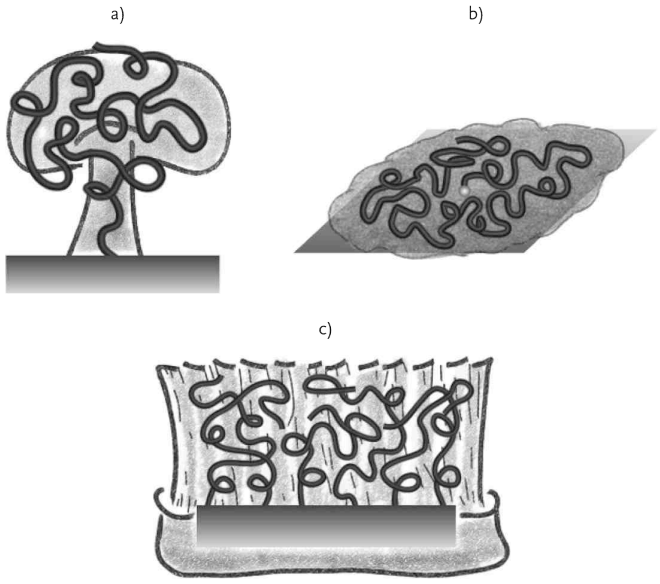

Figure 10: Artist's perception of the terms (a) "mushroom", (b) "pancake" and (c) "brush" used for the different possible conformations of surface-attached polymers[114]

2.2.1 Polymer grafting

With respect to stability, covalently bonded polymers on surface are the best choice. Grafting can be achieved in various ways that can be classified into three main categories: *Grafting-*

onto, *grafting-through*, and *grafting-from*. Schematic representations of the three grafting pathways can be seen in

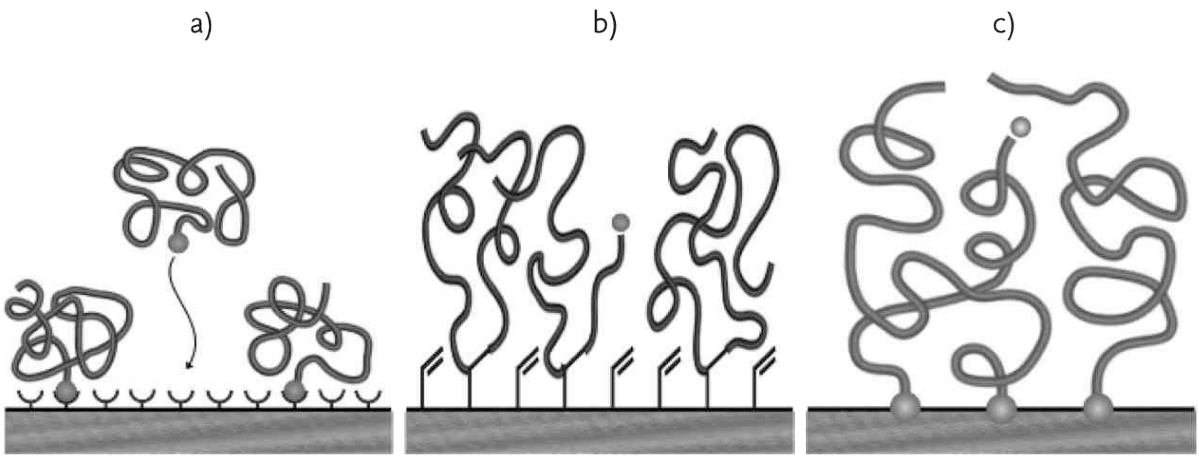

Figure 11: Schematic illustration of different processes used for the attachment of polymers to surfaces: (a) "grafting-onto"; (b) grafting via incorporation of surface-bound monomeric units (grafting-through) (c) "grafting from/surface-initiated polymerization"

In the *grafting-onto* approach, a preformed polymer with reactive groups, either in the backbone or at the chain end, is covalently bonded to the surface. However, by this process grafting density achieved is relatively low due to the diffusion barrier created by already grafted polymer chains, leading to layers of 1-5 nm dry film thickness.[114] Recently, *grafting-onto* has become increasingly important for the generation of polymer brushes at surfaces due to click-chemistry reactions facilitating grafting.[115-119]

The *grafting-through* approach consists of a reactive monomer species on the surface, which takes part in polymerization. Basically, it is polymerization in the presence of a surface-immobilized monomer. Both *grafting-onto* with reactive groups in the backbone and *grafting-through* do not lead to polymer chains attached to the surface on one end, but on one or possibly more points along the backbone.

In the *grafting-from* approach, polymerization is initiated at the surface, leading to polymerization from the surface and thus to polymer chains attached by only one chain end. This surface-initiated polymerization (SIP) has been applied to nearly any surface to generate covalently linked polymer brush systems. SIP has been carried out on many substrates such as gold, silica, glass, but also on semiconductor substrates such as silicon, gallium arsenide, or indium phosphide. The conventional approach for SIP involves the formation of a self-

assembled monolayer (SAM) of initiator molecules or initiator precursors attached to the surface. These initiator molecules are bifunctional, containing an anchor group for surface attachment and an initiator/precursor group that can start the polymerization from the surface. Many different polymerization types have been realized through this concept, including free radical polymerization[120], living radical polymerization[121,122], living cationic[123,124], living anionic[125], ring-opening metathesis polymerization[126], and lately group transfer polymerization.[127] During the last decade, even polycondensations proceeding via a chain-growth reaction have been carried out as surface-initiated polycondensations[128].

Although normal surface-initiated polymerizations are initiated thermally or by addition of an initiator compound, polymerization can also be induced by irradiation with light, mainly in the UV regime. Yang and Rånby[129,130] demonstrated that acrylic and methacrylic monomers can be grafted from polymer surfaces via UV irradiation in the presence of benzophenone, a commonly used photosensitizer. The grafting process is started via abstraction of a hydrogen atom from the polymer surface by a photoexcited triplet-state benzophenone.

This method of photoinitiation has also been used in a "living" sequential photografting approach.[131,132] In this two-step process, benzophenone abstracts a hydrogen atom from the surface and the radical is then capped with another BP molecule, forming a surface-grafted photoinitiator species. In the second step, surface-grafted BP is detached under UV irradiation in presence of a monomer, leaving behind a surface radical from which polymerization can take place. Figure 12 depicts the reaction involved in this grafting method

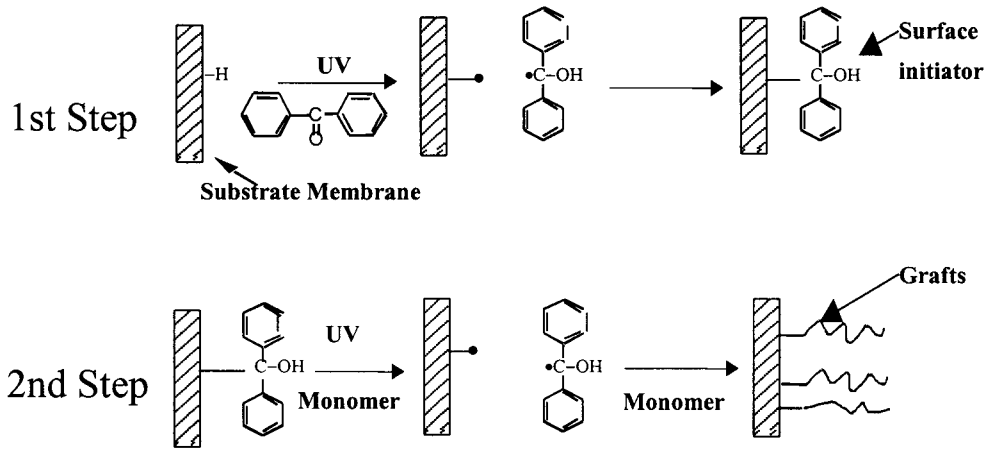

Figure 12: Schematic mechanism of the sequential "living" photografting[131,132]

Although these methods are very effective for generation of polymer-grafted membranes, it turned out that benzophenone as photosensitizer was not needed to obtain grafted polymer

when styrene was used.[133] The model that is used to explain this grafting involves a styrene molecule that is activated by UV irradiation and relaxing into a triplet state via intersystem crossing. This triplet state is in equilibrium with a styrene biradical that can react with H-donors by hydrogen abstraction. After hydrogen abstraction, the monoradical can start polymerization in solution. The surface radical generated by hydrogen abstraction can in turn, react with monomers in a surface-initiated free radical polymerization. This reaction was named "Self-Initiated Photografting and Photopolymerization" (SIPGP) by Wang and Brown,[134] who reported this reaction for acrylic monomers. One of the prerequisites for SIPGP are abstractable hydrogen atoms on the substrate surface. Otherwise, grafting cannot take place via the SIPGP mechanism. In order to be abstractable, the bond dissociation energy (BDE) of the bond has to be lower than ~ 100 kcal/mol. This number comes from the highest energy triplet state T_3, which is 112.5 kcal/mol for acrylic acid[134,135] and 104 kcal/mol for styrene[136]. A reaction scheme of this SIPGP process is shown in Figure 13.

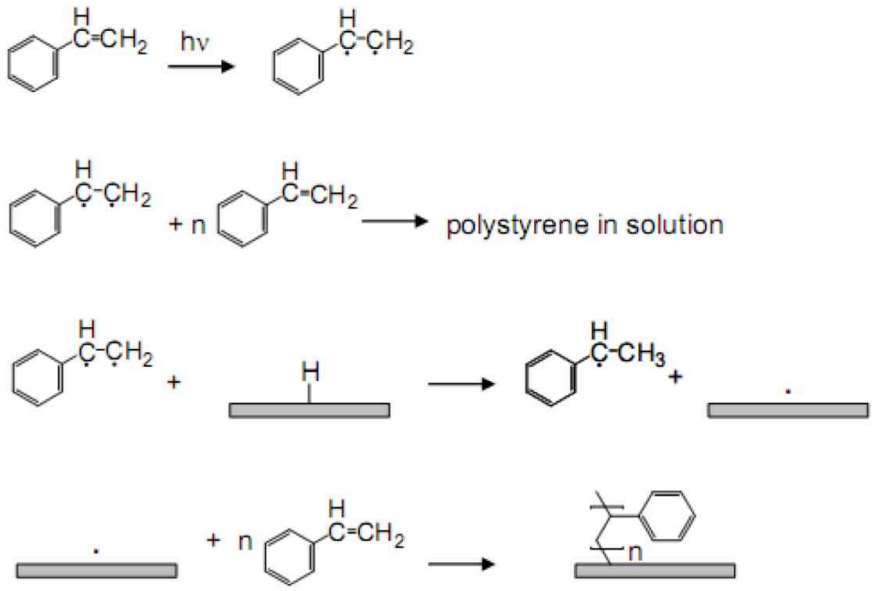

Figure 13: Reaction scheme of the SIPGP photografting method with styrene as monomer

SIPGP has been used for the functionalization of many substrates. Besides polymers, also various other substrates have been grafted from. SIPGP of acrylic and styrenic monomers has been carried out on glassy carbon,[137,138] silicon,[127,139] silicon carbide,[79] pyrogenic silica[140], diamond,[141,142], graphene,[143] crosslinked nanosheets on gold,[144] and on a variety of carbon-templated substrates (e.g., Si, Si_3N_4, Ge, GaAs, GaN, mica, glass, Al).[145]

Polymer brushes grafted *via* SIPGP are highly stable due to their covalent bonding and therefore can be modified via a broad range of post-polymerization modification reactions, such as sulfonation, nitration and aminomethylation with subsequent bioconjugation e.g. with enzymes or proteins, which can be seen in **Figure 14**.

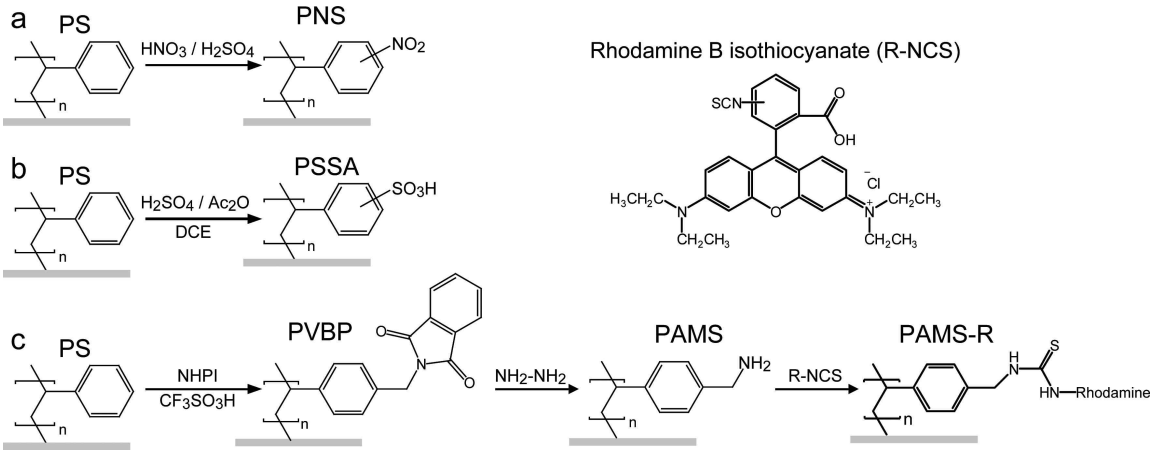

Figure 14: Outline of the different polymer analogue reactions of PS grafts reported by Steenackers *et al.*[141] (a) Nitration of PS grafts with fuminic nitric acid results in poly(nitrostyrene) (PNS) grafts. (b) Sulfonation by acetylsulfuric acid results in poly(styrene sulfonic acid) (PSSA) grafts. (c) Amidoalkylation of PS grafts results in poly((4-aminomethyl)styrene) (PAMS) grafts. In addition, the schematic also shows the grafting of the fluorescent label rhodamine B to PAMS grafts.

2.2.2 Free-radical polymerization

Free-radical polymerization (FRP) is possibly the most frequently used and most intensively studied polymerization method, mainly due to its high industrial relevance.[146] It is tolerant against many functional groups und impurities and can be carried out in bulk as well as in solution, emulsion or suspension even in water.

Generally, the mechanism of FRP consists of four steps: Initiation, start, chain growth, and termination. In the initiation step, an initiator is dissociated. This initiator can be cleaved in several ways, including heat, light, or electron transfer. By homolytic cleavage of the initiator, two radicals are created. The dissociation of such an initiator molecule can be expressed via

$$I \xrightarrow{k_i} 2\,R\cdot$$

In the start reaction, radicals $R\cdot$ react with a monomer molecule at the rate constant

$$R\cdot + M \xrightarrow{k_{st}} R-M\cdot$$

This activated monomer can add to other monomers in a chain-growth reaction with k_p being the polymerization rate constant

$$R-M\cdot +(n-1)M \xrightarrow{k_p} R-(M)_n\cdot$$

The reactivity of the growing chain towards a monomer can be regarded as independent from the chain length but can be influenced by the monomer or by solvation.
Chain termination can occur *via* combination or disproportionation of two growing polymer chains, limiting the concentration of active radicals to around 10^{-8} mol/l.
The termination rate constant is composed of the rate constant of termination by combination of two radical chain ends and the one of termination by disproportionation.
Moreover, transfer reactions can occur, terminating the growth of one chain but generating another radical that can start polymerization.[147]

All of these reactions also take place in surface-initiated FRP, but with some distinct differences. Firstly, in SIPGP there is no cleavage of an initiator but formation of a biradical upon light absorption. Upon abstraction of a hydrogen atom from the surface, only one instead of two radicals are generated on the surface. Also transfer reactions from a growing polymer chain on the surface to a solvent or monomer molecule can be considered termination reactions, since the chain growth from the surface thereby stops.

However, termination reactions of two polymer chains, one in solution and one attached to the surface is highly unlikely, since the radical in solution has to diffuse against the concentration gradient within the polymer film.[148] This is not only true for two growing polymer chains, but also for the transfer reaction between a growing polymer chain in solution and an abstractable hydrogen atom on the surface.

Furthermore, radical abstraction in SIPGP can also occur from already grafted polymer chains on the surface, thereby leading to a "*grafting-from-grafting*" scenario resulting in branched polymer morphologies (dendrigraft polymers / arborescent polymers).[132,149,150]

2.2.3 Copolymers

A copolymer is a polymer comprised of two or more different monomers. Depending on the monomer unit sequences, copolymers can be statistical, alternating, block, or graft copolymers, as will be illustrated by a binary copolymer consisting of two different monomer units A and B.

For a statistical copolymer, the sequential distribution of the monomeric units obeys known statistical laws (AABABBBABAABBBABBABAB....). A random copolymer is a special case of a statistic copolymer, where the monomer units are added to the reactive chain end with the same probability. In an alternating copolymer, the monomer units are incorporated in an exact order along the polymer chain (ABABABABABABABABABA…….). Block copolymers consist of longer sequences (or blocks) of each monomer (AAAAAAAAAAABBBBBBBBBB….). Graft copolymers consist of polymer chains where blocks of one monomer are grafted to the polymer backbone of the other (AAA[BBBBB….]AAA[BBBB….]AAAA[BBBB…]AA…).

By copolymerization, various types of polymers with different properties can be obtained from relatively few monomer species. Most technically relevant copolymerizations are radical in nature because most monomers can be radically polymerized, those monomers are relatively low-cost and the sequential statistics can be manipulated more facile than in other types of polymerization.

2.2.4 Free-radical Copolymerization

Compositions and sequential statistics of copolymers are usually described by the *terminal model*. In this model, the assumption is made that, in a binary system, only the last monomer units M_1* and M_2* of the growing polymer chains exert control over addition of monomer molecules M_1 and M_2. This corresponds to a first-order Markovian statistic. If, however, also the penultimate units have influence on the addition of monomers, four active species, M_1M_1*, M_1M_2*, M_2M_1*, and M_2M_2* are operative. This *penultimate model* corresponds to a second-order Markovian statistic. The terminal model describes the momentary composition of copolymers very well (with some exceptions), however, distribution of diads, triads, etc., rate constants and therefore also polymerization rates can not be described very precisely.

In the easiest case of a copolymerization, the active chain ends react irreversibly with monomers M_1 and M_2. If the polymerization rate is only influenced by the last monomer units on the growing active chain end M_1* and M_2*, this results in four different growth rates and four different rate constants for the four addition reactions.

$$M_1* + M_1 \xrightarrow{k_{11}} M_1* \text{ (homopropagation)}$$

$$M_1* + M_2 \xrightarrow{k_{12}} M_2* \text{ (cross-propagation)}$$

$$M_2* + M_1 \xrightarrow{k_{21}} M_1* \text{ (cross-propagation)}$$

$$M_2* + M_2 \xrightarrow{k_{22}} M_2* \text{ (homopropagation)}$$

The rates of consumption for each monomer that are equal to the rates of addition of each monomer to the growing chain end, can be described as

$$-\frac{d[M_1]}{dt} = k_{11}[M_1*][M_1] + k_{21}[M_2*][M_1]$$

$$-\frac{d[M_2]}{dt} = k_{12}[M_1*][M_2] + k_{22}[M_2*][M_2]$$

Division of those two equations leads to the ratio at which the two monomers are incorporated into the copolymer:

$$\frac{d[M_1]}{d[M_2]} = \frac{k_{11}[M_1*][M_1] + k_{21}[M_2*][M_1]}{k_{12}[M_1*][M_2] + k_{22}[M_2*][M_2]}$$

Since the concentration of M_1* and M_2* in the steady state, their rates of interconversion have to be equal.

$$k_{21}[M_2*][M_1] = k_{12}[M_1*][M_2]$$

Introducing reactivity parameters r_1 and r_2 with

$$r_1 = \frac{k_{11}}{k_{12}} \quad \text{and} \quad r_2 = \frac{k_{22}}{k_{21}}$$

and rearrangement gives

$$\frac{d[M_1]}{d[M_2]} = \frac{[M_1](r_1[M_1] + [M_2])}{[M_2]([M_1] + r_2[M_2])}$$

This equation is known as the *copolymerization equation* or *Mayo-Lewis equation* and r_1 and r_2 are called *monomer reactivity ratios*.

Through knowledge of r_1 and r_2 for a copolymer system, the composition of the copolymer can be predicted, however the validity of the prediction can only be assumed for low conversions. According to the monomer reactivity ratios, different types of copolymerization behavior can be distinguished.

Ideal copolymerization: $r_1 r_2 = 1$

When the product of the monomer reactivity ratios is close to unity, both monomers are incorporated with equal probability, independent from the active end group, since

$$\frac{k_{11}}{k_{21}} = \frac{k_{12}}{k_{22}} \text{ or } r_2 = \frac{1}{r_1}$$

Alternating copolymerization: $r_1 = r_2 = 0$

When both r_1 and r_2 are 0, copolymerization proceeds in a strictly alternating way leading to alternating copolymers.

Block copolymerization: $r_1 > 1$, $r_2 > 1$

When both r_1 and r_2 are greater than 1, block copolymers are formed. For the very unlikely case of r_1 and r_2 being much larger than unity, simultaneous homopolymerization of the two monomers occurs, leading to the formation of a polymer blend.

For the case of $0 < r_1 < 1$ and $0 < r_2 < 1$, both monomers are incorporated into the polymer in a statistic way, leading to a statistical copolymerization. An example for this type of copolymerization is free radical copolymerization of styrene and methyl methacrylate (r_1 = 0.52, r_2 = 0.46).

2.2.5 Polymer Brushes as Macroinitiators

When polymers are grafted to a surface, the possibility arises of using them as macroinitiators for a consecutive surface-initiated polymerization. Applying this route, thick polymer layers can be grafted even from low grafting density polymer brush layers, due to the high steric demand of these "bottle-brush brushes" generated. Advantages of this method over conventional initiator monolayers are the high stability of this macroinitiator layer and the high density of initiator moieties provided by the three-dimensional morphology of the macroinitiator layer. Examples for the use of polymer brushes as macroinitiator layer for surface-initiated polymerization include surface-initiated atom-transfer polymerization (SI-ATRP),[151] surface.initiated living cationic ring-opening polymerization (SI-LCROP) of 2-alkyl-2-oxazolines[137,142], and surface-initiated Kumada catalyst-transfer polycondensation (SI-KCTP).

An example for surface-initiated living cationic ring-opening polymerization is given in Figure 15. After SIPGP of 2-isopropenyl-2-oxazoline (iPOx), the macroinitiator is formed by addition of methyl triflate to yield the positively charged macroinitator. This also leads to a decoiling of the polymer chains because of electrostatic repulsion along the chain. Addition of 2-alkyl-2-oxazoline then leads to the formation of poly(2-alkyl-2-oxazoline)-grafted poly(2-isopropenyl-2-oxazoline).

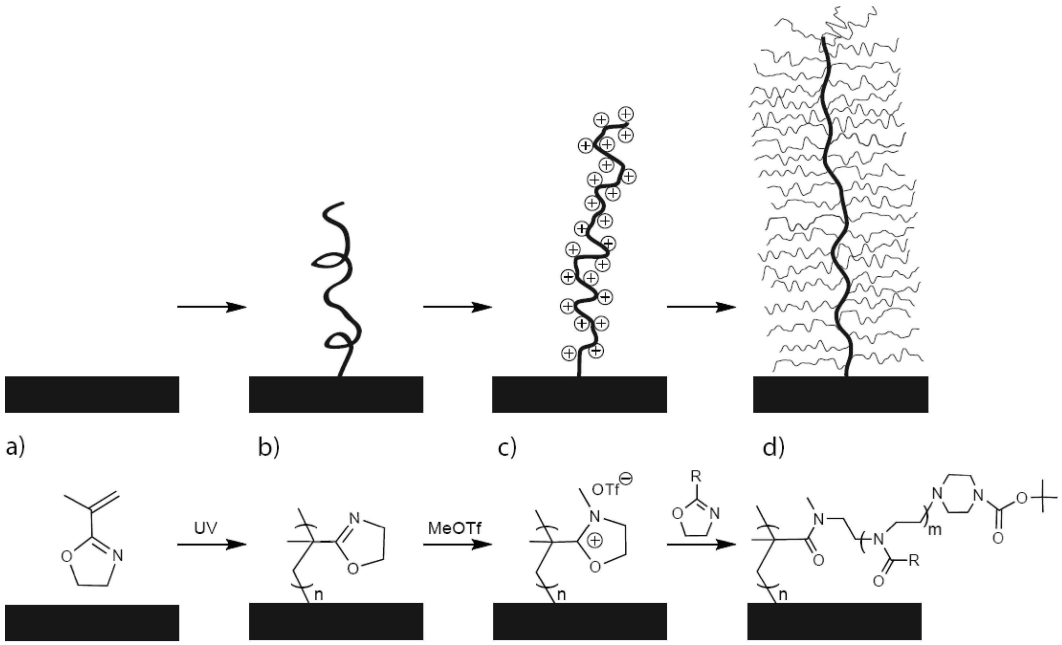

Figure 15: Schematic of the SIPGP of 2-isopropenyl-2-oxazoline on glassy carbon, subsequent initiation with methyl triflate to form a macroinitaor species and SI-LCROP of 2-alkyl-2-oxazoline to yield surface-grafted bottle-brush brushes. Reprinted from reference [137]

Another application of polymer macroinitiators is SI-KCTP. In studies reported by Senkovskyy *et al.*[152], photo-crosslinked brominated polystyrene (PS-Br) is reacted with $Ni(PPh_3)_4$ to form a surface-attached macroinitiator and polymerization is started by addition 2-bromo-3-hexyl-5-chloromagnesiothiophene. By this route, poly(3-hexylthiophene) (P3HT) brushes can be grafted from PS-Br in a living polycondensation. A schematic of this process can be seen in Figure 16.

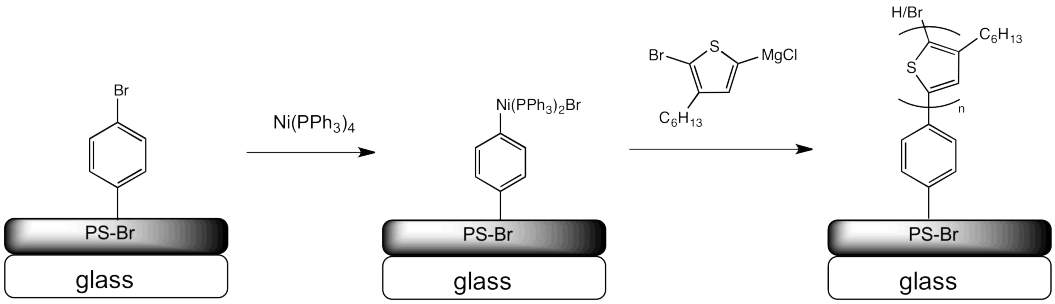

Figure 16: Scheme of the SI-KCTP procedure applied to photo-crosslinked brominated polystyrene

Another method of using polymer brushes as macroinitiator for surface-initiated polymerization is the surface-initiated group transfer polymerization (SI-GTP) of poly(vinylphosphonate)s and was recently published by our group[127]. In this approach, a bifunctional methacrylate (ethylene glycol dimethacrylate EGDM) is polymerized to form a surface-grafted, partially crosslinked polymer network with functional methacrylate sites on which a lanthanidocene catalyst can be immobilized. Polymerization is started by addition of the monomer vinylphosphonate and proceeds *via* a living anionic coordination polymerization mechanism. A scheme of this method is depicted in Figure 17.

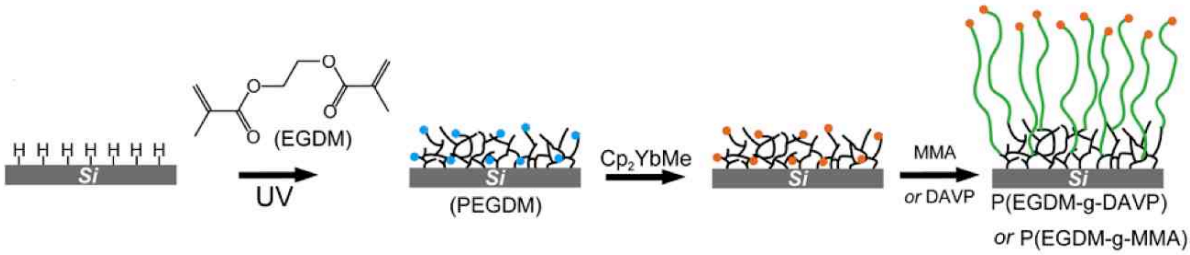

Figure 17: Scheme of SI-GTP initiated from surface-immobilized lanthanide catalyst species to yield stably surface-grafted poly(vinylphosphonate) brushes.

3 Purpose and Objectives

Functionalization of rigid semiconductor surfaces with flexible organic polymers might open up a whole new field of applications as sensors, optoelectronic devices or even photovoltaic applications. But as a journey of thousand miles begins with a small step, fundamentals had to be laid first. Thus, before directly going into application-oriented device design, fundamental processes had to be understood.

The aim of this work was to develop and understand the processes involved during (mainly) photoinduced polymer grafting from semiconductor surfaces in general and silicon surfaces in particular. The main question was, whether it is possible to directly graft polymer brushes from hydrogen-terminated silicon surfaces possessing abstractable hydrogen atoms *via* a convenient one-step protocol, and if so, whether layer thickness could be controlled by varying reaction time. Additionally, ways to accelerate the surface grafting reaction were to be found.

Moreover, the properties of those grafted layers should be determined and also if the grafted layer influences the electronic properties of the substrate material.

Based on these preliminary studies, a follow-up target was the generation of functional polymer grafts on the semiconductor surfaces and the investigation of their stability towards post-polymerization modification as these functional inorganic-organic hybrid materials could be of high interest for e.g. ChemFETs.

After gaining a basic understanding about the processes involved in photoinduced surface grafting from planar silicon, this knowledge had to be applied to polymerization from nanocrystalline silicon, as this presents a large window of opportunity towards optoelectronics due to the unique properties of this material (quantum confinement, luminescence, multiple exciton generation). Also with this system, fundamental processes for photoinduced grafting had to be found and understood and then compared with the findings on planar silicon substrates. Comparisons should also be made between silicon nanocrystals and nanocrystals of other silicon-based materials, namely silicon carbide and silicon nitride.

As work went on and proved to be very successful, it should be examined if the processes developed on silicon surfaces could also be applied on other emerging semiconductor materials gallium nitride and graphene. Especially for graphene, applications in sensing and as a replacement material for transparent conductive oxide (TCO) are in near sight.

Based on these potentials, the general feasibility of grafting conductive polymers from those semiconductor surfaces should also be investigated, potentially leading to use in photovoltaics.

4 Results and Discussion

4.1 Photoinduced Polymerization from H-terminated Si(100)

4.1.1 Background

Despite the high importance of semiconductors material, functionalization of silicon with polymers is a relatively unexplored area of surface chemistry. The conventional approach for grafting polymers from a silicon surface is attachment of an initiator SAM to the native oxide layer of silicon.[121,153,154] From this layer, polymerization can be started. However, these Si-O-C bonded polymer layers are not stable against hydrolysis and the functionalization involves several steps. Moreover, electronic properties of oxide-covered silicon are inferior to H-terminated silicon. Approaches involving direct grafting of the initiator SAM onto H-terminated silicon yielding stable, Si-C bonded polymer grafts also proceed with multi-step protocols.[155-158]. Moran and Carter[159] presented a convenient method for direct passivation of hydrogen-terminated Si(100) surfaces with a variety of polymers, including styrene, 4-vinyl pyridine and several acrylic monomers. In this work, "*chain attachment was found to occur through hydride abstraction by a propagating radical and coupling of a subsequent chain to the resulting dangling bond...*". The initiation of this polymerization took place in solution and the growing chains reacted with the H-terminated silicon surface in a transfer reaction, leading to surface silyl radicals, which, in turn, could react with growing chain ends in a radical recombination reaction to form surface-grafted polymer. This fact, however leads to a mechanism that is more similar to a *grafting-onto* than to a *grafting-from* and is also supported by the fact that polymer layer thickness remained below 15 nm in all cases. Their publication has shown that polymers can be directly grafted from or onto hydrogen-terminated silicon by means of H-abstraction. Also in the work of Moran and Carter they could not rule out that surface silyl radicals can themselves start polymerization by addition of monomers.

Based on these findings, we used H-Si(100) as a substrate for self-initiated photografting and photopolymerization (SIPGP) as it would be a simple one-pot, one-step procedure that might yield high layer thickness and grafting densities. Moreover, its applicability to a wide range of monomers makes it very versatile.

The grafting mechanism we envisioned can be described as follows:

Irradiation with UV light in the region of 300 to 400 nm (λ_{max} = 350 nm) leads to a highly reactive biradical, which can then abstract a hydrogen atom from the Si-H surface. The surface radical (dangling bond) may act as the initiating site for the free-radical polymerization of a vinyl monomer. As the prerequisite for this process is assumed to be a bond dissociation energy (BDE) of the respective X-H bond below ~ 100 kcal/mol. Hydrogen-terminated silicon might be ideal for this process as the BDE of a Si-H bond is reported to be around 90 kcal/mol.[38] The reaction scheme is outlined in Figure 18.

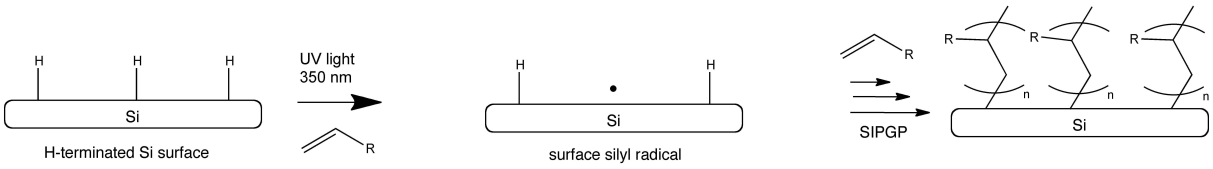

Figure 18: Mechanism of the self-initiated photografting and photopolymerization process on hydrogen-terminated silicon

4.1.2 Proof of Principle

First reactions were carried out by irradiating H-terminated silicon substrates immersed in the monomer styrene (see Figure 19) with UV light and analysis of the substrate after grafting by FTIR spectroscopy, AFM, ellipsometry, and contact angle measurements .

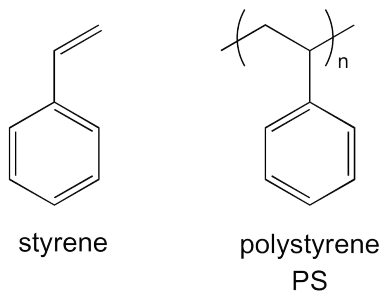

Figure 19: Structural formulas of styrene and polystyrene (PS)

Therefore, Si wafer substrates were cleaned by ultrasonication in acetone for 10 min and then rubbed with a cotton swab. Afterwards, wafers were boiled for 20 min in a 5 wt.% solution of sodium peroxodisulfate in Millipore water. For etching, silicon substrates are immersed in 50% HF in H_2O for 2 min, then rinsed with Millipore water, ultrasonicated in Millipore water for 10 s, then rinsed with Millipore water and blow-dried with an air stream.

The freshly etched substrates were immersed in approx. 1 ml bulk monomer, degassed *via* three freeze-pump-thaw cycles to avoid oxygen contamination and irradiated with UV light (λ_{max} = 350 nm) for the desired duration. After irradiation, the surfaces were immersed in a

good solvent for the respective polymer (toluene for styrene, acetone for most acrylates and methacrylates, and ethanol for polar monomers such as vinyl pyridine) and sonicated for 5 min. The samples were then rinsed with the solvent and immersed, in turns, into toluene, acetone, and ethanol. This leads to a alternating swelling (in a good solvent) and coiling of the surface-grafted polymer chain which also leads to a removal of non-grafted material. After three cycles of alternating immersion in different solvents, the surface is rinsed with semiconductor grade ethanol and blow-dried under a stream of filtered pressurized air. This ensures a removal of particles from the surface.

In order to obtain surface-sensitive IR spectra from the grafted species, variable grazing angle attenuated total reflection (variGATR) measurement was employed. variGATR is a special observation mode of ATR IR spectroscopy, were the substrate is brought in close contact to a germanium crystal with high refractive index. The incident angle in this device can be varied, but was set 62.5 ° in all of our measurements to provide reproducible measurements. The grazing incidence leads to an enhancement of evanescent waves on the surface, which increases the surface sensitivity. By this method it is even possible to detect monolayers on metallic or semiconducting substrates, such as crystalline silicon.

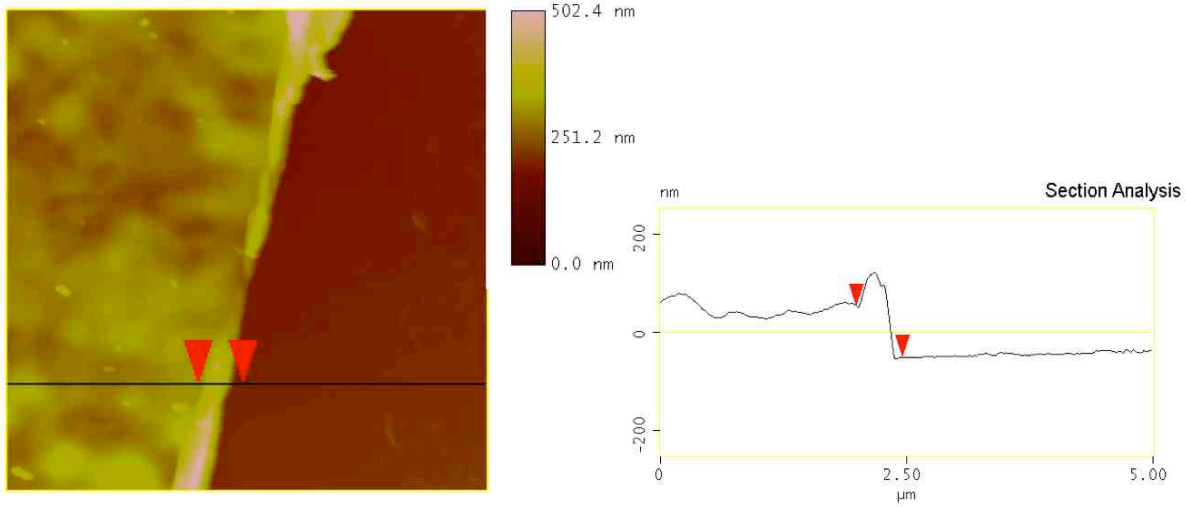

Figure 20: AFM image and section analysis of a hydrogen-terminated silicon surface grafted with styrene for 12 h

Figure 20 shows an AFM image of an H-terminated Si substrate that was irradiated with UV light in the presence of bulk styrene for 12 h. It can be seen that a homogeneous polymer layer is grafted to the surface. An ATR spectrum of the surface is shown in Figure 21. The

presence of grafted polystyrene at the surface was confirmed by FTIR *via* the aromatic C-H stretching bands, aromatic C=C stretching at 1660 cm^{-1} and 1600 cm^{-1} and the methylene backbone bending at 1450 cm^{-1}. Interestingly, Si-H stretching bands at around 2100 cm^{-1} and Si-O stretching vibrations at 1100 cm^{-1} are absent, which is a good indication for a thick and complete layer of polymer grafted on the surface and the absence of oxidation of the Si substrate. Figure 21 shows the disappearance of the Si-H stretching signal even after short irradiation (2 h) in bulk styrene.

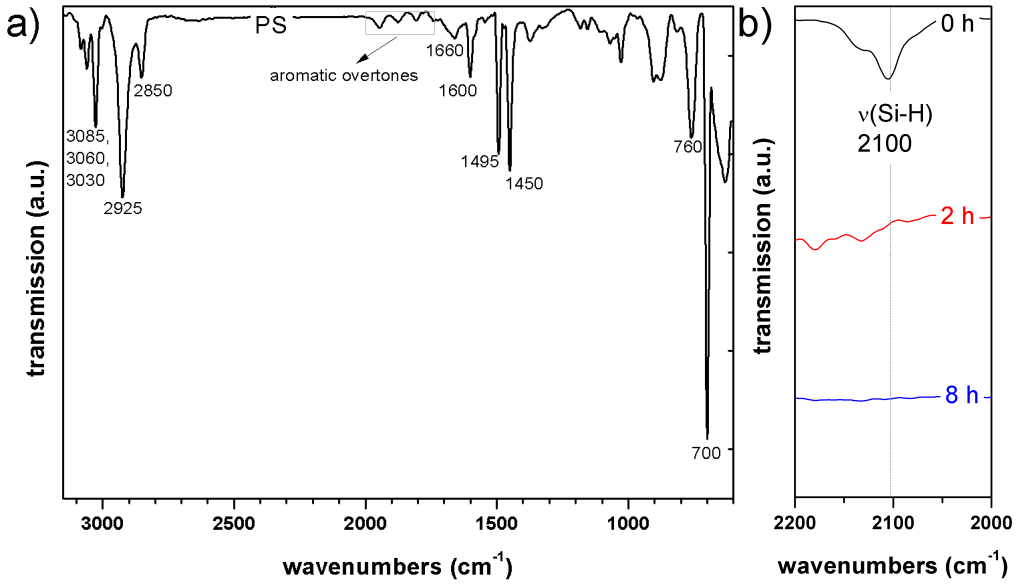

Figure 21: IR spectra of a H-terminated Si substrate after 8 h UV irradiation in bulk styrene (a) and close-up of the characteristic Si-H stretching band region around 2100 cm^{-1} of H-terminated Si substrates after different irradiation times in bulk styrene (b)

The contact angle of this surface was measured to be 91.7 ± 0.15°, being in agreement with the value expected for a PS grafted surface of around 88.42 ± 0.28°.[160]

4.1.3 Grafting kinetics of styrene on H-Si

To obtain more information about the reaction process, H-terminated Si substrates were irradiated in bulk styrene for different polymerization times and the thickness of the grafted polymer layer was measured by AFM. As can be seen in Figure 22, there is an almost linear dependency of polymer layer thickness on grafting time for the first 12 hours of irradiation. The second regime (12 h to 18 h grafting) in polymer layer thickness growth can be attributed to the gel effect (Trommsdorff-Norrish effect) and, more importantly, to grafting from already grafted polymer brushes, leading to branched and/or crosslinked polymer grafts (dendrigraft

brushes). Afterwards, polymer layer thickness increases significantly faster until the reaction solution becomes highly viscous due to the high amount of free polymer generated and hinders further increases in layer thickness. Therefore, irradiation durations longer than 20 hours have not been investigated in this work.

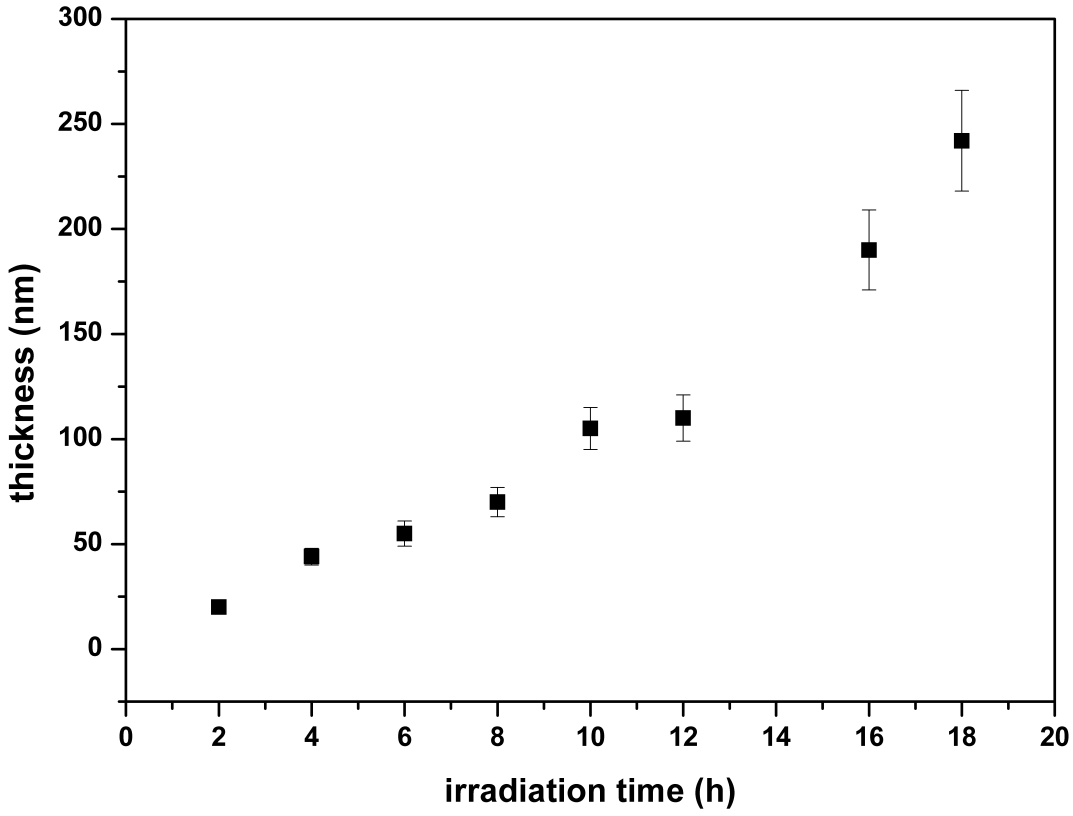

Figure 22: *Ex-situ* kinetics measurement of H-terminated Si(100) in bulk styrene

The linear increase of grafting thickness over time for the first 12 hours is in accordance with results of Steenackers on diazo-functional crosslinked aminobyphenyl thiol layer (k = 9.8 nm/h) and the results reported by Rühe *et al.* on diazo-functional initiator monolayers (16.7 nm/h).[161,162]

Comparing these kinetics to SIPGP from oxidized silicon modified with aminopropyl triethoxysilane (APTES) conducted by Korfmann shows a comparable tendency (8.5 nm/h on APTES-SiOx vs. 9.2 nm/h on H-Si). A possible explanation for the slightly higher grafting rate on H-Si is the lower BDE of the Si-H bond leading to easier H-abstraction and the higher density of Si-H on a Si(100) surface compared to an APTES-modified SiO_x surface, leading to a higher grafting density of the polymers.[140]

4.1.4 SIPGP of (meth)acrylate monomers

Comparing the photografting of styrene from H-terminated silicon to the photografting of acrylates and methacrylates, it can be seen that the latter are much less effective. Monomers methyl methacrylate (MMA), tert.-butyl methacrylate (tBMA) , N,N-dimethylaminoethyl methacrylate (DMAEMA), 2-hydroxyethyl methacrylate (HEMA), and ethyl acrylate (EA) (as seen from Figure 23) were used as candidates for SIPGP on H-terminated Si.

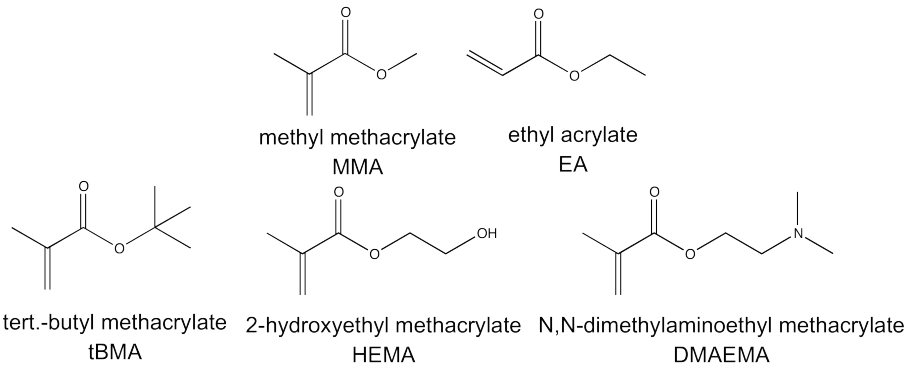

Figure 23: Structural formulas of the (meth)acrylic monomers methyl methacrylate (MMA), ethyl acrylate (EA), tert.-butyl methacrylate (tBMA), 2-hydroxyethyl methacrylate (HEMA), and dimethylaminoethyl methacrylate (DMAEMA)

Grafting resulted only in thin polymer layers, while high conversions in bulk monomer were observed. However, characteristic bands and contact angles in agreement with the respective polymers show that grafting takes place. After 6 h photografting with MMA on H-terminated Si, absence of Si-H stretching bands in the IR spectrum shows a high degree of functionalization. The presence of PMMA after 6 h UV irradiation could be confirmed by presence of characteristic absorption bands, as can be seen in Figure 24**.** *Via* ellipsometry, the thickness of this grafted layer was determined to be around 17 ± 2 nm.

Figure 24 shows an IR spectrum of a H-Si surface grafted with several different (meth)acrylates for different durations. The most prominent band in this spectrum at can be assigned to the C=O stretching vibration of PMMA. Together with the strong band at 1450 cm^{-1} indicating a CH_2-bending vibration and at 1100 for the C-O stretching of the methyl ester, it can be concluded that PMMA is present at the Si surface. The contact angle was measured to be 69.0 ± 0.08° which is congruent with expected values.[163] For the substrate irradiated in bulk MMA for 6 h, thickness of the grafted PMMA layer was determined to be 17 ± 2 nm *via* ellipsometry, the other grafted polymer layers were all < 5 nm.

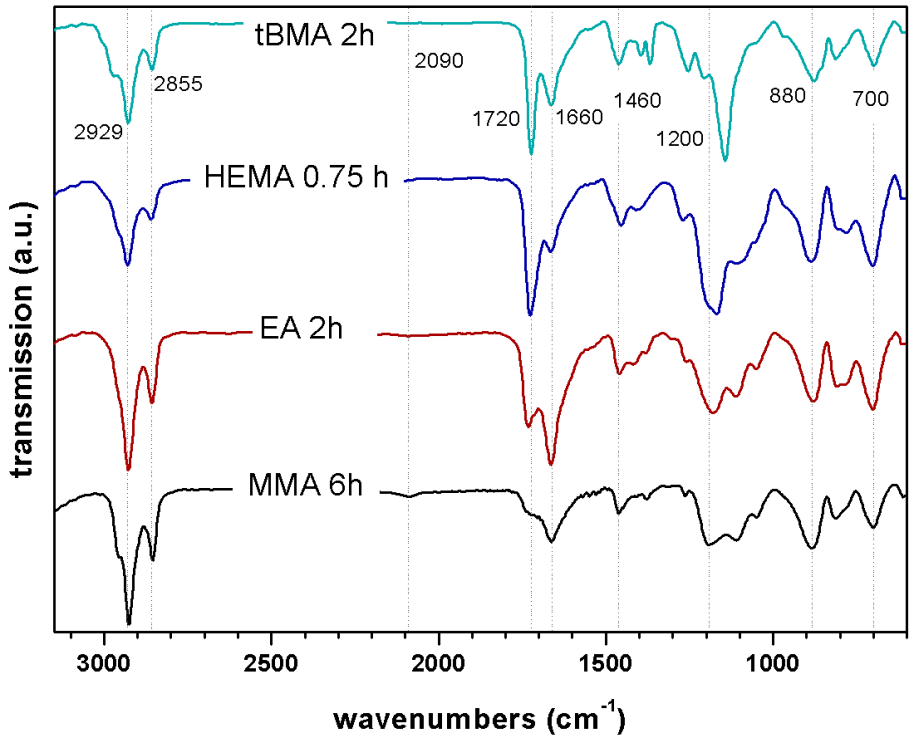

Figure 24: IR spectrum of H-terminated Si(100) surface irradiated in bulk MMA for 6 h (left) and in bulk EA, HEMA and tBMA (right)

Explanations for the difference in grafting effectiveness between styrene and (meth)acrylates can be found in the high affinity of activated alkenes like acrylates and methacrylates for the addition to silyl radicals.[164] This might lead to very strong competition between polymerization initiated from silyl radicals on the surface and a surface chain reaction leading to a hydrosilylated acrylate/methacrylate monolayer. Moreover, negative polarization on the silicon-bonded hydrogen atom and positive polarization of the alkene terminal carbon atom facilitates orientation of the monomer towards the surface and abstraction of the hydrogen atom. This increased reactivity of acrylics towards surface chain hydrosilylation decreases the grafting density of the polymer brushes by decreasing the number of surface dangling bonds taking part in polymerization. This results in lower thickness of grafted polymer layers. Although, it is basically possible to graft from these hydrosilylated monolayers, hydrogen atoms on these layers are harder to abstract than from an Si-H bond and monomers have to diffuse against the concentration gradient in the already grafted polymers.

Regarding the mechanism for this grafting method, different surface reactions have to be taken into account. It is well known that irradiation of a hydrogen-terminated silicon surface in presence of reactive alkenes or alkynes leads to monolayer formation via a surface chain-reaction that is at least twice as fast as polymerization in the case of styrene.[25] This leads to a

strong competition of polymerization and the hydrosilylation chain reaction on the surface and a potentially lower grafting density as not all radicals that are generated on the surface immediately also start polymerization in the first stage of the reaction. However, isolated hydrogen atoms with no or only few neighboring hydrogen atoms can be easily abstracted and start polymerization.

The proposed reaction pathways of the competing reactions are summarized in Figure 25.

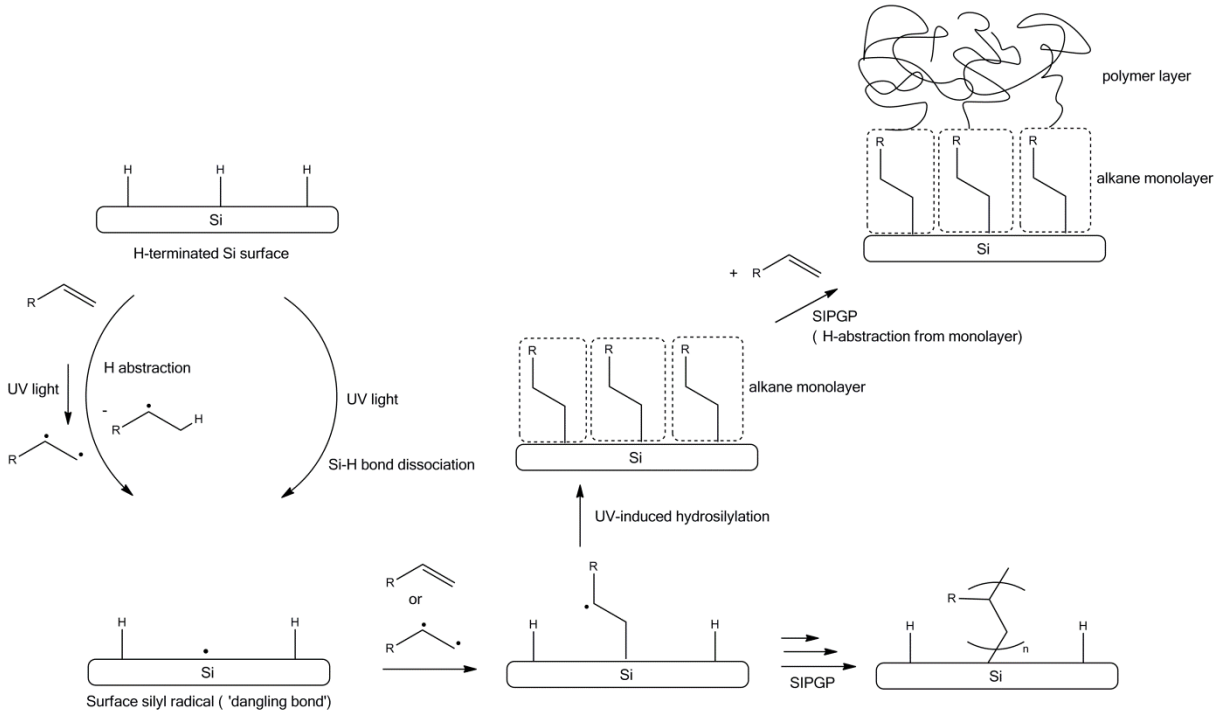

Figure 25: Different pathways for grafting and hydrosilylation during irradiation of H-Si with UV light in presence of UV-active monomers

4.1.5 SIPGP on thermally hydrosilylated H-Si surfaces

To further elucidate the mechanism, a thermally hydrosilylated layer of MMA on H-Si was obtained by immersing H-terminated Si at 40°C for 48 h. This temperature is not sufficient for a thermal initiation of MMA polymerization, as a thermally MMA-grafted blind sample showed no polymer formation. Subsequently, the substrate was irradiated for 2 hours, resulting in a polymer layer thickness of over 200 nm. From this experiment we conclude that polymerization from a thermally pregrafted monolayer with easily abstractable hydrogen atoms facilitates the photografting process by avoiding the competing surface chain reaction. Thus, every radical formed can directly initiate polymerization from the grafted (sub)monolayer.

After the monolayer of the alkene – or MMA monomer as in this case – has been formed, grafting can proceed by a normal photografting and photopolymerization process from the monolayer, resulting in a thick, yet slightly branched polymer layer. For styrene, this grafting from a dense monolayer is shown to be not very facile, as aromatic C-H bonds have a high bond dissociation energy (BDE) and thus are hard to graft from. For PMMA, grafting from the monolayer is much more facile due to the somewhat lower BDE of the C-H bonds of the methyl groups. For that reason, grafting of PMMA from a MMA monolayer on Si occurs much faster in the beginning.

4.1.6 Electronic properties

Major reasons for working with H-terminated surfaces as compared to oxidized silicon are the better electronic properties of the latter due to their less electronically perturbed surface. Low recombination rates of electrons and holes at the interface are essential for low-noise electronic devices and high-efficiency solar energy converters. With this recombination rate being dependent on the density of electrical surface "trap" states (defects, dangling bonds), ways are to be found for effective saturation and passivation of a silicon surface. One of the main routes for this is chemical functionalization.[165,166] By etching the native oxide layer of silicon with 50% hydrofluoric acid, the surfaces becomes H-terminated. This hydrogen termination leads to a saturation of surface defects (dangling bonds) and minimizes electronic perturbation of the surface. Thus, lifetime of surface minority charge carriers, as measured by microwave photoconductivity decay, is much higher in freshly HF-etched silicon than it is in oxidized silicon. It has been shown that a grafted organic monolayer on silicon surfaces can conserve electronic properties. It can also make the surface more stable against oxidation than H-terminated surfaces, which are oxidized over time by insertion of atmospheric oxygen into Si-Si bonds. We examined if a polymer layer obtained by direct photografting from H-terminated silicon layers yields in similar well-passivated and stable Si surfaces.

Surface recombination velocity measurements were collected using a contactless microwave photoconductivity apparatus. Electron–hole pairs were photogenerated using a coherent pulsed diode laser. The photoinduced conductivity in the Si sample was monitored using the reflected signal from a radio frequency coil. A simplified schematic of this method can be seen in Figure 26.

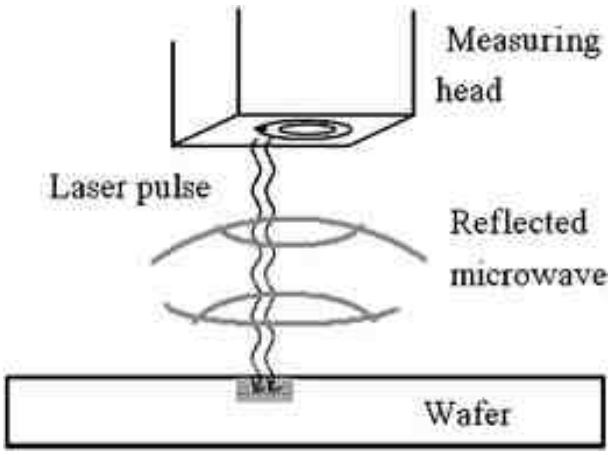

Figure 26: Schematic of the microwave photoconductivity decay measurements to obtain charge-carrier lifetimes[167]

The conductivity (probed by microwave reflectivity which is correlated to minority charge-carrier concentration) decreases as the charge carriers recombine with surface-localized trap states. Charge-carrier lifetimes (τ) are extracted from the absorbed RF signal (128 trace average) by fitting the data to a single-exponential decay:[168]

$$A = y_0 + a\, e^{-t/\tau}$$

with τ being the measured charge-carrier lifetime. The surface recombination velocity, *S,* can be obtained from τ through[169]

$$\frac{1}{\tau} = \frac{1}{\tau_b} + \frac{2S}{d}$$

with τ_b as the bulk lifetime, and *d* as the sample thickness. For all measurements $\tau_b >> \tau$ is valid, so that $S \approx d/2\tau$. Thus, surface recombination velocity can be compared by comparison of the charge carrier lifetimes obtained from microwave photoconductivity decay measurements.

It can clearly be seen that for oxidized silicon, the lifetimes are short in comparison with hydrogen fluoride etched surfaces, due to charge recombination at surface defects. It is also interesting to see that minority charge carrier lifetime for PS-grafted Si is about in the same range or even higher as for freshly etched silicon. This can be caused by an additional hydrophobization of the Si surface, which can hinder the absorption of water that can lower the charge carrier lifetimes by inducing dipols on the surface. The values for poly(allyl amine) grafted for 16 h also show relatively high lifetimes. From these measurements it can also be concluded that a grafted polystyrene polymer layer not only leads to a retention of the

electronic properties but also passivate against oxidation by atmospheric oxygen as measurements of PS grafted surfaces after exposure to air 48 h showed only a small decrease in charge-carrier lifetime (see Table 1).

Table 1: Charge-carrier lifetime values of silicon substrates grafted with polystyrene for 8 h and poly(allyl amine) for 16 h compared to HF-etched and native oxide coated silicon

Sample	Lifetime τ (μs)
Polystyrene grafted for 8 h	19.6
Polystyrene grafted for 8 h after 48 h air exposure	12.3
Poly(allyl amine) grafted for 16 h	10.4
Poly(allyl amine) grafted for 16 h after 48 h air exposure	10.2
HF-etched reference	15.6
Native oxide	6.5

4.1.7 Photoinitiated Grafting of Copolymers

As a next step towards generation of functional polymer architectures, copolymerization reactions of styrene with different monomers were also investigated to obtain a broad range of functional polymer brushes on Si with polymer layer thicknesses beyond only a few nm. As monomers for that approach 2-hydroxyethyl methacrylate (HEMA), 2-dimethylaminoethyl methacrylate (DMAEMA) and 2-isopropenyl-2-oxazoline (*i*POx) were selected, which all possess a double bond suitable for SIPGP and free radical polymerization (see Figure 27).

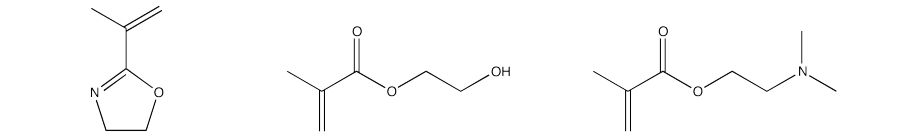

2-isopropenyl-2-oxazoline *i*POx | 2-hydroxyethyl methacrylate HEMA | N,N-dimethylaminoethyl methacrylate DMAEMA

Figure 27: Structural formulas for the monomers used together with styrene in the copolymerization approach, 2-isopropenyl-2-oxazoline (*i*POx), 2-hydroxyethyl methacrylate (HEMA), and dimethylaminoethyl methacrylate (DMAEMA)

As mentioned above, trials to polymerize bulk HEMA on H-Si *via* SIPGP resulted in complete gelation of the bulk monomer within 90 minutes of irradiation and very thin (< 5 nm) grafted layers. Polymerization of bulk DMAEMA on H-Si resulted in thin and inhomogeneous polymer layers. Bulk *i*POx was successfully grafted from H-Si, however, the grafted layer was relatively thin and the grafting rate was very low (25 ± 2 nm after 36 h irradiation).

However, copolymerization of all these monomers with styrene resulted in homogenously grafted polymer brush layers, which is in congruence with similar results from our group obtained for SIPGP copolymerizations on graphene.[170]

For the copolymerization of styrene with HEMA ($r_1 = 0.27$, $r_2 = 0.49$)[171] at a molar ratio of 4:1, all characteristic bands for both monomeric units are present in the IR spectrum (Figure 28), indicating the formation of a copolymer. The contact angle was measured 81.4 ± 0.52 ° (in comparison to 69.7 ± 0.10° for a homo-PHEMA grafted Si surface). The thickness of the grafted polymer layer was determined to be 370 ± 15 nm.

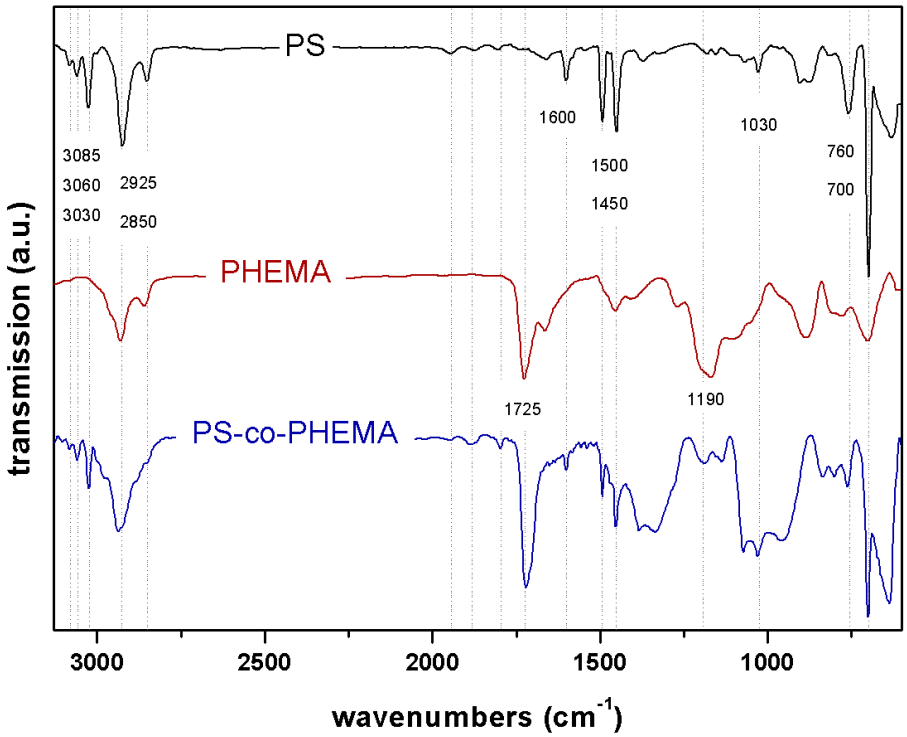

Figure 28: Comparison of IR spectra of polystyrene, poly(hydroxyethylmethacrylate) and poly(styrene-co-hydroxyethylmethacrylate) brushes on silicon

For the copolymerization of styrene with DMAEMA (r_1 = 0.22, r_2 = 0.42)[172] at 4:1 molar ratio, all characteristic bands are present in the IR spectrum, also indicating a copolymer. The contact angle was measured 84.2 ± 0.08° (in comparison to 57.9 ± 0.22° for a homo-PDMAEMA grafted Si surface). The thickness of the grafted polymer layer was determined to be 220 ± 5 nm.

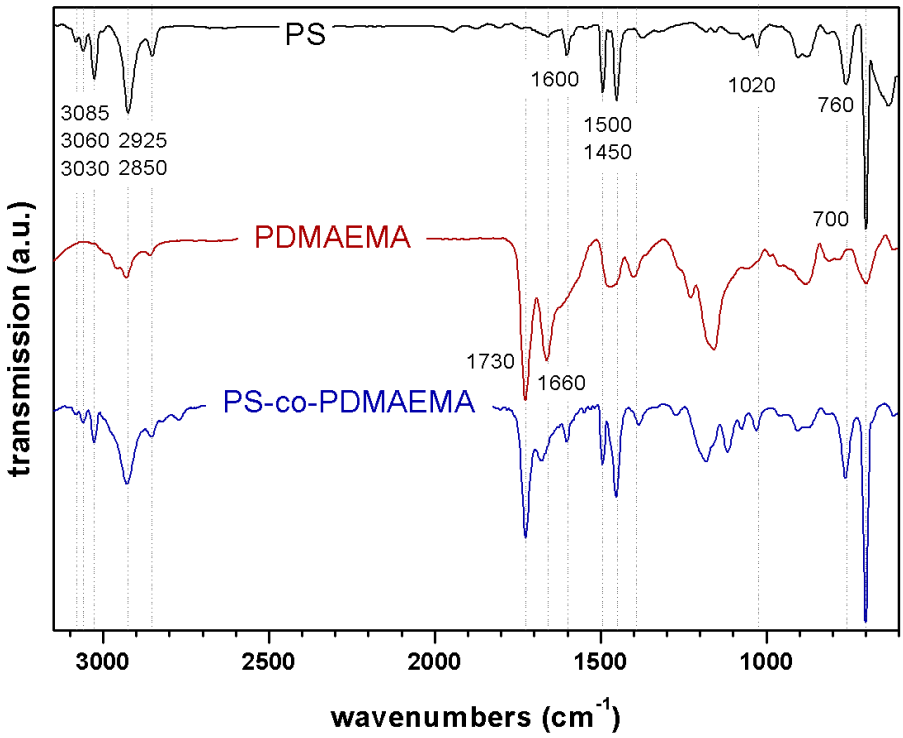

Figure 29: Comparison of IR spectra of polystyrene, poly(DMAEMA) and poly(styrene-co-DMAEMA) brushes on silicon

Copolymerization of styrene with *i*POx (r_1 = 0.67, r_2 = 0.64)[173] was carried out with a 1:1 molar ratio. Layer thicknesses of 20 ± 2 nm after 18 h and 80 ± 8 nm after 66 hours show a faster growth rate than for bulk *i*POx alone.

4.1.8 Bottle-brush brushes on H-Si

One of the major advantages of the direct photografting process is the superior stability of the polymer brushes resulting from the direct Si-C bond established through photografting. This bond is more resistant chemically than siloxane-grafted polymer layers, for example against treatment with hydrofluoric acid.

To prove the retained reactivity of the radically polymerized oxazoline units of PiPOx, a surface initiated cationic ring opening polymerization (SI-CROP) of 2-ethyl-2-oxazoline from each of the P*i*POx covered surfaces was carried out similar to previous reports.[137] A general scheme for this type of SIPGP grafting with subsequent LCROP can be seen in Figure 30.

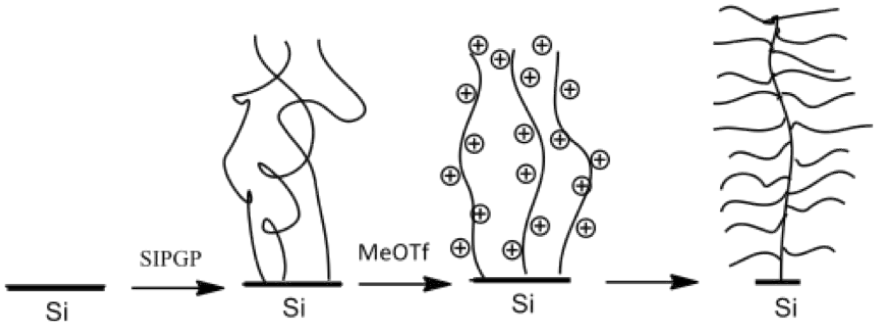

Figure 30: Schematic of the grafting of bottle-brush brushes on silicon by SIPGP of *i*POx and subsequent LCROP of EtOx

Thicknesses of PiPOx and PS-co-PiPOx polymer brush layers before and after LCROP of EtOx are summarized in Table 2.

Table 2: Thicknesses of grafted PiPOx- and PS-co-PiPOx polymer brush layers before and after grafting of EtOx, determined by AFM

Monomers	UV grafting [h]	Thickness [nm]	Thickness after EtOx grafting [nm]
IPOx	36	25	60
IPOx/Sty 1:1	18	20	50
IPOx/Sty 1:1	66	80	400

Results show that for the same time of LCROP of EtOx, layer ticknesses increase around 2.5 to 5-fold due to the formation of cylindrical brushes. These results indicate a high flexibility of the initial polymer layer on the surface and good accessibility of the initiator species methyl triflate during the initiation step of the polymerization. Presence of grafted poly(2-ethyl-2-oxazoline) is confirmed by IR spectroscopy (see Figure 31).

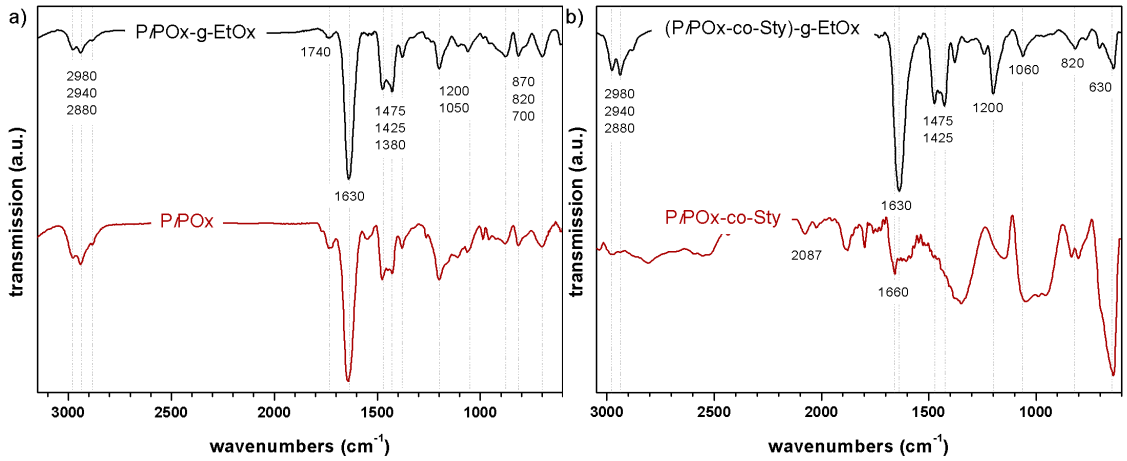

Figure 31: IR spectra of PS-co-P*i*POx brushes before and after LCROP of EtOx and IR spectrum of a Si substrate grafted with P*i*POx-g-EtOx bottle-brush brush

4.1.9 Structured Polymer Brushes

As a further aim of this work, we conducted experiments on the direct photolithographic patterning of H-Si surfaces. By this method, silicon surfaces can be functionalized with patterned polymer brushes in a convenient one-step procedure. A further advantage over the use of a photoresist is the higher cleanness, since photoresist residues may remain on the sample surface and would then act as initiation spots for polymerization and thereby compromise pattern quality. The procedure used herein was carried out as follows:

A silicon substrate was etched with a 50% hydrofluoric acid mixture for 2 min and then cleaned by ultrasonication and rinsing with millipore water. A TEM grid was then placed on the surface, further covered with a thin steel plate with a hole secured with a clamp (see Figure 32).

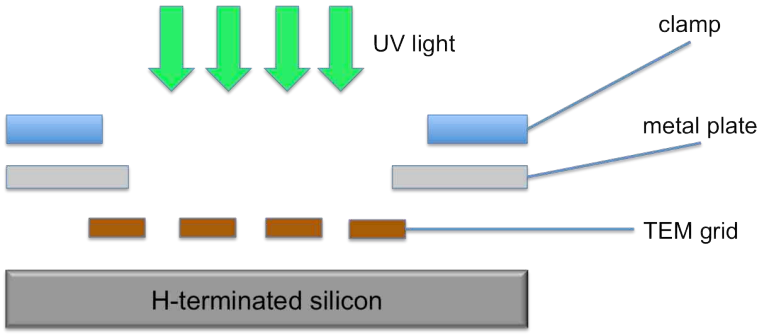

Figure 32: Experimental setup used for the photopatterning experiments

The sample was immersed in bulk liquid monomer solution and irradiated by UV light. After the reaction, the sample was taken out, the setup disassembled and the surface was cleaned via the standard procedure. The samples were investigated by optical microscopy, IR spectroscopy, and SEM.

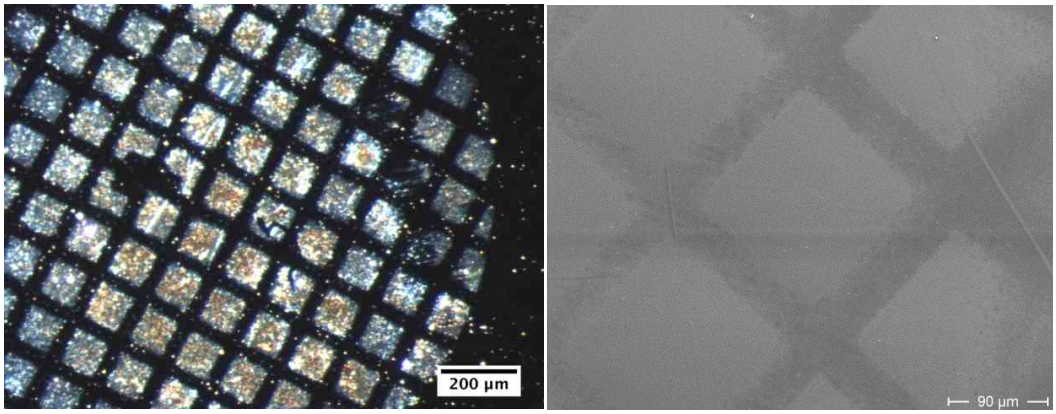

Figure 33: Optical microscope (a) and SEM image (b) of structured PS brushes on H-Si (18 h irradiation)

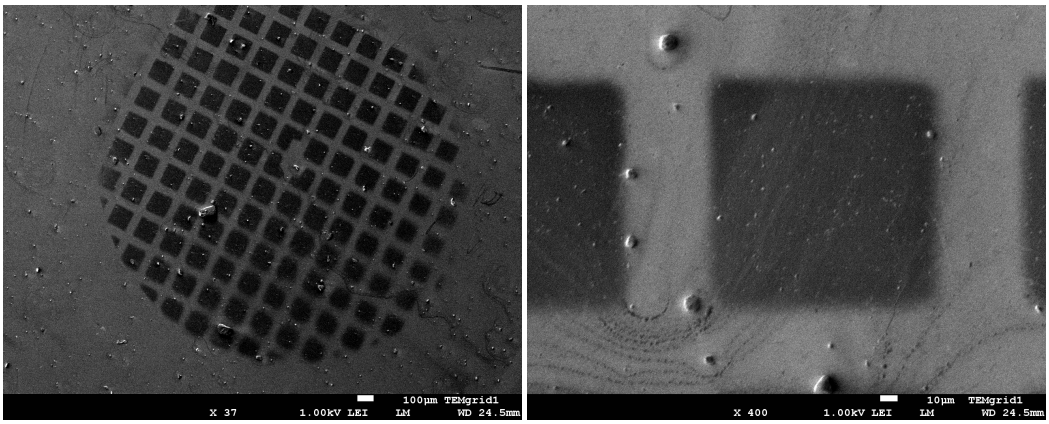

Figure 34: SEM images of structured PS-co-PHEMA brushes on H-Si (18 h irradiation)

From Figure 33 and Figure 34, the good quality of the patterns can be seen. IR spectra confirmed the presence of grafted polymer on the Si surface. Ellipsometry measurements gave a thickness of grafted polymer brush layer of over 300 nm for PS-patterned and even over 400 nm for PS-co-PHEMA-patterned Si surfaces.

4.1.10 Structured Binary Brushes

Building upon the results of these first photolithographic experiments, the possibility to obtain patterned binary polymer brushes was investigated. The simple procedure targeted in a first

set of experiments involved direct photolithography on H-terminated Si, subsequent oxidation of the remaining unfunctionalized areas with successive SI-ATRP on the oxidized silicon. A schematic of this process is outlined in Figure 35.

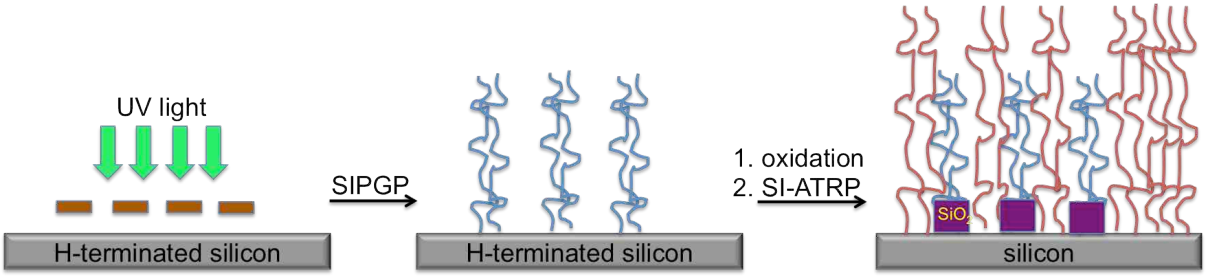

Figure 35: Schematic of the synthesis of structured binary brushes by direct photolithography

A similar approach for creating binary polymer brushes has already been reported in literature by Xu *et al.*, employing a combination of ATRP and radical addition fragmentation transfer (RAFT) polymerization.[174] However, in that process an additional step for the immobilization of the initiator monolayer is required.

Unfortunately, in this work, trials for the generation patterned binary polymer brushes by direct photolithography and successive SI-ATRP from reoxidized surfaces did not to turn out to be successful. This was maybe caused by the way the surfaces were oxidized. In our process, Si-H surfaces were left to oxidize in ambient air at room temperature. This route might not have been sufficient to introduce silanol groups on the surface necessary for the immobilization of APTES.

Hence, a different and slighty more complex method was employed (see **Figure 36**).

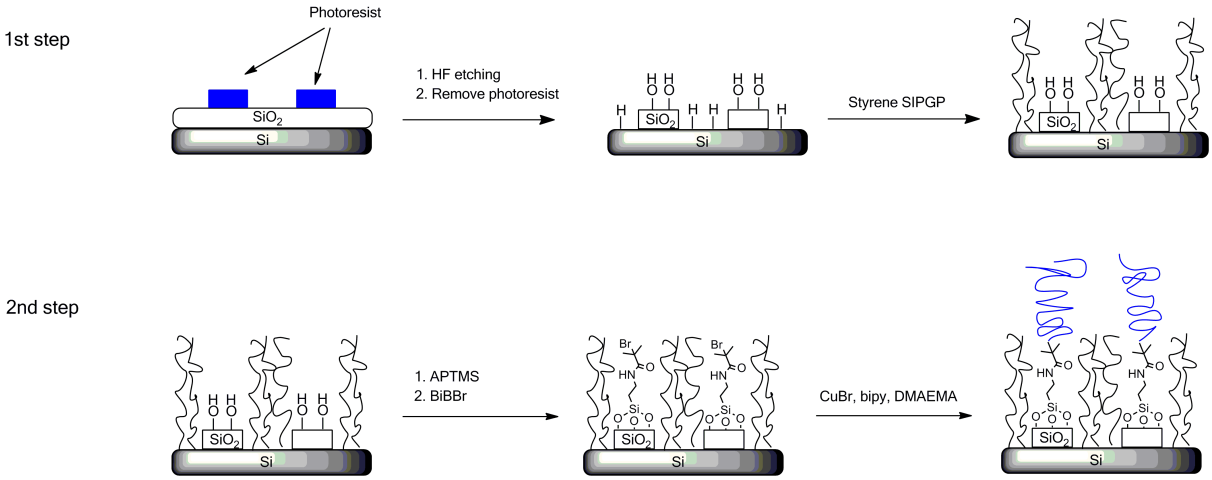

Figure 36: Schematic of the process used for the synthesis of structured binary brushes of PS and PDMAEMA

In order to obtain patterned polymer brushes, a silicon substrate was coated with structured photoresist on its native oxide layer. A SEM image of a single structure feature ("F") can be seen in Figure 37. The substrate was then etched with aqueous HF (50%), leading to an H-terminated surface in the areas not protected by the photoresist. The areas covered with photoresist during HF etching were expected to retain the native silicon oxide layer.

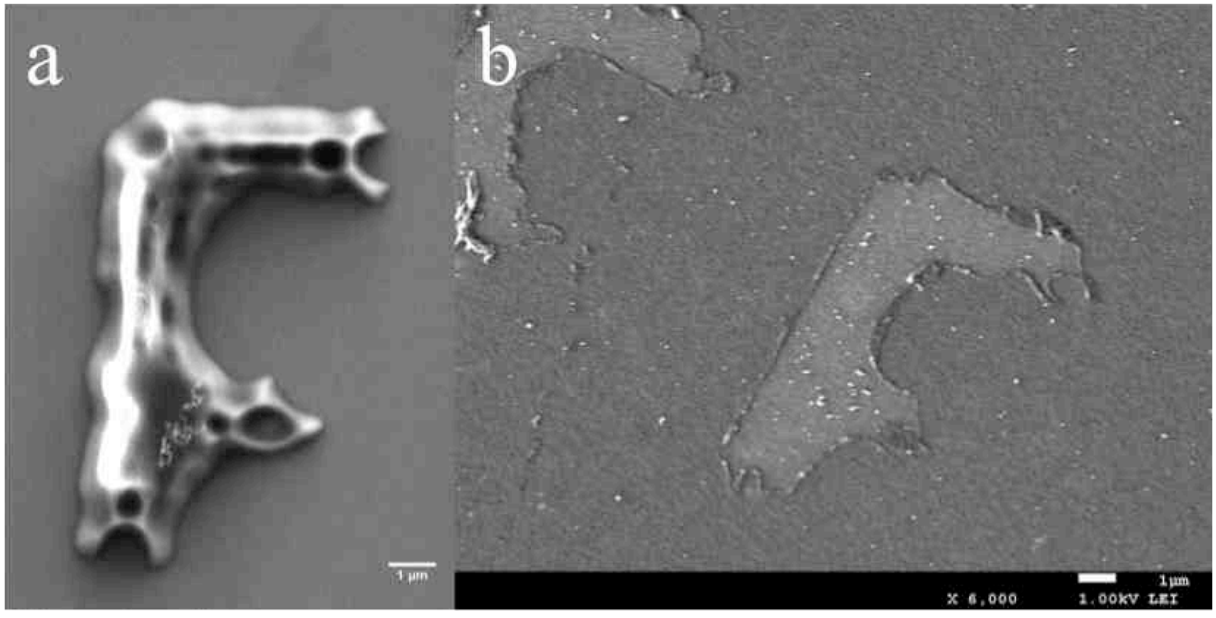

Figure 37: SEM images of the original photoresist structure (left) and the same substrate after etching, removal of photoresist, and UV-induced grafting with PS (right)

In the second step of the structuring process, the partly etched Si substrate was photografted with styrene for five hours to obtain structured polystyrene brushes of approx. 50 nm in

thickness. The presence of these structured polymer brushes serves also as a direct proof that no polymer is formed on the native oxide layer on silicon, which can be seen in Figure 37.

As the third step, the remaining silicon oxide layer is functionalized with 3-aminopropyltrimethoxysilane through condensation of the siloxane groups with the oxide layer on silicon. Afterwards, the amino groups of the APTMS layer on silicon oxide are reacted with α-bromoisobutyryl bromide to form an initiator species for SI-ATRP. The surface was then immersed into a degassed solution of DMAEMA in water, and Cu(I)Cl salt and bypyridine were added subsequently to start the polymerization.

After 18 h of polymerization at room temperature, the surface was cleaned and analyzed with DRIFT IR spectroscopy, AFM, and SEM. Figure 38 shows an optical microscope as well as AFM image of the resulting surface. The structure features have a height of approx. 350 nm (see Figure 38d), and structural resolution is retained. Figure 39 shows an SEM image of these features.

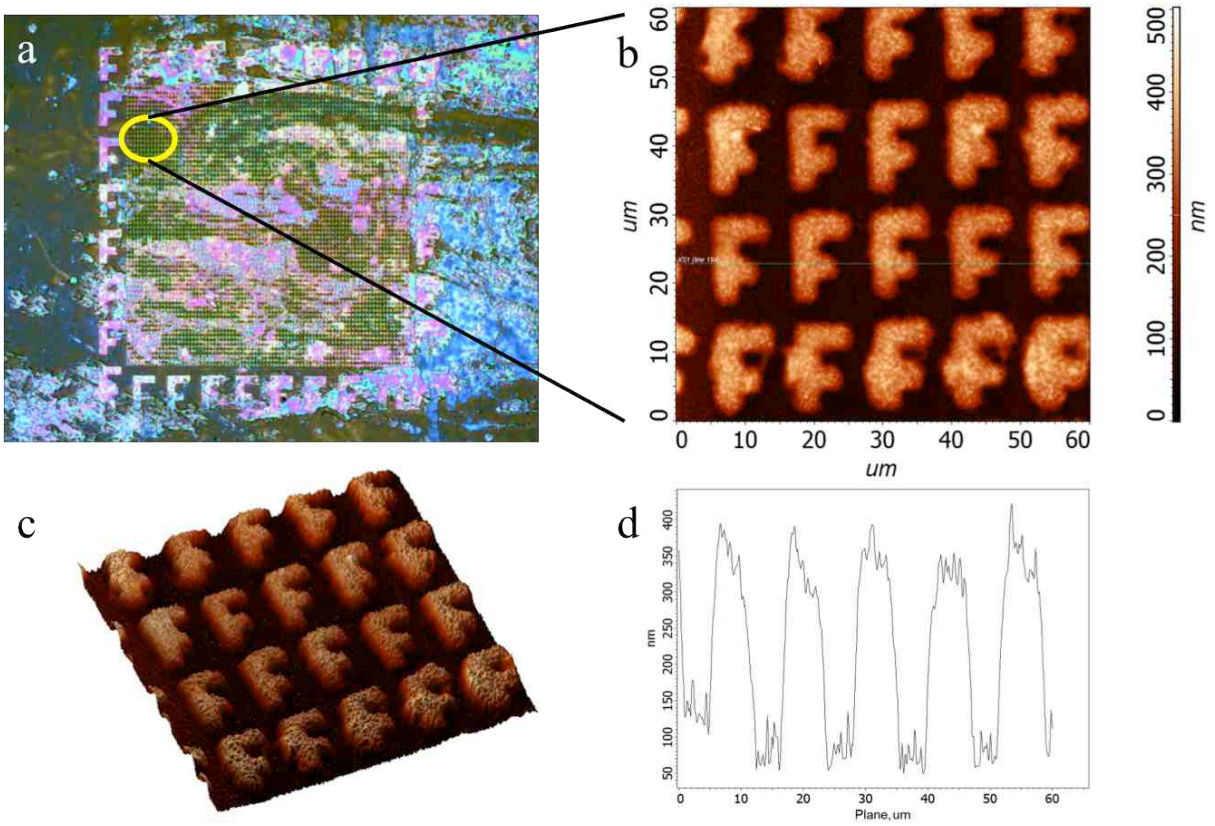

Figure 38: Optical microscope (a) and AFM image (b) with cross section (d) of the substrate with patterned polymer brushes of PDMAEMA ("F" structures) and PS (surrounding). Subfigure (c) shows a 3D representation of the AFM measurement (not to scale)

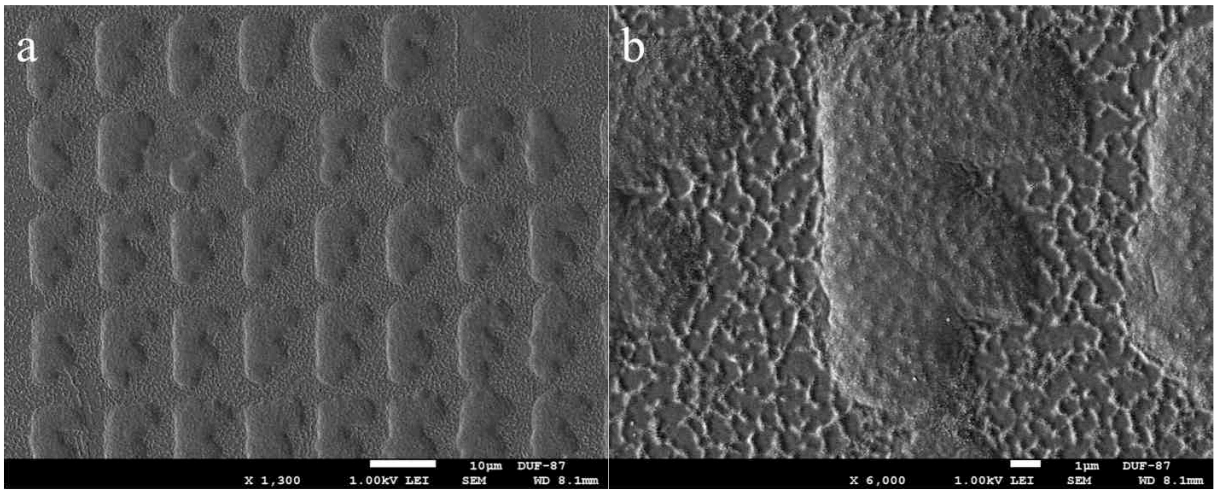

Figure 39: SEM image (a) and close-up (b) of the final structured binary brushes of PDMAEMA ("F" structure) and PS (surrounding)

From this SEM images (Figure 39) the polystyrene layer between the structure features can be seen. To proof the presence of polystyrene as well as PDMAEMA in the corresponding areas, local energy dispersive x-ray (EDX) measurements have been conducted on the respective areas of the substrate, which are shown in Figure 40.

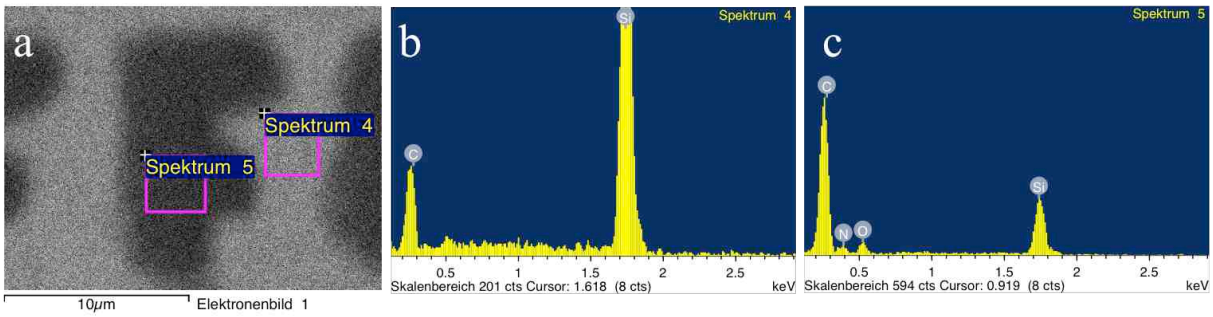

Figure 40: SEM image of binary brush grafted surface (a) and EDX spectra of PS-grafted surface (b) and the PDMAEMA structure features (c)

From the EDX spectrum in Figure 40b, the presence of polystyrene on the surface can be concluded due to the carbon peak. The high intensity of the silicon-related peak comes from the silicon background due to the high penetration depth of the electron beam into the sample. Similarly, the presence of grafted PDMAEMA in the “F” structure can be concluded from the EDX spectrum in Figure 40c. The peaks for carbon, oxygen and nitrogen correspond to PDMAEMA on the surface and the lower intensity of the silicon peak is in accordance with the higher thickness of these features. The fact that polystyrene is still present in the surrounding of the “F” features also indicates a high stability of the grafted brushes.

4.2 Sequential Photografting

4.2.1 Background

To improve the performance of the photografting method on silicon, an alternative route was investigated that could enable grafting of acrylates and methacrylates as well as accelerate grafting rates of styrene grafting. The method that was envisioned herefore was the sequential grafting approach reported by Ma *et al.*[131] Therefore, a conventional photoinitiator compound, benzophenone (BP) or isopropyl thioxanthone (ITX) (see Figure 41), was immobilized on the silicon surface in a first step *via* UV irradiation.

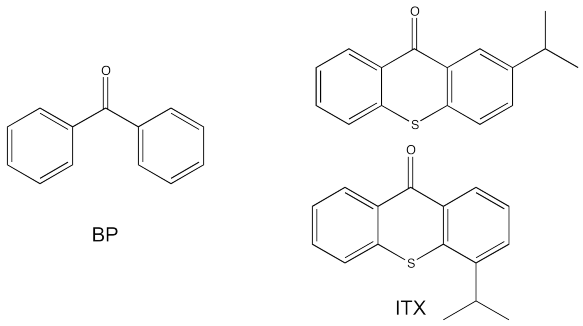

Figure 41: Chemical formula of benzophenone (BP) and of isomers of 2- and 4-isopropyl thioxanthone (ITX)

As postulated by Ma and coworkers, this immobilized photoinitiator layer acts as an initiator in the second step, where the functionalized surface is irradiated with UV light in presence of a monomer. The photoinitiator is expected to detach upon UV irradiation under formation of a surface silyl radical, which then initiate a free radical polymerization. An examplary reaction scheme of the process with benzophenone as initiator is depicted in Figure 42.

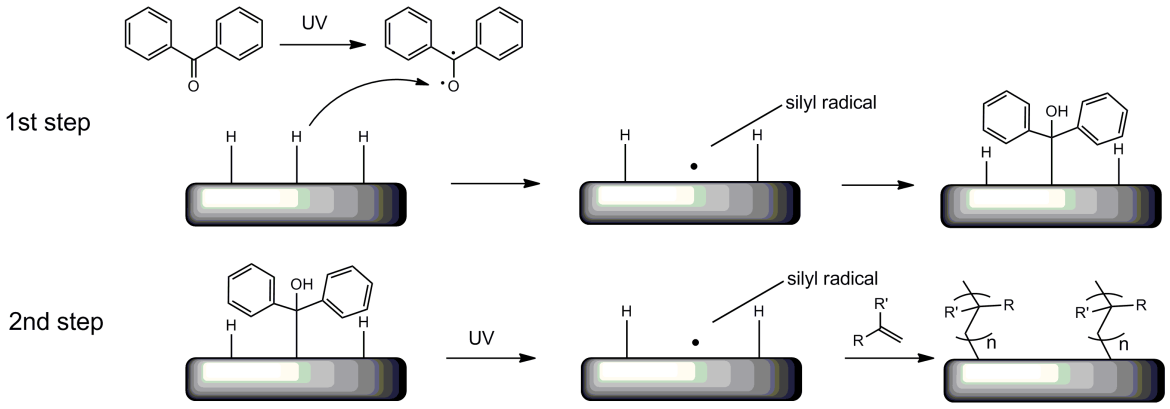

Figure 42: Schematic of the sequential photografting process on hydrogen-terminated silicon with benzophenone as photoinitator

4.2.2 Proof of Principle

First experiments showed that a sequentially performed process improves grafting efficiency over the one-pot process, since a one-pot synthesis with 6.7 wt% BP in MMA resulted in a polymer layer of only 3 nm after 2 h of irradiation at 350 nm wavelength.

Therefore, the two-step procedure according to Ma *et al.* was employed. In the first step, H-Si substrates were irradiated in a solution of 6.7 wt% BP in cyclohexane for different durations. After irradiation for a certain amount of time, substrates were removed from the reaction vial, washed three times with 1 ml toluene each, and sonicated for 5 min in 2 ml toluene. Subsequently, the substrates were rinsed with ethanol and blow-dried under an air-stream.

Thereafter, substrates were immersed in 1 ml of monomer, degassed with three freeze-pump-thaw cycles and irradiated for the desired amount of time. Workup was carried out as described previously.

Table 3 gives an overview over miscellaneous monomers grafted with the sequential photografting method for different durations.

Table 3: Grafting results of different monomers by sequential photografting with BP (6.7 wt% in cyclohexane)

Monomer	Irradiation time Benzophenone [h]	Irradiation time monomer [h]	Thickness [nm]
One-step MMA	-	2	3
MMA	6	5	216
GMA	5	1	77
HEMA	5	1	574
HEMA	1	0.75	90
tBMA	5	3	82
styrene	5	18	99
styrene	3	8	345
vinyl acetate	3	42	82
N-vinyl carbazole	3	18	6
DMAEMA	3	2	36
allyl mercaptan	3	18	7

From the results in Table 3 it can be seen that with this method even thick layers of poly(meth)acrylates can be directly grafted on H-terminated Si if in a first step BP is immobilized on the surface.

To gain a better understanding of the processes involved, analysis of the surface-grafted initiator layer as well as the resulting polymer layer was conducted and kinetics were investigated of both BP and ITX-induced grafting of styrene. For these experiments, a 5 wt% solution of BP in benzene was used. Benzene was chosen because of its low reactivity in grafting reactions due to the high BDE of aromatic C-H bonds.[175] The concentration of ITX was chosen equimolar to BP, corresponding to a 7 wt% solution of ITX in benzene. Figure 43 shows an ATR IR spectrum of a H-Si surface irradiated for 3 h in a 5 wt% solution of BP in benzene.

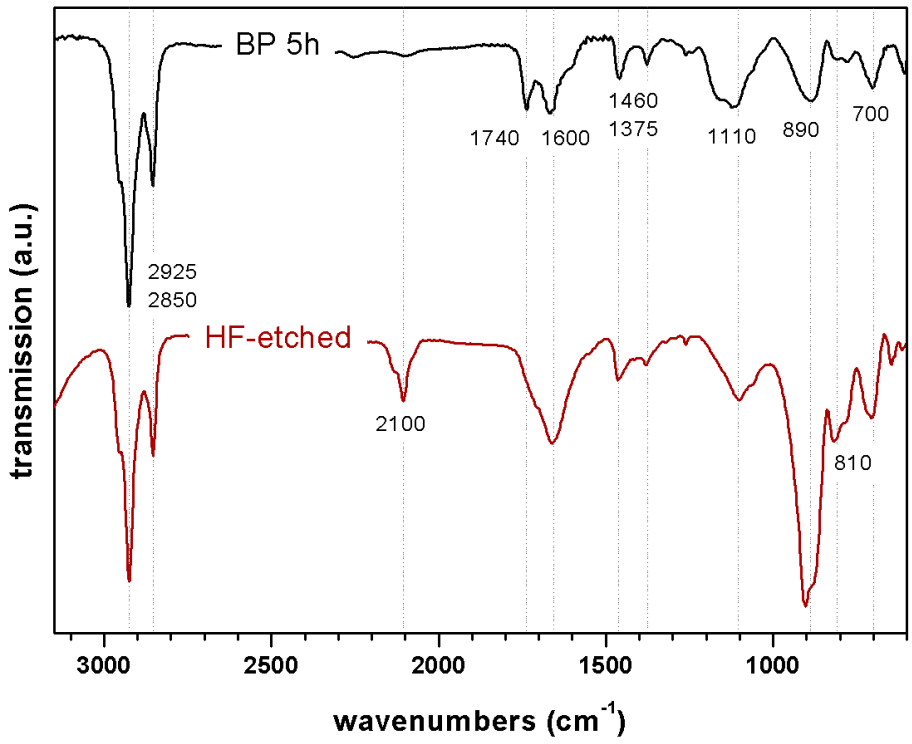

Figure 43: ATR IR spectrum of H-Si irradiated for 3 h in 5 wt% BP solution in benzene

The IR spectrum presented in Figure 43 shows characteristic bands of surface-bonded BP. Small shoulders at 3050 cm^{-1} indicate aromatic C-H stretching bands, and bands at 1660 and 1600 cm^{-1} confirm the presence of aromatic C=C bands. Bands at ~ 1100 cm^{-1} indicate presence of either Si-O- or C-O- stretching bands. This arises from the possibility that BP can also bind through Si-O- bonds to the silicon surface due to the high oxygen affinity of silicon (shown in Figure 44).

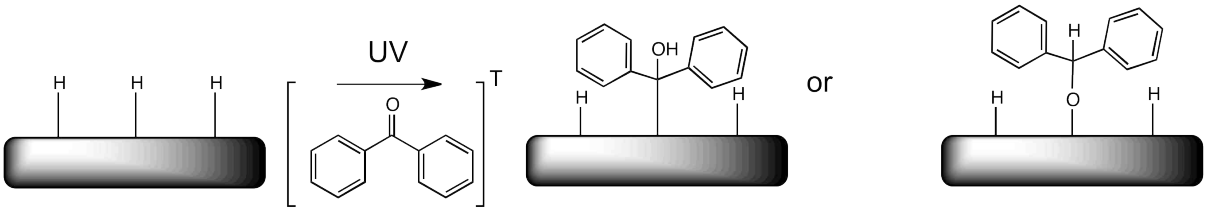

Figure 44: UV activation of BP leading to two different bonding morphologies on H-Si

Both ways of bonding, however, can facilitate polymer grafting. This can be explained via two different mechanisms. One is degrafting of the BP (or ITX) moiety under UV irradiation and another one is grafting from the photoiniator monolayer. The second pathway seems also realistic, since grafted photoinitiator BP and ITX possess either hydroxyl groups or benzylic protons stabilized by two phenyl rings. Both of these groups are easily to be grafted from, due to the low bond dissociation enthalpy of those X-H groups.[175]

In any case, polymer brushes of styrene could be effectively grafted with this method. An ATR IR spectrum of a H-Si substrate irradiated for 5 h with BP and subsequently for 6 h with styrene is shown in Figure 45.

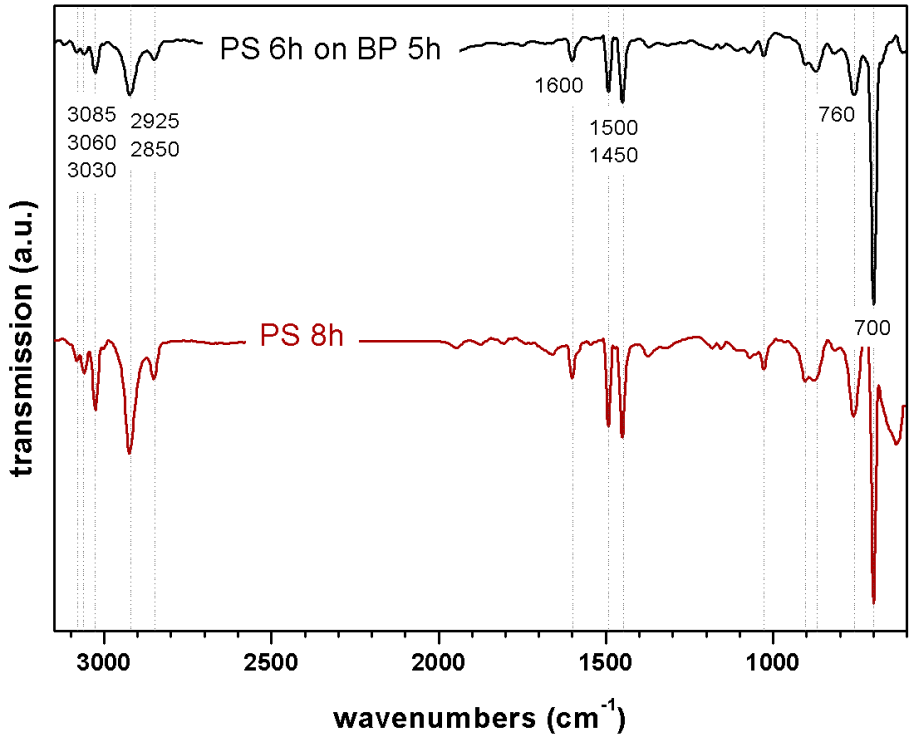

Figure 45: ATR IR spectrum of H-Si pregrafted 5 h with BP irradiated for 6 h in styrene

Figure 45 clearly indicates the feasibility of this concept, independent from the mechanism involved in grafting.

To gain a better understanding about the influence of different parameters on the grafting process, *ex situ* kinetics measurements were conducted both with BP and ITX to correlate grafted polymer layer thickness with irradiation time – both of photoinitiator and monomer.

In a first series, grafting of styrene over irradiation time was investigated in correlation with BP grafting time, and in a second series, the same set of experiments was carried out with an equimolar amount of ITX.

4.2.3 Sequential grafting kinetics of styrene with BP

For a better overview of the data in this section, Figure 46 gives a summary of the grafted polystyrene layer thicknesses achieved with the sequential benzophenone photografting method, which will be discussed in more detail on the following pages.

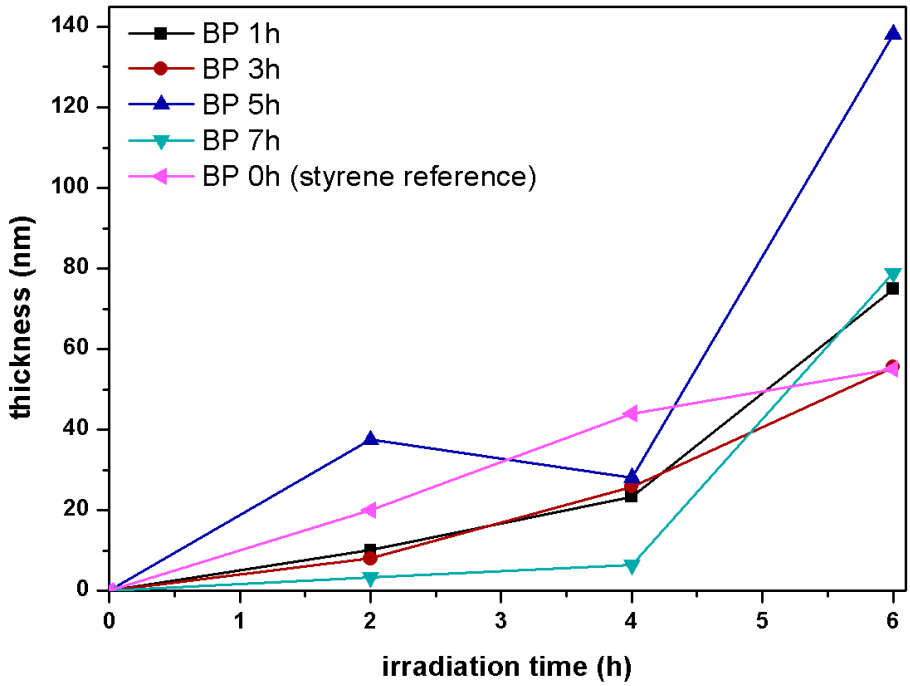

Figure 46: Correlation of grafted layer thickness with irradiation time in styrene (determined by ellipsometry) of H-Si substrates pregrafted with BP for different durations in comparison with non-pregrafted H-Si

1 h and 3 h BP immobilization

For samples irradiated in 5 wt% solution of BP in benzene, contact angles were in the range of 60 ± 10° for 1 h BP irradiation and ~ 55 ± 3° for 3 h BP irradiation compared to ~ 80° in case of H-terminated Si(100). This shows a clear tendency towards a more hydrophilic surface, potentially arising from surface-immobilized BP. The presence of bands being attributed to BP can be found in IR spectroscopy. BP-grafted substrates were then immersed

in styrene, degassed via three freeze-pump-thaw cycles and irradiated for 2, 4 and 6 hours respectively. Figure 47a shows the correlation of grafted polymer layer thickness with irradiation in styrene for a H-Si substrate irradiated with BP for 1 h and 3 h.

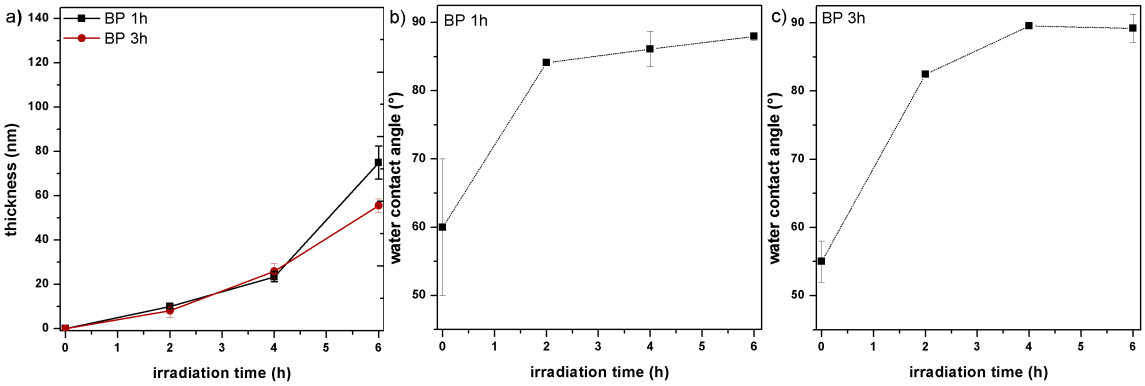

Figure 47: Layer thickness over irradiation time in styrene for H-Si grafted with BP for 1 h and 3 h (a) and correlation of water contact angle with irradiation time of silicon grafted with BP for 1 h (b) and 3 h (c) (error bars represent standard deviation)

From Figure 47a it can be seen that for 2 h and 4 h irradiation time in styrene, layer thickness is in both cases lower than for styrene alone, and for 6 h irradiation it is slightly higher for 1 h BP irradiation and approximately the same for 3 h BP irradiation.

Water contact angle measurements shown in Figure 47b and c reveal that even after short grafting time in styrene contact angles are close to the value expected for polystyrene and thus showing that the grafting process effectively leads to PS-grafted silicon surfaces via this route.

5 h BP immobilization

With 5 h BP irradiation, grafting results were better than for 1 h and 3 h irradiation. Figure 48 shows the correlation of layer thickness with irradiation time for 5 h BP irradiated substrates.

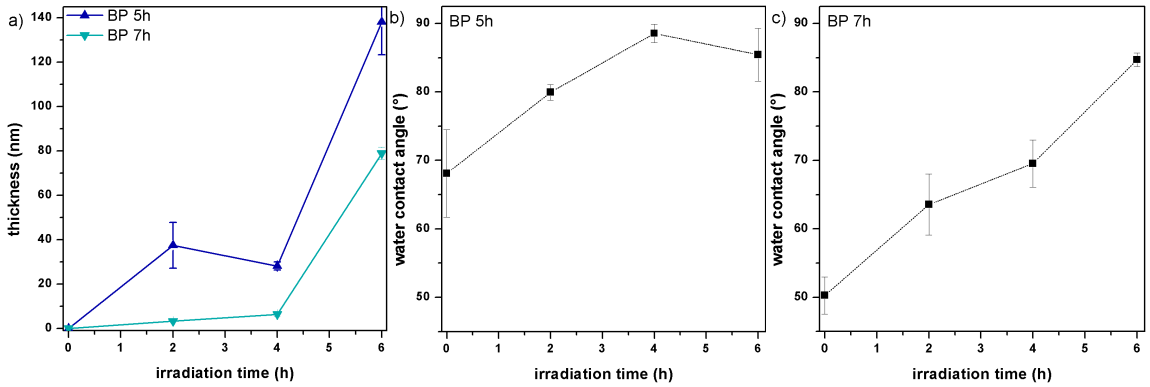

Figure 48: Layer thickness over irradiation time in styrene for H-Si grafted with BP for 5 h and 7 h (a) and correlation of water contact angle with irradiation time of silicon grafted with BP for 5 h (b) and 7 h (c) (error bars represent standard deviation)

From Figure 48a it can be seen that already after 2 h styrene grafting, layer thickness is already at 40 ± 10 nm. After 6 h irradiation with styrene, the thickness is around 140 nm, exceeding the value of styrene grafted alone more than twofold. These results clearly show the advantage of this sequential photografting method over the conventional one-step approach with respect to grafting rates.

Figure 48b shows that water contact angles for those samples are also around 90°, the value expected for PS-grafted surfaces.

7 h BP immobilization

For the irradiation in styrene of substrates pregrafted with BP for 7 h, the results were different to the aforementioned ones with respect to grafting rate.

As Figure 48a shows, grafted layer thickness of styrene in 7 h BP irradiated surfaces were much lower than for the preceding experiments. Especially for 2 h and 4 h styrene grafting, layer thicknesses were much lower than in previous experiments.

What can be seen from Figure 48c is that the water contact angle of the PS-grafted surfaces increases only slowly from the initial value. The low contact angle in the range for that of native oxide also gives indication for a high degree of surface oxidation. This oxidation can take place by degrafting immobilized initiator during the first step when the irradiation time is chosen too long. Especially since for these type of photoinitiator the wavelength for immobilization and detachment are the same, irradiation time in the first step has to be chosen carefully to maximize the amount of grafted initiator and avoid early degrafting.

4.2.4 Sequential grafting kinetics of styrene with isopropyl thioxanthone (ITX)

To obtain more information about grafting with a surface-immobilized photoinitiator, sequential photografting was also investigated with ITX. This molecule possesses the possibility to detach also under irradiation with visible light at 532 nm wavelength, which makes it interesting for biological applications.[176] It is also commonly used as a photoiniator for printing. A schematic for the sequential photografting process using ITX can be seen in Figure 49.

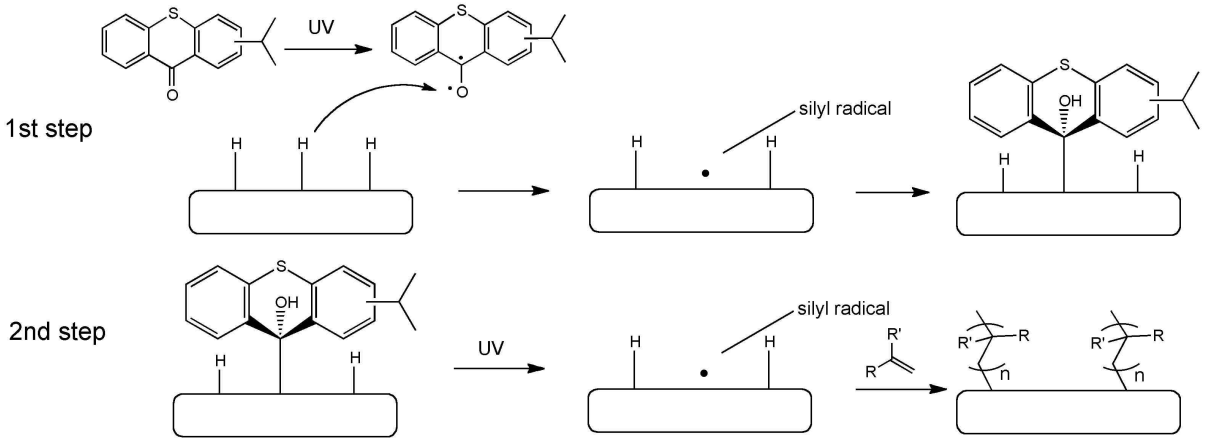

Figure 49: Schematic of the sequential photografting process on hydrogen-terminated silicon with ITX as photoinitator

For the sequential photografting experiments with ITX, all parameters were investigated analogous to BP grafting. Therefore, a concentration of 7 wt% ITX in benzene, equimolar to 5 wt% BP in benzene was used. All other parameters were kept constant.

Figure 50 shows an ATR IR spectrum of a H-Si surface irradiated with 7 wt% ITX in benzene at 350 nm for 5 h.

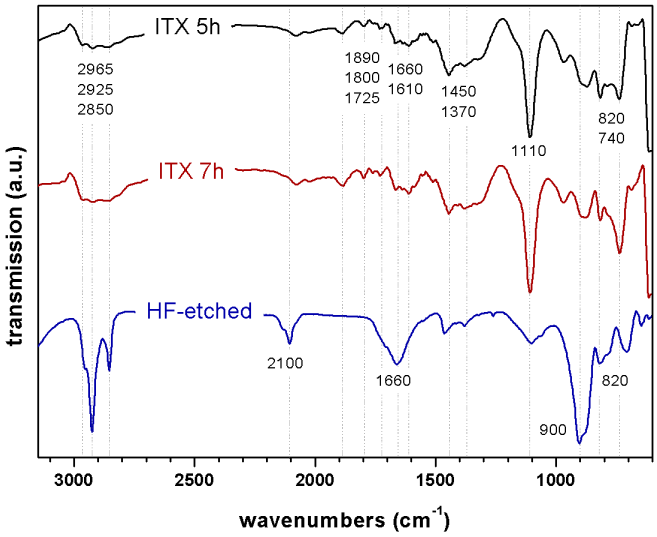

Figure 50: ATR IR spectrum of H-Si irradiated in 7 wt% ITX solution in benzene

It can be seen (Figure 50) that IR absorption bands corresponding to ITX are present. Aliphatic as well as aromatic C-H stretching vibrations can be detected on the surface and stretching bands attributed to aromatic C-C stretching can be seen at 1660 to 1600 cm^{-1}. As the most prominent band in this spectrum, the band at 1100 cm^{-1} can be seen. Similarly to BP-grafted surfaces, this could either arise from a Si-O or a C-O bond.

An ATR IR spectrum of PS grafted successfully with ITX can be seen in Figure 51.

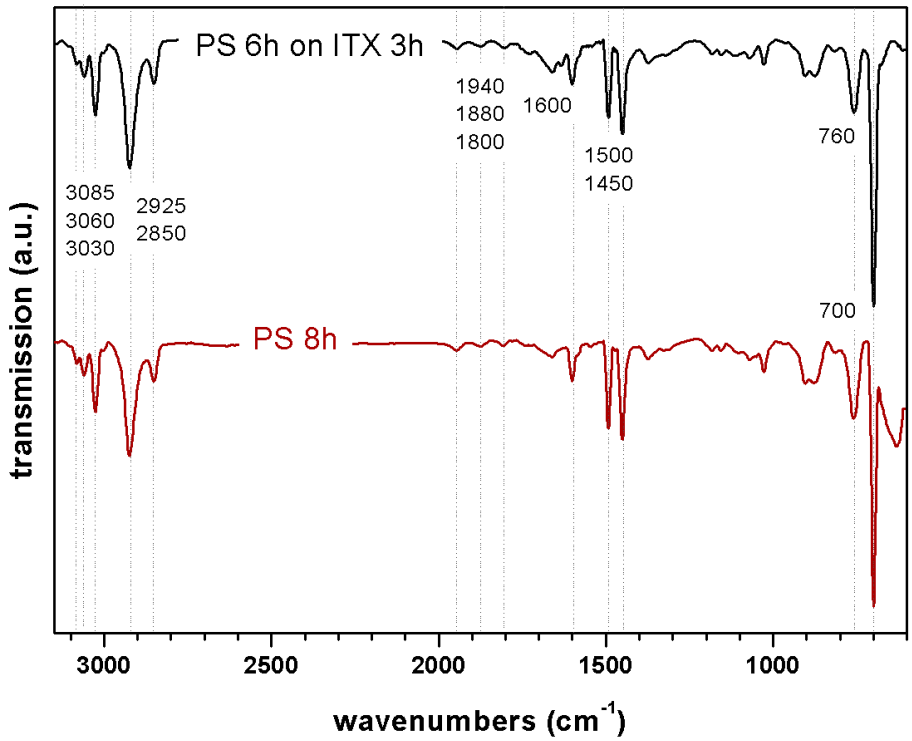

Figure 51: ATR IR spectrum of H-Si pregrafted 3 h with ITX irradiated for 6 h in styrene

The high degree of accordance of the bands for the ITX-pregrafted substrate with a non-pregrafted reference spectrum clearly proves the feasibility of this grafting route also for ITX.

Since a more thorough presentation and discussion of correlations of layer thickness and water contact angle with styrene irradiation time for samples pregrafted with photoinitiator for different durations was already conducted for BP grafting, results for ITX will be presented in a more condensed form and directly put into comparison with those of BP. Figure 52 gives an overview over the graft layer thicknesses achieved with the ITX photografting method.

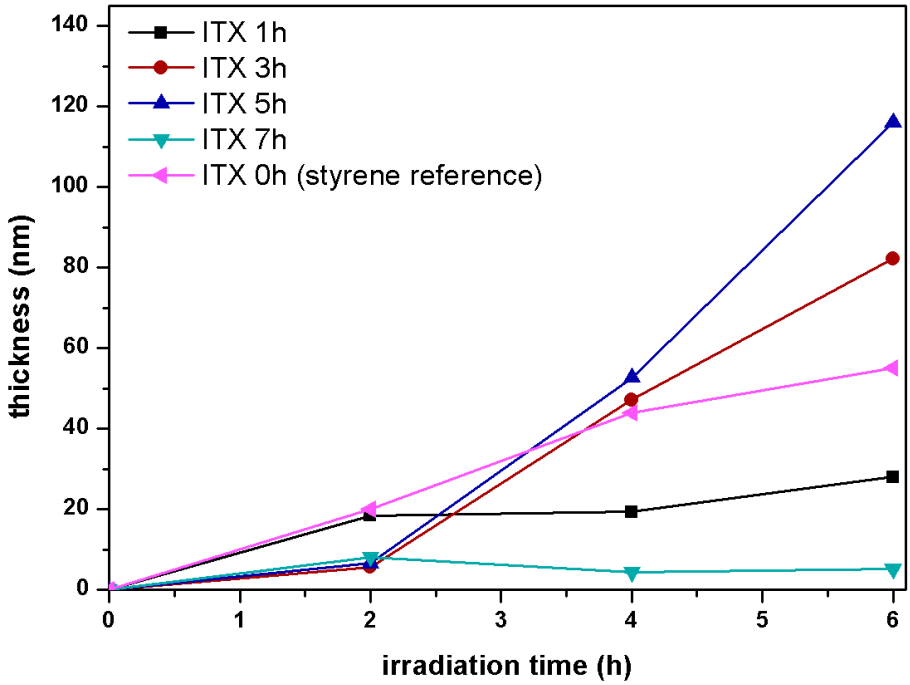

Figure 52: Correlation of grafted layer thickness with irradiation time in styrene (determined by ellipsometry) of H-Si substrates pregrafted with ITX for different durations in comparison with non-pregrafted H-Si

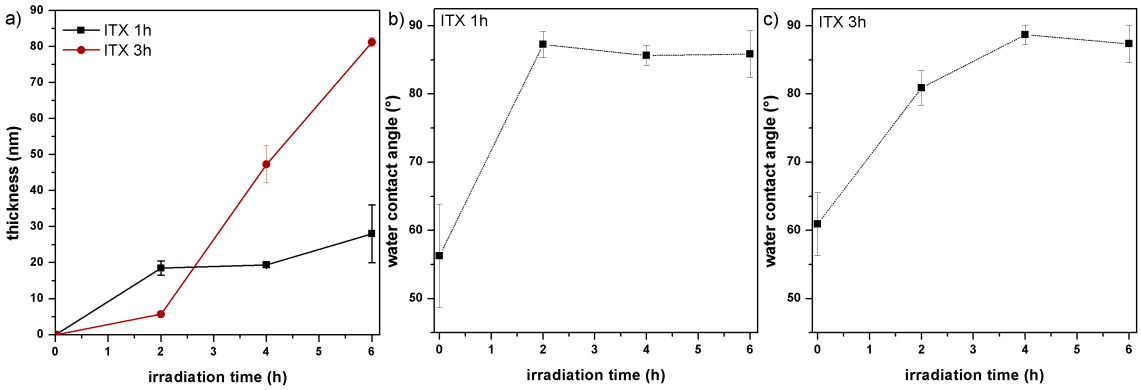

Figure 53: Layer thickness over irradiation time in styrene for H-Si grafted with ITX for 1 h and 3 h (a) and correlation of water contact angle with irradiation time of silicon grafted with ITX for 1 h (b) and 3 h (c) (error bars represent standard deviation)

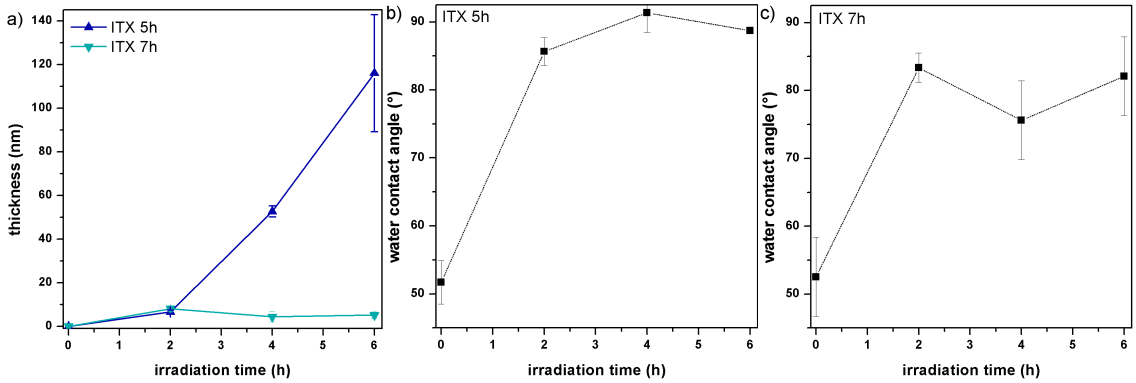

Figure 54: Layer thickness over irradiation time in styrene for H-Si grafted with ITX for 5 h and 7 h (a) and correlation of water contact angle with irradiation time of silicon grafted with ITX for 5 h (b) and 7 h (c) (error bars represent standard deviation)

It can be seen that the general trends visible from these experiments are similar to those of BP grafting. For 1 h and 3 h immobilization of ITX, layer thickness increases monotonously with irradiation time in styrene (see Figure 53a) and also the water contact angles (Figure 53bc) show no distinct difference to the behavior of the BP-pregrafted substrates. Thicknesses of grafted PS layers also show a maximum for 5 h pregrafting duration of ITX and for 7 h immobilization, thicknesses are very low. Water contact angles show a fast increase from the initial values (50 ~ 60° in all cases) to around 90° for polystyrene-grafted surfaces.

A comparison of the thicknesses of BP grafting with those of ITX is shown in Figure 55.

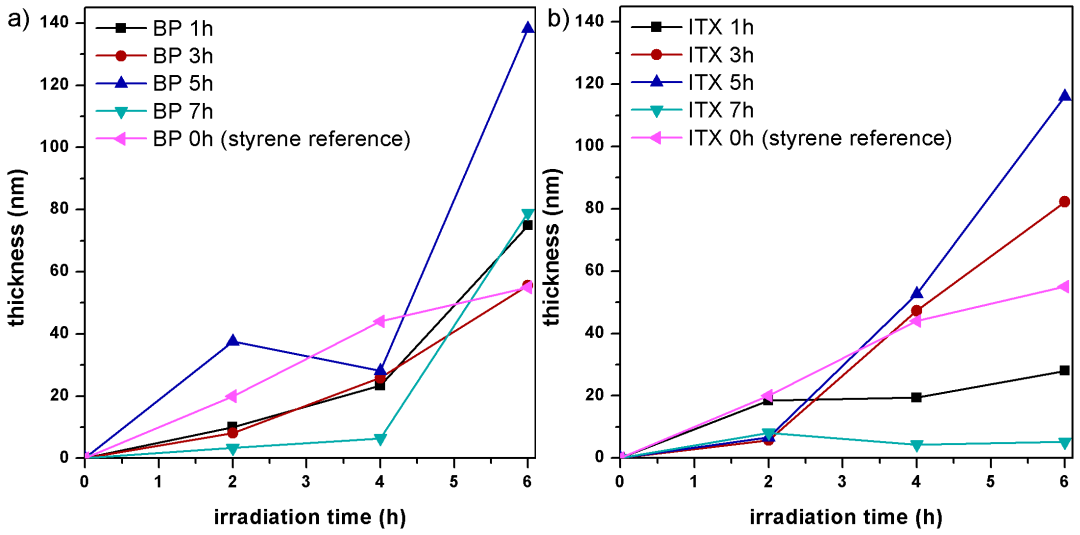

Figure 55: Correlation of layer thickness with irradiation time for different pregrafting durations of (a) BP and (b) ITX

From this comparison it is obvious that certain trends are present in both systems. One trend is the relatively slow increase of layer thickness in the beginning of the polymerization, possibly resulting from a multilayer that is detaching and thereby degrafting polymer chains grafted onto it. 5 h of irradiation in photoinitiator solution show best results with respect to layer thickness in both cases. This could be attributed to an equilibrium of maximum coverage of the surface with the photoinitiator and multilayer formation which might decrease grafting thickness.

4.2.5 Sequential Photografting from Thermally Hydrosilylated BP layers

To see the extent to which multilayer formation plays a role in polymer chain degrafting, only a single layer of photoinitiator molecules on the H-Si surface should be investigated. This was achieved by thermal hydrosilylation of the photoinitiator. It is known in literature, that unsaturated C=O bonds for example in phenylmethyl ketone or benzophenone add to Si-H surfaces in a surface hydrosilylation chain reaction.[177] This method was therefore used as a mild method to obtain a (sub)monolayer of BP on the Si substrate. It has to be mentioned, however, that in this case bonding almost exclusively takes place via Si-O bonds, thus possibly altering the degrafting process. Nevertheless, it was expected to deliver important information about the grafting and degrafting process.

To yield thermally BP-grafted substrates, H-terminated silicon was reacted for 24 h at 60°C in a 5 wt% BP solution in benzene.

Figure 56 shows ATR IR spectra of an H-Si surface thermally hydrosilylated with BP for 24 h (a) and the same surface after irradiation for 6 h in styrene (b).

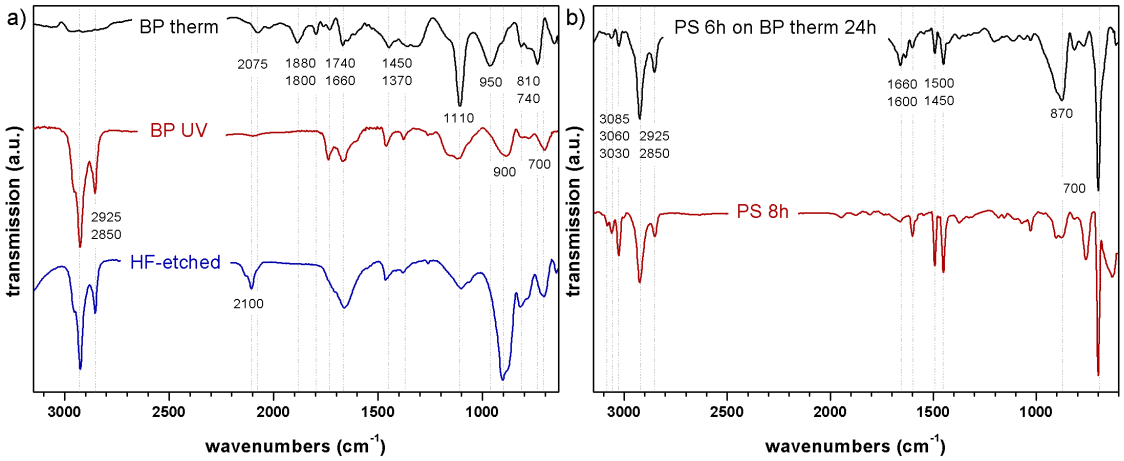

Figure 56: ATR IR spectra of H-Si (a) after thermal hydrosilylation with BP (24 h, 60°C) compared to a UV-irradiated BP-grafted substrate and a freshly HF-etched reference substrate and (b) same sample after 6 h irradiation in styrene compared with a reference sample grafted for 8 h in bulk styrene *via* the conventional one-step procedure

As can be seen from Figure 56a, there is still a considerable amount of Si-H bonds present on the surface, confirmed by the Si-H stretching band at 2075 cm^{-1}, which corresponds with the formation of a submonolayer with a surface coverage < 100 %. Aliphatic as well as aromatic C-H stretching bands together with aromatic overtone bands from 1880 to 1800 cm^{-1} indicate the presence of grafted BP on the surface. The strong band at 1110 cm^{-1} indicates either Si-O or C-O bonds, however, the O-H stretching vibration expected for a C-O-H moiety in S-C grafted BP is much less pronounced than in UV grafted samples (not shown in the spectra) which is an indication for BP being bonded via Si-O-C bonds. This is indicative of the benzophenone being grafted presumably by a hydrosilylation chain reaction.

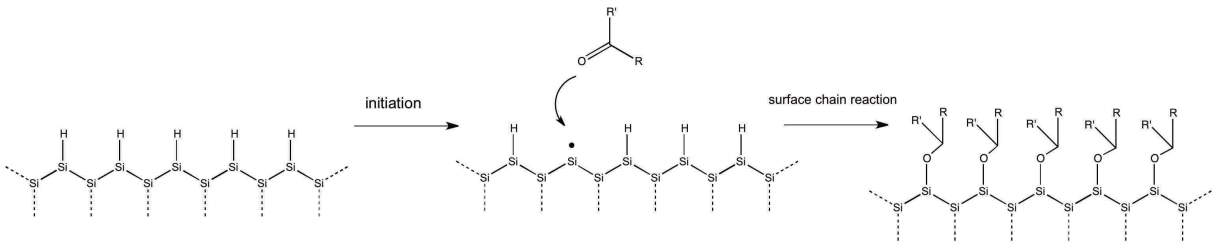

Figure 57: Thermal hydrosilylation chain reaction of aldehydes and ketones on H-Si

After irradiation for 6 h in styrene, these bands at 1100 cm^{-1} are of much weaker intensity, which means that either degrafting of BP moieties from the Si surface took place or PS bands are so strong that those bands are superposed. However, Si-H bands also disappeared indicating good functionalization of the Si substrate with styrene.

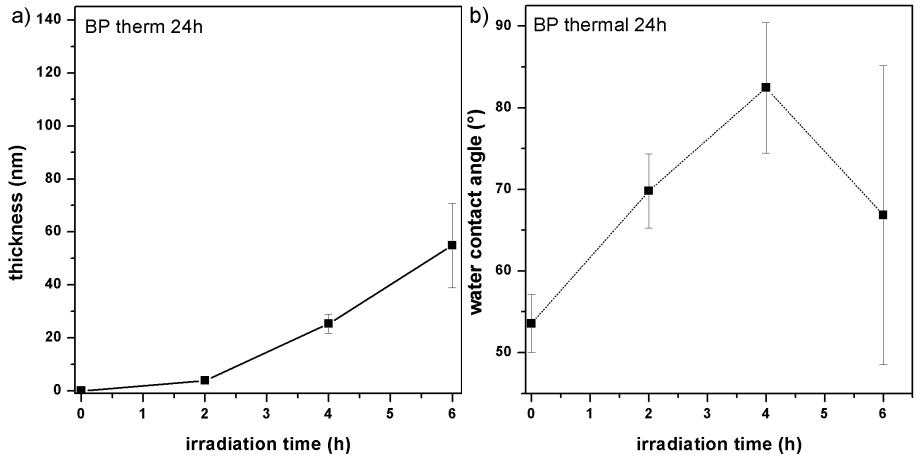

Figure 58: Correlation of irradiation time in styrene with (a) grafted layer thickness and (b) water contact angle for thermally hydrosilylated H-Si with BP

In Figure 58a, it can be seen that it is possible to graft polymer layers on silicon with this method. However, grafting thicknesses remain much lower than for 5 h UV immobilization with BP and, more importantly, do not exceed the values for grafting from unmodified H-Si surfaces. Moreover, water contact angles reveal a more polar and thus more oxidized surface than for the UV-grafted sequential polymerization. Therefore it can be stated that grafting the photoinitiator under UV irradiation is far more effective than thermal hydrosilylation of the photoinitiator.

4.2.6 Sequential Photografting in Air

As it has been shown that with the sequential photografting method a variety of polymers could be grafted from H-terminated silicon, it was further to be investigated if this process was applicable in non-degassed conditions, potentially widening its range of applications.

Therefore, an experiment was conducted analogously to the conventional sequential photografting route with the exception that the degassing steps were omitted. The ATR IR spectra of a sample after irradiation for 5 h in non-degassed BP solution and after 6 h irradiation in styrene are shown in Figure 59 a and b.

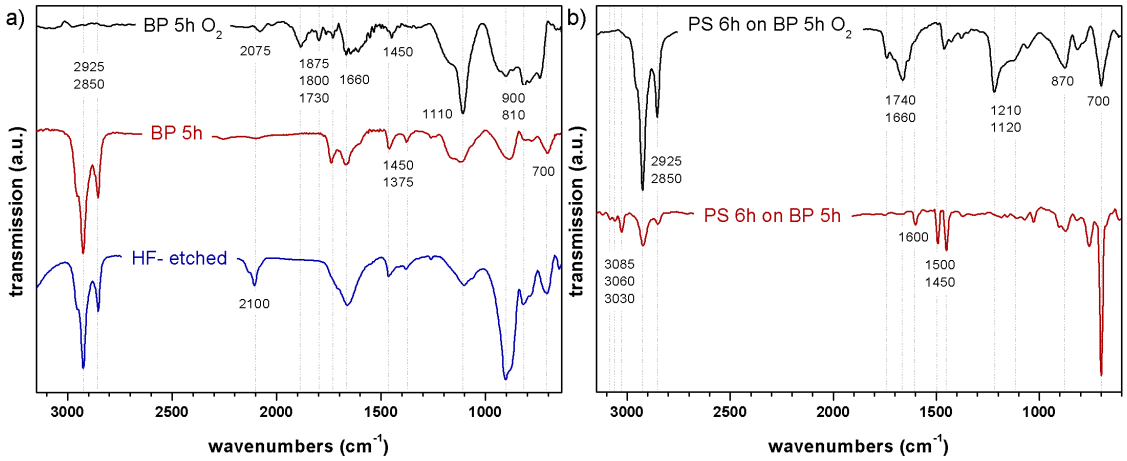

Figure 59: ATR IR spectra of an H-Si substrate irradiated in (a) 5 wt% BP in benzene for 5 h and (b) same sample after irradiation in styrene for 6 h (both without degassing)

From the IR spectrum in Figure 59a it can be seen that some amount of BP has been grafted to the surface. However, the strong shoulder around 1200 cm^{-1} indicates a high level of oxidation. After irradiation in styrene, no aromatic C-H stretching bands could be observed and the silicon oxide band at 1200 cm^{-1} has become more pronounced.

The contact angle of the Si substrate after BP grafting is 46.20 ± 8.49° and after grafting with styrene for 6 h it is still 59.85 ± 4.31 and layer thickness was determined to be as low as 5 nm by ellipsometry.

From these results it can be concluded that polymer cannot be grafted by sequential photografting without prior degassing. The reason for this can be found in the first step, where hydrogen atoms are abstracted from a Si-H bond, generating silyl surface radicals. These radicals are highly reactive and can react with the C=O double bond of the initiator or with oxygen in the solution which will then lead to an unreactive oxidized surface.

4.2.7 Conclusion

In this chapter it could be shown that photografting on silicon surfaces can both be applied to other monomers and grafting can be accelerated by a factor of 2 with the sequential photografting approach.

Ex situ kinetics measurements show that for a 5 wt% solution of both BP and ITX in benzene, maxima of grafting rates are obtainable by irradiation for 5 h in photoinitiator solution. Polymer layer thicknesses after 6 h irradiation in styrene are 138.2 ± 14.8 nm for 5 h BP

irradiation and 116.0 ± 26.8 nm for 5h irradiation in ITX, both exceeding the value for styrene alone twofold.

The possibility of thermal attachment of the photoinitiator layer has also been shown, reaching values of 55 ± 16 nm after 6 h irradiation in styrene. As the values lie in the same regime as pure styrene photografting, it is still to be evaluated if this method possesses advantages over the conventional approach.

Owed to the limited amount of time available, many questions have been left unanswered, e.g. if the photoinitiator concentration has an effect on the consecutive grafting reaction. As a first set of experiments has been carried out at a somewhat higher BP concentration and showed better results, especially for the grafting of acrylates, this should be subject of further investigations.

4.3 Polymerization on Nanocrystalline Silicon

4.3.1 Background

As of now, only few examples of polymer grafting from nanocrystalline silicon (nc-Si) have been reported. Clark *et al*. [178] and Ruckenstein *et al*.[179] have observed polymerization on acrylic acid on nc-Si under irradiation with UV light. Polymer-grafted nc-Si showed high dispersibility and stable luminescence properties. However, Ruckenstein *et al*. stated that analysis of AAc-grafted nc-Si "…*indicate a negligible amount of grafted PAAc*." and Clark *et al.*[178] observe formation of acrylic acid oligomers (8-9 repeating units).

Xu *et al.*[180] report on grafting of poly(methacrylic acid) from nc-Si *via* thermal grafting, although not really going into detail about the amount of grafted polymer, its molecular weight or nature of bonding.

To apply the general basic understanding of the processes and mechanisms involved in grafting polymers from planar H-terminated silicon surfaces, H-terminated silicon nanocrystals were studied as substrate material. Besides opening the door towards new hybrid nanomaterials through this route, it should also be clarified if growth of polymer takes place or not during irradiation of nc-Si in a monomer, as this contradicts some of the current reports in literature. For a typical experiment, ~100 mg nc-Si was dispersed in EtOH and sonicated. Approx. 0.5 ml of 48% aqueous HF were added under vigourous stirring and the stirring is continued for 15 min. Afterward, the dispersion is sonicated for 1 min and then filtered over a 0.2 μm PTFE membrane in a pressure filter unit. The substrate is washed with copious amounts of EtOH and then dried *in vacuo*. This etching procedure is accompanied by a weight loss of the nc-Si of around 50% (see Appendix), indicating a very high initial oxygen content (as seen in Figure 60a).

The etched nc-Si shows a strong Si-H absorption band at ~2100 cm^{-1}, indicating successful hydrogen-termination of the particle surface. However, the strong absorption band attributed to Si-O stretching vibrations at ~1100 cm^{-1} show a high degree of surface oxidation even after etching, which can also be caused by fast reoxidation of the hydrogen-terminated nc-Si due to its high surface area.

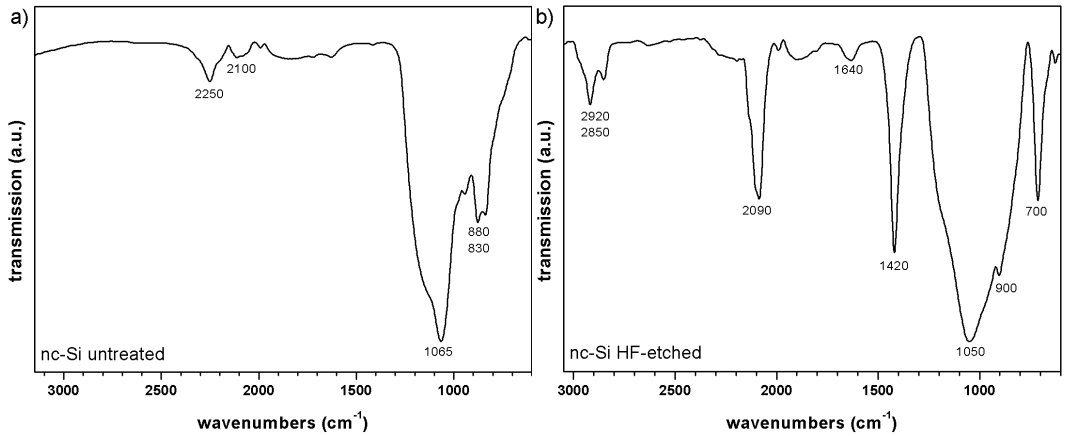

Figure 60: DRIFT spectra of untreated nc-Si (a) and hydrogen-terminated nc-Si after HF-etching (b)

H-terminated nc-Si was dispersed in monomer and irradiated with UV light for the wanted duration after degassing. After workup (filtration and washing and dryning *in vacuo*), the functionalized particles were analyzed by DRIFT spectroscopy, TGA measurements, TEM, and dispersibility experiments.

4.3.2 SIPGP of styrene on nc-Si

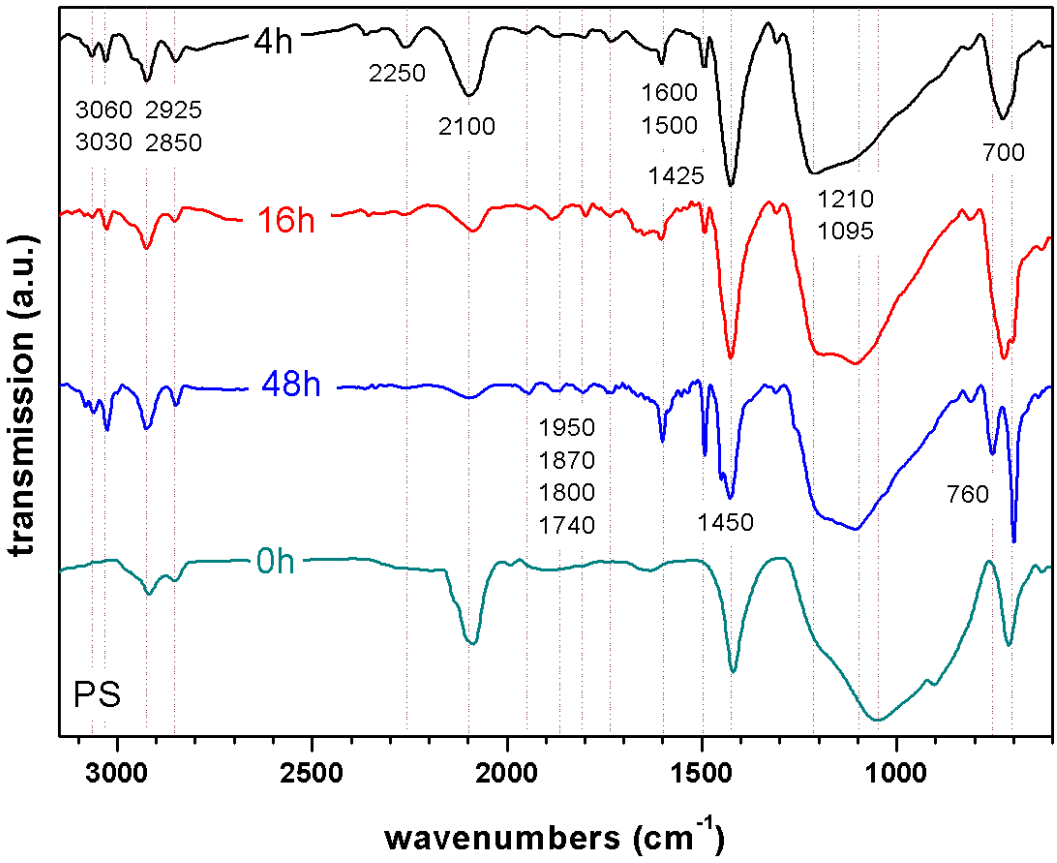

Figure 61: DRIFT spectra of H-terminated nc-Si irradiated for 4 h, 16 h and 48 h in styrene compared to the HF-etched reference

As apparent from Figure 61, polystyrene can readily be grafted from H-terminated silicon nanocrystals. DRIFT spectra of nc-Si in styrene after UV irradiation show absorption bands characteristic for polystyrene.

This can be seen from the occurrence of aromatic C-H valence vibrations of the three non-equivalent protons at 3085, 3060 and 3030 cm^{-1} and C-H stretching bands from CH- and CH_2 groups in the polymer backbone at 2925 and 2850 cm^{-1}. Further weaker absorption bands at 1950, 1870, 1800, and 1740 cm^{-1} are caused by aromatic overtones. Two further medium strong absorption bands of the C=C valence stretching at 1600 and 1500 cm^{-1} and one from the CH and CH_2 deformation at 1425 cm^{-1} are visible. In the fingerprint region, an absorption band from the aromatic C-H deformation vibration (*out of plane*) for five neighboring protons at 760 cm^{-1} gives hint to a monosubstituted aromatic ring. Besides that, further aromatic fingerprint bands between 1000 and 1220 cm^{-1} can not be detected because they superpose with Si-O valence stretching. Additional to the polystyrene bands, absorption bands from Si-H valence vibrations at 2100 cm^{-1} as well as Si-O-Si-H valence stretching bands at 2250 cm^{-1}

can be seen. The intensity of the absorption bands of these Si-H and Si-O-Si-H valence stretching vibrations decreases in comparison to the polystyrene signals with increasing irradiation time. Based on this observation it can be concluded that despite better functionalization of nc-Si with PS can be obtained at longer irradiation times, no complete functionalization of the surface could be achieved. This could be owed to the fact that some of the surface Si-H moieties are not accessible for reactions due to steric hindrance by the already grafted layer of molecules. The presence of the absorption bands from Si-O-Si-H valence vibrations indicates a certain degree of surface oxidation by insertion of oxygen in Si-Si bonds. Also, the Si-O valence stretching bands suggest either a reoxidation after or during etching or an insufficient removal of the very thick oxide layer. Elemental analysis carried out on the unetched substrate used in our experiments revealed an silicon oxide content of ~ 50 wt%. Thus, complete removal of this oxide is difficult. Besides the absorption bands mentioned, no significant bands occurred, so that coarse impurities can be excluded. Only a broad absorption band at ~ 3500 cm^{-1} (not shown in the above spectra) can be seen, resulting either from residual solvent within the polymer shell or from Si-OH valence vibrations.

For a direct proof of this assumed polymer layer around the silicon nanoparticles, TEM images were recorded (see Figure 62). From these images, a polymer layer around each particle can be seen, which indicates good functionalization as well as separation of the particles.

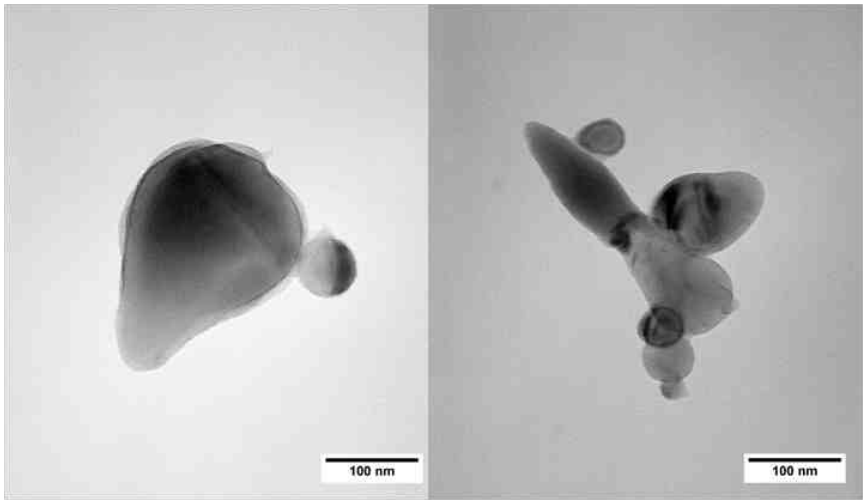

Figure 62: TEM images of nc-Si grafted with styrene for 48 h. Around each particle, a thin polymer layer can be seen.

To investigate the grafting rate on nc-Si, *ex situ* kinetics studies were carried out irradiating 0.1 wt% dispersions of nc-Si in styrene for different durations and correlating the TGA weight loss with the irradiation time. This correlation can be seen in Figure 63.

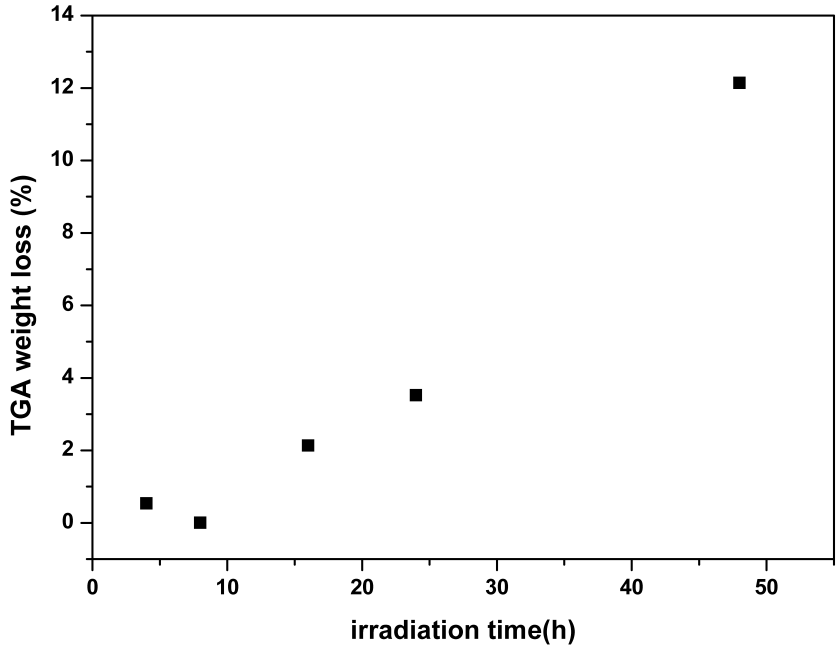

Figure 63: Correlation of TGA weight loss with the irradiation time for nc-Si irradiated in bulk styrene monomer

The TGA measurements give a more quantitative information about the amount of grafted polymer than DRIFT spectroscopy measurements. TGA data shown in Figure 63 gives a nearly linear increase of grafted polymer with irradiation time. Interestingly, the free polymer that passed through the filter in the sample irradiated for 48 h showed a slightly yellowish color, being an indication for very small but very well functionalized Nc-Si that passed through the filter.

Free polymer formed in the bulk monomer upon irradiation was precipitated from the filtrate, washed, and dried *in vacuo*. Afterwards, it was subjected to GPC analysis to obtain information about molecular weight and dispersity (seeTable 4), which could in turn yield information about processes involved in grafting.

Table 4: GPC data of free bulk polymer from samples of 0.1 wt% dispersions of nc-Si in styrene irradiated with UV light

Irradiation time (h)	$\bar{M}_w$ (kg/mol)	$\bar{M}_n$ (kg/mol)	Đ
4	249	65	3.85
16	583	188	3.10
24	614	149	4.11
48	611	182	3.36

It can be seen that the dispersity Đ is around 4 in all cases, which is not unusual for the SIPGP process, as new radicals are generated over the whole reaction time, leading to high dispersity values.

4.3.3 SIPGP of MMA on nc-Si

Another class of monomers to be grafted from nc-Si with the SIPGP method were methacrylates. The exact same procedure was followed using bulk MMA monomer instead of bulk styrene to disperse the nc-Si. Concentration of nc-Si in MMA also was 0.1 wt%.

Figure 64 depicts IR spectra of nc-Si irradiated in bulk MMA for 4, 16 and 48 h compared to the HF-etched reference.

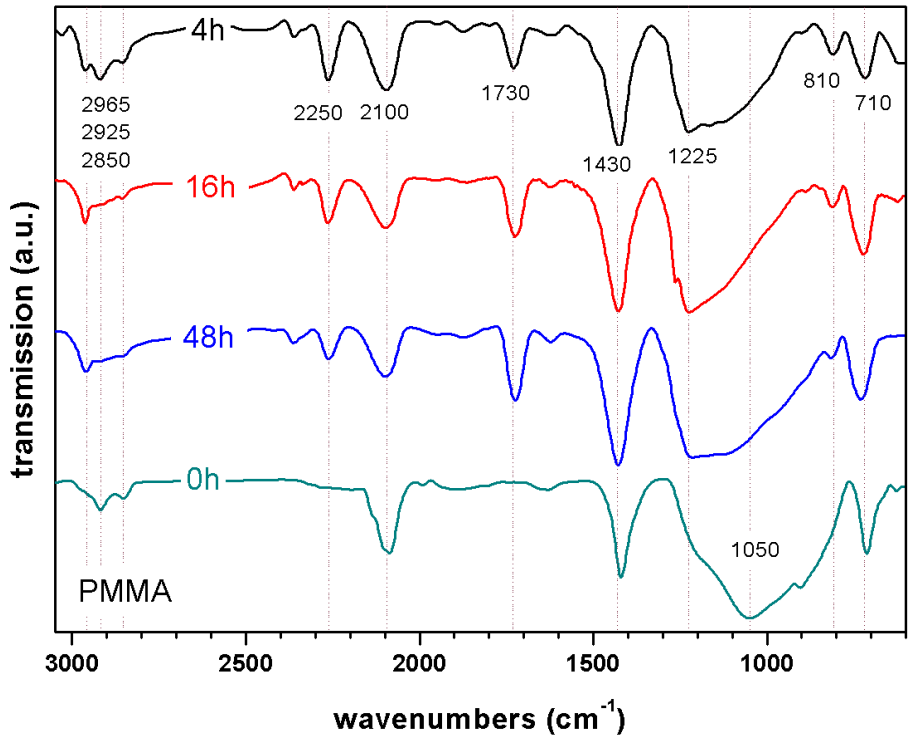

Figure 64: DRIFT spectra of nc-Si grafted with PMMA for 4 h, 16 h, and 48 h compared to HF-etched nc-Si

From Figure 64, the presence of grafted PMMA on the nc-Si surface can unambiguously be seen. The DRIFT IR spectra show two neighboring bands centered at 2965 and 2925 and 2850 cm^{-1}, which can be attributed to CH, CH_2, and CH_3 stretching vibrations and a strong absorption band at 1730 cm^{-1} to the C=O valence vibration. Especially the vibration band at 2965 cm^{-1} is indicative for an alkene double bond $C=CH_2$ stretching, which in turn means that a significant amount of MMA is grafted via Si-O-C and not Si-C bonds. As the Si-O-C grafted monomers are not starting a polymerization reaction but can only participate in already initiated polymerizations *via* a *grafting-through* mechanism, grafting density is expected to be significantly lower than for styrene.

Furthermore, in the IR spectra CH_n deformation bands can be detected at 1430 cm^{-1} (which superpose with the reference however), and two broad, partly superposed absorption bands at 1615 and 1167 cm^{-1} of the C-O stretching vibration of the ester moiety. Comparison to corresponding IR spectra from literature show a high degree of agreement [181]. Additionally, Si-H and Si-O-Si-H valence vibrations occur at 2100 and 2250 cm^{-1}. Based on the strong Si-H absorption band it can be concluded that only an incomplete functionalization of hydrogen sites with PMMA has taken place. This is also affirmed by the observation that the intensity of the absorption bands related to PMMA does not increase further in comparison to e.g. the

Si-H bands even at longer irradiation durations. However, this in turn shows the good passivation of Si-H sites through PMMA polymer, since the particles were handled in air for several hours before measuring the IR spectra. Taking this into account, it can be assumed that a thin layer of PMMA together witha Si-O-C bonded MMA submonolayer is formed in a very short amount of time (< 4 h), which both hinders further grafting and effectively passivates the nc-Si substrate.

This is further confirmed by TGA measurements on nc-Si irradiated in bulk MMA for different times, shown in Figure 65.

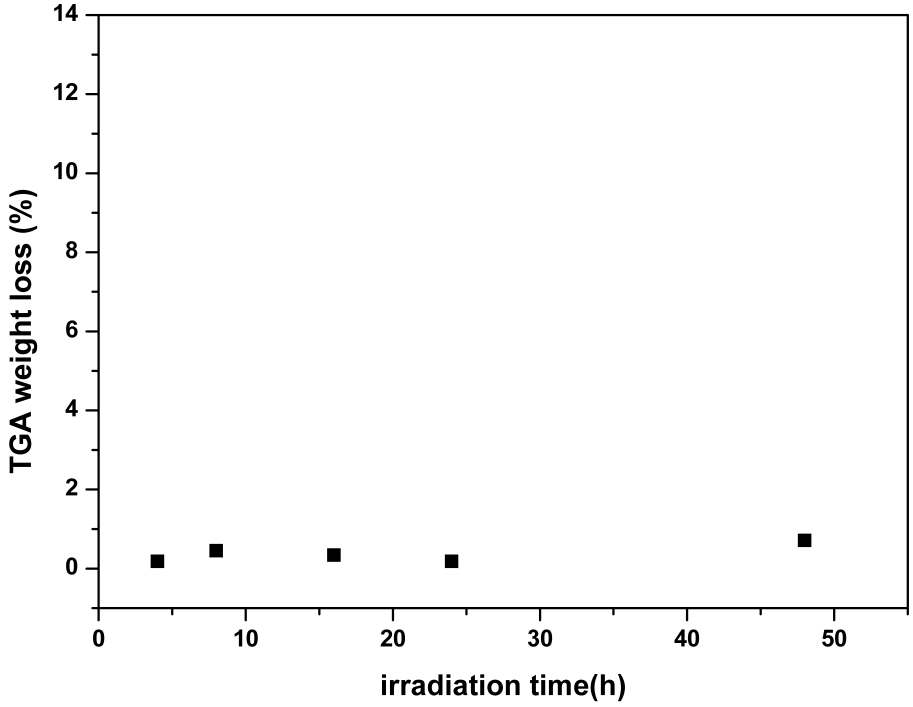

Figure 65: Correlation of TGA weight loss and irradiation time for PMMA-grafted nc-Si

Grafted PMMA amounts to a maximum of 1 wt% even after 48 h of irradiation, indicating no further grafting after initial formation of a PMMA layer. Furthermore, TEM images reveal the presence of a complete layer (~ 5-10 nm) around each nanocrystal and no formation of agglomerates, as can be seen in **Figure 66**. This indicates, that the surface grafting leads to functionalization of nc-Si with thin, homogenous polymer layers, as oxidized nc-Si readily forms agglomerates in almost any solvent.

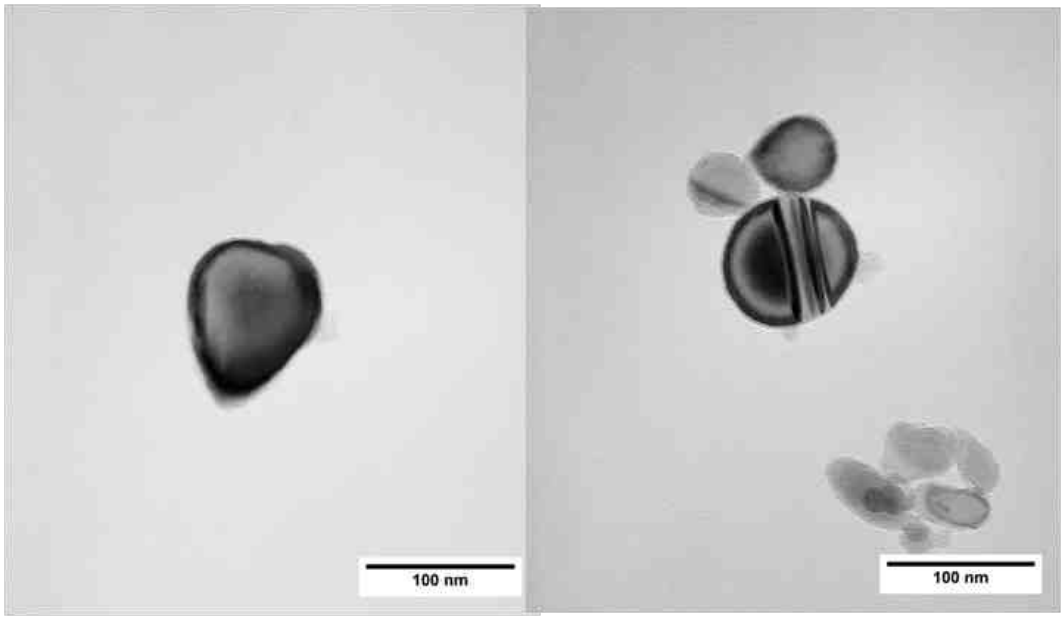

Figure 66: TEM images of nc-Si after 16 h grafting with PMMA

During workup, only small amounts of free bulk polymer could be precipitated. This was highly unexpected, as acrylates and methacrylates give very high amounts of free polymer when irradiated with UV light as observed for experiments with planar silicon substrates. A possible explanation for the low amount of free polymer is the strong light absorption by nc-Si on the one hand, leading to less intensity available for initiating polymerization and grafting. On the other hand, silicon nanocrystals also strongly interfere with normal radical polymerization, especially in acrylates. A high concentration of Si-H bonds can lead to a significant amount of transfer reactions,[182] thereby terminating the free radical polymerization reaction and leading to low molecular mass polymer.[183]

4.3.4 SIPGP of tBMA on nc-Si

As another relevant methacrylate monomer, tert.-butyl methacrylate (tBMA) was grafted from nc-Si. The reason for using tBMA is the convenient post-polymerization hydrolysis of the formed polymer PtBMA to obtain polymethacrylic acid (PMAAc) brushes, which can be used for immobilization of redox-active moieties or even enzymes.[113]

The procedure used was the same as in the previous experiments with bulk tBMA instead of styrene or MMA. All other parameters were kept the same to ensure compatibility of the results. DRIFT IR-spectra of samples irradiated for different durations (4 h, 16 h, and 48 h) is shown in Figure 67.

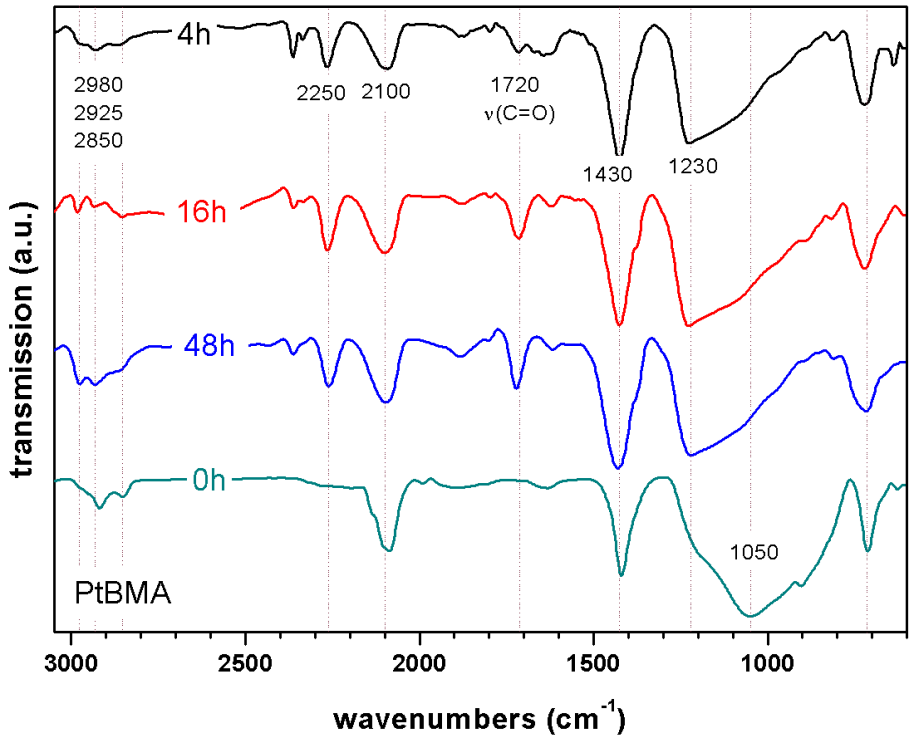

Figure 67: DRIFT spectra of nc-Si grafted with PtBMA for 4 h, 16 h, and 48 h

DRIFT IR spectra of nc-Si after UV irradiation with tBMA suggest the presence of grafted PtBMA, also here together with some Si-O-C bonded tBMA. Absorption bands from CH_n valence vibrations at 2976 and 2925 and 2850 cm^{-1}, from the C=O valence stretching at 1730 cm^{-1}, CH_n deformation bands at 1429 cm^{-1}, and a CH_2 rocking band at 716 cm^{-1} can be detected. Si-H stretching bands at 2096 cm^{-1} and Si-O-Si-H stretching bands at 2250 cm^{-1} indicate incomplete functionalization and partial oxidation. As already observed with MMA grafting, the relation of intensities of PtBMA-related absorption bands and Si-H stretching bands does not change even at high irradiation times and thus indicates low grafting rates, being further confirmed by TGA analysis shown in Figure 68.

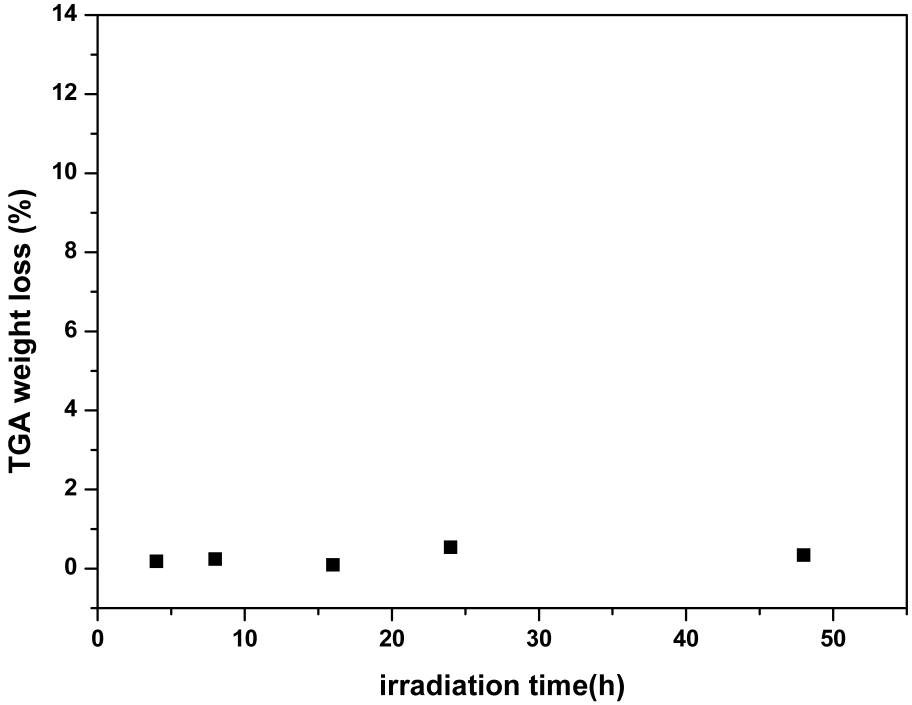

Figure 68: Correlation of TGA weight loss and irradiation time for PtBMA-grafted nc-Si

Furthermore, no free polymer could be precipitated. From this can be concluded that also with tBMA hydrosilylation is preferred, leading to a monolayer and if polymers are grafted, grafting density is very low. Since the tert.-butyl group is sterically more demanding than the methyl group in MMA, Si-H bonds are even more shielded, leading to lower degrees of functionalization. However, even with PtBMA, a complete layer of polymer could be formed around each particle, as can be observed in the TEM images shown in **Figure 69**.

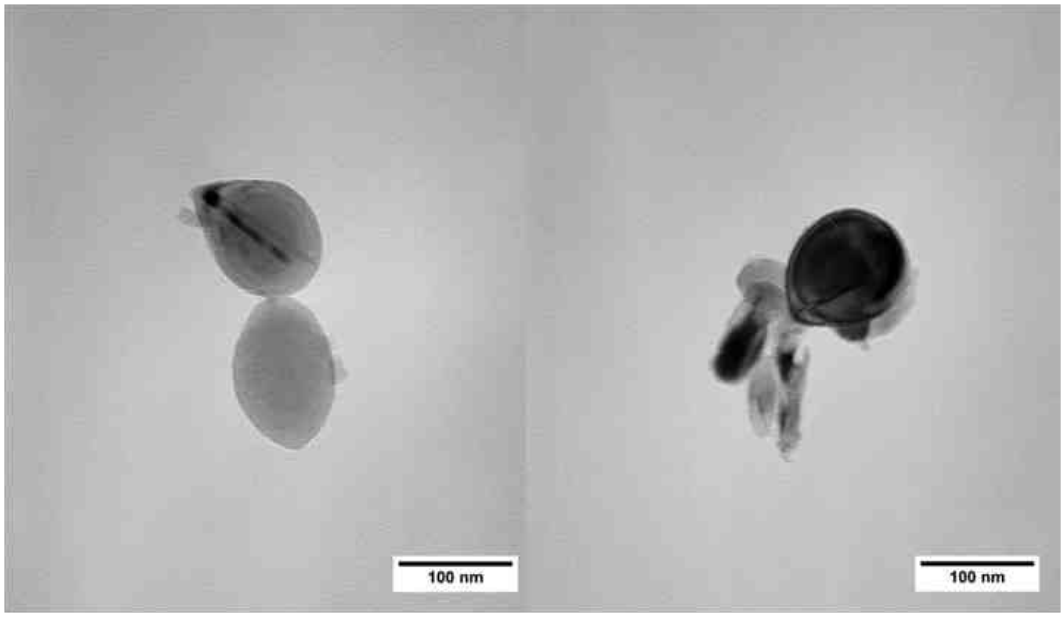

Figure 69: TEM images of nc-Si after 16 h grafting with tBMA

4.3.5 SIPGP of DMAEA on nc-Si

Another monomer to be grafted was dimethylamino ethylacrylate (DMAEA). It was chosen because of its inherent multiresponsivity to pH, temperature, and ion strength potentially leading to stimuli-responsive nanohybrids.

A 0.1 wt% dispersion of H-terminated nc-Si in DMAEA monomer was degassed and irradiated for 16 h. Figure 70 shows a DRIFT spectrum of the sample after filtration, washing, and drying *in vacuo*.

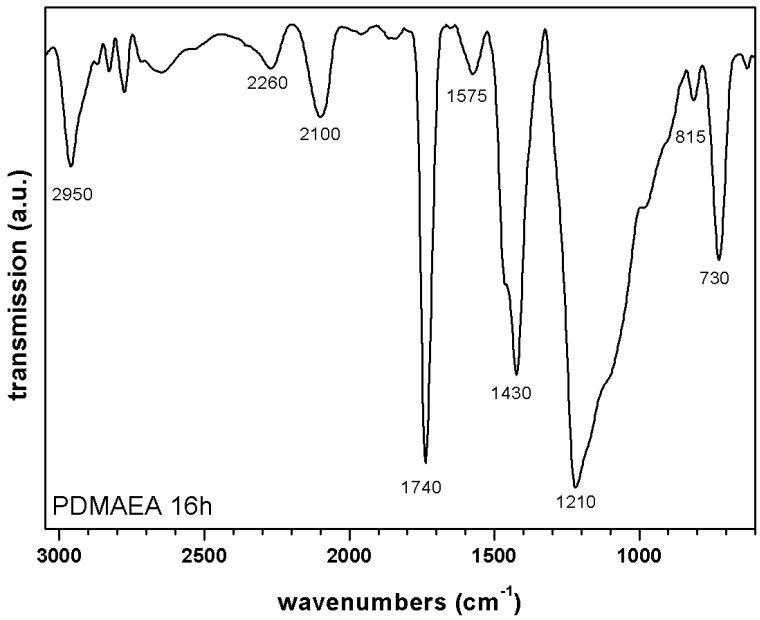

Figure 70: DRIFT spectrum of Nc-Si grafted with PDMAEA for 16 h

The DRIFT spectrum of nc-Si irradiated for 16 h with UV light in DMAEA shows weak to medium CH_n valence stretching bands - shifted by the amine group – at 2950, 2825, and 2775 cm^{-1}, a strongly superposed absorption band of the CH_n and C=O deformation vibration at 1424 cm^{-1}, a very strong absorption band of the C=O valence stretching at 1740 cm^{-1}, and several strong, superposed absorption bands of the ester C-O and Si-O valence stretching between 1000 and 1219 cm^{-1}. Latter could, as already mentioned, arise from incomplete removal of the native silicon oxide or from subsequent oxidation of the nanoparticles. Furthermore, Si-H and Si-O-Si-H valence stretching vibrations at 2100 and 2270 cm^{-1} point towards incomplete conversion of the surface Si-H groups, despite being weaker than in the PMMA- and PtBMA-grafted samples. Surprisingly, TGA measurements revealed 2.77 wt% of grafted polymer after 16 h of grafting. Together with the results from IR spectra analysis, functionalization of nc-Si with DMAEA can be regarded successful. The reason for this might be found in the nature of DMAEA as a tertiary amine. It has been reported in literature that tertiary amines can be used as initiator layers for SIPGP[184]. Thus, grafting from nc-Si with DMAEA does not stop after the monolayer has been formed but continues by grafting easily from the DMAEA layer.

4.3.6 SIPGP of 4-Vinyl Pyridine on nc-Si

Grafting of VP from nc-Si was also done within this work, as P4VP shows pH sensitivity and also nanoparticles can be synthesized within the P4VP brushes that can be used for catalysis.[185-189]

A 0.1 wt% dispersion of H-terminated nc-Si in 4-VP monomer was degassed and irradiated for 16 h. Figure 71 shows a DRIFT spectrum of the sample after the reaction, washing and drying.

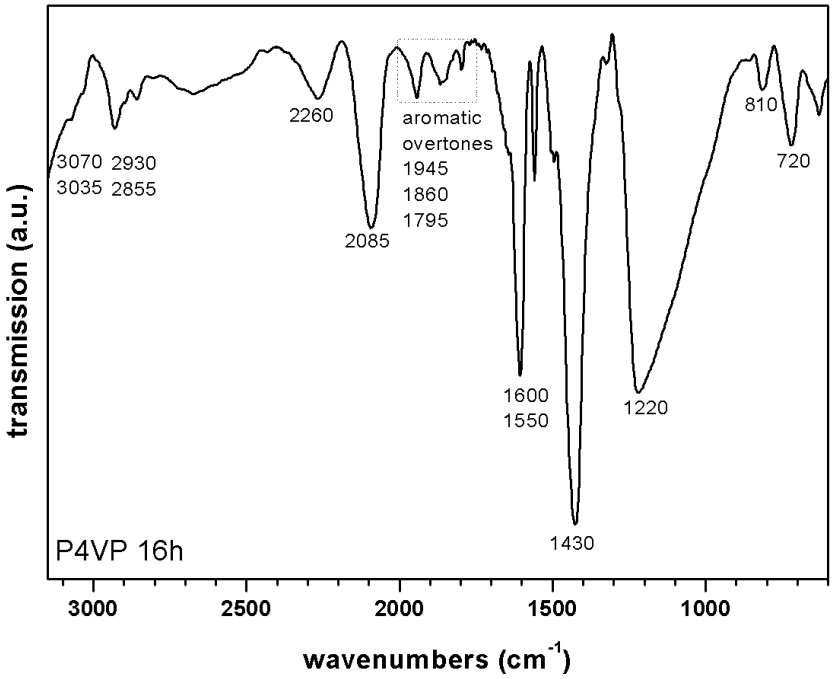

Figure 71: DRIFT spectrum of Nc-Si grafted with P4VP for 16 h

The DRIFT spectrum of nc-Si after 16 h irradiation in 4-VP shows a weak absorption band of aryl CH valence stretching at 3070 and 3030 cm^{-1} and CH_n valence stretching band from the polymer backbone at 2930 and 2855 cm^{-1}. Further absorption bands of aromatic overtones at 1945, 1860, and 1795 cm^{-1}, two medium strong bands of the C=C valence stretching at 1600 and 1550 cm^{-1}, and a strong CH_n deformation band at 1430 cm^{-1} can be seen. Absorption bands of aromatic CH stretching vibrations over 3000 cm^{-1} superpose with the OH stretching of residual solvent and are thus not detectable. Besides the absorption bands attributed to P4VP, there are also Si-H absorption bands at 2100 cm^{-1} and Si-O-Si-H absorption bands at 2260 cm^{-1}, that are also present in all other samples for the aforementioned reasons. However, those bands are not very strong compared to the P4VP-related bands. Moreover, taking into account the calculated amount of grafted polymer of 2.73 wt% determined by TGA, it can be concluded that grafting was successful.

4.3.7 Photoinduced Grafting of Copolymers from nc-Si

As a convenient way to obtain functional polymer grafts on silicon, the photoinduced grafting of copolymers has already been demonstrated in Chapter 4.1.7. In a first try to apply this process to grafting from nc-Si a 0.1 wt% dispersion of H-terminated nc-Si in a 10:1 mixture of styrene and HEMA was irradiated for 16 h. Figure 72 shows a DRIFT spectrum of the sample after filtration, washing, and drying *in vacuo*.

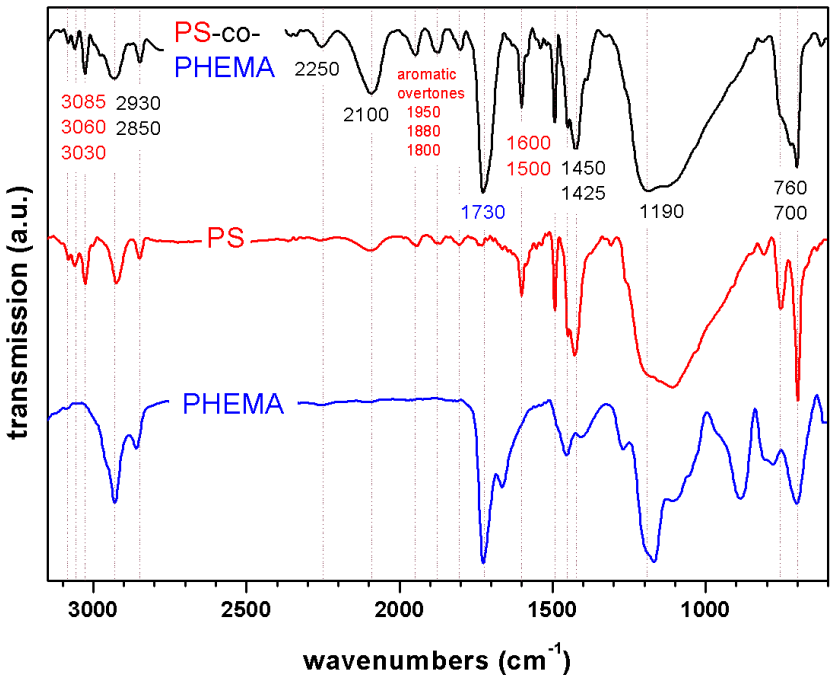

Figure 72: DRIFT spectrum of nc-Si grafted with 10:1 styrene/HEMA for 16 h

The DRIFT spectrum of nc-Si after 16 h irradiation in styrene/HEMA 10:1 shows the absorption bands expected for the statistical copolymer. Aromatic CH valence stretching bands of the three non-equivalent protons of polymeric styrene can be seen at 3085, 3060, and 3030 cm^{-1}, two superposed absorption bands at 2930 and 2850 cm^{-1} from the CH, CH_2 and CH_3 valence vibrations of the polymer backbone and methacrylic CH_3 groups, medium strong absorption bands at 1950, 1880, and 1800 cm^{-1} from aromatic overtone modes, two relatively strong absorption bands at 1600 and 1500 cm^{-1} from C=C valence stretching, an absorption band at 1425 cm^{-1} from CH_n deformation vibrations and a broad absorption band of the HEMA OH group at 3500 cm^{-1}. Latter could also be caused by residual adsorbed solvent ethanol. However, as the strong C=O valence stretching band at 1730 cm and the CH_3 umbrella deformation vibration as a shoulder at 1380 cm^{-1} can be clearly detected, presence of HEMA in the copolymer could be confirmed. In the fingerprint region, aryl-H deformation vibrations at 760 cm^{-1} originating from five neighboring protons can be seen, indicating a

monosubstituted aromatic compound. Weak absorption bands of Si-H at 2100 cm^{-1} and of Si-O-Si-H at 2250 cm^{-1} also occur. TGA revealed a six-fold higher weight loss than for 16 h homo-PS grafted nc-Si, namely 12.63 %. From this it can be stated that functionalization has been carried out very effectively similar to planer silicon substrates, although the nc-Si surface has not been completely functionalized. This can be attributed, as already mentioned, to steric shielding of the surface by the grafted polymers with its sterically demanding phenyl and ester moieties.

4.3.8 SIPGP of Allylamine on nc-Si

Originally, grafting of allylamine onto nc-Si was planned to be carried out as a normal hydrosilylation leading to monolayer. The allylamine monolayer could then be used as a linker for the immobilization of catalysts. Therefore, a 0.1 wt% dispersion of H-terminated nc-Si in allylamine was degassed and irradiated for 16 h. Figure 73 shows a DRIFT spectrum of the sample after filtration, washing, and drying *in vacuo*.

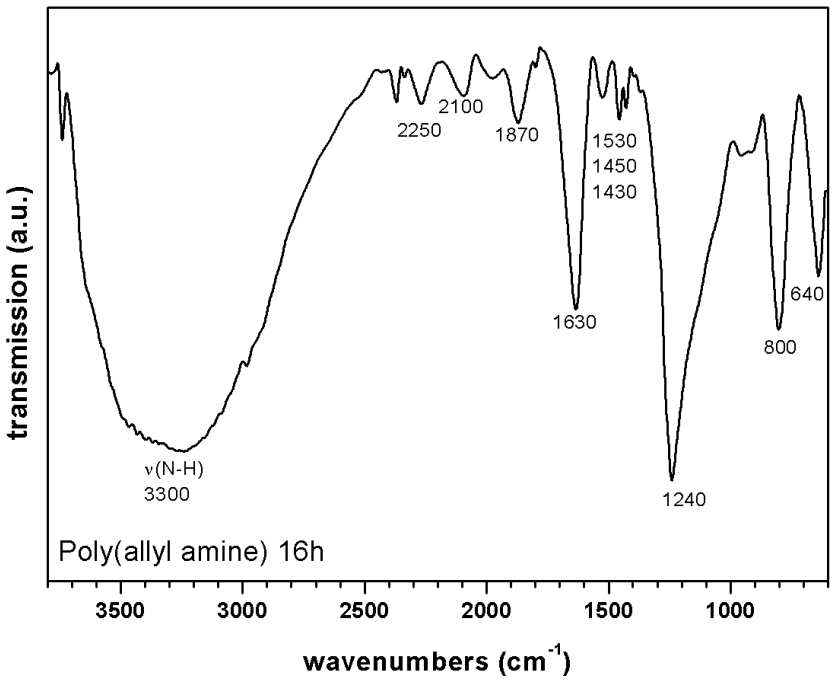

Figure 73: DRIFT spectrum of Nc-Si grafted with allylamine for 16 h

The DRIFT spectrum of nc-Si after 16 h irradiation in allylamine shows a broad, strong absorption band of the NH_2 valence stretching vibration at ~ 3300 cm^{-1}, a superposed absorption band at 2985 cm^{-1} resulting from CH_n valence stretching, a strong absorption band from the NH_2 deformation vibration (NH_2 scissoring), and three weak bands at 1530, 1450,

and 1430 cm^{-1} from CH_n deformation modes. Furthermore, Si-H and Si-O-Si-H absorption bands can be detected at 2100 and 2250 cm^{-1}. TGA measurements revealed a weight loss of 9.26 wt% after only 16 h of grafting. This value can be regarded as exceptionally high, especially with regard to the fact that no free polymer could be precipitated.

4.3.9 Influence of nc-Si Concentration on Grafting

Since nc-Si shows very strong absorption of light, it was interesting to see the effect of diluting the concentration of nc-Si in the monomer. Samples with a concentration of 0.05 wt% (1/2 of the usual concentration) and 0.025 wt% (1/4 of the usual concentration) of H-terminated nc-Si were prepared while all other parameters were kept constant. The samples were degassed and irradiated for 16 h. Figure 74 shows DRIFT spectra of the two sample after filtration, washing, and drying *in vacuo*.

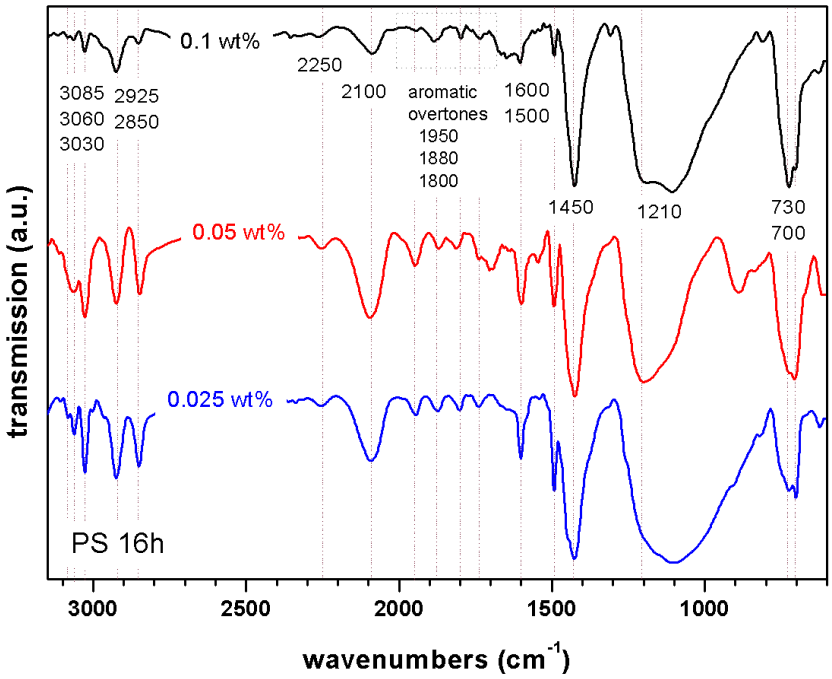

Figure 74: DRIFT spectra of 0.05 wt% (black) and 0.025 wt% (red) Nc-Si in styrene irradiated for 16 h

DRIFT spectra of 0.05 and 0.025 wt% nc-Si in styrene after 16 h irradiation show the same absorption bands as for 0.1 wt% and will therefore not be discussed in detail. It can be seen that the intensities of the Si-H bands decrease with decreasing dilution but do not completely disappear, however, due to steric shielding by polystyrene chains. Further unwanted Si-O-Si-H and SiH_n valence stretching bands show a relatively low intensity in comparison. TGA

measurements reveal grafted amounts of polymer to be 3.88 % for half the normal concentration and 4.77 % for the quartered normal concentration. This corresponds to a increase in comparison to 0.1 wt% of 81% and 124%, both even exceeding the amount of grafted PS of the 0.1 wt% dispersion irradiated for 24 h. These results can be easily explained by the fact that less light absorption by nc-Si is taking place, leading to better activation of styrene and therefore higher grafting performance. Furthermore, concentration of Si-H moieties is decreased that could potentially take part in transfer reactions with growing polymer chains.

4.3.10 The "one-pot" method

In an effort to simplify the grafting process on the one hand and improve the quality of the functionalization on the other hand, an alternative procedure was developed: The "one-pot" procedure. As the nc-Si was etched in the conventional procedure, the solution was not degassed during etching. After etching, cc-Si was handled under ambient atmosphere and were thus subject to oxidation. It was envisioned that exclusion of oxygen from the system would avoid oxidation of the nc-Si surface and thus improve the grafting efficiency.

For this reason the experimental procedure was slightly altered: Untreated nc-Si was dispersed in the monomer, and a small amount of HF solution was added after degassing. Then, the evolving SiF_4 gas was removed by short evacuation and the dispersion was irradiated with UV light as usual. Workup was also carried out as usual, by filtration over a 0.2 μm PTFE filter membrane in a pressure filtration setup and washed with copious amounts of a good solvent for the formed monomer and then with ethanol. After drying *in vacuo*, the samples were analyzed *via* TGA and DRIFT spectroscopy.

4.3.10.1 "One-pot" Grafting of Styrene

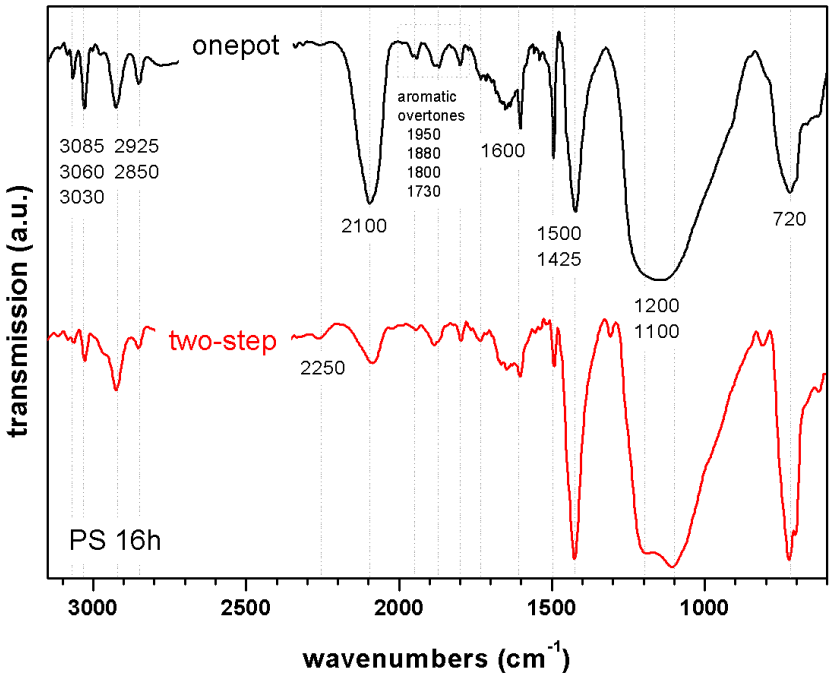

Figure 75: DRIFT spectrum of nc-Si grafted with PS for 16 h via the "one-pot" method compared to the two-step reference

From the DRIFT spectrum (Figure 75), the presence of grafted PS can be concluded since all characteristic polystyrene absorption bands are observable. An exact assignment of bands can be found in the appendix. In comparison to the conventionally treated sample irradiated for 16 h, the most prominent difference is the very strong Si-H absorption band at ~ 2100 cm^{-1}. In contrast Si-O-Si-H absorption bands, expected at 2250 cm^{-1} are merely visible. This indicates a very low amount of oxidation by insertion of oxygen into Si-Si bonds. Surprisingly, TGA measurements revealed only 0.26 wt% grafted polystyrene determined *via* TGA weight loss, representing a decrease of 59 % compared to the conventional process. Thus, it has to be stated that the one-pot procedure did not lead to higher grafting performance in the case of styrene, but reoxidation could be avoided, as seen by the low intensity of Si-O-Si-H bands.

4.3.10.2 "One-pot" Grafting of MMA

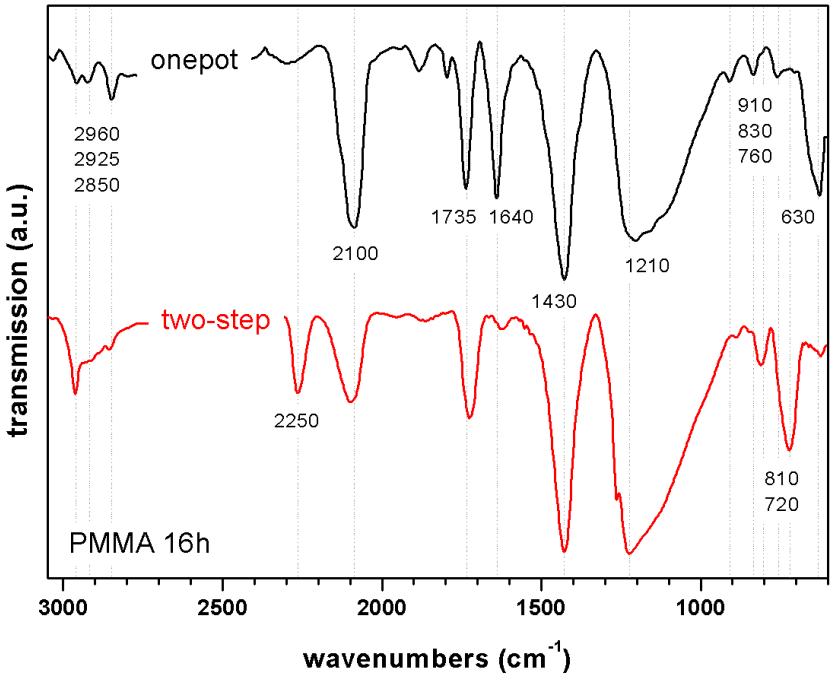

Figure 76: DRIFT spectra of nc-Si grafted with PMMA for 16 h via the "onepot" and the two-step method

As in the previous sample, several bands assigned to grafted PMMA can be detected from the DRIFT spectrum in Figure 76. Also here, a strong decrease in the intensity of the Si-O-Si-H absorption band can be seen together with a very strong Si-H band. Exact assignment of absorption bands can be found in the appendix. TGA measurements give 0.55 wt% of grafted PMMA, indicating an increase of 62 % compared to the conventional process. This can be caused by the possibility of HF to remove Si-O-C bonded MMA layer, which regenerates Si-H sites for grafting.

4.3.10.3 "One-pot" Grafting of tBMA

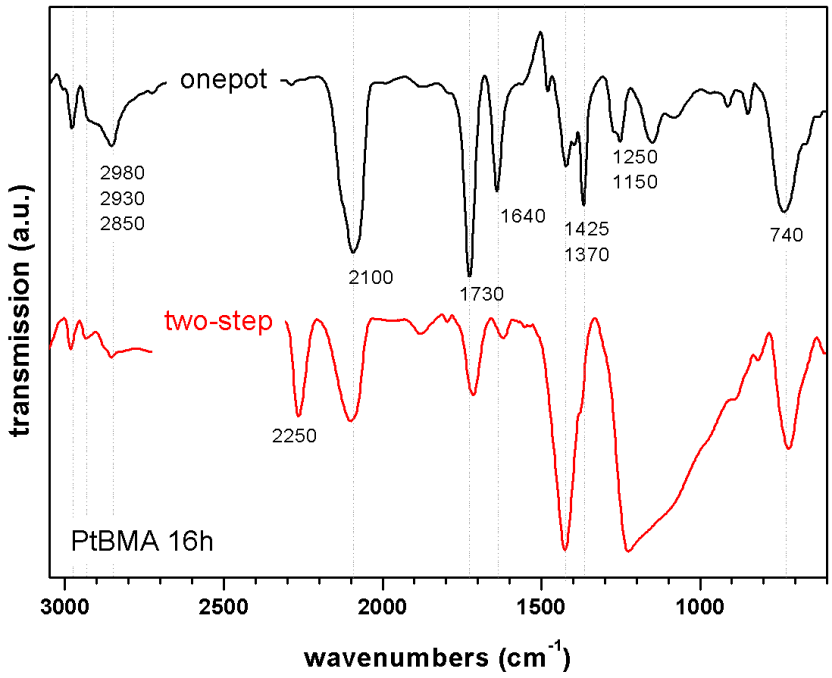

Figure 77: DRIFT spectrum of nc-Si grafted with tBMA for 16 h via the "one-pot" method

In the DRIFT spectrum in Figure 77, several absorption bands expected for grafted PtBMA can be detected. Exact assignments can be found in the Appendix). In comparison to the conventionally treated sample, no Si-O-Si-H absorption bands can be detected. However, the intensity of the Si-H stretching bands shows a strong increase compared to the normal sample. However, TGA weight loss was determined to be 1.3 %, being 16-fold higher than the conventional sample. This represents a possibility to enhance grafting of acrylates on nc-Si.

4.3.10.4 "One-pot" Grafting of Allylamine

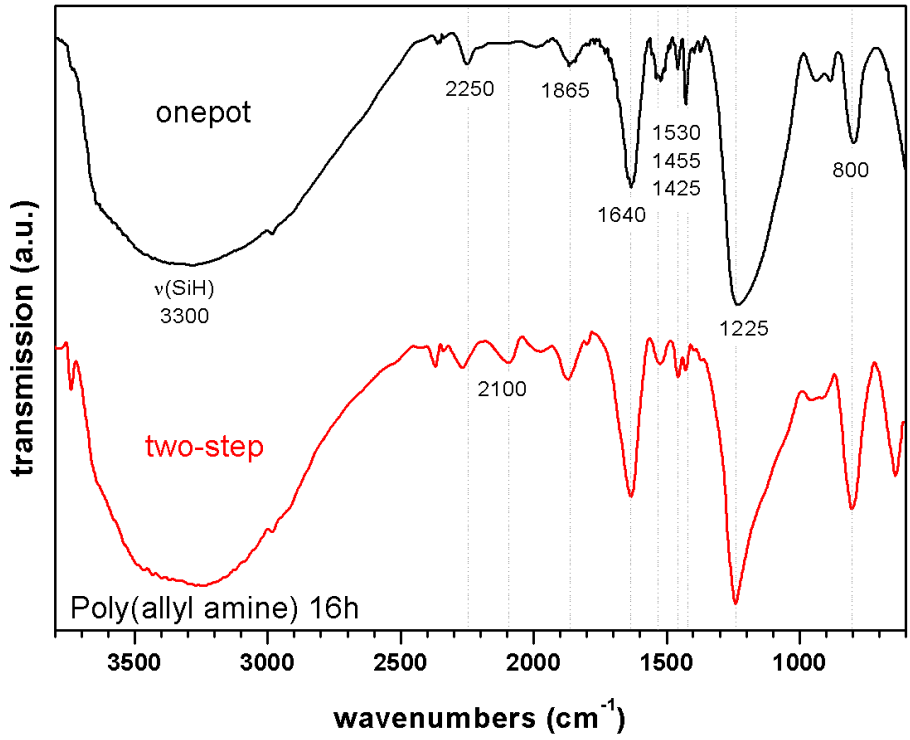

Figure 78: DRIFT spectrum of nc-Si grafted with poly(allyl amine) for 16 h via the "one-pot" method

From the DRIFT spectrum in Figure 78, a successful grafting of PAAm can be concluded. Moreover, the DRIFT spectrum looks very similar to that of the conventionally treated sample. Exact assignments of IR bands and their intensities can be found in the appendix. The most prominent difference in comparison to the conventional allyl amine grafting is the much lower intensity of the Si-H band, indicating a higher degree of grafting. Also the Si-O-Si-H band shows a somewhat lower intensity. The higher amount of grafted polymer was also confirmed by TGA measurements, as TGA weight loss was determined to be 32.8 %, being an increase of 60.7 % from the conventionally grafted nc-Si. The high grafting performance of allylamine on the surface could potentially be explained by the nature of the initiation process. As in these experiments no free polymer could be precipitated from solution despite the high amount of grafted polymer, it could be possible that initiation of allylamine polymerization does not take place via the normal SIPGP mechanism but is initiated directly by photoinduced dangling bonds on the silicon surface, as already reported for grafting of allylamine from diamond.[190]

From these results it can be stated that photoinduced grafting of allylamine from H-terminated silicon surface constitutes a convenient method for obtaining amino-functional polymer

brushes, having a wide range of applications due to their versatile chemistry (e.g. protein/enzyme coupling, immobilization of redox-active moieties, and good water-solubility). Additionally, the fact that only low amount of ungrafted polymer are produced makes this method very efficient.

4.3.11 Sequential Photografting on nanocrystalline silicon

Since good results in terms of more efficient grafting could be achieved via the sequential photografting procedure on planar silicon substrates, it was to be investigated if this method could also be applied to nanocrystalline silicon.

As in the case of planar silicon substrates, sequential photografting on nc-Si was carried out in a two-step procedure. In the first step, freshly H-terminated nc-Si was dispersed in a 5 wt% solution of benzophenone in benzene to give a 0.1 wt% dispersion with respect to nc-Si. The dispersion was then degassed via three freeze-pump-thaw cycles and irradiated for 3, 5, and 16 h, respectively.

In Figure 79, DRIFT spectra of nc-Si after BP-grafting for 3 h and 5 h can be seen.

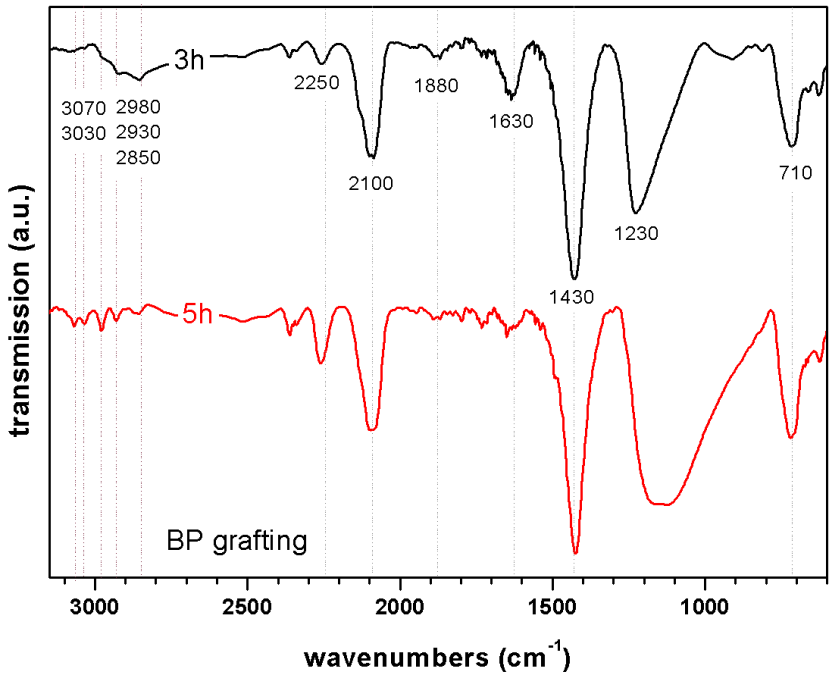

Figure 79: DRIFT spectra of nc-Si grafted with BP for 3 h (black) and 5 h (red)

Both DRIFT spectra indicate the presence of grafted benzophenone. Aromatic C-H stretching at 3070 and 3030 cm^{-1} as well as aromatic C=C stretching bands at ~ 1630 cm^{-1} confirm the presence of an aromatic compound. The Si-O stretching band at ~ 1100 cm^{-1} and the Si-O-Si-H band at ~ 2250 cm^{-1} show an increased intensity for the sample grafted for a longer time. This could be caused by reoxidation of nc-Si during or after functionalization and also by alternative binding of BP onto the nc-Si surface over an Si-O-C bond. The question if BP attached via such an Si-O-C bond can still degraft under UV irradiation could not be fully answered in our experiments.

Afterwards, BP-grafted nc-Si was dispersed in styrene to obtain 0.1 wt% dispersions. The dispersions were irradiated with UV light for 16 h and analyzed via DRIFT spectroscopy and TGA.

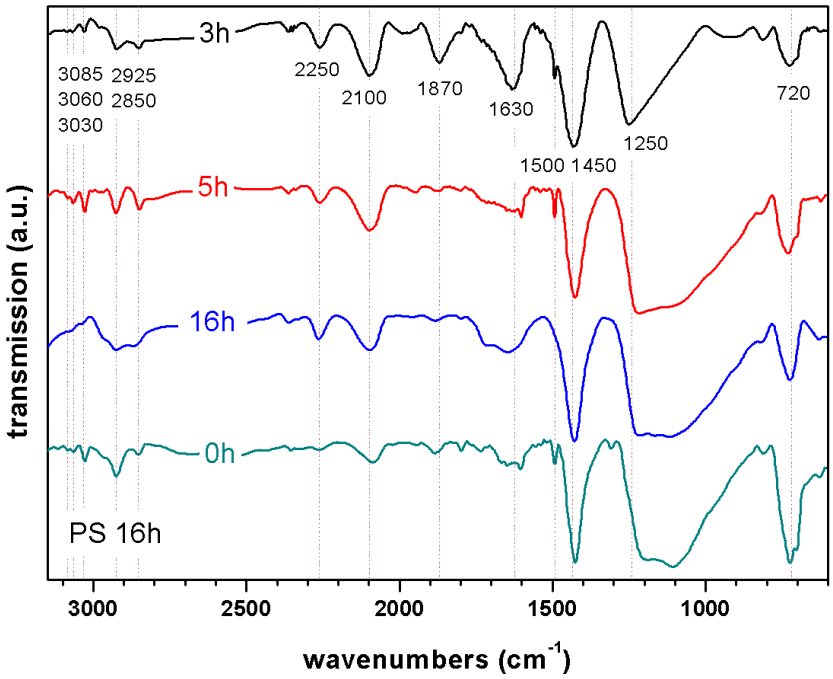

Figure 80: DRIFT spectra of nc-Si grafted with BP for 3 h (black), 5 h (red), and 16 h (blue) and 0 h (reference sample) after 16 h irradiation in styrene

In Figure 80, only the DRIFT spectra of nc-Si sequentially grafted with styrene after BP grafting for 3 h and 5 h show clear presence of absorption bands assignable to grafted polystyrene. Especially for the 5 h BP-grafted nc-Si sample, aromatic C-H stretching bands can be clearly detected. Exact assignments of absorption bands can be found in the appendix. It is interesting to see that the intensity of the Si-O-Si-H band in comparison to the Si-H

stretching band is decreasing for the 5 h BP-grafted sample and increasing for the 3 h BP-grafted one (see Figure 79). No statement can be made about the 16 h BP-grafted sample, since DRIFT spectroscopy was not carried out after BP grafting. For 3 h and 5 h BP grafting however, several conclusions can be drawn. Since the Si-H band is decreasing in the 3 h BP-grafted sample, there were still accessible Si-H bonds on the surface after BP grafting that took part in the PS grafting. For the 5 h BP-grafted sample, Si-H bands could have also become weaker, but Si-O-Si-H bands showed an even stronger decrease. This means that either Si-O-Si-H bonds are more reactive towards hydrosilylation or, which is more likely, that BP molecules attached via a Si-O-C bond seem to degraft under UV irradiation, leading to a reversible oxidation of the surface. It has to be stated, nevertheless, that no direct proof for this theory could be given in the scope of this work due to the limitation of the analytical methods available.

Taking into account the calculated weight loss values from the TGA measurements (all lower than for the conventional process), no improvement of the grafting process on nc-Si could be achieved with the sequential photografting method.

4.3.12 Thermally-Induced Grafting from nc-Si

A common problem in UV-induced grafting is unwanted light absorption. If the substrate absorbs a high amount of light, the process becomes less efficient since either very high intensities or long durations have to be employed. Within this chapter, two different approaches are discussed: An easy and convenient one-step thermal grafting procedure and a more sophisticated sequential thermal polymerization using TEMPO as a mediator.

In the one-step procedure, H-terminated nc-Si is dispersed in a monomer capable of thermal autopolymerisation. In our case, styrene was used for reasons of comparability, but acrylates and methacrylates could also potentially be used for this kind of grafting. 0.1 wt% dispersions were produced, degassed via three freeze-thaw-cycles and reacted for a certain amount of time at 120°C. Work-up was done according to the general procedure.

As for the initiation mechanism, two different possibilities were recognized. One is the conventional thermal autoinitiation mechanism of styrene, as also described in literature. Hereby, two styrene molecules react *via* a thermal Diels-Alder cycloaddition to form a Diels-Alder adduct. This species is highly reactive as it can regain its aromaticity by transfer of a hydrogen atom to another molecule, thereby generating to radicals.[191] These radicals can

start polymerization in solution and also, by H-abstraction or transfer reactions, on the Si surface. A scheme of the initiation mechanism is depicted in Figure 81.

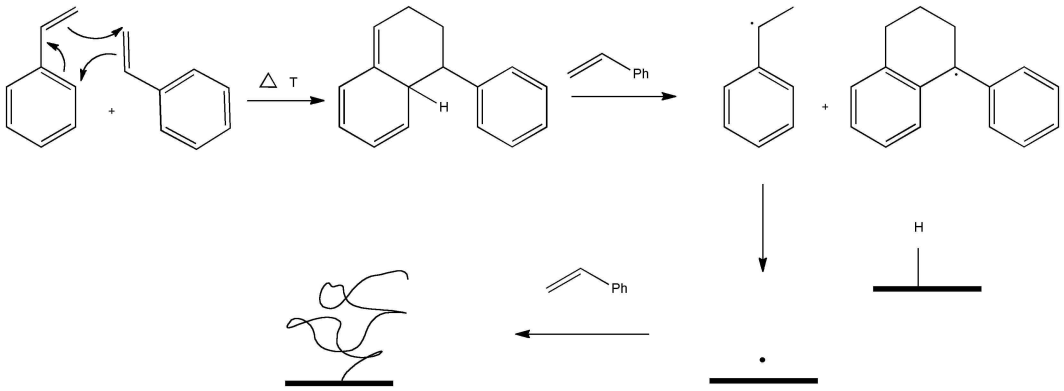

Figure 81: Scheme of the thermal autoinitiation mechanism of styrene leading to grafting from/onto a H-Si surface [159,191]

The problem with this mechanism is that only low grafting densities and thus only low amounts of grafted polymer can be obtained, since the grafting mechanism is more likely to be of the grafting-onto type, as also reported by Moran and Carter.[159]

Another possible initiation mechanism is the thermally induced dissociation of Si-H bonds at the H-terminated silicon surface, leading to surface silyl radicals that can initiate polymerization through a grafting-from mechanism.

One-step Thermoinitiated Grafting

A 0.1 wt% dispersion of H-terminated nc-Si in styrene was degassed via three-freeze-pump-thaw cycles and reacted for 4 h at 120°C. Workup was carried out according to the general procedure.

Figure 82 shows a DRIFT spectrum of nc-Si after 4 h of thermal grafting with styrene.

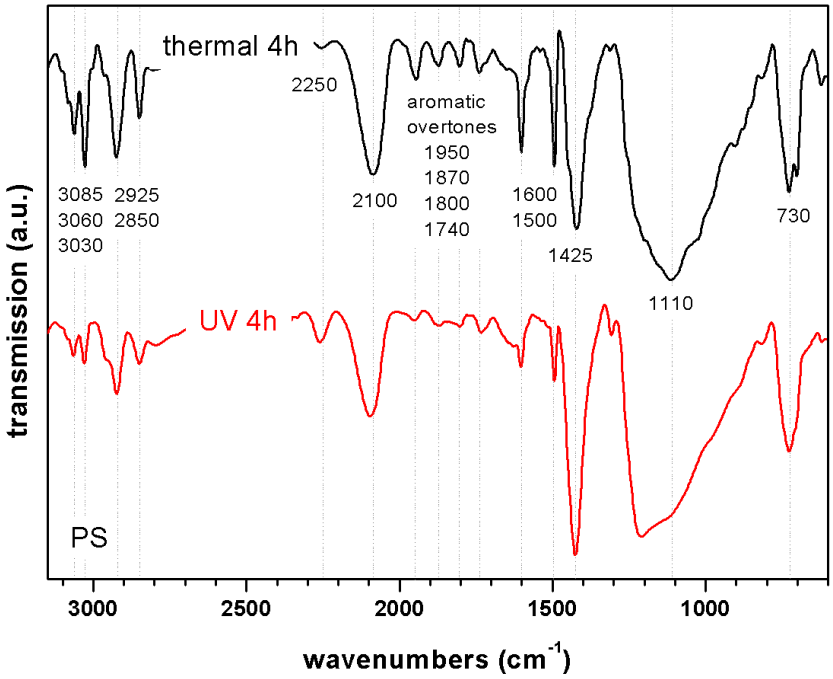

Figure 82: DRIFT spectrum of nc-Si thermally grafted (120°C) with styrene

The DRIFT spectrum in Figure 82 shows clear presence of grafted polystyrene. Exact values and assignments can be found in the appendix. Weight loss determined by TGA was 1.72 %, constituting three times the amount of grafted polystyrene compared to photoinduced grafting. Thus, the thermally initiated grafting on silicon represents a highly effective, fast and convenient way for the functionalization of nc-Si and light absorption by the particles is not of high importance any longer. It has to be taken into account, nevertheless, that viscosity of the samples shows a very steep increase, making work-up very difficult for samples with long reaction times. Besides an increase in grafted polymer, also free polymer showed a strong increase. Compared with the photografted process, the thermally initated method generated 50 times as much polymer, compromising its efficiency. GPC measurements of the precipitated free polymer showed higher molar masses and narrower dispersities for the thermal method in contrast to the photoinduced method. Values can be found in Table 5. Reasons for that can be found in the higher amount of radicals generated in the photoinduced method compared to thermal autoinitiation. If the thermally initiated polymerization is compared to a blind sample of styrene polymerized thermally without addition of initiator, it can be seen that molar masses are even higher and dispersity is lower than for the sample with nc-Si. This clearly shows that nc-Si is involved in transfer reactions with the growing polymer chains, which is not astonishing due to the low BDE of Si-H.

Table 5: M_w, M_n and Đ values for free polymer of nc-Si in styrene (thermal/photochemical) and blind sample of styrene (thermal)

	$\bar{M}_w$ [kg/mol]	$\bar{M}_n$ [kg/mol]	Dispersity Đ
nc-Si in styrene (4 h / 120°C)	405	127	3.18
styrene (4 h / 120°C)	492	176	2.79
nc-Si in styrene (4 h / 350 nm)	249	65	3.85

Sequential Thermoinitiated Grafting

As thermally induced grafting turned out to be very successful in terms of grafting effectiveness, improvements were still to be made. One goal still to be achieved was to obtain an efficient grafting process that would have polymerization taking place only on the particles and not in solution, as this would drastically increase the applicability of this process by minimizing waste and facilitating work-up. An approach that was envisioned to achieve both effectiveness and efficiency was a "true" surface-initiated polymerization using TEMPO both as initiator and mediator for polymerization. In literature surface-initiated NMP (SI-NMP) has already been reported using surface grafted NMP initiators. The attachment of an NMP initiator to a silicon surface has to take place through immobilization of a linker molecule that is hydrosilylated (for H-terminated Si) or condensed (for oxidized Si) to form an initiator monolayer.

In the process used in this work, the initiator and mediator are the same. Literature reports on attachment of TEMPO to silyl dangling bonds, leading to TEMPO layers on silicon.[192,193] Although only reported under UHV conditions, this method should be also applicable for solution processes. As a second step, the TEMPO-grafted silicon substrate is subjected to high temperatures, leading to detachment of TEMPO and radical formation at the surface. From these radicals, we envisioned that polymerization is initiated. A schematic of the process is shown in Figure 83.

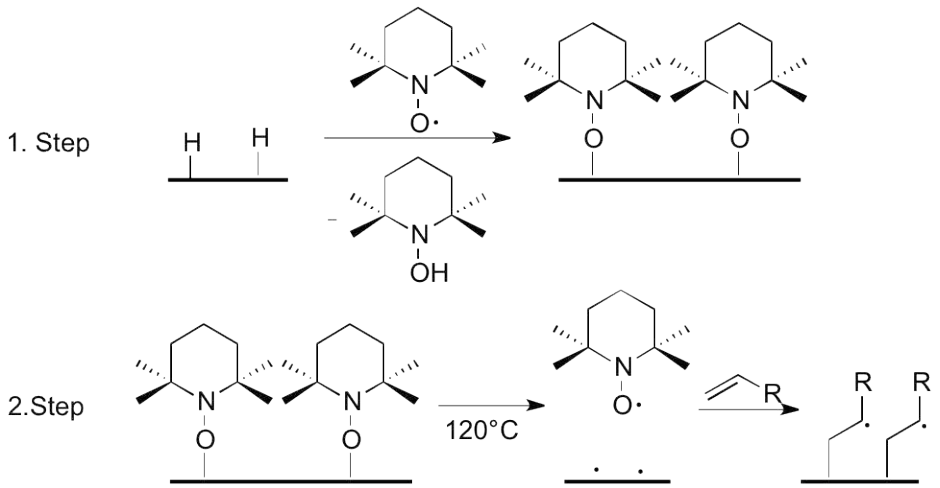

Figure 83: Schematic of the sequential thermoinitiated polymerization using TEMPO

The advantage of this process over the one-step approach is the higher number of radicals generated on the surface compared to the solution and the prevention of the surface hydrosilylation chain reaction by lowering the amount of Si-H bonds. Moreover, detached TEMPO molecules can react with radicals and growing chains formed in solution to control and inhibit polymerization in solution.

For this polymerization method, H-terminated nc-Si were dispersed in a 5 wt% solution of TEMPO in mesitylene to obtain a 0.1 wt% dispersion. The dispersion was reacted for 4 h at 120°C. Figure 84 shows a DRIFT spectrum of nc-Si grafted with TEMPO for 4 h compared to the same substrate after polymerization of styrene (4 h, 120°C) and a UV-grafted reference sample

.

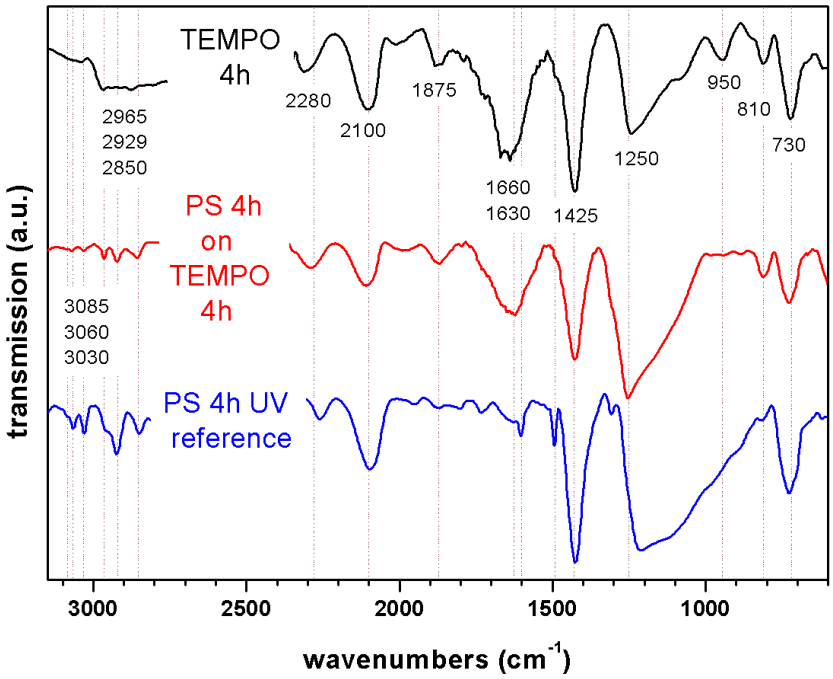

Figure 84: DRIFT spectrum of nc-Si grafted with TEMPO for 4 h at 120°C compared to the same substrate after polymerization of styrene (4 h, 120°C) and a UV-grafted reference sample

The DRIFT spectrum in Figure 84 reveals CH_n stretching vibrations at 2986 cm^{-1} and Si-O-Si-H absorption bands at ~ 2280 cm^{-1}. Si-H stretching bands are also seen at 2100 cm^{-1}, strong NR_3 deformation bands at 1644 cm^{-1}, and CH_n deformation bands at 1425 cm^{-1}. The strong absorption band at 1231 cm^{-1} indicates a high amount of Si-O bonds, that could be from oxidized silicon but also from Si-O-N bonds resulting from the attachment of TEMPO. It can also be mentioned that TEMPO-grafted nc-Si showed a weight increase of 7.59 % after vacuum-drying, indicating good functionalization with TEMPO.

After analysis, TEMPO-grafted nc-Si was dispersed in styrene (0.1 wt) and reacted at 120°C for 4 h and also 16 h. As the dispersion reacted for 16 h could not be filtered, analysis by DRIFT spectroscopy and TGA was only carried out on the sample reacted for 4 h after normal workup. The DRIFT spectrum of the sample is shown in Figure 84.

The spectrum shows characteristic polystyrene absorption bands. Exact assignments can be seen in the appendix. During workup, only 2.6 mg of free polymer could be precipitated. This indiactes that TEMPO is detached from nc-Si and is able to suppress polymerization in solution, thus making the process very efficient since side products are minimized. From the TEM images in Figure 85, the polymer layer around the particles can be clearly recognized.

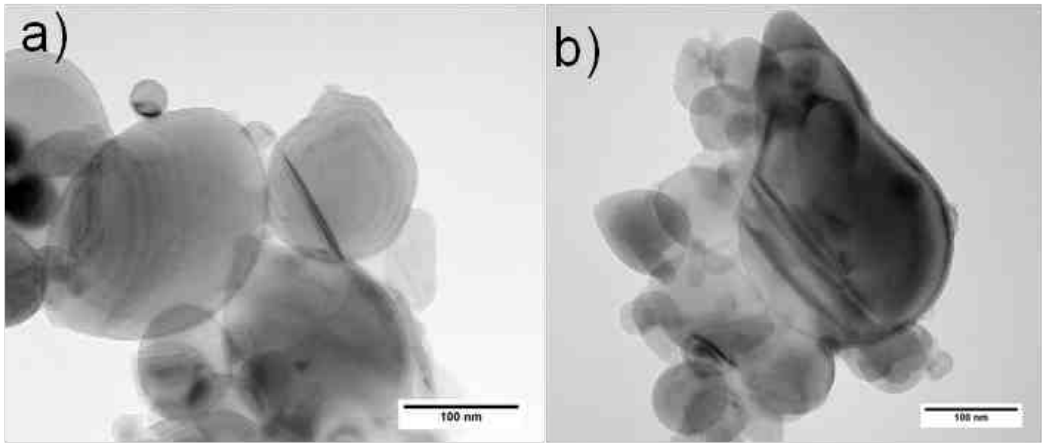

Figure 85: TEM images of TEMPO-nc-Si after 16 h grafting with styrene

Grafted polymer determined by TGA was 2.45 wt%, showing both good grafting effectiveness and efficiency. It can be stated that the sequential thermoinitiated grafting process with TEMPO is a convenient method for the grafting of polymer from nc-Si while minimizing the amount of free polymer formed in solution, thus being a "true" surface-initiated polymerization method.

4.3.13 SIPGP on SiC and Si_3N_4 nanoncrystals

Due to the success of applying the SIPGP procedure on silicon nanocrystals, also other nanocrystalline materials should were testes with respect to their compatibility with the procedure. Silicon carbide, SiC, and and silicon nitride, Si_3N_4, also have a wide range of potential applications, some of them being sensors or optical waveguide materials. In literature, first reports show the possibility of generating monolayers or polymers on SiC[79] and Si_3N_4.[81,82] A hypothetical mechanism of their functionalization was published by Rosso *et al.* [77,78,84] which claims the formation of radicals and/or ions on the surface that are reactive towards unsaturated compounds. These reactive species arise from photoinduced hemolytic cleavage of Si-Si, Si-H, Si-O, Si-N, or O-H bonds and the formation of electron-hole pairs, respectively. The biggest difference between Si and SiC or Si_3N_4 nanocrystals is the surface termination after HF-etching. Since all of the materials bear a native oxide layer, it has to be removed prior to the photografting procedure. After HF-etching, SiC and and Si_3N_4 are not purely Si-H terminated, but with Si-OH and C-OH in case of SiC and Si-H, Si-NH, or Si-NH_2 in case of Si_3N_4.

Experimentally, nc-SiC and nc-Si_3N_4 (obtained from Sigma-Aldrich) was dispersed in monomer to obtain a 0.1 wt% dispersion, degassed *via* three freeze-pump-thaw cycles and etched for 15 min by addition of 0.5 ml 5 % HF in ethanol under protective gas atmosphere. After short degassing to remove evolving SiF_4, the dispersions were irradiated with UV light for 16 h. Workup was done using the general procedure (filtering, washing, drying). Samples were analyzed by DRIFT spectroscopy and TEM.

DRIFT spectra of Si_3N_4 before and after functionalization with styrene are shown in Figure 86.

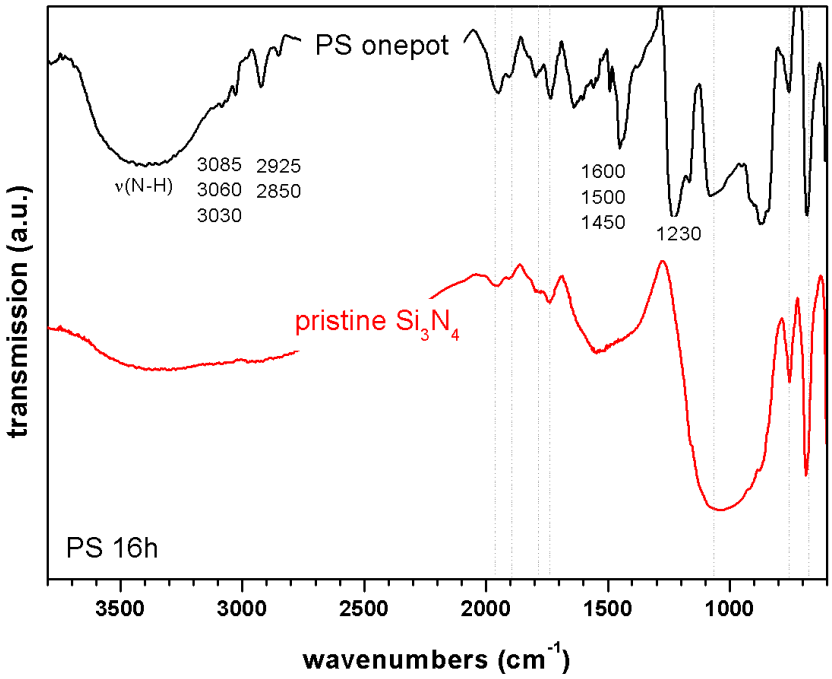

Figure 86: DRIFT spectra of Si_3N_4 untreated (red) and after 16 h photografting in styrene with the "one-pot" route (black)

Exact assignments of absorption bands can be seen in the appendix. Prominent bands in the DRIFT spectrum of PS-grafted Si_3N_4 nanocrystals are resulting from aromatic overtone modes, CH_n stretching, and C=C valence stretching. TGA measurements revealed a weight loss of 4.49 %. This is very high in comparison to both the photografted nc-Si samples (two-step and one-pot method). A reason for this better grafting might be lower light absorption by Si_3N_4, leading to more light available for initiation of polymerization.

As for grafting on SiC, reactivity and surface termination depends on the crystal polytype and on the surface orientation, which was also reported previously.[79] For the polymerization on SiC, it can be stated that under UV irradiation with λ_{max}=350 nm, polymerization only takes place at C-OH facets, since abstraction enthalpy for an Si-O-H hydrogen atom is too high.

Figure 87 shows DRIFT spectra of nc-SiC untreated and after irradiation in styrene for 16 h at 350 nm with the one-pot method.

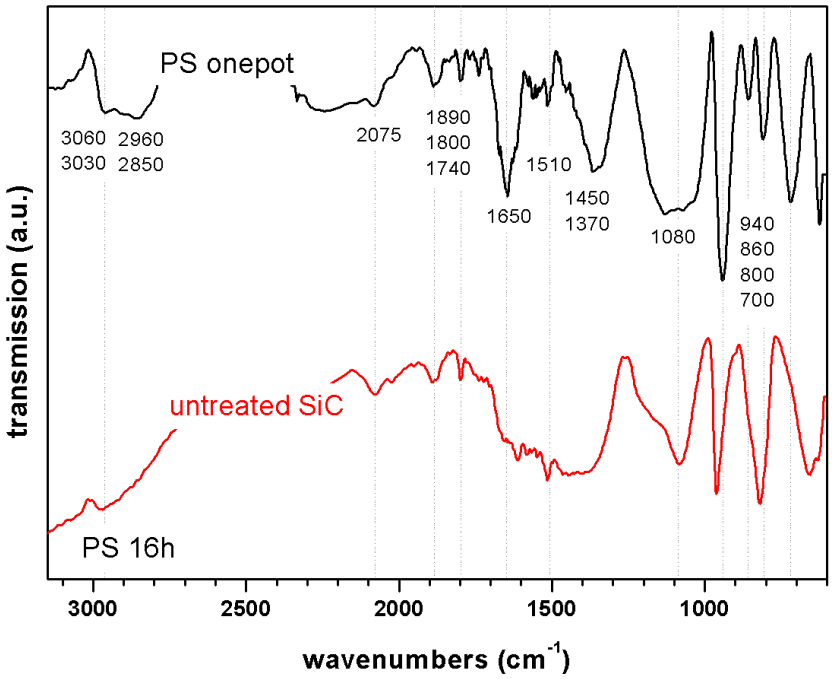

Figure 87: DRIFT spectra of SiC untreated (red) and after 16 h irradiation in styrene (black)

From Figure 87 presence of grafted polystyrene can be concluded. Exact assignments of the absorption bands can be found in the appendix. Together with the TGA weight loss of 2.55 wt%, effective polymer grafting can be confirmed.

Anisotropic Grafting SiC with DMAEMA

In order to see if this reactivity contrast of different facets of SiC with regard to photoinduced grafting is also present in the nanomaterial, SiC nanocrystals were functionalized via photochemical grafting with DMAEMA *via* the "one-pot" route for 15 min.

Figure 88 shows TEM images of untreated nc-SiC and nc-SiC irradiated for 15 min in DMAEMA.

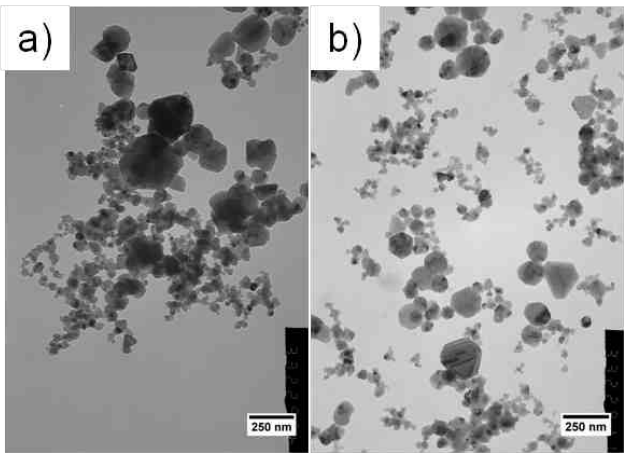

Figure 88: TEM images of nc-SiC before (left) and after 15 min grafting with DMAEMA with the "one-pot" route

As visible in Figure 88, polymer grafting leads to a better dispersion of the agglomerates through steric stabilization of the nanocrystals. This also manifests in better dispersion in a good solvent like ethanol.

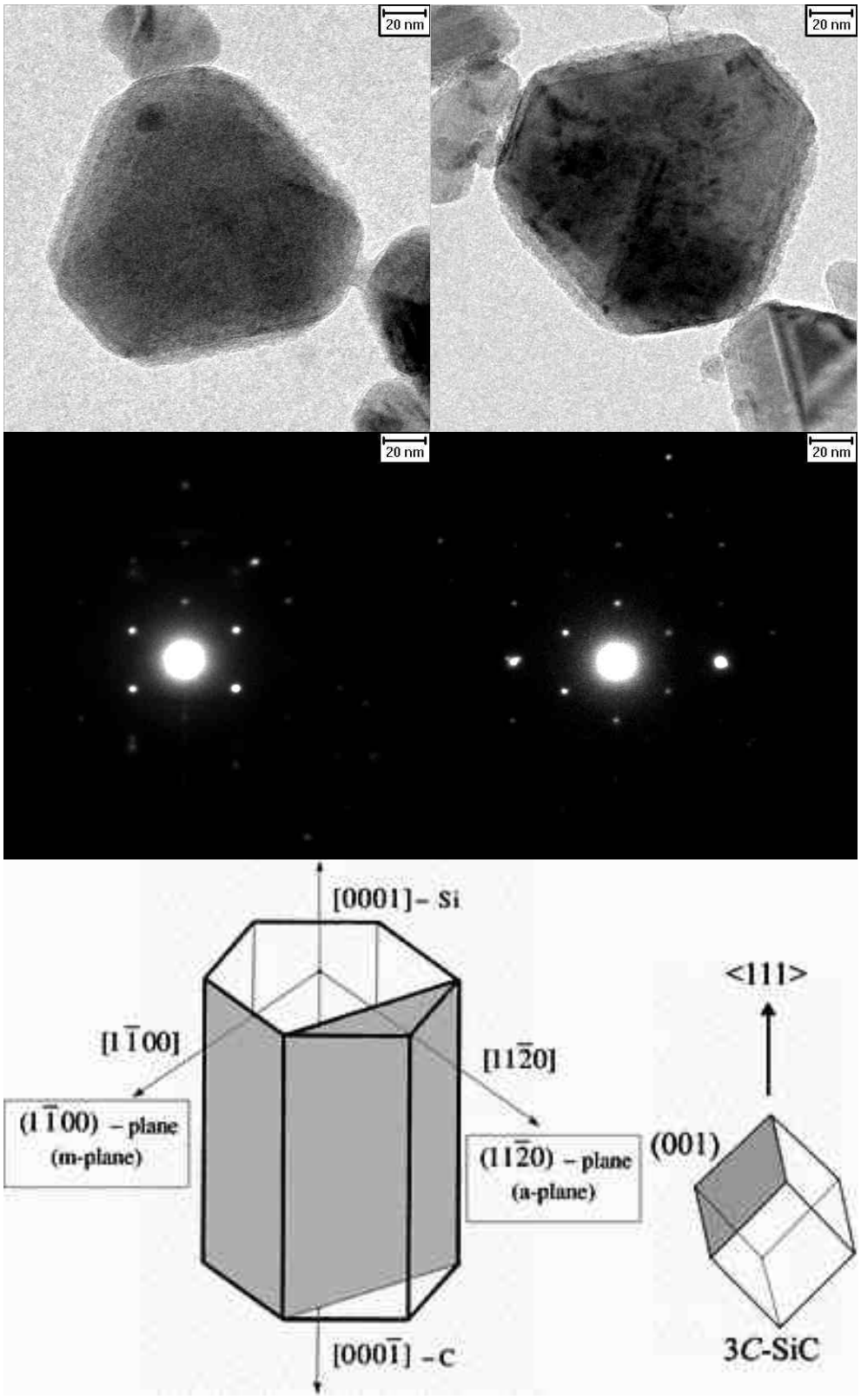

Figure 89: TEM images of SiC nanocrystals and corresponding transmission electron diffraction patterns and illustration of crystallographically inequivalent facets in hexagonal SiC compared to cubic SiC[194]

From the close-up TEM images in Figure 89 and their diffractograms, a difference between the facets can be clearly seen. When polymer is grafted on one facet, the diametrically opposite facet is not grafted with polymer. This confirms the results from literature.[79] However, these results only hold true for hexagonal SiC. As in these experiments, predominantly cubic SiC (as also confirmed by powder x-ray diffractometry) was used, these hexagonal crystals can be regarded as impurities. **Figure 90** shows TEM images of isotropically grafted cubic nc-SiC also present in the sample.

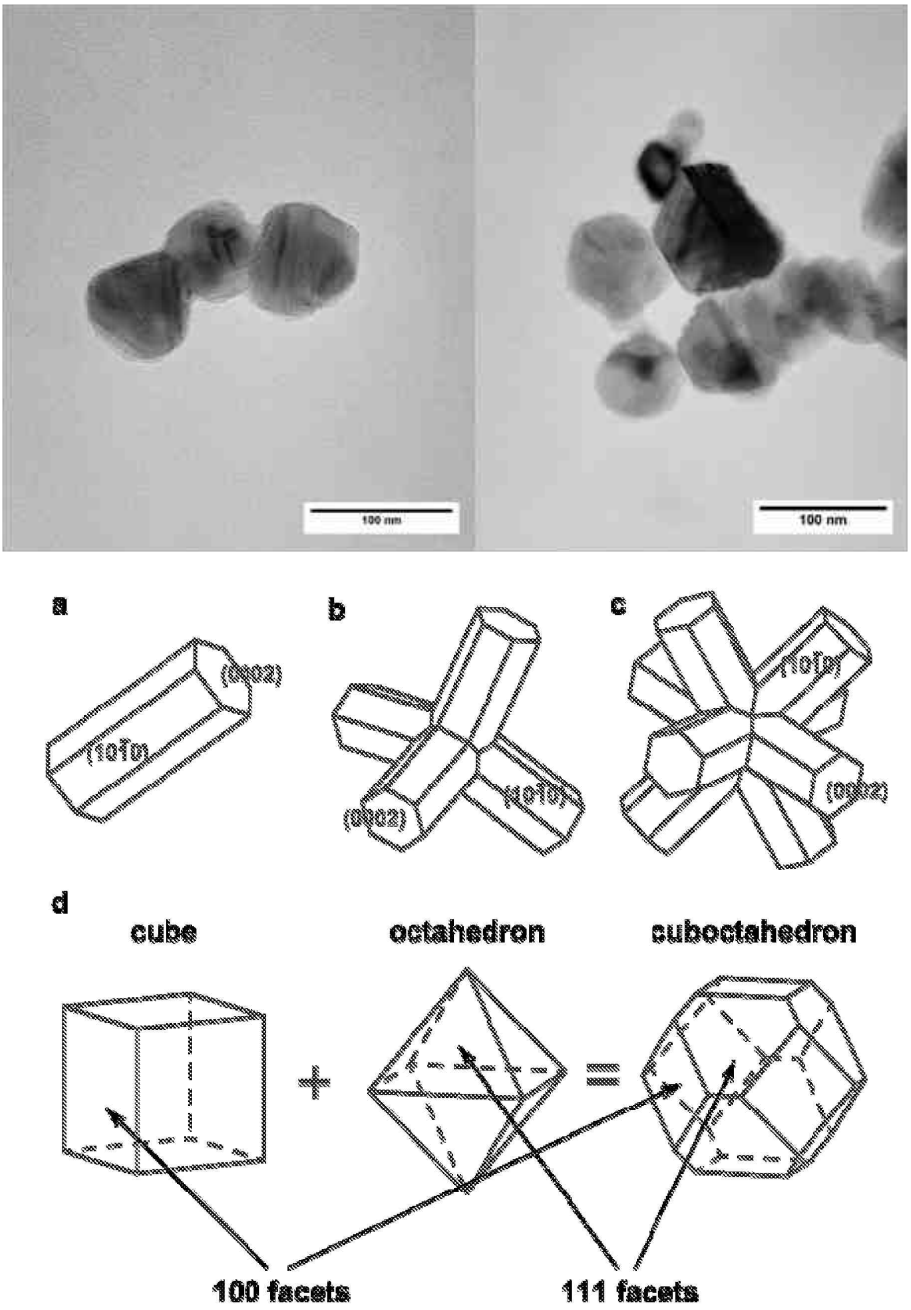

Figure 90: TEM image of nc-SiC cuboctahedra functionalized with DMAEMA for 15 min via the one-pot route and illustration of the cuboctahedron shape[195]

However, on both cubic and hexagonal SiC, a polymer layer can be clearly detected from the TEM images. This can be seen even more clearly in the HRTEM image depicted in Figure 91.

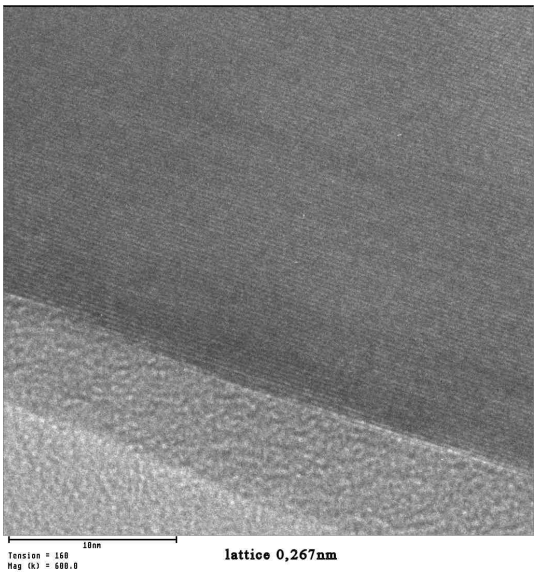

Figure 91: HRTEM image of hexagonal nc-SiC facet with polymer

In the HRTEM image, lattice planes of SiC can be seen with polymer attached to the facet. The lattice spacing of 2.67 Å indicates a hexagonal phase, as also confirmed by the diffraction patterns in Figure 89.[196]The thickness of the grafted PDMAEMA layer can be determined to be approx. 5 nm.

The results obtained from SIPGP on nc-SiC are quite intriguing. Since these nanocrystals show anisotropic reactivity in their hexagonal polytype, there exists a possibility for anisotropic functionalization of those particles. This could in turn enable the convenient synthesis of nc-SiC grafted with two different polymers or functionalities. A possible method for this might be SIPGP in the first step, leading to grafting from C-OH terminated facets and subsequent functionalization of Si-OH groups on the remaining, unfunctionalized facets. This might eventually represent an easy route for the synthesis of novel bifunctional Janus nanoparticles.

4.4 Photoinduced Grafting on Gallium Nitride Substrates

In an effort to test the possibility of grafting onto other relevant semiconductor substrates, gallium nitride was chosen. As a wide bandgap III-V seminconductor, GaN is a potential material for short-wavelength optoelectronic devices.[85] Besides that, GaN possesses high

mechanical, thermal and chemical stability. Together with its biocompatibility, GaN represents an interesting semiconductor material to be functionalized with polymer brushes.

In this work, GaN was first HF-etched to remove the oxidic layer and afterwards OH-terminated in an O_2 plasma. Thus, Ga-OH groups are formed that can be functionalized via the SIPGP process. Unfortunately, a value for the BDE of these Ga-OH hydrogen atoms could not be obtained from the literature.

Experimentally, OH-terminated GaN single crystal substrates were immersed in monomer, degassed via three freeze-pump-thaw cycles and irradiated with UV light for the desired duration. Workup was carried out following the general procedures. Polymerization was performed with the (meth)acrylic monomers methyl methacrylate (MMA), 2-hydroxyethyl acrylate (HEA), 2-hydroxyethyl methacrylate (HEMA), and glycidyl methacrylate (GMA) as well as with styrene and its derivatives 4-bromostyrene (4BS) and pentafluoro styrene (PFS).

Results obtained for grafting of these monomers onto p-type and n-type GaN are summarized in Table 6.

Table 6: Summary of layer thicknesses for different monomers polymerized on n-type and p-type GaN. "*" indicate values at lower UV intensity which are not comparable.

	monomer	polymerization time (h)	layer thickness *via* AFM (nm)
n	styrene	7	100
p		16	125
n	4-bromostyrene	3.5	15*
p		3.5	26
n	pentafluoro styrene	24	55*
p		24	150
n	MMA	2	225
p		3.5	400
n	HEA	3	75
p		-	-
n	HEMA	0.5 (diluted 1:3 in THF)	150

p		0.5 (diluted 1:3 in THF)	25*
n	GMA	3 (diluted 1:1 in THF)	200
p		3 (diluted 1:1 in THF)	122

The results in Table 6 indicate the feasibility of applying the SIPGP procedure to GaN. Unfortunately, the intensity of the UV lamp decreased during some of the experiments, so that not all values are directly comparable. Those values are marked with an asterisk (*). Due to this fact, no direct conclusions could be made about the reactivity contrast between n-type and p-type GaN towards the different monomers. Nevertheless, some general trends could be derived from these experiments. As expected and unlike with silicon, grafting of (meth)acrylates proceeded faster than grafting of styrenics. A problem only appearing during grafting of (meth)acrylates was fast gelation. In case of polymerization in neat GMA, polymer layer thickness was as low as 25 nm and after 150 min of irradiation layer thickness was around 42 nm whereas the bulk monomer already solidified. This indicates very fast polymerization in solution leading to high viscosity very early, preventing effective grafting. To improve grafting performance with GMA, it was diluted with THF a good solvent for both GMA and the resulting polymer that was expected not to take part in the polymerization. This should slow down the increase of viscosity in the bulk monomer, enabling grafting to take place for a longer time until the gelation of monomer. This way, polymer layer thicknesses up to 200 nm could be achieved. HEMA showed a similar behavior, resulting in fast gelation of the bulk monomer after ~ 30 min of irradiation. However, layer thicknesses of over 400 nm could be obtained. Diluting the monomer in a 1:3 ratio in THF resulted in lower layer ticknesses (150 nm after 30 min irradiation for n-type GaN).

When explaining the resulting grafted film thicknesses, several factors have to be taken into account. While external factors like light intensity and monomer purity can be more or less kept constant, other factors resulting from the nature of the different monomers and also reactivity differences between n-type and p-type GaN can strongly influence the grafting process. One single factor strongly affecting polymer grafting is the bond dissociation enthalpy of the surface hydrogen atoms. It is generally expected that lower BDE are attended by higher layer thicknesses due to higher grafting densities. However, as could be shown in the previous chapter on functionalization of silicon, too low BDE can also lead to preference of a surface chain reaction. Unfortunately, no literature values about BDE of GaN could be found in the literature.

To quantifiy the grafting performance, grafting rates (in nm/h) were estimated from the experiments and compared to literature values of the polymerization rate constants. The results can be seen in Table 7.

Table 7: Comparison of grafting rates and propagation rates for different monomers. All data on k_p, estimated at T = 50°C from Ref.[197] unless stated otherwise, except for HEA, estimated at T = 40°C from Ref. [198]

Monomer	Propagation rate k_p ($lmol^{-1}s^{-1}$)	Grafting rate (nm/h)
Styrene	160	14.3 (n-GaN), 7.8 (p-GaN)
4-Bromostyrene	212	4.3* (n-GaN), 7.4 (p-GaN)
Pentafluorostyrene	no data available	2.3* (n-GaN), 6.3 (p-GaN)
MMA	648	112.5 (n-GaN), 114.3 (p-GaN)
HEA	26800	25.0 (n-GaN)
HEMA	2563	300 (n-GaN, 1:3 in THF), 50* (p-GaN, 1:3 in THF)
GMA	~ 1200	66.7 (n-GaN, 1:1 in THF), 40.7 (p-GaN, 1:1 in THF)

From the values in Table 7, a difference in grafting rate of styrenics in comparison to (meth)acrylates can be clearly recognized. Even diluted GMA and HEMA showed much higher grafting rates than styrenics, which can be attributed to the faster propagation rates. The results obtained from grafting of HEA, however, seem a bit peculiar, but due to the limited amount of data, conclusions can not be made.

In order to obtain more exact information about grafting rates, *ex situ* kinetics were measured for the polymerization of styrene, HEA and GMA on n-type GaN, which can be seen in Figure 92.

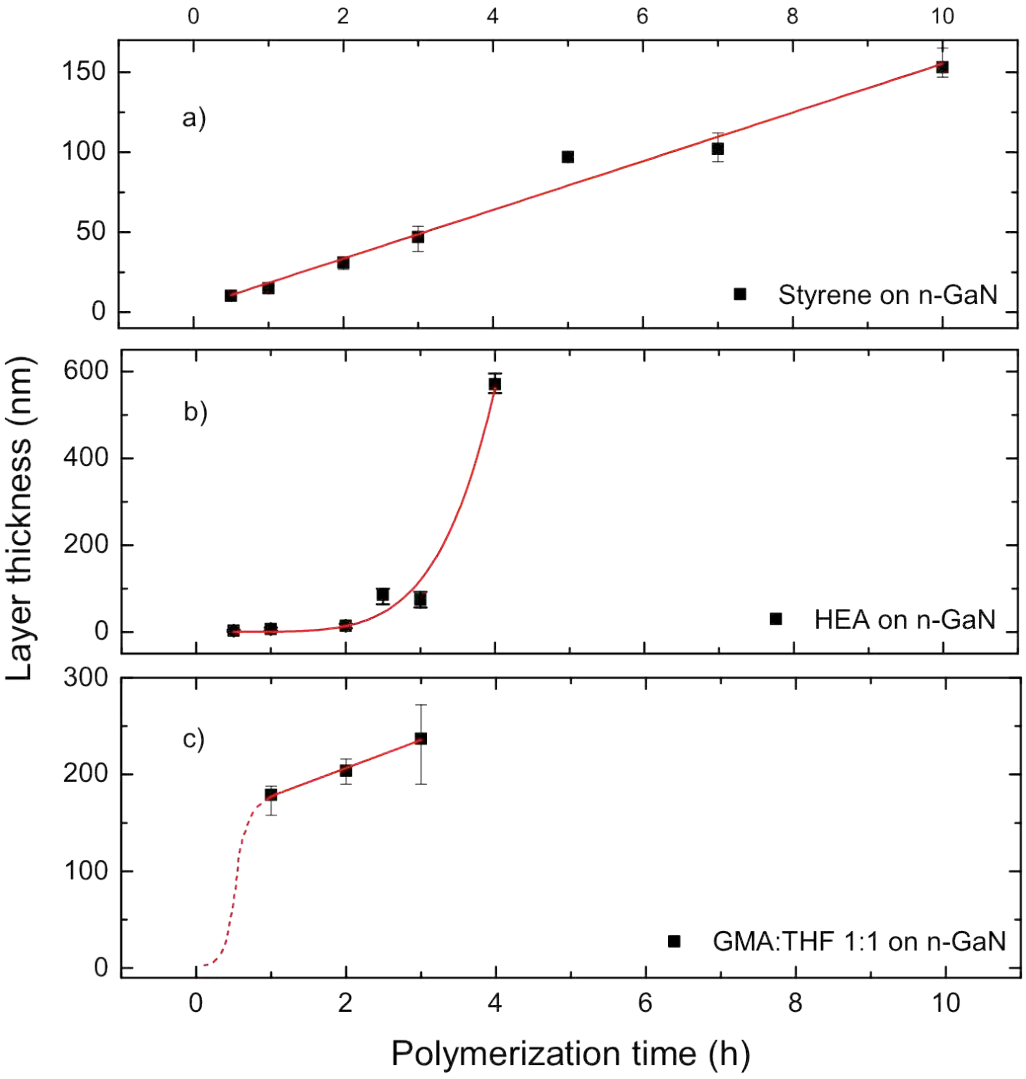

Figure 92: Correlation between layer thickness and polymerization time for (a) styrene, (b) HEA, and (c) GMA 1:1 in THF.

From Figure 92a, a linear correlation of layer thickness with polymerization time for the first 10 h of irradiation can be concluded. For the grafting of n-GaN with neat HEA, an exponential increase after 4 h can be observed. Longer grafting times could not be investigated due to solidification and unwanted crosslinking of the bulk monomer. Grafting of GMA diluted 1:1 in THF shows saturation after ~ 3 h, after which solidification and crosslinking of the bulk monomer prevented further investigation.

In conclusion it can be stated that grafting from both n-type and p-type GaN is feasible for all of the monomers investigated. As expected grafting rates of (meth)acrylic monomers exceeded that of styrenics. Differences in reactivity between n-type and p-type GaN could not be revealed in our experiments and need further investigation.

4.5 Photoinduced Grafting using Graphene as a Substrate

As a relatively new material, graphene has drawn considerable interest from the scientific community in the past decade. Recent work done by our group suggests that the SIPGP can be carried out on graphene as well. Although grafting from perfect graphene cannot be carried out, defects in the form of sp^3-hybridized carbon atoms, preferentially terminated with hydrogen, can be harnessed for grafting. As shown earlier by our group, polymer brushes can be generated by irradiation of graphene in styrene and even photolithographic structuring is possible.[143] Compared to other methods of functionalizing graphene, our procedure has the advantage of not introducing further defects, but using the defects available. In order to prove that theory, polymerization was carried out on graphane, which is hydrogenated graphene. This graphane was synthesized by exposing graphene to hydrogen plasma, effectively converting sp^2-hybridized carbon to H-terminated sp^3-hybridized carbon. By adjusting the plasma's acceleration voltage, surface density of sp^3-carbon and thereby defect density could be controlled. Density of defects can be monitored by Raman spectroscopy via the I_D/I_G ratio.

A correlation of I_D/I_G ratio with acceleration voltage of the H_2 plasma can be seen in Figure 93. Selected hydrogen-terminated graphene samples were then immersed in styrene and irradiated for 8 h and 16 h, respectively and layer thickness was determined by AFM after transferring to silicon substrate. A correlation of polymer layer thickness for 8 h and 16 h grafting and acceleration voltage can be seen in Figure 93.

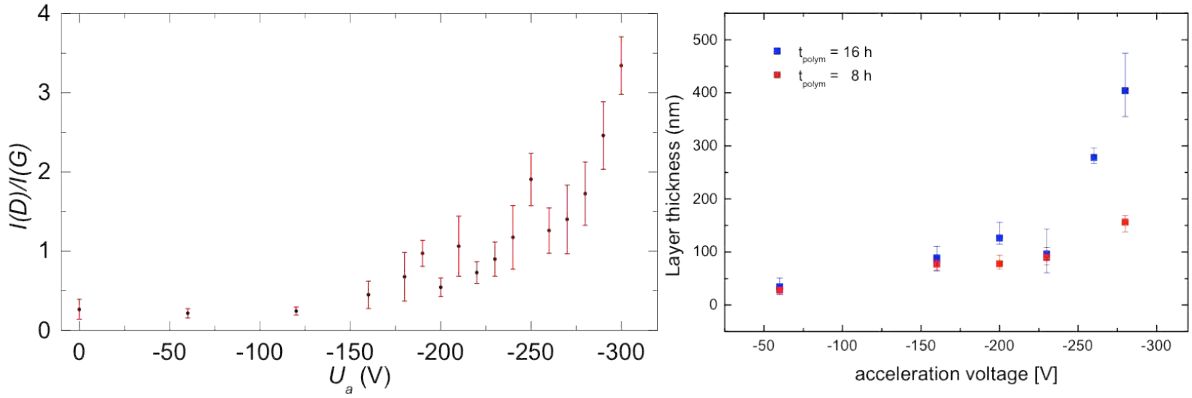

Figure 93: Correlation of acceleration voltage with (left) I_D/I_G ratio and (right) grafted PS layer thickness after 8 h and 16 h grafting

From Figure 93, a dependency of layer thickness from defect density can be seen, which is even more clearly visible when plotting these two parameters against each other, as done in Figure 94.

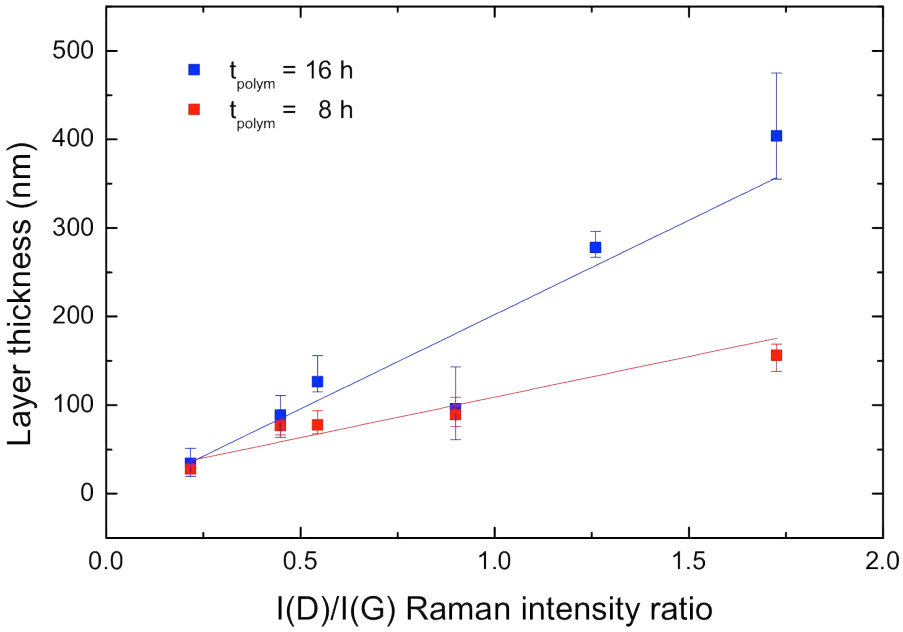

Figure 94: Correlation of grafted PS layer thickness and I_D/I_G ratio

As clearly visible from Figure 94, layer thickness for 8 h and 16 h styrene grafting on hydrogenated graphene shows a linear increase with I_D/I_G ratio. This is not surprising taking into account that polymer layer thickness increases linearly with grafting density. This in turn serves as a proof for our hypothesis that SIPGP starts at sp^3-defects on graphene.

As the general feasibility for the SIPGP procedure on graphene and graphane is shown, also other monomers were to be tested that could eventually lead to graphene grafted with functional polymers. Among the monomers investigated were MMA, DMAEMA, methacrylatoethyl trimethyl ammonium chloride (METAC), 4VP, but none of these lead to grafting on graphene. As a specific monomer-substrate interaction was assumed, grafting of styrene derivatives 4-bromostyrene and pentafluorostyrene (structures can be seen in Figure 95) was investigated.

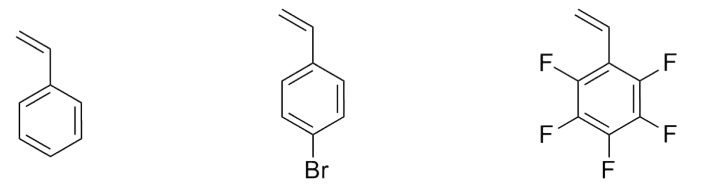

Figure 95: Structural formulas of styrene, 4-bromostyrene and pentafluorostyrene

All of these monomers have a common structural feature, the aromatic carbon six-membered ring. This ring is assumed to exert a specific interaction with the graphene substrate, most presumably π-π interactions. This might lead to a favored preorientation or better proximity to the substrate, allowing a more effective abstraction of hydrogen atoms.

Table 8 gives an overview over layer thicknesses of styrene, 4BS and PFS grafted on pristine graphene.

Table 8: Polymerization of styrene and two styrene derivatives on graphene results in different layer thicknesses after different polymerization times. †: T = 40 ◦C, data from Ref. [197].

monomer	t_{polym} (h)	Layer thickness (nm)	Propagation rate k_p ($lmol^{-1}s^{-1}$)
styrene	16	34	160
4BS	5	150	212
PFS	24	160	not available

If a linear increase of polymer layer thickness is assumed, then styrene grafting rate on graphene is around 2.13 nm/h, PFS has a rate of 6.67 nm/h and 4BS a rate of 30 nm/h. The differences in grafting rates can be attributed to different propagation rates on the one hand and to different initiation efficiencies on the other. Moreover, branching could also influence grafting rates. When comparing styrene to PFS, differences in grafting rates are not very pronounced. However, since no date on the propagation rate constant of PFS could be obtained, no conclusion could be made about that. The grafting rate of 4BS is about an order of magnitude higher than for styrene, also polymerization rate constant lie in the same regime. This might be explained by the fact that the C-Br bond is weak compared to an aromatic C-H bond. At only 272 kJ/mol, bromine radicals can be easily abstracted by activated monomers, leading to a high degree of grafting. Moreover, it is possible that the initiation mechanism in

general and the intersystem crossing in particular is more effective for 4BS due to the heavy atom present.

Copolymerization and graft-Copolymerization

Since only grafting of styrene derivatives was successfully achieved on graphene, methods to graft other monomers were still to be found. Although the bromine moiety of P4BS is in principle accessible for post-polymerization modifications of the polymer brushes generated via the SIPGP process, reactions involved are cumbersome and necessitate the use of a catalyst and harsh reaction conditions in many cases. Therefore, the use of (meth)acrylic monomers with inherent functionalities, like DMAEMA or HEMA, is still an interesting topic. As a model system to test these reactions styrene/MMA was chosen as it was known to from statistical copolymers when polymerized radically. The reactivity ratios of styrene (A) and MMA (B) are $r_A = 0.52$ and $r_B = 0.46$. To compare results, a second approach was also tested, namely the grafting of polystyrene and subsequent grafting of PMMA to the polystyrene primer layer. Both approaches were carried out on graphene as well as on graphane and analyzed via DRIFT spectroscopy and AFM.

Table 9 shows a summary of the AFM results.

Table 9: Layer thicknesses observed for copolymerization of styrene and MMA on graphene and graphane, compared to the layer thicknesses observed for homopolymerization of styrene.

	styrene	**MMA**	**styrene-co-MMA**	**styrene-graft-MMA**
graphene	16 h, 34 nm	5 h, 0 nm	24 h, 46 nm	16 h (PS) + 5 h (PMMA), 135 nm
graphane	24 h, 150 nm	5 h, 0 nm	24 h, 150 nm	16 h (PS) + 5 h (PMMA), > 600 nm

To verify presence of both monomer unit in the graft, DRIFT spectroscopy was carried out. A comparison of DRIFT spectra of graphene grafted with pure polystyrene, poly(styrene-stat-MMA), and poly(styrene-graft-MMA) can be seen in Figure 96.

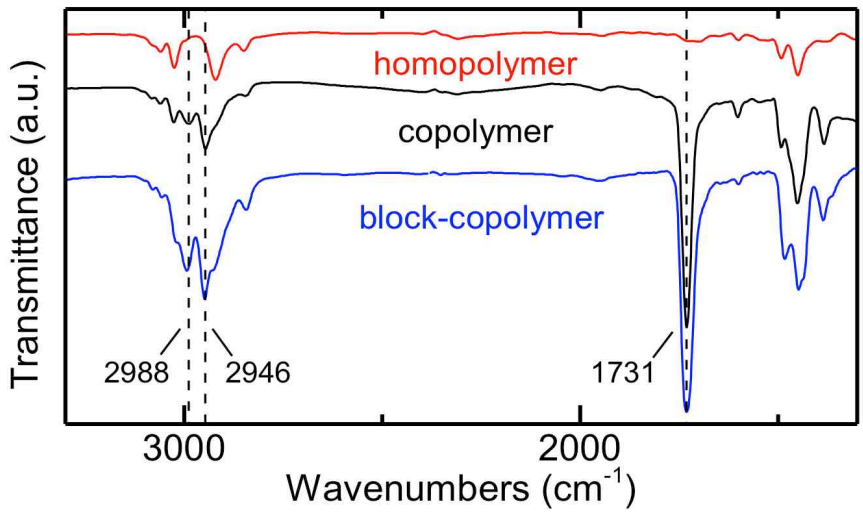

Figure 96: DRIFT spectra of polystyrene, poly(styrene-stat-MMA), and poly(styrene-graft-MMA) grafted from graphene

From the DRIFT spectra of both copolymers, presence of grafted MMA beside styrene can be confirmed. This can be most unambiguously proven by presence of the C=O stretching of the MMA unit at 1731 cm^{-1}.

In order to obtain functional polymer brushes directly in a one-step procedure, styrene was copolymerized with both HEMA and DMAEMA, which do not polymerize on graphene when polymerized alone. 1:1 mixtures of styrene with both monomers were grafted on graphene and analyzed with DRIFT spectroscopy to prove the presence of methacrylic units in the polymer chains.

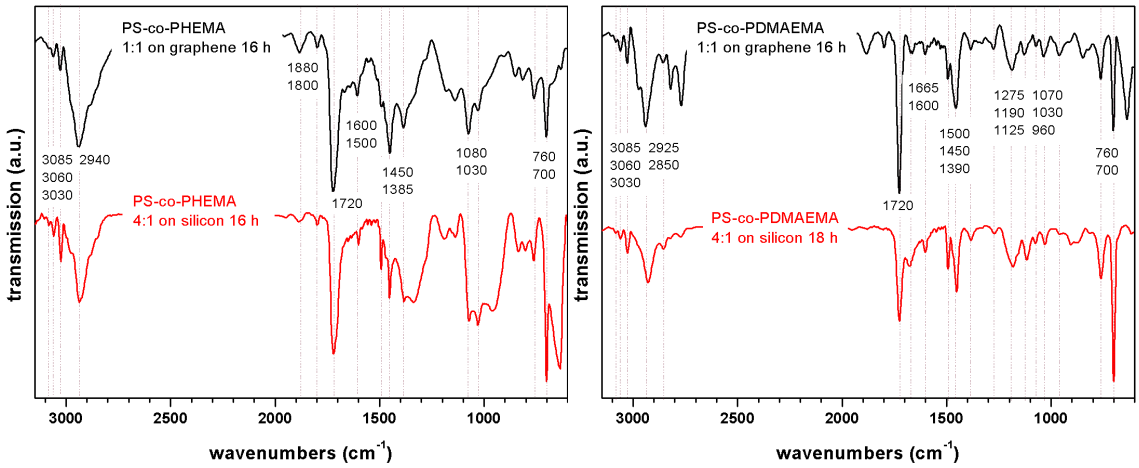

Figure 97: IR spectrum of PS-co-PHEMA and PS-co-PDMAEMA grafted from pristine graphene (both 1:1 molar ratio, 350 nm, 18 h) in comparison to the copolymer-grafted silicon substrates from chapter 4.1.7

From the very close accordance of the IR spectra of copolymer-grafted graphene compared with Si substrates grafted with the same copolymer systems, the presence of grafted functional copolymers on graphene can be proven.

Thus, this method represents a versatile route for the grafting of functional polymers from graphene substrates, that could then be further modified to yield chemically-sensitive graphene transistors.

4.7 Conductive Polymer/Semiconductor Nanohybrids by Surface-Initiated KCTP

Functionalization of semiconductor surfaces with conductive polymers is of special interest with regard to photovoltaic applications. Therefore, methods are to be found to obtain a stable grafting of conductive polymer to various semiconductor substrates.

As Senkovskyy *et al*. already showed, poly(3-hexylthiophene) P3HT can be grafted from brominated polystyrene *via* Surface- Initiated Kumada Catalyst-Transfer Polycondensation (SI-KCTP) to yield P3HT grafts stably attached to a glass surface.[152]

In our work, we combined the facile surface photografting method to generate surface-grafted poly(4-bromostyrene) P4BS that can be used as an initiator precursor for SI-KCTP. Advantages of this method lie in the synthetic ease of this combination of the two methods, involving a straightforward two-pot synthesis protocol.

4.7.1 P3HT bottle-brush brushes on Si(100)

In a first set of experiments, P4BS was grafted from H-terminated silicon *via* the two-step photografting method described in chapter 4.2. The sequential photografting was chosen since one-step grafting of 4-BS resulted only in very thin polymer layers.

The P4BS initiator layer was analyzed with IR spectroscopy. IR spectra of the Si surface after sequential grafting and P4BS one-step reference substrate are shown in Figure 98 and confirm the presence of grafted P4BS on the surface. The P4BS layer thickness was 40 nm.

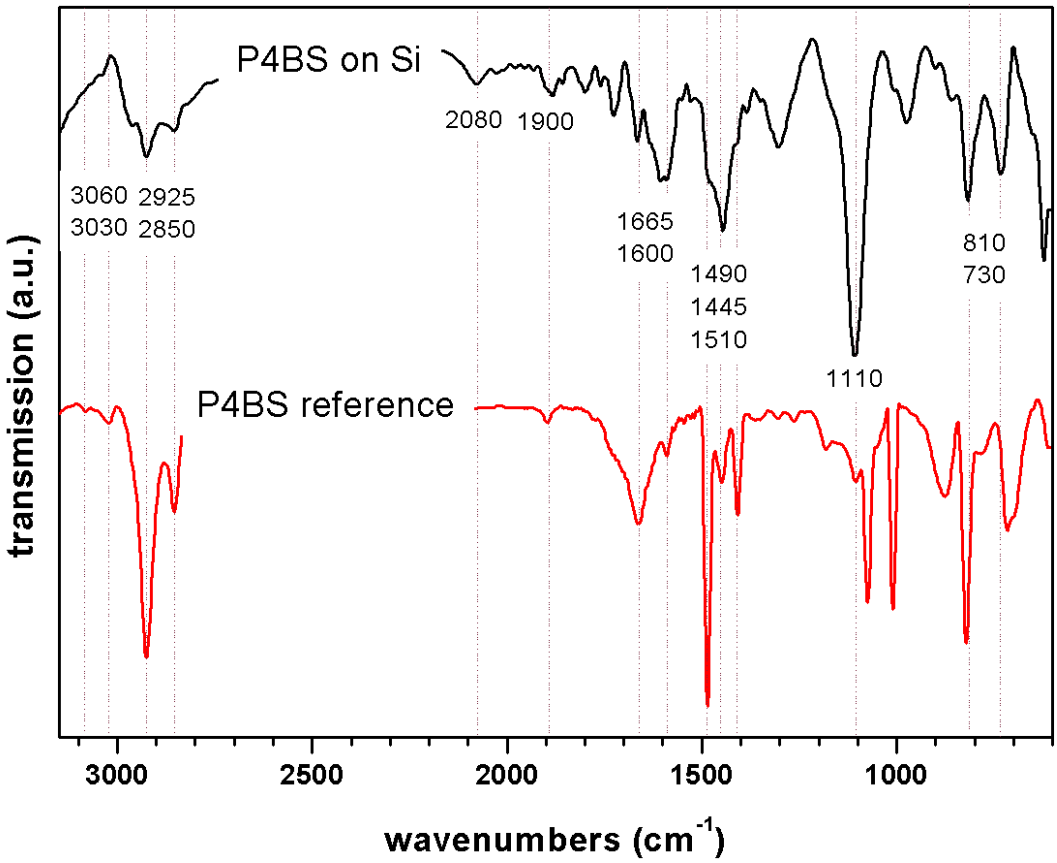

Figure 98: IR spectra of P4BS-grafted silicon substrate (3 h BP pregrafting, 12 h irradiation in bulk 4BS) and P4BS reference (4 h UV grafting in bulk 4BS)

Afterwards, the substrate was immersed over night in a 0.5 wt% solution of $Ni(PPh_3)_4$ in toluene. Then, dppp ligand was added to initiate a ligand exchange. After 2 h of ligand exchange, monomer 2-bromo-5-chloromagnesio-3-hexylthiophene was added to start polycondensation and the reaction was allowed to proceed over night.

After quenching with HCl/MeOH, the surface was cleaned by sonication and washing in different solvents.

IR spectroscopy (see Figure Figure 99) proves presence of P4BS-g-P3HT and polymer layer thickness was determined to be 140 nm after P3HT grafting *via* AFM.

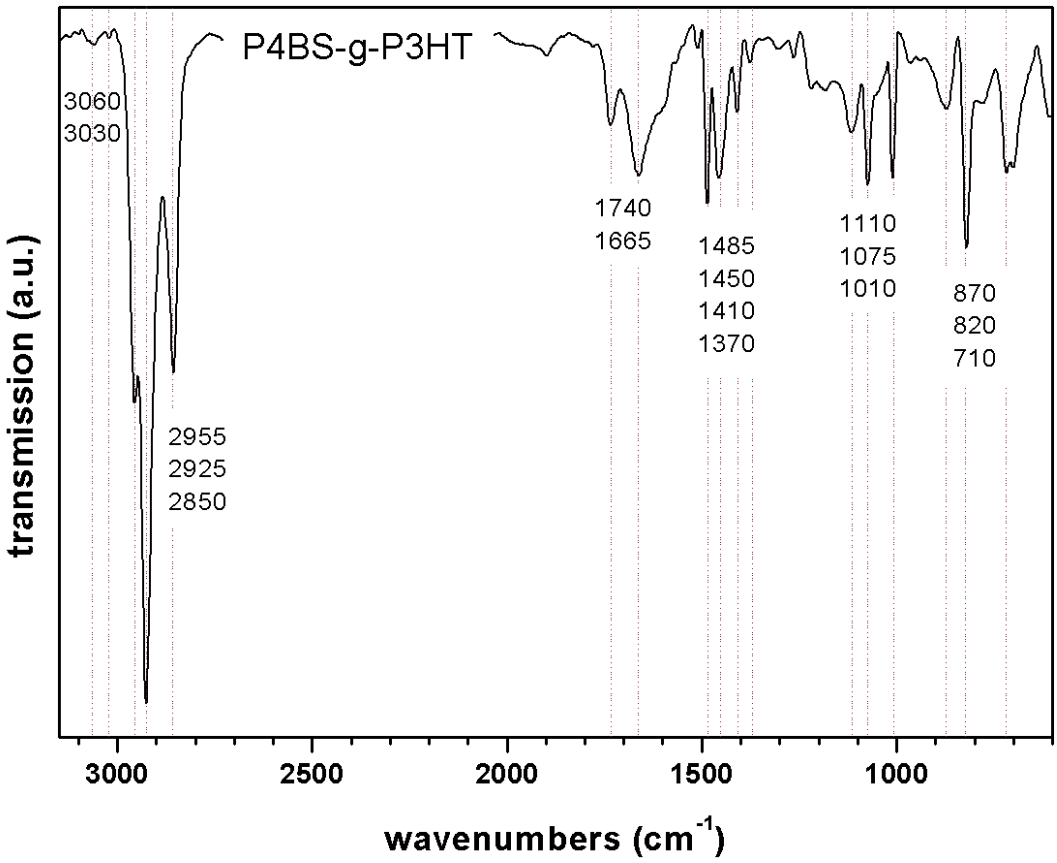

Figure 99: IR spectrum of silicon surface grafted with P4BS-g-P3HT bottle-brush brushes

4.7.2 P3HT-grafted nanocrystalline silicon

As this grafting process is a way to generate conductive-polymer/semiconductor hybrid materials, it should be applied nc-Si. These new hybrid nanomaterials could have interesting electronic properties and might be used in thin-film photovoltaics.

For the grafting of P3HT on nc-Si, the process was slightly altered. Instead of photografting of P4BS, a monolayer of 4-bromophenylacetylene (BPA) was immobilized on H-terminated nc-Si via thermally induced hydrosilylation. Therefore, freshly HF-etched nc-Si was dispersed in a solution of BPA in toluene, the dispersion was degassed and reacted at 100°C for 18 h. After filtration, washing and drying, the sample was analyzed by IR spectroscopy.

In the second step, the BPA-grafted nc-Si was immersed over night in a 0.5 wt% solution of $Ni(PPh_3)_4$ in toluene. Then, dppp ligand was added to initiate a ligand exchange. After 2 h of ligand exchange, monomer 2-bromo-5-chloromagnesio-3-hexylthiophene was added to start polycondensation and the reaction was allowed to proceed over night.

After quenching with HCl/MeOH, the particles were cleaned by filtration and washing and then dried *in vacuo*. The sample was analyzed by IR spectroscopy and TEM.

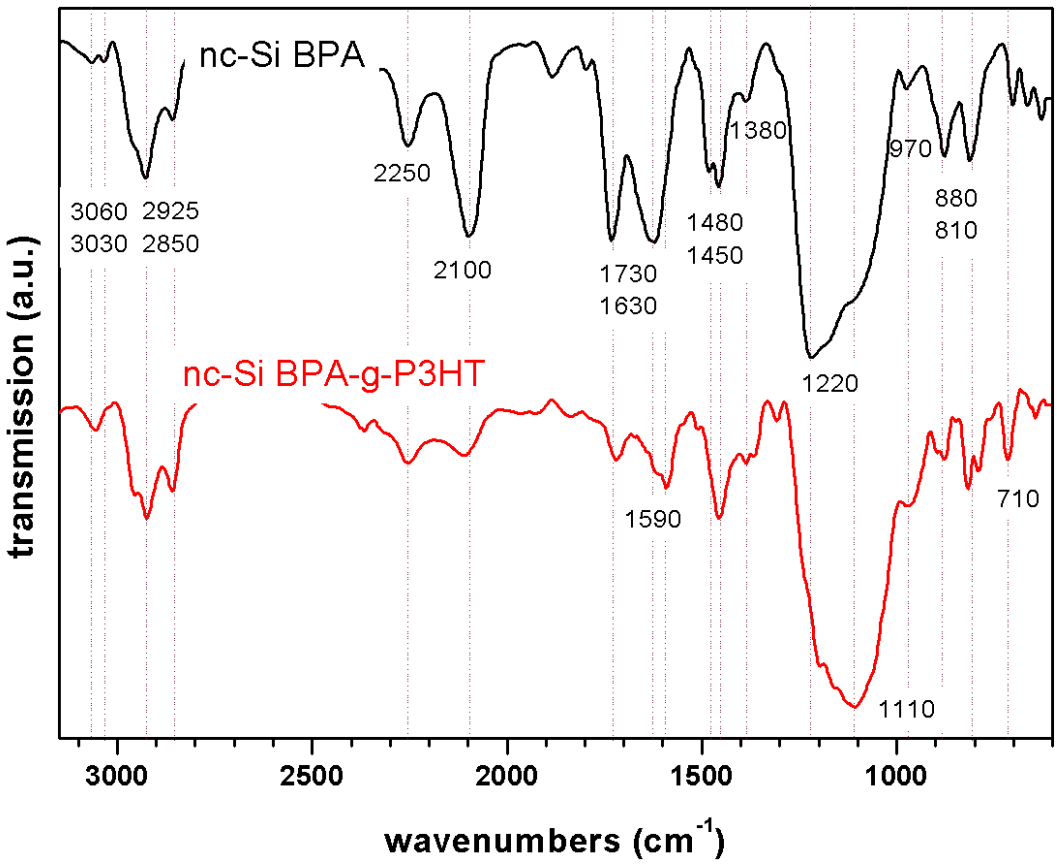

Figure 100: Nanocrystalline silicon after grafting with BPA (100°C, 18 h) and after subsequent P3HT grafting

From the IR spectra in Figure 100 no direct evidence for presence of grafted layer can be made, although a certain amount of organic material can be detected on the nc-Si. The small difference in the IR spectra, however, does not allow for a exact assignment of BPA- or P3HT-related vibration bands. Nevertheless, a first indication for successful grafting is the color of the particles, which changed from light-brown to very dark brown, presumably due to additional absorption of light by grafted P3HT.

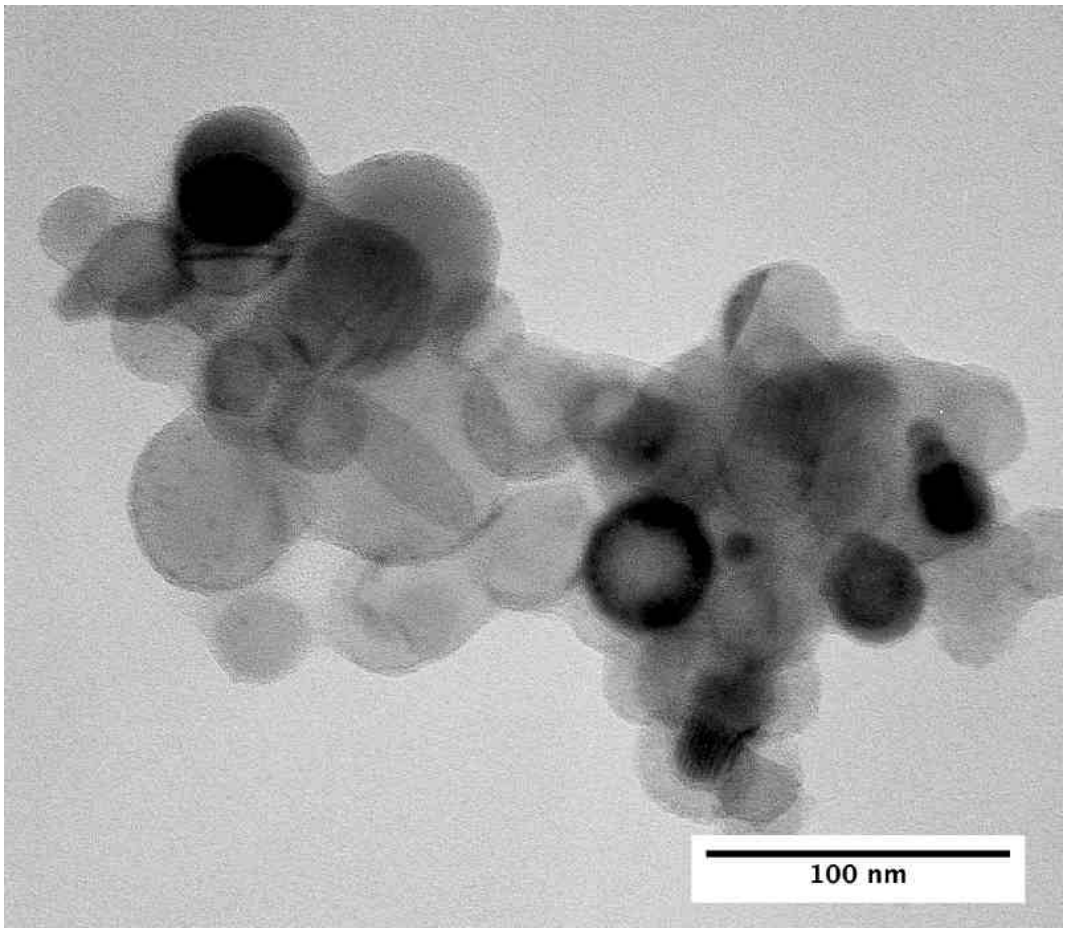

Figure 101: TEM image of nc-Si grafted with P3HT

From the TEM image in Figure 101, a thin homogeneous layer of polymer can be seen around each particle. However, particles are agglomerated or even aggregated and polymer can also be seen between single particles.

From these first preliminary studies, the feasibility of this grafting process for the generation of functional P3HT-Si-nanohybrid could be shown. In future experiments, P3HT grafts on luminescent nc-Si will be investigated with respect to their optical properties and their application in nc-Si/P3HT thin-film photovoltaics similar to those reported in literature.[69]

4.7.3 P3HT bottle-brush brushes on graphene

Grafting of conductive polymers on graphene is of high potential relevance, since graphene is projected as a cheap replacement for ITO in hybrid organic-inorganic solar cells. For this application, stable grafting of conductive polymer onto graphene is crucial.

Therefore, we developed a method for covalent grafting of P3HT from pristine graphene via a aryl bromide initiator/linker layer. For the generation of this layer, two different concepts are utilized, which are shown in **Figure 102**.

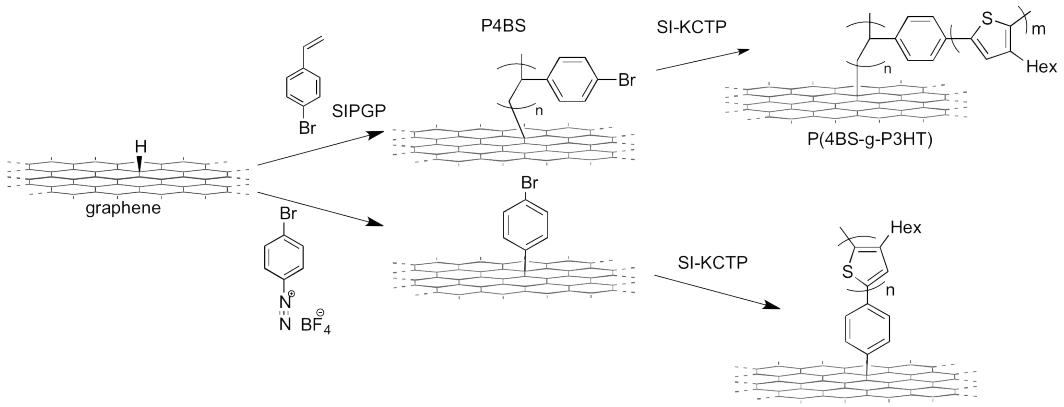

Figure 102: Schematic drawing of the two different routes for functionalization of graphene with P3HT

The first route utilizes grafting of a diazonium salt, 4-bromophenyldiazonium tetrafluoroborate to obtain bromophenyl moieties directly linked to graphene. The second route involves functionalization of already present hydrogen defect sites via the self-initiated photografting and photopolymerization (SIPGP) of 4-bromostyrene. AFM images of these two initiator layers can be seen in Figure 103.

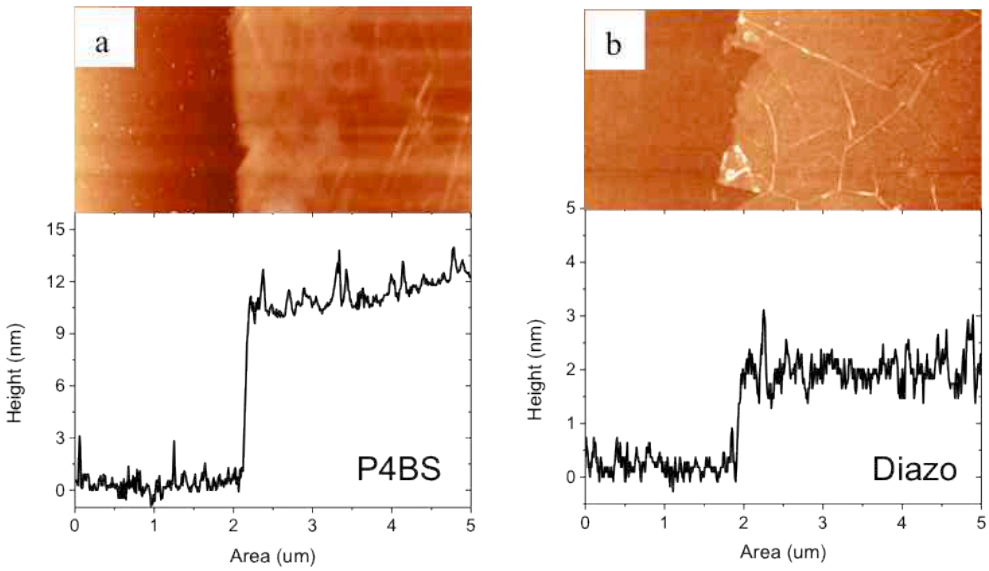

Figure 103: AFM and height profiles at scratch edges following functionalization of graphene with (a) bulk 4-bromstyrene (40 min UV) and (b) 4-bromophenyl diazonium tetrafluoroborate in water (1 h at room temperature)

The height of the P4BS-grafted graphene was determined as approx. 10 nm and the diazonium-grafted graphene was approx. 2 nm. This also accords with the different structures formed for the two processes, polymer brushes in case of P4BS-grafting and mono- or multilayers in case of diazonium grafting.

Independent from the route chosen for the generation of the initator layer, the bromophenyl-grafted graphene is immersed in a catalyst solution for generation of a first initiator species and a ligand exchange step is carried out to obtain a more stable catalyst species. After catalyst immobilization, a 3-hexylthiophene monomer with both a bromine and a chloromagnesium Grignard functionality is added which then polymerizes via a Kumada catalyst-transfer polycondensation starting from the surface-immobilized catalyst species.

Figure 104 gives a comparison between P3HT-grafted graphene synthesized with the two different methods.

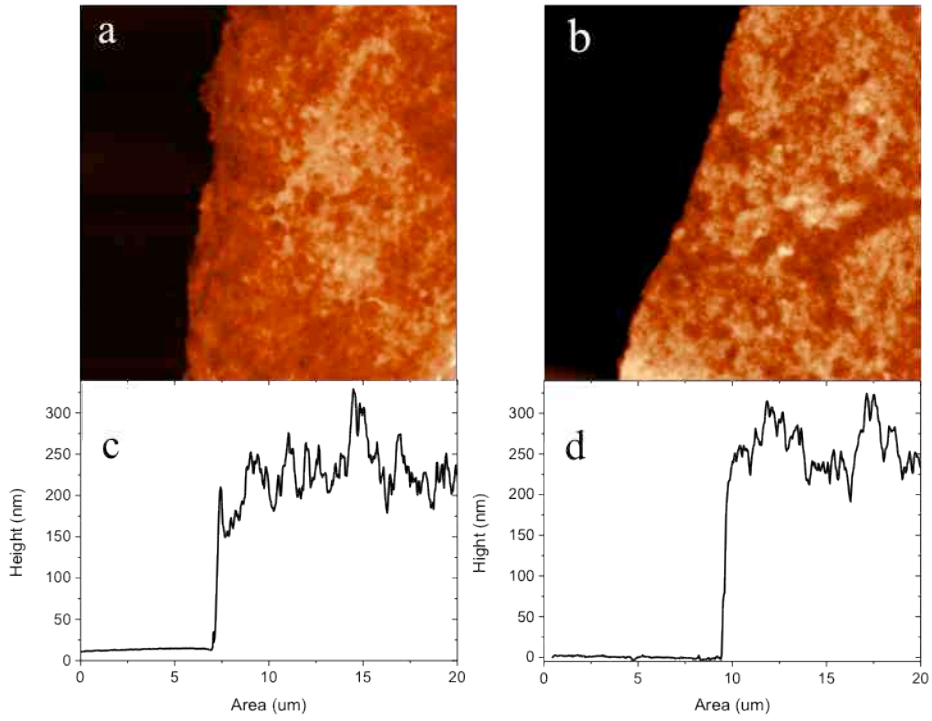

Figure 104: AFM topography images (a, b) and cross-sections (c, d) of the scratched area of grpahene grafted with PSBr-g-P3HT bottle-brush brushes (left) and diazonium-g-P3HT brushes (right).

Height analysis of the AFM images in Figure 104 gives a polymer layer thickness of 200 nm for P4BS-g-P3HT-grafted graphene and 250 nm for phenyl-g-P3HT-grafted graphene.

At first, these results seem surprising when the initial heights of the graphene sheets with grafted immobilization layer are taken into account. While the thickness of the P4BS initiator layer was around 10 nm, the phenyl bromide grafted graphene had around 2 nm in thickness. However, thicknesses after grafting of P3HT even show a higher layer thickness for the diazonium grafted than for the P4BS-grafted graphene. A possible explanation for this finding lies in the nature of the different grafting reactions. As in the P4BS grafting only already existing defects are grafted from, the diazonium salt route is known to induce additional defects, which could lead to a higher grafting density in the subsequent P3HT grafting which leads to thicker layers. The generation of these defects was probed by Raman spectroscopy of the different graphene substrates, which is shown in Figure 105.

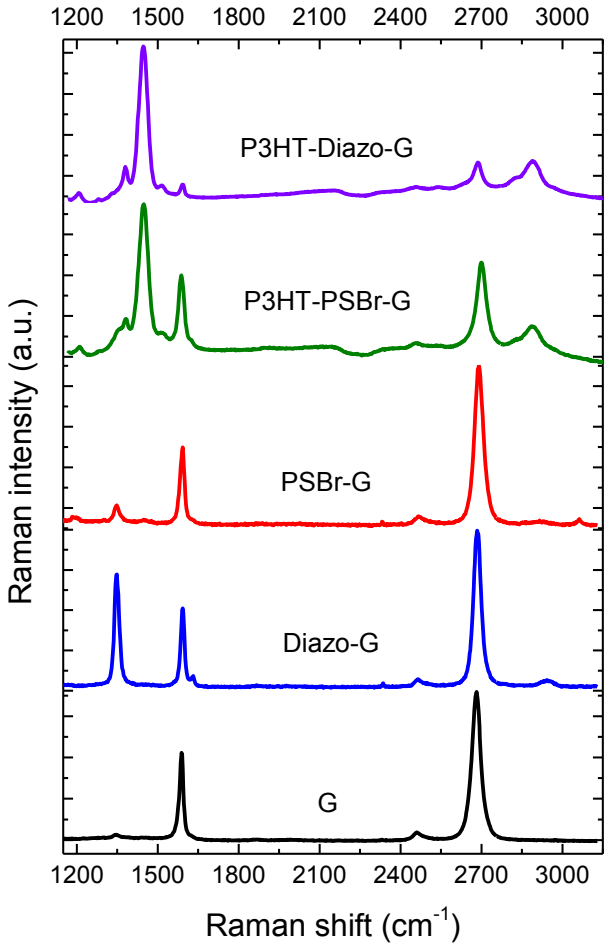

Figure 105: Comparative Raman spectra from as-grown graphene and bromophenol initiator poly(4-bromostyrene) (PSBr-G) or 4-bromobenzene diazonium tetrafluoroborate (Diazo-G) immobilized graphene and further modified by SI-KCTP with P3HT.

As results from these measurements illustrate (see Figure 105), the photoinduced grafting of bromostyrene does not lead to an increase in the I_D/I_G intensity ratio of the graphene substrate, whereas the diazonium route indeed induces a high amount of defects (sp^3-hybridized carbon atoms). This is in accordance with the two different mechanisms because grafting *via* SIPGP only takes place at already existing defect (C-H) sites, while diazonium grafting proceeds *via* electrophilic attack with the introduction of defects.

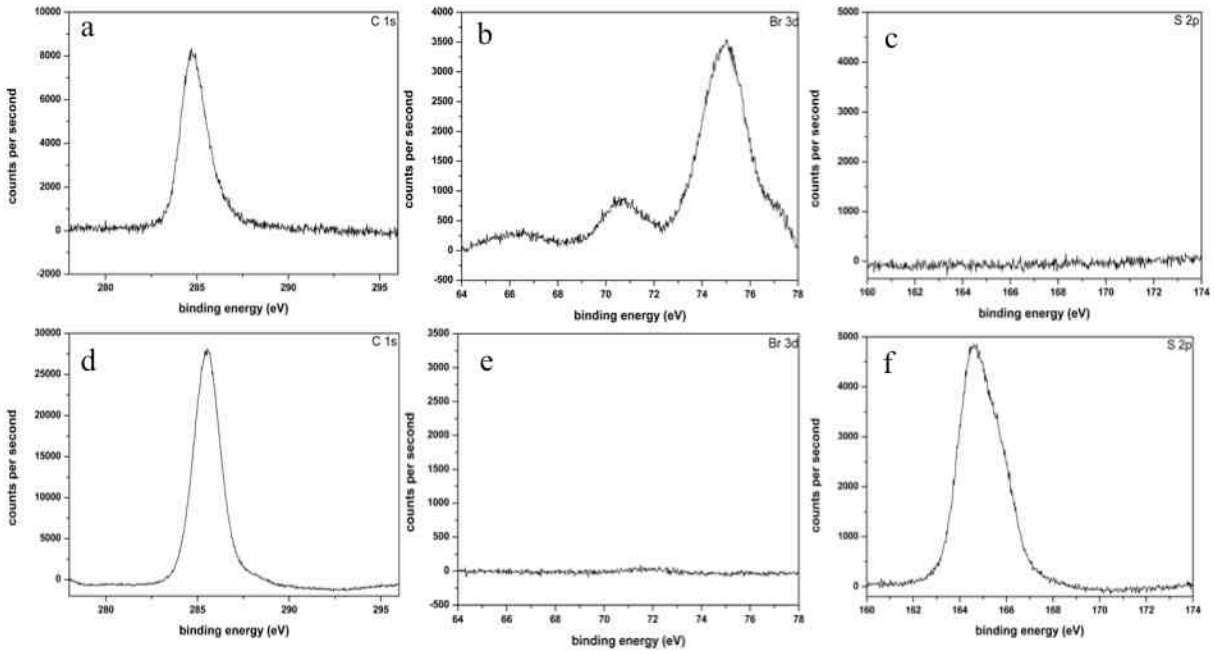

Figure 106: XPS spectra of a graphene sheet grafted with 4-phenyldiazonium tetrafluoroborate before (a,b,c) and after (d,e,f) SI-KCTP for the elements carbon (a,d), bromine (b,e), and sulfur (c,f)

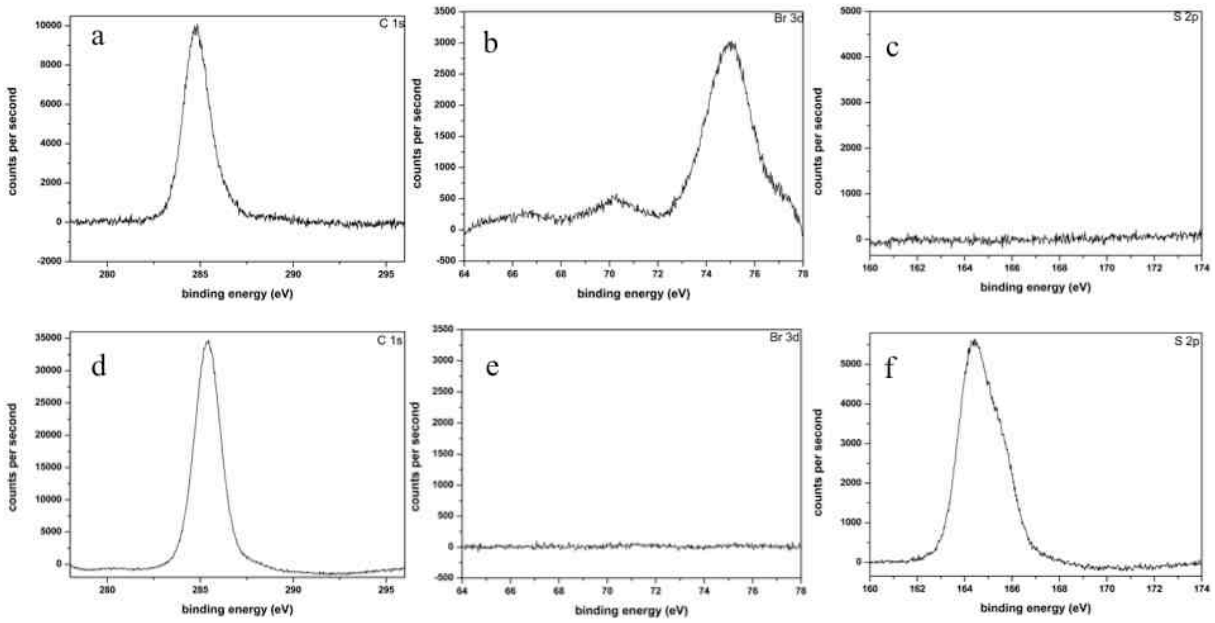

Figure 107: XPS spectra of a graphene sheet grafted with poly(4-bromostyrene) before (a,b,c) and after (d,e,f) SI-KCTP for the elements carbon (a,d), bromine (b,e), and sulfur (c,f)

As can be seen in Figure 106 and Figure 107, the presence of the grafted layers of phenyl bromide and poly(4-bromostyrene) was confirmed *via* x-ray photoelectron spectroscopy (XPS), where carbon and bromine are detected on the intitiator layers. After P3HT-grafting, the bromine peaks in the XPS spectrum have disappeared and sulfur peaks are now clearly detectable. The presence of immobilized nickel catalyst in the intermediate step has not been confirmed, as the catalyst-impregnated graphene was directly processed without intermediate characterization.

Grafted P3HT on graphene could also be seen with the bare eye as **Figure 108**a shows. The P4BS-grafted graphene on copper foil shown on the left is colorless. After grafting, the P4BS-g-P3HT-grafted graphene has dull brownish color when immersed in a solvent in which the polymer is not well soluble and violet when immersed in a good solvent. **Figure 108**b shows UV spectra of P4BSg-P3HT-grafted graphene transferred to glass slides. With increasing thickness of the graft polymer layer, absorption bands around 460, 500 and 560 nm can be seen.

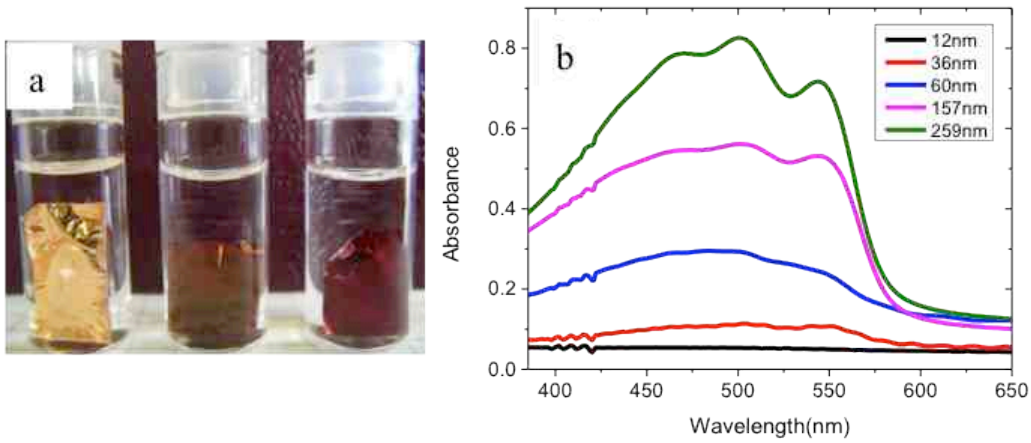

Figure 108: (a) Photographs of the 170 nm thick P3HT brush prepared on graphene (copper as substrate) starting with PSBr thin layer as initiator in methanol (middle) and in dichloromethane (right), PSBr thin layer as control (left). (b) UV-vis absorption spectra of the PSBr-g-P3HT film with various thickness (40 min P4BS polymerization followed by different time grafting with P3HT).

For a closer investigation of the SI-KCTP grafting step, *ex-situ* grafting kinetics measurements on P4BS-grafted graphene have been carries out, which can be seen in Figure 109.

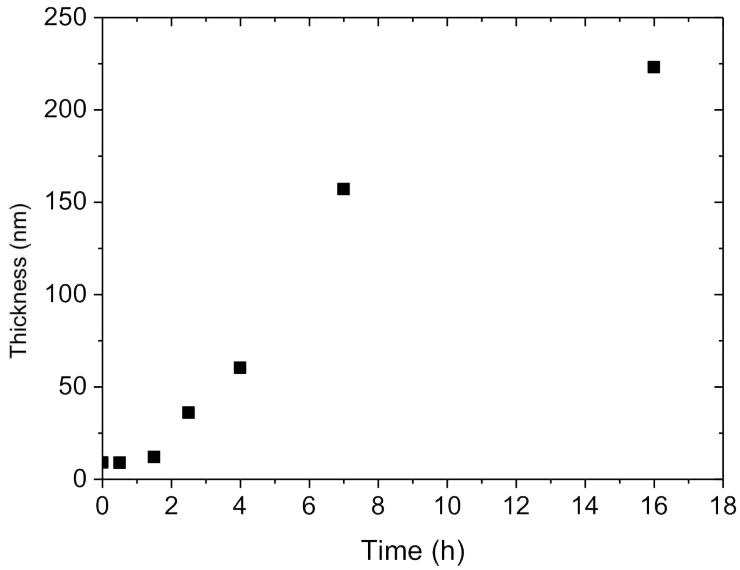

Figure 109: Dry-state thickness of P4BS-g-P3HT bottle-brush brush films grown at different SI-KCTP polymerization times

From the AFM thicknesses in Figure 109, a linear increase of P4BS-g-P3HT layer thickness from 2 to 16 h grafting time can be seen. This is in good accordance with the grafting mechanism, which is reported to be a living polycondensation.

Comparing the two different mechanisms for the generation of the initiator layer, a big advantage of the SIPGP over the diazonium route lies in the possibility of photopatterning. To illustrate this, a graphene sample has been illuminated with UV light through a photomask with hexagonal features in bulk 4-bromostyrene.

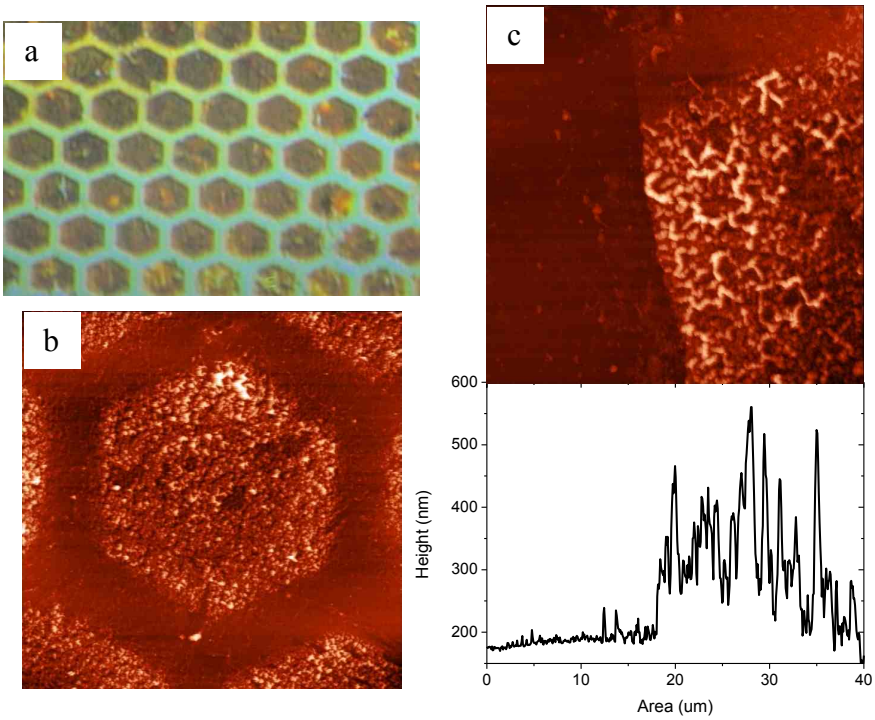

Figure 110: Optical microscope (a) and AFM (b) images as well as section height analysis (c) of patterned polymer bottle-brush P4BS-g-P3HT layers on single layer graphene prepared by UV illumination through a mask in bulk 4-bromo styrene, following with normal surface-initiated kumada catalyst-transfer polycondensation. Surface polymerization occurs selectively in illuminated regions of the material.

This patterning process leads to structured P4BS-g-P3HT grafts on graphene (see **Figure 110**) in the illuminated areas, while no grafted polymer can be detected in the regions darkened during SIPGP.

In summary, we present the first surface-initiated Kumada catalyst-transfer polycondensation to covalent grafting conducting P3HT brushes from single layer graphene. Self-initiated

photografting and photopolymerization (SIPGP) and diazonium salt addition are alternative and conceptually different strategies, which can be used to generate inimers for embedding of Ni species for grafting. The unique graphene-based structure morphology, so-called polymer carpets, prepared by these grafts may lead to interesting conductivity and electroluminescent behavior. Further work will include electronical and optical characterization the preparation of functional devices. As compared to the diazonium salt reaction, the SIPGP occurred at already existing defect sites and that there was no disruption of the basal plane conjugation of graphene. This method thus offers a route to define graphene functionality with conjugated polymer without apparently degrading its electronic properties. Furthermore, we demonstrated that P3HT brushes can be locally and selectively grafted on graphene surface via the SIPGP routes using a photomask. This advance opens up avenues for the preparation of microstructured conductive polymer brushes on single layer graphene, which can be further exploited in the fabrication of novel optoelectronic devices and sensors.

4.8 Linear Polythioethers *via* Photoinduced Click-Polyaddition of α,ω-Alkylene Sulfides

In an effort to obtain silicon surfaces with a grafted monolayer of propylene thiol, H-terminated silicon was irradiated with UV in bulk allyl mercaptan. Therefore, a freshly H-terminated Si(110) surface was immersed in freshly distilled bulk allyl mercaptan (prop-2-ene thiol), degassed via three freeze-pump-thaw cycles and irradiated with UV for 42 h. After irradiation, the surface was taken out of the reaction vial, sonicated for 5 min in THF, then repeatedly immersed in toluene, ethyl acetate and ethanol and eventually rinsed with ethanol before blow-drying with an air-stream. The surface was analyzed with DRIFT-IR spectroscopy and ellipsometry.

However, to our surprise, the reaction did not stop at a monolayer, but a layer of 7.21 nm (determined by ellipsometry) was obtained. Moreover, the bulk allyl mercaptane became viscous upon irradiation. The assumption of polymer formation could be comfirmed by precipitation of the produced polymer in ethanol and analysis *via* GPC, NMR, and DRIFT-IR spectroscopy. As can be seen from Figure 111, the IR spectra of the allyl mercaptane grafted surface and the precipitated polymer poly(trimethylenesulfide) are in very good congruency, so that the presence of the polythioether at the Si surface can be confirmed.

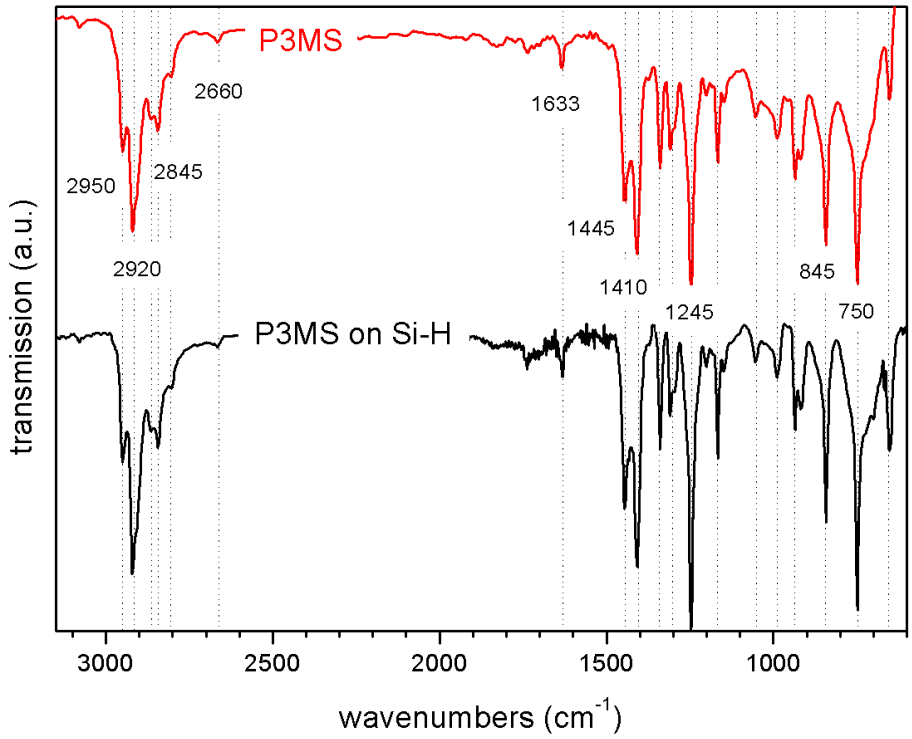

Figure 111: Direct comparison of P3MS-grafted silicon substrate and precipitated polymer from bulk solution after 42 h UV irradiation

Since we were intrigued by the photoinduced homopolymerization of this α,ω–unsaturated thiol compound, we decided to investigate this type of polymerization as a side-project.

The addition of a thiol to a non-activated carbon-carbon double bond known as the thiol-ene click reaction, recently developed into a widely used reaction in synthetic chemistry. Its simplicity, selectivity and efficiency makes the thiol-ene click reaction ideally suited for quantitative polymer analog reactions, surface functionalizations and synthesis of bioorganic hybrids.[199-201] Even though, this reaction is known for over 100 years,[202] the thiol-ene click reaction only recently receives much attention for polymer network synthesis, polymer functionalization, dendrimer synthesis, and modification of three-dimensional objects as it can be induced by light, is metal-free and orthogonal to various other ligation reactions.[203,204]

A direct route to polythioethers, is the photoinduced polyaddition of α,ω-alkylene thiols as first described in the late 1920s by Braun *et al.*[205,206] Much later, Oswald *et al.*[207] used allylic sulfides and in a series of papers Nuyken *et al.*[208-213] studied the polyaddition of styrenic thiols. Based on a first report by Mayo *et al.* [214] and Ketley *et al.*[215] Bowman and coworkers[216-218] investigated the photocopolymerization of thiols with different comonomers and confirmed the step-growth mechanism. They also pointed out several unique advantages of the thiol-ene photopolymerization being photoinitiator/catalyst free, oxygen tolerant and

specifically suited for the production of coatings. Surprisingly, and to the best of our knowledge no work has been reported so far that describes the simplest route to poly(thioether)s from α,ω-alkylene thiols.

A set of four α,ω-alkylene thiols were selected for the thiol-ene click polyaddition. While prop-2-ene thiol (allyl thiol) is commercially available, the other monomers as listed in Table 1 could be readily prepared in high yields and with high purity according to the literature.[219,220] Monomers were stored in the dark at -20°C and did not show any sign of decomposition over a period of one week. Prop-2-ene thiol has been freshly distilled prior to use in polymerization reactions. The polymerization was carried out in a 2 M solution under vigorous stirring at room temperature and constant irradiation with UV light for 24 h. Analog to the previous results from Oswald, chloroform was found to be the most suitable solvent. While in benzene the polyaddition reaction proceeds but only low molar mass products were obtained, in pentane already oligomeric products precipitated, polymerization of allylic thiols in chloroform yielded polymer products in all cases.[207]. Table 1 summarizes the results of the reactions for all monomers used so far.

Table 10: Molar mass average, dispersity and conversion for poly(thioether)s prepared from α,ω-alkylene thiols by UV irradiation in chloroform (2 M) for 24 h or bulk monomer for 48 h (*).

Poly(thioether)	Monomer	M_n[a] (kg/mol)	M_w[a] (kg/mol)	n[b]	Đ[c]	Conversion[d] (%)
Poly(propylene sulfide)	Prop-2-ene thiol	2.3	5.5	74	2.37	98.6
Poly(butylene sulfide)	But-3-ene thiol	2.9	3.7	42	1.27	97.6
		8.5*	16.1*	183*	1.90	99.5*
Poly(pentylene sulfide)	Pent-4-ene thiol	2.5	3.7	36	1.48	97.3
Poly(undecylene sulfide)	Undec-10-ene thiol	4.4	7.3	39	1.65	97.4

[a] Number average (M_n) and weight average (M_w) molar mass as determined by gel permeation chromatography; [b] degree of polymerization; [c] dispersity, $Đ = M_w/M_n$; [d] calculated by Carothers' equation: $c = 1 - 1/n$

Polymer purification by precipitation in methanol was straightforward and in all cases odor free and colorless polymers were obtained. ^{1}H-NMR spectroscopy of the obtained polymers unambiguously confirmed the formation of the desired poly(thioether)s and revealed a very high monomer conversion as judged from the signal intensity of olefinic protons at 5.1 and 5.8 ppm (see appendix). Gel permeation analysis gave dispersity values around 2 or lower and molar masses from 3.7-7.3 kg/mol. Oswald et al.[207] reported the synthesis of poly(propylene sulfide) with M_w = 0.5 to a maximum of 5 kg/mol. Significantly higher molar mass could be realized by longer irradiation times (48 h) and irradiation of bulk monomer. As listed in Table 1, this resulted in e.g. poly(butylene sulfide) with n = 180 (M_w = 16 kg/mol, Đ = 1.9). However, although ^{1}H and ^{13}C NMR spectra of Poly(undecylene sulfide) indicate formation of disulfides (see appendix), the obtained polymer shows a high degree of polymerization, see Table 1. Thus, it is suggested that disulfides, if formed during polymerization reaction, can be cleaved by UV irradiation or by reaction with other radicals present[221,222] and consequently do not impede a step growth polymerization mechanism. Another explanation for the origin of

disulfide bonds could be their formation after polymer precipitation under oxidative air atmosphere by oxidation of thiols.[223]

In Figure 112, the development of the molar mass and dispersity with the irradiation time is shown for a 6 M solution of prop-2-ene thiol in chloroform as analyzed by GPC. The observation that the reaction proceeds more slowly than one would expect from results depicted in table 1 might be attributed to the increased monomer concentration. The viscosity of the reaction mixture increases significantly when a concentration of 6 M is used compared to 2 M. The observation that the molar mass is leveling off at around 2 kg/mol might be a result of trace amounts of oxygen that enter reaction vessel when aliquots necessary for GPC measurements are taken.

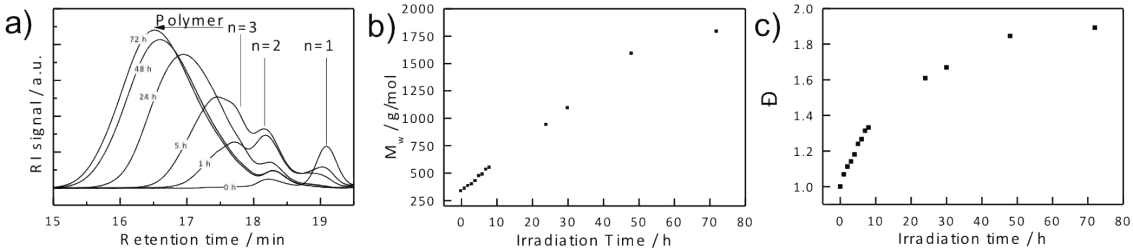

Figure 112: a) GPC traces of aliquots of a 6 M solution of prop-2-ene thiol in chloroform under constant UV irradiation sampled at indicated times. b) Development of the weight average molar mass (Mw) and c) dispersity (Đ) with the irradiation time.

GPC analysis of freshly distilled prop-2-ene thiol already revealed existence of monomers along with a small fraction of dimers. This was corroborated by ^{1}H NMR spectroscopy, approx. 3.2 mol.% dimer was determined (Figure 112a). At 1h UV irradiation, mostly dimers (CH_2=C_2H_3-S-C_3H_6-SH) and trimers are formed, similar to the findings of Oswald *et al.*[207] At 5 h already oligomers are detectable and with ongoing polymerization time higher molar mass poly(propylene sulfide) is formed with a typical development of M_w and Đ with the reaction time (Figure 112b,c). Analog investigations for the other monomers were not possible since the photopolymerization proceeded too fast for the sampling procedure. For pent-4-ene thiol, after 10 min UV irradiation the conversion of double bonds was already > 90% as determined by ^{1}H NMR spectroscopy. All results so far indicate a conversion of α,ω-alkylene thiols via a photoinduced polyaddition reaction. This was further investigated by *ex situ* kinetic measurements in which we determined the double bond conversion with time as determined by ^{1}H spectroscopy (Figure 113).

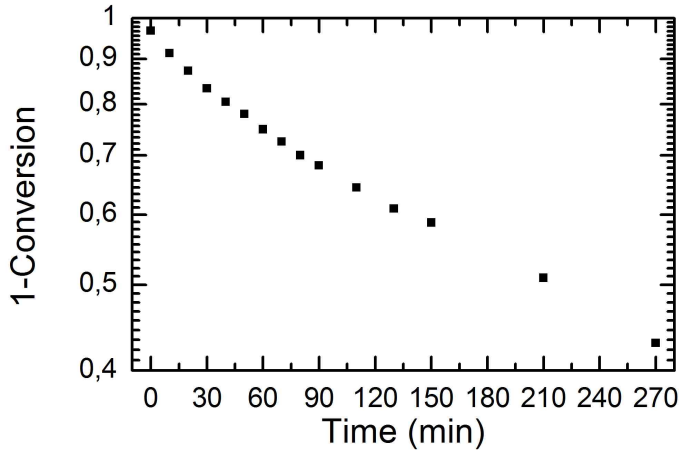

Figure 113: *Ex situ* NMR kinetics of double bond conversion over time for the photoinduced thiol-ene click polyaddition of prop-2-ene thiol solution in chloroform (2 M).

The conversion of one function of the AB monomer system (here the olefin function) follows nicely the typical trend for a step-growth reaction. A similar double bond conversion was found by Bowman *et al.*[218] for the photopolymerization of dithiols and dienes monitored by real time FT-IR spectroscopy. Moreover, GPC investigation of a reaction mixture aliquot at 40% conversion (at 150 min) revealed an average molar mass of 150 g/mol which most probably corresponds to a dimer ($M_{theor.}$ = 148.29 g/mol). Neither ^{1}H NMR spectroscopy nor GPC analytical data gave hints for the formation of significant amounts of cyclic thioethers.[224] Even excessive dilution of the reaction mixture did not result in a dectectable amount (by ^{1}H NMR spectroscopy) of ring formation. In a solution of but-3-ene thiol diluted in benzene, no signals attributed to tetrahydrothiophene (thiolane) at chemical shifts of 2.53 and 1.55 ppm could be detected. A solution of pent-4-ene thiol in benzene also showed no signals that could be attributed to the sulfur-containing heterocycle, thiane, expectable at 2.29 ppm. Although formation of cyclic monomers was not observed by ^{1}H NMR spectroscopy, formation of macro cycles cannot be excluded. It is to be mentioned that also analysis by mass spectroscopy cannot distinguish between linear and cyclic products as, resulting from the addition reaction, their molecular formulas are identical.

So far, all results indicate step-growth polyaddition mechanism of the α,ω-alkylene thiols which is conveniently induced by UV irradiation. Based on our results and in agreement with earlier studies by Bowman *et al.*,[217,218] we propose a mechanism for the photoinduced thiol-ene click reaction as depicted in Figure 114.

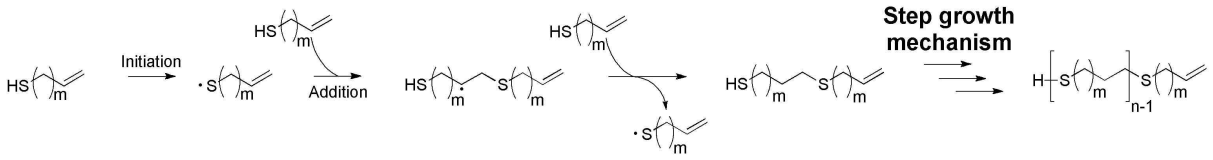

Figure 114: Proposed reaction mechanism for the photoinduced thiol-ene polyaddition of α,ω-alkylene thiols leading to linear poly(thioether)s.

Furthermore, we investigated first properties of the novel poly(thioether)s such as the melting temperature as a function of the main chain methylene group number (number of CH_2 units = m+2). Differential scanning calorimetry (DSC) was performed with the poly(thioether)s of methylene segment lengths, m = 1, 2, 3, 9. The results are summarized in Figure 115. The DSC data show that higher m lead to a systematic increase of the melting temperatures.

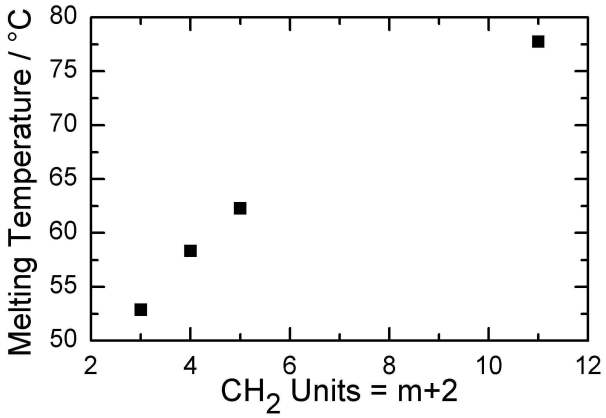

Figure 115: Melting temperature of the homologue series of poly(thioether)s as a function of the number of main chain methylene units as determined by DSC.

Disulfide formation was only observed in case of poly(undecenylene sulfide). This was not the case for all other polymers under the reaction and under standard storing conditions. As disulfides can participate in radical reactions,[221,222] the thiol as well as the ene - terminal functions are readily available for further functionalization of the polymer chain termini by e.g. consecutive thiol-ene click coupling reactions to form block copolymers, defined endfunctionalized polythioethers or other hybrid materials.

5 Summary and Outlook

At the beginning of this thesis, the question was if it is possible to graft polymers from selected semiconductor surfaces *via* photoinduced grafting to obtain a functional polymer layer that is stable enough for both passivation and post-synthetic modification. First of all, the answer is yes.

Photoinduced grafting from hydrogen-terminated silicon. It could be shown that polystyrene could be grafted from H-terminated silicon surface by irradiating the surface in presence of the monomer. Layer thickness increases monotonously with time, yielding thick polymer layers. Trials to graft (meth)acrylates with this method showed much lower thicknesses, most presumably owed to the high reactivity of Si-H bonds to (meth)acrylates regarding hydrosilylation. As a way to work around this problematic and to introduce (meth)acrylic functional unit to the polymers, a copolymerization approach was applied by simply using a monomer mixture of styrene and the desired monomer, obtaining stable and homogenous copolymer brushes. In order to prove the extraordinary stability of those Si-C bonded polymer grafts, post-polymerization modifications were carried out employing harsh conditions. Not only that the polymer brushes turned out to be stable under these conditions, this also provides routes for building up bottle-brush brush morphologies using poly(2-alkyl-2-oxazolines).

The procedure used for photografting of styrene was also shown to be suitable both for direct lithography and for lithography exploiting the reactivity contrast between hydrogen-terminated and oxide-covered silicon. Using this route, binary polymer brush structures were obtained by a combination of self-initiated photografting and photopolymerization (SIPGP) of styrene on H-terminated silicon and SI-ATRP on oxide-covered silicon.

Sequential photografting from H-terminated silicon. Regarding grafting rates, it was accomplished to accelerate grafting two-fold by using a sequential photografting procedure with immobilization of photoinitiator benzophenon or ITX in the first step and irradiation of the so-functionalized surface in the second step. *Ex-situ* kinetics measurements revealed grafting rate to be dependent from pre-grafting time as well as photoinitiator concentration. The general feasibility of directly creating functional polymer brushes this way could also be shown and insight could be gained in the mechanism involved in grafting as well as initiator immobilization.

Direct Photografting from nanocrystalline silicon. After fundamentally understanding the processes involved during photografting from planar silicon, the process could be successfully applied to nanocrystalline silicon, silicon carbide and silicon nitride, respectively. General trends observed in grafting from planar silicon could also be seen in polymerizing from nanocrystalline silicon. Grafting of styrene resulted in a monotonous increase of attached polymer over irradiation time, being in congruency with results on planar Si substrate. Grafting of MMA and tBMA showed no increase of attached polymer over time, however, DRIFT spectroscopy and dispersibility experiments gave strong hints towards successful grafting of short polymer chains or oligomers, respectively. Grafting of 4-vinylpyridine, diethylaminoethyl acrylate, and allyl amine all resulted in grafting of at least oligomeric material from the surface as determined by DRIFT spectroscopy. GPC analysis of free polymer precipitated from the reaction solution provided useful insight into reaction involved between the nc-Si surface and growing polymer chains. Moreover, thermally initiated grafting of styrene from nc-Si was also shown to be feasible and straightforward.

Photoinduced polymerization from graphene. The influence of hydrogenation on SIPGP from graphene substrate was investigated. It could be shown that polymer layer thickness of grafted polystyrene increased exponentially with defect density due to increasing grafting density of the resulting polymer chains. While styrene, 4-bromostyrene and pentafluorostyrene could be easily grafted from graphene, grafting of acrylates and methacrylates was not possible. To obtain (meth)acrylic-functional polymers on graphene, the copolymerization approach described in chapter 4.1.7 was successfully applied, yielding PS-co-PMMA and PS-g-PMMA grafted graphene. The process was also shown to be possible with copolymer systems styrene/HEMA and styrene/DMAEMA, being potential candidates for graphene-based sensing.

Surface-initiated Kumada Catalyst-Transfer Polycondensation. In order to obtain semiconductor surfaces grafted with conductive polymer brushes, we applied SI-KCTP to polymerize P3HT from silicon as well as from graphene. In case of silicon, SI-KCTP was conducted from a P4BS brush grafted via sequential photografting. P4BS-g-P3HT brushes were analyzed via ATR IR spectroscopy and showed an approx. threefold increase in layer thickness by SI-KCTP. Grafting from nc-Si was conducted from bromophenyl acetylene layers. Grafting from graphene was done both from P4BS-grafted and bromophenyl-functionalized graphene, which both led to homogeneous P3HT layers of around 170 nm thickness.

Linear Polythioethers via Photoinduced Click-Polyaddition of α,ω-Alkylene Sulfides.

α,ω– alkylene thiols were polymerized to telechelic poly(thioether)s by photoinduced thiol-ene click polyaddition. The poly(thioether)s were found to be linear and semi-crystalline. The melting points increase systematically with the count of the main chain methylene groups.

In this work, convenient and straightforward one-step and two-step strategies for the functionalization of semiconductor surfaces, predominantly hydrogen-terminated silicon, have been demonstrated. By this approach, it is possible to generate inorganic-organic hybrid nanostructures that combine the advantages of both material classes.

Further work will include the development of polymer-functionalized devices using this approach. For example, functionalization of graphene with a copolymer of DMAEMA and styrene will lead to multiresponsive graphene-transistor sensors responsive to pH, temperature and ion strength. P3HT-grafted graphene could eventually be used in hybrid solar cells, where good linkage between P3HT polymer and graphene could lead to higher stability and better charge transfer.

Regarding polymer-modification of silicon, possibilities are also vast. Functional polymer brushes grafted from silicon can be used as an organic linker for the immobilization of redox-active catalyst systems, leading to new electrode or sensor materials. This is also underlined by the high importance of p-doped silicon as a substrate material for artificial photosynthesis. Another possibility is the passivation of silicon surfaces *via* SIPGP, leading to long-term stability. Taking into account the ongoing trend to miniaturization of silicon-based electronics, regimes where surface properties start playing a dominant role are not very far any more.

Another window of opportunity is the functionalization of nanocrystalline silicon with polymers. Until now, this is an area that has not attracted much attention, but this will only be a matter of time. Having the possibility to tailor surface chemistry of nc-Si by straightforward surface-initiated polymerization will create a whole new range of applications for the resulting organic-inorganic core-shell nanomaterials, some of them being bioimaging, drug delivery, nanolithography, photovoltaics, and energy storage.

6 Zusammenfassung und Ausblick

Zu Beginn dieser Arbeit stellte sich die Frage, ob es möglich ist, Polymere direkt auf ausgewählten Halbleiteroberflächen mittels photoinduzierter Pfropfung zu erzeugen, die sowohl stabil genug sind, um die Oberfläche zu passivieren als auch um postsynthetisch modifiziert werden zu können. Diese Frage kann nun mit Ja beantwortet werden.

Photoinduzierte Propfung von wasserstoff-terminiertem Silicium. Es konnte gezeigt werden, dass Polystyrol durch Bestrahlung einer H-terminierten Si-Oberfläche in Gegenwart des Monomers auf dieser polymerisiert werden kann. Die Schichtdicken steigen monoton in Korrelation zur Bestrahlungsdauer was zur Bildung von dicken (>200 nm), homogenen Polymerschichten. Versuche, (Meth)Acrylate mit dieser Methode zu pfropfen resultierte in weitaus dünneren Schichten, wahrscheinlich aufgrund der hohen Reaktivität der Si-H Bindungen auf der Oberfläche gegenüber (Meth)Acrylaten bezüglich Hydrosilylierung. Um diese Problematik zu umgehen und dennoch Acrylgruppen in die Polymere einzuführen, wurden die entsprechenden Acrylmonomere mit Styrol copolymerisiert, was zu stabilen und homogenen Copolymerschichten führte. Um die außergewöhnliche chemische Stabilität dieser Si-C-gebundenen Polymerbürsten zu demonstrieren, wurden postsynthetische Modifikationsreaktionen unter harschen Bedingungen durchgeführt. Neben der Tatsache, dass die Polymerbürsten nachweislich unter diesen Bedingungen stabil sind, stellt dies auch eine Route dar, um zylindrische Polymerbürsten („bottle-brush brushes“) mittels der oberflächeninduzierten lebenden kationischen Ringöffnungspolymerisation von 2-Alkyl-2-oxazolinen zu erzeugen.

Es konnte zudem gezeigt werden, dass diese Art der Photopfropfung sowohl für direkte Lithographie als auch für Lithographie unter Ausnutzung des Reaktivitätsunterschieds zwischen H-terminiertem und oxidbedecktem Silicium geeignet ist. Auf diese Weise können sogar binäre Polymerbürstensysteme durch eine Kombination der selbstinitiierten Photopfropfung und Photopolymerisation (SIPGP) von Styrol auf H-terminiertem Si und oberflächeninitiierter Atomtransfer Radikalpolymerisation (SI-ATRP) von oxidbedecktem Silicium erzielt werden.

Sequenzielle Photopfropfung. Die Wachstumsraten der Polymerschichtdicken konnten auf das Doppelte beschleunigt werden. Dies wurde erzielt durch die Einführung einer sequenziellen Prozedur mit der Immobilisierung eines Photoinitiators auf der Oberfläche im ersten Schritt und Bestrahlung der so funktionalisierten Silicumoberfläche in Gegenwart eines

Monomers im zweiten Schritt. *Ex-situ* Kinetikmessungen zeigten, dass die Wachstumsraten sowohl von der Konzentration des Photoinitiators als auch der Dauer der Immobilisierung im ersten Schritt abhängig sind. Die grundsätzliche Möglichkeit, funktionelle Polymerbürsten auf diese Weise zu erzeugen, wurde demonstriert und es konnte Einblick in die Mechanismen der Pfropfung sowie der Immobilisierung gewonnen werden.

Direkte Photopfropung auf nanokristallinem Silicum. Aufbauend auf einem grundlegenden Verständnis der Prozesse während der Photopfropfung von Polymeren auf planarem Silicum sollte dieser Prozess auf nanokristallines Silicum, Siliciumcarbid und Siliciumnitrid angewendet werden. Generelle Trends, die auch schon auf planarem Silicium beobachten wurden, zeigten sich auch bei der Pfropfung von nanokristallinem Si. Die Pfropfung von Styrol führte zu einem linearen Anstieg der Menge des gepfropften Polymers mit der Bestrahlungsdauer, was mit der Pfropfung auf planarem Si übereinstimmt. Die Pfropfung mit MMA und tBMA zeigte keinen Anstieg der Menge an gebundenem Polymer mit der Zeit, jedoch deuten Ergebnisse aus der DRIFT Spektroskopie sowie aus Dispersibilitätsexperimenten auf eine erfolgreiche Funktionalisierung mit Monolagen, kurzen Polymerketten oder Oligomeren hin. Die Pfropfung von 4-Vinylpyridin, Dimethylaminoethylacrylat und Allylamin resultierte in der Pfropfung von Polymeren und Oligomeren, was durch DRIFT Spektroskopie bestätigt wurde. GPC Analysen der ausgefällten ungebundenen Polymere aus den Reaktionen lieferten nützliche Einsichten in die Reaktion zwischen der nc-Si Oberfläche und den wachsenden Polymerketten. Darüber hinaus konnte gezeigt werden, dass eine thermoinitiierte Pfropfung von Styrol auf unkomplizierte Weise durch Erhitzen von H-terminiertem nc-Si in Styrol durchgeführt werden kann.

Photoinduzierte Polymerisation auf Graphen. Es wurde der Einfluss der Hydrogenierung von Graphen auf die Photopfropfung untersucht. Es konnte gezeigt werden, dass die Schichtdicke einer Polymerschicht exponentiell mit der Defektdichte (C-H) ansteigt, aufgrund einer Zunahme der Pfropfdichte der resultierenden Polymerketten. Während Styrol, 4-Bromstyrol und Pentafluorstyrol problemlos auf Graphen gepfropft werden konnten, schlug die Funktionalisierung mit Acrylaten und Methacrylaten fehl. Um dennoch (meth)acrylfunktionale Polymere auf Graphen zu erhalten, wurde der Copolymerisationsansatz aus Kapitel 4.1.7. erfolgreich auf Graphen übertragen, was zur Funktionalisierung von Graphen mit PS-co-PMMA- und PS-g-PMMA-gepfropftem Graphen führte. Dieser Prozess wurde auch auf die Copolymersysteme Styrol/HEMA und

Styrol/DMAEMA erfolgreich angewendet, welche potenzielle Kandidaten für Graphen-basierte Sensoren darstellen.

Oberflächeninitiierte Kumada Katalysatortransferpolykondensation.

Um Halbleiteroberflächen funktionalisiert mit leitfähigen Polymeren zu erhalten, wurde SI-KCTP sowohl auf Silicium als auch auf Graphen angewendet. Im Fall von planarem Si wurde die SI-KCTP von einer P4BS Initiatorschicht durchgeführt. Die P4BS-g-P3HT Polymerbürsten wurden mittels ATR IR Spektroskopie analysiert und zeigten einen ca. dreifachen Anstieg der Schichtdicke durch die SI-KCTP. Die Pfropfung von P3HT auf nc-Si wurde auf Bromophenylacetylen-funktionalisiertem nc-Si durchgeführt und deutet auf eine erfolgreiche Funktionalisierung hin. Die Pfropfung auf Graphen wurde sowohl von P4BS-gepfropftem als auch von Bromophenyl-funktionalisiertem Graphen durchgeführt, was beides zu homogenen P3HT Schichten von 170 nm Dicke nach 18 h SI-KCTP führte.

Lineare Polythioether durch die photoinduzierte Klick-Polyaddition von α,ω-Alkylensulfiden. α,ω– Alkylenthiole wurden durch photoinduzierte Thiol-En Klick-Polyaddition zu telechelen Polythioethern polymerisiert. Diese Polythioether waren linear und semikristallin und die Schmelzpunkte stiegen systematisch mit der Anzahl der Methylengruppen in der Hauptkette.

In dieser Arbeit wurden unkomplizierte und praktische Wege zur Funktionalisierung von Halbleiteroberflächen, insbesondere wasserstoff-terminiertem Silicium, mit Polymeren u.a. mittels Photopolymerisation demonstriert. Auf diese Weise ist es möglich, anorganisch-organische hybride Nanomaterialen zu generieren, welche die Vorteile beider Materialklassen kombinieren. Neben der generellen Machbarkeit wurden zudem die Stabilität der so erzeugten Strukturen und die Übertragbarkeit auf andere Morphologien und Substrate gezeigt.

Darauf aufbauende Arbeiten werden sich mit Entwicklung polymerfunktioneller Halbleiterbauteile unter Anwendung der hier entwickelten Methoden beschäftigen.

Beispielsweise führt die Funktionalisierung von Graphen mit einem Copolymer aus Styrol und DMAEMA potenziell zu multiresponsiven Graphentransistoren, die sensitiv gegenüber pH-Wert, Temperatur und Ionenstärke sind. P3HT-funktionales Graphen könnte schließlich in Hybridsolarzellen Anwendung finden, wo gute Anbindung zwischen P3HT Polymer und dem

Graphen, zusammen mit dem Erhalt der elektronischen Eigenschaften des Graphens trotz Pfropfung, zu einer höheren Stabilität und besserem Ladungstransfer führt.

Was die Modifikation von Silicium mit Polymeren angeht, sind die Möglichkeiten enorm. Funktionelle Polymerbürsten auf Silicium können als organischer Linker für die Anbindung von redox-aktiven Katalysatorsystemen genutzt werden, was zu neuartigen Elektroden- oder Sensormaterialen führen könnte. Dies wird auch durch die große Bedeutung von p-dotiertem Silicium als Substrat für die künstliche Photosynthese unterstrichen. Eine weitere Möglichkeit ist die Passivierung von Siliciumoberflächen mittels SIPGP, was zu hoher Langzeitstabilität führt. In Anbetracht des andauernden Trends zur Miniaturisierung von siliciumbasierter Elektronik sind die Größenordnungen, wo oberflächenbasierte Effekte eine dominante Rolle zu spielen beginnen, nicht mehr weit entfernt.

Eine weitere großartige Gelegenheit stellt die Funktionalisierung von nanokristallinem Silicium mit Polymeren dar. Bisher ist dies ein Gebiet, dem noch nicht allzu viel Aufmerksamkeit zuteil wurde, was aber nur eine Frage der Zeit sein wird. Mit der Möglichkeit, die Oberflächeneigenschaften des nc-Si gezielt mittels einer einfach durchzuführenden Oberflächenmodifikation durch Polymere maßzuschneidern, führt zu einer ganzen Palette von neuen Anwendungen für die daraus resultierenden organisch-anorganischen Hybridmaterialien, beispielsweise Bioimaging, Drug Delivery, Photovoltaik, Optoelektronik und Energiespeicherung.

7 Experimental

7.1 Materials

Chemicals

Chemicals were purchased from suppliers Sigma-Aldrich, Acros and Fisher Scientific. Styrene was purified by recondensation in vacuum. All other monomers were purified by passing over basic alumina.

Substrate Materials

Silicon wafers (100, p-doped) were obtained from CrysTec GmbH, Sigma-Aldrich and WACKER Chemie AG.

Nanocrystalline silicon and silicon carbide were obtained from Sigma-Aldrich.

Nanocrystalline silicon nitride was obtained from PlasmaChem GmbH.

Graphene Growth

The CVD growth apparatus, which was used for production of the graphene samples in this work consists of a resistively heated glass tube into which a 5 × 5 cm^2 piece of copper foil (Alfa Aesar, 0.025 mm, 99.8 % Cu) is loaded. One end of the glass tube is attached to a rotary vacuum pump via a butterfly valve. On the other end of the reaction tube, mass flow controllers adjust the flux of the three process gases: Ar, H_2, and P5. P5 is a commercially available gas mixture containing 5% methane in Ar. Methane is the carbon source for the graphene formation, and its high dilution in argon ensures that the methane concentration remains below the explosive threshold in air. Therefore, no additional gas sensors are required for this process. Capacitance manometers are utilized for process pressure measurement. In order to control the temperature, a thermocouple is inserted into the hot zone of the oven and attached to a Eurotherm PID controller, which regulates the current in the resistively heated oven.

Graphene growth is a two-step process. First, the surface of the copper foil is etched under a H_2/Ar atmosphere at 1000 °C for approximately 15 minutes in order to create a pristine, non-oxidized surface. In the second step, graphene growth occurs by exposure of copper to a

CH_4/H_2/Ar atmosphere for ten minutes at 1000 °C. The sample is then cooled down to room temperature while maintaining the growth gas flow conditions. The sample is dismounted after approximately three hours of cooling.

7.2 Methods

Atomic force microscopy (AFM)

AFM scans were obtained with a Nanoscope IIIa scanning probe microscope from Veeco Instruments using standard tips in tapping mode (driving amplitude of approx. 1.25 V at a scan rate of max. 0.5 Hz).

Contact Angle Measurements

Water contact angles were determined with a full-automated Krüss DSA 10 Mk2 contact angle goniometer and three points were measured on each surface. The data were obtained with the aid of the Krüss Drop Shape Analysis v3 software package.

Ellipsometry

Ellipsometric measurements were carried out on a SD 2300 ellipsometer of Philips Analytica Technology GmbH with a wavelength of 633 nm.

GPC measurements

Measurement and evaluation of GPC analyses was done with a Varian PLGPC at 35 °C in THF *via* a refractive index detector relative to polystyrene standard.

Infrared spectroscopy (FT-IR)

Fourier transform infrared spectroscopy (FT-IR) was performed on an Bruker Vertex 70 instrument equipped with a VariGATR variable grazing angle ATR setup from Harrick Scientific (for ATR measurements) or a DRIFT setup from *Spectra Tech* and a mercury–cadmium–telluride (MCT) detector. For each spectrum, 500 scans were accumulated with a spectral resolution of 4 cm^{-1}. Background spectra were recorded with 250 scans.

Microwave Synthesis

Microwave-assisted synthesis was performed using a CEM Discover LabMate system.

Microwave Photoconductivity Decay

Light source: 1064 nm emission from a Continuum Minilite II Nd:YAG laser with ~100 uJ/cm^2.

Microwave source: Gunn diode oscillator with an output frequency of 38.3 GHz , operating with an output power of 200 mW.

Detection: The detector is a Schottky diode finline detector, with the time-dependent microwave reflectivity detected using a Tektronix DPO 3052 oscilloscope.

Data was normalized and fitted (non-linear fit) with the Origin software package to obtain lifetime values.

Transmission Electron Microscopy (TEM)

TEM images were recorded with a JEOL 2010.

Scanning Electron Microscopy (SEM)

SEM images were recorded on a JEOL 7500F.

Nanocrystal Filtration

Filtration was done with a pressure filter unit from *Satorius Stedim Biotech* and PTFE filter membranes (0.2 μm/0.45 μm) from *Grace* and *Sartorius* .

7.3 Syntheses

7.3.1 Sample pretreatment

Si wafer substrates are cleaned by ultrasonication in acetone for 10 min and then rubbed with a cotton swab. Afterwards, wafers were boiled for 20 min in a 5 wt.% solution of sodium peroxodisulfate in Millipore water.

For etching, silicon substrates are immersed in 50% HF in H_2O for 2 min, then rinsed with millipore water, ultrasonicated in millipore water for 10 s, then rinsed with Millipore water and blow-dried with an air stream.

Gallium nitride substrates were hydroxylated in an oxygen plasma.

Graphene substrates were used as-grown still attached to the copper foil without further pretreatment.

7.3.2 Self-initiated photopolymerization and photografting (SIPGP)

These procedures apply to grafting on all planar substrates used in this work, including silicon, gallium nitride and graphene.

For polymerizations, substrates were immersed into 1 ml of bulk monomer. Degassing was carried out via three freeze-thaw cycles and the container was subsequently put under protective argon atmosphere. The sample containers were then placed over a UV photoreactor tube (8 W, intensity maximum around 350 nm wavelength) and irradiated from below for the desired duration.

After irradiation, the substrates were taken out of the reaction containers and cleaned by ultrasonication in an appropriate solvent (toluene for styrene, acetone for acrylates and methacrylates) for 5 min to remove ungrafted polymer. It has to be noted here that graphene samples were not sonicated since this could lead to damage of graphene layers. The substrate was then immersed in turns into toluene, ethyl acetate and ethanol (three cycles) to further remove ungrafted polymer chains from the substrate. As a last step, the substrate was rinsed with ethanol and blow-dried in an air stream.

7.3.3 Living cationic ring-opening polymerization (LCROP)

The poly(2-isopropenyl-2-oxazoline) (PIPOx) modified Si substrates were submerged in a solution of 2 ml dry and freshly distilled acetonitrile (ACN) with an excess amount of methyl trifluoromethane sulfonate (MeOTf) at approximately -35°C under a dry argon atmosphere. After stirring for 3 h at 0°C, the mixture was allowed to equilibrate to RT and stirred for 60 min before 2-ethyl-2-oxazoline (EtOx) was added under argon atmosphere. The reaction solution was irradiated by microwaves for 20 min with a temperature setting of 130°C. Finally, an excess of piperidine was added to selectively terminate the LCROP. After allowing the sample to stand overnight, it was removed from the reaction solution and thoroughly washed with a saturated solution of potassium carbonate in deionized water (Millipore). Final cleaning was performed by sequential ultrasonication in deionized water, ethanol, ACN and ethyl acetate for 5 min each.

7.3.4 Structured binary polymer brushes

A Si substrate coated with structured photoresist was etched by immersing into aqueous HF (50%) for 1 min and rinsing with millipore water and blow-drying. The photoresist was removed by ultrasonication in 1:1 isopropanol/acetone, wiping with a cotton swab in acetone, rinsing with ethanol and blow-drying.

The partly etched Si substrate was immersed in styrene, degassed via three freeze-pump-thaw cycles and irradiated for 5 hours with UV light. After irradiation in styrene, the Si substrate was cleaned by ultrasonication in toluene. The substrate was then immersed in turns into toluene, ethyl acetate and ethanol (three cycles) to further remove ungrafted polymer chains from the substrate. As a last step, the substrate was rinsed with ethanol and blow-dried in an air stream. For preparation of SI-ATRP, the partly PS-grafted partly oxide terminated Si substrate was immersed into 3 ml of dry ethanol and 0.3 ml 3-aminopropyl trimethoxysilane (APTMS) were added. After 1 hour, the substrate was taken out of the solution, rinsed with ethanol and dried. The substrate was then put into a solution of 3 ml dichloromethane (DCM), 0.3 ml triethyl amine (NEt_3) and 0.03 ml α-bromoisobutyryl bromide (BiBBr) and left to react for 30 min. After rinsing of the substrate with DCM, it was immersed into 3ml of degassed millipore water. Subsequently, 0.017 g copper (I) bromide CuBr, 1 ml of DMAEMA and 0.031 g 2,2´-bipyridine were added under argon atmosphere to prevent oxidation of Cu^I. After additionally degassing via three freeze-pump-thaw cycles, the reaction was reacted for 18 h at room temperature. Eventually, the substrate was taken out of the reaction vial, cleaned by ultrasonication in millipore water for 5 min and immersed in turns into water, ethanol, and ethyl acetate (three cycles) to further remove ungrafted polymer chains from the substrate. As a last step, the substrate was rinsed with ethanol and blow-dried in an air stream.

7.3.5 Sequential photografting on hydrogen-terminated silicon

H-terminated Si(100) substrates were immersed in a solution of benzophenone (6.7 wt% or 5 wt%) or ITX (7 wt%) and degassed *via* three freeze-pump-thaw cycles. After irradiation for a certain amount of time, substrates were removed from the reaction vial, washed three times with 1 ml toluene each, and sonicated for 5 min in 2 ml toluene. Subsequently, the substrates were rinsed with ethanol and blow-dried under an air-stream.

The BP- or ITX-grafted samples were then analyzed with contact angle measurements and VariGATR IR spectroscopy.

Thereafter, substrates were immersed in 1 ml of monomer and irradiated for the desired amount of time. Workup was carried out as described previously.

7.3.6 SIPGP on H-terminated nanocrystalline silicon

For hydrogen-termination nc-Si is dispersed in ethanol to obtain a 0.5 wt dispersion that is sonicated for 15 min. To this dispersion, 0.5 ml aqueous HF (50 %) are added under stirring and the dispersion is stirred for 10 min. During stirring, gas formation can be observed, which is probably due to SiF_4, and darkening of the dispersion. After etching, the dispersion is filtered through a pressure filtration unit with 0.2 μm PTFE membrane and washed three times with 50 ml ethanol each. Nc-Si is dried on the filter in high vacuum.

7.3.6.1 SIPGP of styrene, MMA and tBMA on H-terminated nc-Si

H-terminated nc-Si was dispersed in the respective monomer to obtain a 0.1 wt% dispersion and sonicated for 5 min. The dispersion is degassed in a sealed pyrex microwave reaction vial *via* three freeze-thaw cycles. Dispersions are irradiated for 4, 8, 16, 24, and 48 h respectively with UV light (λ_{max}=350 nm, 8 mW/cm^2) under stirring.

Workup of the irradiated samples was done by dilution of the dispersion with a suitable solvent for the resulting polymer (toluene for polystyrene, acetone for PMMA and PtBMA, ethanol for P4VP and poly(allylamine)) and filtration with a pressure filter over 0.2 μm PTFE membrane. Polystyrene-grafted samples were washed three times with 50 ml toluene each, three times with 50 ml acetone each and three times with 50 ml ethanol each. PMMA and PtBMA samples were washed with three times with 50 ml acetone each. The polymer-grafted nc-Si was dried on the filter membrane *in vacuo*.

The toluene fractions from the polystyrene samples and the actone fractions from the methacrylates were concentrated on a rotary evaporator and precipitated in ethanol (polystyrene) or pentanes (polymethacrylate). The polymer was washed with the corresponding solvent (ethanol for PS, pentane for acrylics) and dried *in vacuo* for further analysis.

The corresponding initial and final weights of polymer-grafted nc-Si and of free polymer after drying *in vacuo* are listed in the following table.

monomer	irradiation time (h)	initial weight	monomer (ml)	output weight nc-Si	non-grafted polymer	mass difference nc-Si

		(mg)		(mg)	(mg)	(%)
St	4	23.6	2.3	20.8	13.3	-11.9
	8	25.0	2.5	43.0	4.0	+72.0
	16	25.0	2.5	7.7	47.1	-69.2
	24	25.0	2.5	9.7	59.9	-61.2
	48	25.0	2.5	12.2	105.4	-51.2
MMA	4	29.0	2.9	28.2	0.7	-2.76
	8	29.0	2.9	26.1	-	-10.0
	16	29.0	2.9	26.1	0.4	-10.0
	24	29.0	2.9	27.2	0.3	-6.21
	48	29.0	2.9	26.9	1.4	-7.24
*t*BMA	4	25.0	2.5	24.9	-*	-0.40
	8	25.0	2.5	25.5	-*	+2.00
	16	25.0	2.5	25.7	-*	+2.80
	24	25.0	2.5	19.2	-*	-23.2
	48	25.0	2.5	23.7	-*	-5.20

* no free polymer was obtained

7.3.6.2 SIPGP of DMAEA-, 4-VP-, Styrol/HEMA and allylamine from H-terminated nc-Si

H-terminated nc-Si are dispersed in the respective monomer to obtain a 0.1 wt% (0.2 wt% in case of allyl amine) dispersion and sonicated for 5 min. The dispersion is degassed in a sealed pyrex microwave reaction vial *via* three freeze-thaw cycles. Dispersions are irradiated for 16 h with UV light (λ_{max}=350 nm, 8 mW/cm^2) under stirring, anaologous to the experiments decribed in chapter 7.3.6.1.

The P4VP-grafted nc-Si sample is diluted with 10 ml ethanol and filtered three times with 50 ml ethanol each over a 0.2 μm PTFE membrane. The filtrate is concentrated to ~ 5 ml and precipitated from 100 ml pentane.

Workup of poly(styrene-co-HEMA)-grafted nc-Si was performed anaologous to the workup of styrene-grafted nc-Si described in chapter 7.3.6.1.

The filtrate obtained during workup of the poly(allylamine)-grafted nc-Si was transparent but yellowish in color, most presumably by poly(allylamine)-functionalized nc-Si that have passed through the filter due to their small size. Interestingly, the filtrate showed blue to yellow luminescence under irradiation with 365 nm UV light.

The corresponding initial and final weights of polymer-grafted nc-Si and of free polymer after drying *in vacuo* are listed in the following table.

monomer	irradiation time (h)	initial weight (mg)	monomer (ml)	output weight nc-Si (mg)	non-grafted polymer (mg)	mass difference nc-Si (%)
DMAEA	16	22.0	2.2	26.4	15.8	+20.0
4-VP	16	48.1	4.8	51.1	166.2	+6.24
St/HEMA	16	26.2	2.6	24.0	12.8	-8.40
AAM	16	16.6	3.0	19.9	-	+19.9

7.3.6.3 SIPGP of styrene on H-terminated nc-Si at lower concentrations

SIPGP of styrene from H-nc-Si at concentrations of 0.05 and 0.025 wt% was performed analogous to experiments described in chapter 7.3.6.1 and workup was done accordingly. Irradiation time was 16 h in both cases.

The corresponding initial and final weights of polymer-grafted nc-Si and of free polymer after drying *in vacuo* are listed in the following table.

monomer	irradiation time (h)	initial weight	monomer	output weight nc-	non-grafted polymer	mass difference

		(mg)	(ml)	Si (mg)	(mg)	nc-Si (%)
St	16	21.5	4.3	9.9	112.8	-53.9
St	16	10.8	4.4	10.3	87.7	-4.63

7.3.6.4 "One-pot" SIPGP of styrene, MMA, tBMA and allylamine on H-terminated nc-Si

In a reaction vial with magnetic stirrer, nc-Si was dispersed in 4.0 ml monomer to obtain a 0.1 wt% dispersion. This dispersion was sonicated for 15 min, degassed *via* three freeze-pump-thaw cycles and subsequently, 0.5 ml of a 5 vol% solution of HF in ethanol (obtained by mixing 1 part 50 % aqueous HF with 9 parts ethanol) were added slowly under strong stirring. Gas formation (SiF_4) can be observed and pressure is equilibrated by short evacuation. Samples were irradiated for 16 h and workup was performed analogous to chapter 7.3.6.1.

The corresponding initial and final weights of polymer-grafted nc-Si and of free polymer after drying *in vacuo* are listed in the following table.

monomer	irradiation time (h)	initial weight (mg)	monomer (ml)	output weight nc-Si (mg)	non-grafted polymer (mg)
St	16	40.8	21.2	103.0	-48.0
MMA	16	44.4	23.9	127.8	-46.2
*t*BMA	16	43.7	26.7	205.9	-38.9
AAM	16	41.8	55.5	-	+32.8

7.3.6.5 Thermal grafting of styrene nc-Si

Functionalization of H-nc-Si with TEMPO

In a 25 ml Schlenk flask, H-terminated nc-Si is dispersed together with TEMPO in mesitylene. The dispersion is sonicated for 15 min, degassed *via* three freeze-pump-thaw cycles and stirred for 16 h at 120 °C in an oil bath under argon atmosphere. After the reaction, nc-Si is

filtered over a 0.2 μ, PTFE membrane and washed with toluene, acetone, and ethanol (three times 50 ml each). After drying in high vacuum, TEMPO-grafted nc-Si is obtained for further reactions.

The corresponding initial and final weights of TEMPO-grafted nc-Si after drying *in vacuo* are listed in the following table.

Initial weight H-nc-Si (mg)	TEMPO (mg)	mesitylene (m)]	output weight Si-np (mg)	mass difference nc-Si (%)
72.1	360.8	7.2	73.0	+1.25
75.1	374.9	7.5	80.8	+7.59

Thermal grafting of styrene from TEMPO-nc-Si

TEMPO-nc-Si are dispersed in styrene to obtain a 0.1 wt% dispersion. The dispersion is sonicated for 15 min, degassed *via* three freeze-pump-thaw clycles and reacted under stirring at 120 °C in an oil bath for 4 h and 16 h respectively. After the reaction, the 16 h sample is diluted with copious amounts of toluene (~ 50 ml) due to its high viscosity and afterwards precipitated from ethanol. The sample with 4 h irradiation time was worked up according to the procedure from chapter 7.3.6.1

The corresponding initial and final weights of polymer-grafted nc-Si and of free polymer after drying *in vacuo* are listed in the following table.

Si-np-TEMPO [mg]	styrene (ml)	irradiation time(h)	output weight Si-np (mg)	output weight free polymer (mg)	mass difference nc-Si (%)
73.0	7.3	4	73.4	2.6	+0.55
64.2	6.4	16	4939.7*	-	-

* weight of unfiltrated nc-Si/polystyrene composite

Thermal polymerization of styrene (blind samples)

2.0 ml of styrene are degassed *via* three freeze-pump-thaw cycles and reacted under argon at 120 °C. Reaction times are 4 h and 16 h respectively. Polystyrene was precipitated from 50 ml and washed with three times 50 ml ethanol.

The corresponding final weights of polymer after drying for each sample *in vacuo* are listed in the following table.

styrene (ml)	Reaction time (h)	polymer (mg)
2.0	4	502.2
2.0	16	1043.9

Thermal polymerization of styrene from H-terminated nc-Si

Furthermore, H-terminated nc-Si is dispersed in styrene to obtain a 0.1 wt% dispersion. The dispersions are sonicated for 15 min, degassed *via* three freeze-pump-thaw cycles and reacted in inert atmosphere for 16 h at 120 °C. After the reaction, the sample reacted for 16 h is dissolved in 50 ml of toluene and precipitated from and washed with ethanol (three times 50 ml), and dried *in vacuo*. Workup of the sample reacted for 4 h was done according to chapter 7.3.6.1.

The corresponding initial and final weights of polymer-grafted nc-Si and of free polymer after drying *in vacuo* are listed in the following table.

initial weight nc-Si (mg)	monomer (ml)	reaction time (h)	output weight Si-np (mg)	output weight free polymer (mg)	mass difference nc-Si (%)
26.6	2.6	4	24.0	706.2	-9.77
44.9	4.5	16	2763.4*	-	-

* weight of unfiltrated nc-Si/polystyrene composite

7.3.6.6 Sequential photografting of styrene from H-terminated nc-Si

H-terminated nc-Si and benzophenone are dispersed in benzene. The dispersions are sonicated for 15 min, degassed *via* three freeze-pump-thaw cycles and irradiated under argon atmosphere. After the reaction, the samples are filtrated over 0.2 μm PTFE membranes and washed with toluene, acetone, and ethanol (three times 50 ml each). The initial and output weights of nc-Si for different irradiation times with BP in the UV can be seen in the following table.

irradiation time (h)	initial weight nc-Si (mg)	5 % benzophenone solution in benzene (ml)	output weight nc-Si (mg)	mass difference nc-Si (%)
3	27.6	2.7	30.7	+11.2
5	27.7	2.7	24.0	-13.4
16	23.5	2.4	20.2	-14.0

After functionalization of nc-Si with BP, nc-Si is dispersed in styrene to obtain a 0.1 wt% dispersion. The dispersions are sonicated for 15 min, degassed *via* three freeze-pump-thaw cycles and irradiated with UV light for 16 h in an argon atmosphere. Workup was done according to the procedure reported in chapter 7.3.6.1.

The initial and output weights of BP-grafted nc-Si in styrene for different irradiation times in the UV can be seen in the following table.

BP-grafted nc-Si irradiation time (h)	initial weight nc-Si (mg)	styrene (ml)	output weight nc-Si (mg)	output weight free polymer (mg)	mass difference nc-Si (%)
3	30.7	3.0	23.3	28.4	-24.1
5	24.0	2.4	17.2	23.9	-28.3
16	20.2	2.0	16.0	-	-20.8

7.3.6.7 SIPGP of styrene on SiC and Si_3N_4 with the "one-pot" procedure

SiC and Si_3N_4 is dispersed in 4 ml styrene to obtain 0.1 wt% dispersions. The dispersions are sonicated for 15 min, degassed *via* three freeze-pump-thaw cycles and subsequently etched under stirring in an argon atmosphere with 0.5 ml 5 % HF solution in ethanol (obtained by mixing 1 part 50 % aqueous HF with 9 parts ethanol). Pressure built up by evolution of gaseous SiF_4 is equilibrated by evacuation. Samples are irradiated in the UV for 16 h and worked up according to the procedure described in chapter 7.3.6.1.

The corresponding initial and final weights of polymer-grafted nc-SiC and nc-Si_3N_4 and of free polymer after drying *in vacuo* are listed in the following table.

nanocrystals	initial weight nanocrystals (mg)	irradiation time (h)	output weight nanocrystals (mg)	output weight free polymer (mg)	mass difference nanocrystals (%)
SiC	44.2	16	43.5	361.5	-1.58
Si_3N_4	44.2	16	47.8	593.5	+8.14

7.3.7 Surface-initiated Kumada Catalyst-Transfer Polycondensation (SI-KCTP)

7.3.7.1 Synthesis of 2-bromo-5-chloromagnesio-3-hexylthiophene

In a dried schlenk flask, 113 µl (1.0 mmol) 2,5-dibromo-3-hexylthiophene are dissolved in 10 ml THF under argon atmosphere and 1.0 ml (1.0 mmol) 1 M tert.-butylmagnesium chloride solution in THF are added under stirring. The reaction is allowed to proceed for 2 h at room temperature.

7.3.7.2 SI-KCTP from P4BS-grafted H-terminated silicon

SI-KCTP was carried out under inert gas (Ar) atmosphere in a glovebox.

An H-terminated Si(100) substrate is immersed in 1 ml of a 6.7 wt% solution of benzophenone in cyclohexane in a glass reaction vial. The vial is degassed *via* three freeze-pump-thaw cycles, irradiated with UV light for 3 h and worked up according to the procedures described in chapter 7.3.5. The substrate is then immersed into 1 ml of 4-bromostyrene, degassed *via* three freeze-pump-thaw cycles and irradiated for 90 min with UV light. Workup is done after the procedure described in chapter 7.3.2.

After analysis, the substrate is placed into a dried reaction vial inside a glovebox and 1.5 ml solution of 0.05 wt% tetrakis(triphenylphosphino)-nickel(0) $Ni(PPh_3)_4$ were added. The catalyst solution was allowed to react over night (~ 16 h). After impregnation, 1 mg of 1,3-bis(diphenylphosphino)propane dppp were added and ligand exchange was allowed to take place over 2 h. Subsequently, 1.5 ml of 0.1 M solution of 2-bromo-5-chloromagnesio-3-hexylthiophen are added and the reaction is allowed to stand over night (~ 16 h).

Afterwards, the substrate is removed from the reaction vial, quenched by short immersion in MeOH/HCl, sonicated for 5 min in DCM, washed by swelling/deswelling cycles in toluene/acetone/ethanol, and rinsed with ethanol followed by blow-drying.

7.3.7.3 SI-KCTP from BPA-grafted nc-Si

39.4 mg nc-Si was etched *via* the conventional procedure, filtered, washed and dried.

Freshly HF-etched nc-Si was dispersed in a solution of 21.1 mg BPA in 5 ml toluene, the dispersion was degassed and reacted at 100°C for 18 h. After filtration, washing and drying, the sample was analyzed by IR spectroscopy.

In the second step, the BPA-grafted nc-Si was dispersed in 5 ml of a 0.5 wt% solution of $Ni(PPh_3)_4$ in toluene. Then, 1 mg dppp ligand was added to initiate a ligand exchange. After 2 h of ligand exchange, 1 ml monomer 2-bromo-5-chloromagnesio-3-hexylthiophene was added to start polycondensation and the reaction was allowed to proceed over night.

After quenching with HCl/MeOH, the particles were cleaned by filtration and washing with THF, toluene and ethanol, and then dried *in vacuo*. The sample was analyzed by IR spectroscopy and TEM.

7.3.7.4 SI-KCTP from P4BS-grafted graphene

A graphene sheet on copper is immersed into 1 ml 4-bromostyrene, degassed *via* three freeze-pump-thaw cycles and irradiated for 40 min. Workup is done after the procedure described in chapter 7.3.2 but with the exception that NO SONICATION was applied since this can damage the graphene sheet.

The substrate is then placed into a dried reaction vial under argon atmosphere and 1.5 ml solution of 0.05 wt% tetrakis(triphenylphosphino)-nickel(0) $Ni(PPh_3)_4$ were added. The catalyst solution was allowed to react over night (~ 16 h). After impregnation, 1 mg of 1,3-

bis(diphenylphosphino)propane dppp were added and ligand exchange was allowed to take place over 2 h. Subsequently, 1.5 ml of 0.1 M solution of 2-bromo-5-chloromagnesio-3-hexylthiophen are added and the reaction is allowed to stand over night (~ 16 h).

Afterwards, the substrate is removed from the reaction vial, quenched by short immersion in MeOH/HCl, sonicated for 5 min in DCM, washed by swelling/deswelling cycles in toluene/acetone/ethanol, and rinsed with ethanol followed by blow-drying.

7.3.7.5 SI-KCTP from 4-bromophenyl-grafted graphene

A graphene sheet on copper is immersed into a solution of 100 mg 4-bromophenyldiazonium tetrafluoroborate in water, and left to react for 1 h. The substrate is cleaned by washing in water, ethanol, acetone and toluene and finally blow-dried in an air-stream.

The substrate is then placed into a dried reaction vial under argon atmosphere and 1.5 ml solution of 0.05 wt% tetrakis(triphenylphosphino)-nickel(0) $Ni(PPh_3)_4$ were added. The catalyst solution was allowed to react over night (~ 16 h). After impregnation, 1 mg of 1,3-bis(diphenylphosphino)propane dppp were added and ligand exchange was allowed to take place over 2 h. Subsequently, 1.5 ml of 0.1 M solution of 2-bromo-5-chloromagnesio-3-hexylthiophen are added and the reaction is allowed to stand over night (~ 16 h).

Afterwards, the substrate is removed from the reaction vial, quenched by short immersion in MeOH/HCl, sonicated for 5 min in DCM, washed by swelling/deswelling cycles in toluene/acetone/ethanol, and rinsed with ethanol followed by blow-drying.

8 Bibliography

[1] W.R. Ashurst, C. Yau, C. Carraro, C. Lee, G.J. Kluth, R.T. Howe, R. Maboudian, *Sensor Actuat. A-Phys.* **2001**, *91*, 239-248.

[2] L. Lagutchev, S. Song, H. Huang, Y. Yang, C. Chuang, *Chem. Phys.* **1998**, *226*, 337 - 349.

[3] K.M. Kemner, *Science* **1997**, *276*, 923-926.

[4] B.R. Guidotti, W.R. Caseri, U.W. Suter, *Langmuir* **1996**, *12*, 4391-4394.

[5] H.M. Fagerholm, J.B. Rosenholm, T.J. Horr, R.S. Smart, *Colloid Surface A* **1996**, *110*, 11 - 22.

[6] R. Banga, J. Yarwood, A.M. Morgan, B. Evans, J. Kells, *Langmuir* **1995**, *11*, 4393-4399.

[7] A. Wang, H. Tang, T. Cao, S.O. Salley, K.Y. Ng, *J. Colloid Interf. Sci.* **2005**, *291*, 438-447.

[8] H. Ubara, T. Imura, A. Hiraki, *Solid state commun.* **1984**, *50*, 673-675.

[9] J.M. Buriak, *Chem. Rev.* **2002**, *102*, 1271-1308.

[10] M.R. Linford, C.E.D. Chidsey, *J. Am. Chem. Soc.* **1993**, *115*, 12631-12632.

[11] M.R. Linford, P. Fenter, P.M. Eisenberger, C.E.D. Chidsey, *J. Am. Chem. Soc.* **1995**, *117*, 3145-3155.

[12] T. Strother, W. Cai, X. Zhao, R.J. Hamers, L.M. Smith, *J. Am. Chem. Soc.* **2000**, *122*, 1205-1209.

[13] P. Wagner, S. Nock, J.A. Spudich, W.D. Volkmuth, S. Chu, R.L. Cicero, C.P. Wade, M.R. Linford, C.E. Chidsey, *J. Struct. Biol.* **1997**, *119*, 189 - 201.

[14] Z. Lin, T. Strother, W. Cai, X. Cao, L.M. Smith, R.J. Hamers, *Langmuir* **2002**, *18*, 788-796.

[15] A.R. Pike, L.H. Lie, R.A. Eagling, L.C. Ryder, S.N. Patole, B.A. Connolly, B.R. Horrocks, A. Houlton, *Angew. Chem. Int. Edit.* **2002**, *41*, 615-617.

[16] T. Böcking, K.A. Kilian, K. Gaus, J.J. Gooding, *Langmuir* **2006**, *22*, 3494-3496.

[17] W. Liao, F. Wei, M.X. Qian, X.S. Zhao, *Sensor Actuat. B-Chem.* **2004**, *101*, 361 - 367.

[18] K.-P.S. Dancil, D.P. Greiner, M.J. Sailor, *J. Am. Chem. Soc.* **1999**, *121*, 7925-7930.

[19] Y. Yamanoi, T. Yonezawa, N. Shirahata, H. Nishihara, *Langmuir* **2004**, *20*, 1054-1056.

[20] H. Sugimura, S. Nanjo, H. Sano, K. Murase, *J. Phys. Chem. C* **2009**, *113*, 11643-11646.

[21] C. Lagrost, G. Alcaraz, J.F. Bergamini, B. Fabre, I. Serbanescu, *Acta Crystall. B-Stru.* **2007**, 1050-1052.

[22] W. Feng, B. Miller, *Langmuir* **1999**, *15*, 3152-3156.

[23] N. Shirahata, A. Hozumi, T. Yonezawa, *Chem. Rec.* **2005**, *5*, 145-159.

[24] S.F. Bent, *Surf. Sci.* **2002**, *500*, 879 - 903.

[25] D.D.M. Wayner, R.A. Wolkow, R.A. Wolkow, *J. Chem. Soc., Perkin Trans. 2* **2001**, 23-34.

[26] .B. Sieval, R. Linke, H. Zuilhof, E.J.R. Sudhölter, *Adv. Mater.* **2000**, *12*, 1457-1460.

[27] A.B. Sieval, A.L. Demirel, J.W.M. Nissink, M.R. Linford, J.H. van der Maas, W.H. de Jeu, H. Zuilhof, E.J.R. Sudhölter, *Langmuir* **1998**, *14*, 1759-1768.

[28] A.B. Sieval, V. Vleeming, H. Zuilhof, E.J.R. Sudhölter, *Langmuir* **1999**, *15*, 8288-8291.

[29] R.L. Cicero, M.R. Linford, C.E.D. Chidsey, *Langmuir* **2000**, *16*, 5688-5695.

[30] F. Effenberger, G. Götz, B. Bidlingmaier, M. Wezstein, *Angew. Chem. Int. Edit.* **1998**, *37*, 2462-2464.

[31] T. Strother, R.J. Hamers, L.M. Smith, *Nucleic Acids Res.* **2000**, *28*, 3535-3541.

[32] E.G. Robins, M.P. Stewart, J.M. Buriak, *Chem. Commun.* **1999**, 2479-2480.

[33] Q.-Y. Sun, L.C.P.M. de Smet, B. van Lagen, M. Giesbers, P.C. Thüne, J. van Engelenburg, F.A. de Wolf, H. Zuilhof, E.J.R. Sudhölter, *J. Am. Chem. Soc.* **2005**, *127*, 2514-2523.

[34] L.C.P.M. de Smet, A.V. Pukin, Q.Y. Sun, B.J. Eves, G.P. Lopinski, G.M. Visser, H. Zuilhof, E.J.R. Sudhölter, *Appl. Surf. Sci.* **2005**, *252*, 24-30.

[35] R. Boukherroub, A. Petit, A. Loupy, J.N. Chazalviel, F. Ozanam, *J. Phys. Chem. B* **2003**, *107*, 13459-13462.

[36] J.M. Buriak, M.P. Stewart, T.W. Geders, M.J. Allen, H.C. Choi, J. Smith, D. Raftery, L.T. Canham, *J. Am. Chem. Soc.* **1999**, *121*, 11491-11502.

[37] Y. Liu, S. Yamazaki, S. Yamabe, Y. Nakato, *J. Mater. Chem.* **2005**, *15*, 4906-4913.

[38] M.J.S. Dewar, E.F. Healy, J.J.P. Stewart, J. Friedheim, G. Grady, *Organometallics* **1986**, *5*, 375-379.

[39] R. Walsh, *Acc. Chem. Res.* **1981**, *14*, 246-252.

[40] M.Z. Hossain, H.S. Kato, M. Kawai, *J. Phys. Chem. B* **2005**, *109*, 23129-23133.

[41] M.Z. Hossain, H.S. Kato, M. Kawai, *J. Am. Chem. Soc.* **2005**, *127*, 15030-15031.

[42] R.L. Cicero, C.E.D. Chidsey, G.P. Lopinski, D.D.M. Wayner, R.A. Wolkow, *Langmuir* **2002**, *18*, 305-307.

[43] J.G.C. Veinot, *Acta Crystall. B-Stru.* **2006**, 4160-4168.

[44] J.R. Heath, *Science* **1992**, *258*, 1131-1133.

[45] R.K. Baldwin, K.A. Pettigrew, J.C. Garno, P.P. Power, G.-Y. Liu, S.M. Kauzlarich, *J. Am. Chem. Soc.* **2002**, *124*, 1150-1151.

[46] T. Murthy, N. Miyamoto, M. Shimbo, J. Nishizawa, *J. Cryst. Growth* **1976**, *33*, 1-7.

[47] W.R. Cannon, S.C. Danforth, J.H. Flint, J.S. Haggerty, R.A. Marra, *J. Am. Ceram. Soc.* **1982**, *65*, 324-330.

[48] W.R. Cannon, S.C. Danforth, J.S. Haggerty, R.A. Marra, *J. Am. Ceram. Soc.* **1982**, *65*, 330-335.

[49] U. Kortshagen, *J. Phys. D Appl. Phys.* **2009**, *42*, .

[50] L. Mangolini, E. Thimsen, U. Kortshagen, *Nano letters* **2005**, *5*, 655-659.

[51] L. Mangolini, U. Kortshagen, *Adv. Mater.* **2007**, *19*, 2513-251+.

[52] S.-M. Liu, Y. Yang, S. Sato, K. Kimura, *Chem. Mater.* **2006**, *18*, 637-642.

[53] C.M. Hessel, E.J. Henderson, J.G. Veinot, *Chem. Mater.* **2006**, *18*, 6139-6146.

[54] C.M. Hessel, E.J. Henderson, J.G. Veinot, *J. Phys. Chem. C* **2007**, *111*, 6956-6961.

[55] F.A. Reboredo, A. Franceschetti, A. Zunger, *Phys. Rev. B* **2000**, *61*, 13073-13087.

[56] D. Jurbergs, E. Rogojina, L. Mangolini, U. Kortshagen, *Appl. Phys. Lett.* **2006**, *88*, 233116-233116.

[57] W.D.A.M. de Boer, D. Timmerman, K. Dohnalová, .N. Yassievich, H. Zhang, .J. Buma, T. Gregorkiewicz, *Nat. Nanotechnol.* **2010**, *5*, 878-884.

[58] M.C. Beard, K.P. Knutsen, P. Yu, J.M. Luther, Q. Song, W.K. Metzger, R.J. Ellingson, A.J. Nozik, *Nano Lett.* **2007**, *7*, 2506-2512.

[59] C.J. Murphy, J.L. Coffer, *Appl. Spectrosc.* **2002**, *56*, 16A-27A.

[60] .D. Hirschman, L. Tsybeskov, .P. Duttagupta, .M. Fauchet, *Nature* **1996**, *384*, 338-341.

[61] L. Pavesi, L. Dal Negro, C. Mazzoleni, G. Franzò, F. Priolo, *Nature* **2000**, *408*, 440-444.

[62] Z.F. Li, E. Ruckenstein, *Nano letters* **2004**, *4*, 1463-1467.

[63] T. Holec, T. Chvojka, I. Jelinek, J. Jindrich, I. Nemec, I. Pelant, J. Valenta, J. Dian, *Mater. Sci. Eng. C* **2002**, *19*, 251-254.

[64] M.J. Sailor, E.J. Lee, *Adv. Mater.* **1997**, *9*, 783-793.

[65] T. Timmerman, G. Gregorkiewicz, *Mater. Sci. Eng. B* **2009**, *159–160*, 87 - 89.

[66] V. Švrček, S. Slaoui, M. Muller, *Thin Solid Films* **2004**, *451–452*, 384 - 388.

[67] C.-Y. Liu, Z.C. Holman, U.R. Kortshagen, *Nano Lett.* **2008**, *9*, 449-452.

[68] R. Dietmueller, A.R. Stegner, R. Lechner, S. Niesar, R.N. Pereira, M.S. Brandt, A. Ebbers, M. Trocha, H. Wiggers, M. Stutzmann, *Appl. Phys. Lett.* **2009**, *94*, .

[69] S. Niesar, R. Dietmueller, H. Nesswetter, H. Wiggers, M. Stutzmann, *phys. status solidi A* **2009**, *206*, 2775-2781.

[70] S. Niesar, W. Fabian, N. Petermann, D. Herrmann, E. Riedle, H. Wiggers, M.S. Brandt, M. Stutzmann, *Green* **2011**, *1*, 339-350.

[71] M. Tamborra, M. Striccoli, M.L. Curri, J.A. Alducin, D. Mecerreyes, J.A. Pomposo, N. Kehagias, V. Reboud, C.M. Sotomayor Torres, A. Agostiano, *Small* **2007**, *3*, 822-828.

[72] A. Fissel, *Phys. rep.* **2003**, *379*, 149-255.

[73] Choyke, W. J.; Matsunami, H.; Pensl, G. *Silicon carbide: recent major advances*; Springer Verlag: 2004.

[74] Saddow, S. E.; Agarwal, A. K. *Advances in silicon carbide processing and applications*; Artech House Publishers: 2004.

[75] N.G. Wright, A.B. Horsfall, *J. Phys. D Appl. Phys.* **2007**, *40*, 6345.

[76] R. Yakimova, R.M. Petoral Jr, G.R. Yazdi, C. Vahlberg, A. Lloyd Spetz, K. Uvdal, *J. Phys. D Appl. Phys.* **2007**, *40*, 6435-6442.

[77] M. Rosso, A. Arafat, K. Schroen, M. Giesbers, C.S. Roper, R. Maboudian, H. Zuilhof, *Langmuir* **2008**, *24*, 4007-4012.

[78] M. Rosso, M. Giesbers, A. Arafat, K. Schroen, H. Zuilhof, *Langmuir* **2009**, *25*, 2172-2180.

[79] M. Steenackers, I.D. Sharp, K. Larsson, N.A. Hutter, M. Stutzmann, R. Jordan, *Chem. Mater.* **2009**, *22*, 272-278.

[80] P. Patil, P. Pandey, J.P. Bange, G. Gaikwad, G. Gautam, *Opt. Mater.* **2005**, *27*, 663 - 670.

[81] A. Arafat, K. Schroën, L.C. de Smet, E.J. Sudhölter, H. Zuilhof, *J. Am. Chem. Soc.* **2004**, *126*, 8600-8601.

[82] A. Arafat, M. Giesbers, M. Rosso, E.J. Sudhölter, K. Schroën, R.G. White, L. Yang, M.R. Linford, H. Zuilhof, *Langmuir* **2007**, *23*, 6233-6244.

[83] Y. Coffinier, R. Boukherroub, X. Wallart, J.P. Nys, J.O. Durand, D. Stiévenard, B. Grandidier, *Surf. Sci.* **2007**, *601*, 5492-5498.

[84] M. Rosso, A.T. Nguyen, E. de Jong, J. Baggerman, J.M. Paulusse, M. Giesbers, R.G. Fokkink, W. Norde, K. Schroën, C.J. van Rijn, H. Zuilhof, *ACS Appl. Mater. Interfaces* **2011**, *3*, 697-704.

[85] K. Miwa, A. Fukumoto, *Phys. Rev. B* **1993**, *48*, 7897-7902.

[86] W.C. Johnson, J.B. Parson, M.C. Crew, *J. Phys. Chem.* **1931**, *36*, 2651-2654.

[87] F.A. Ponce, D.P. Bour, *Nature* **1997**, *386*, 351-359.

[88] G. Steinhoff, O. Purrucker, M. Tanaka, M. Stutzmann, M. Eickhoff, *Adv. Funct. Mater.* **2003**, *13*, 841-846.

[89] G. Steinhoff, M. Hermann, W.J. Schaff, L.F. Eastman, M. Stutzmann, M. Eickhoff, *Appl. Phys. Lett.* **2003**, *83*, 177-179.

[90] M. Stutzmann, J.A. Garrido, M. Eickhoff, M.S. Brandt, *phys. status solidi a* **2006**, *203*, 3424-3437.

[91] S. Porowski, *Appl. Phys. Lett.* **1998**, *73*, 668-670.

[92] M. Seelmann-Eggebert, J.L. Weyher, H. Obloh, H. Zimmermann, A. Rar, S. Porowski, *Appl. Phys. Lett.* **1997**, *71*, 2635-2637.

[93] M. Stutzmann, *Appl. Phys. Lett.* **2000**, *77*, 2012-2014.

[94] M. Stutzmann, O. Ambacher, M. Eickhoff, U. Karrer, A. Lima Pimenta, R. Neuberger, J. Schalwig, R. Dimitrov, J. Schuck, D. Grober, *phys. status solidi b* **2001**, *228*, 505-512.

[95] A.K. Geim, *Science* **2009**, *324*, 1530-1534.

[96] L.H. Hess, M. Jansen, V. Maybeck, M.V. Hauf, M. Seifert, M. Stutzmann, I.D. Sharp, A. Offenhäusser, J.A. Garrido, *Adv. Mater.* **2011**, *23*, 5045-5049.

[97] Q. Su, S. Pang, V. Alijani, C. Li, X. Feng, K. Müllen, *Adv. Mater.* **2009**, *21*, 3191-3195.

[98] Y. Xu, H. Bai, G. Lu, C. Li, G. Shi, *J. Am. Chem. Soc.* **2008**, *130*, 5856-5857.

[99] Q.H. Wang, M.C. Hersam, *Nature Chemistry* **2009**, *1*, 206-211.

[100] Y. Liang, D. Wu, X. Feng, K. Müllen, *Adv. Mater.* **2009**, *21*, 1679-1683.

[101] E.Y. Choi, T.H. Han, J. Hong, J.E. Kim, S.H. Lee, H.W. Kim, S.O. Kim, *J. Mater. Chem.* **2010**, *20*, 1907-1912.

[102] E. Bekyarova, M.E. Itkis, P. Ramesh, C. Berger, M. Sprinkle, W.A. de Heer, R.C. Haddon, *J. Am. Chem. Soc.* **2009**, *131*, 1336-1337.

[103] J.R. Lomeda, C.D. Doyle, D.V. Kosynkin, W.-F. Hwang, J.M. Tour, *J. Am. Chem. Soc.* **2008**, *130*, 16201-16206.

[104] J.M. Englert, C. Dotzer, G. Yang, M. Schmid, C. Papp, J.M. Gottfried, H.-P. Steinrück, E. Spiecker, F. Hauke, A. Hirsch, *Nature Chemistry* **2011**, *3*, 279-286.

[105] M.Z. Hossain, M.A. Walsh, M.C. Hersam, *J. Am. Chem. Soc.* **2010**, *132*, 15399-15403.

[106] H. Liu, S. Ryu, Z. Chen, M.L. Steigerwald, C. Nuckolls, L.E. Brus, *J. Am. Chem. Soc.* **2009**, *131*, 17099-17101.

[107] M. Quintana, K. Spyrou, M. Grzelczak, W.R. Browne, P. Rudolf, M. Prato, *ACS Nano* **2010**, *4*, 3527-3533.

[108] M. Maggini, G. Scorrano, M. Prato, *J. Am. Chem. Soc.* **1993**, *115*, 9798-9799.

[109] H. Lim, J.S. Lee, H.-J. Shin, H.S. Shin, H.C. Choi, *Langmuir* **2010**, *26*, 12278-12284.

[110] H. Yang, F. Li, C. Shan, D. Han, Q. Zhang, L. Niu, A. Ivaska, *J. Mater. Chem.* **2009**, *19*, 4632-4638.

[111] J.O. Sofo, A.S. Chaudhari, G.D. Barber, *Phys. Rev. B* **2007**, *75*, 153401.

[112] K.S. Novoselov, *Science* **2009**, *323*, 610-613.

[113] N.A. Hutter, M. Steenackers, A. Reitinger, O.A. Williams, J.A. Garrido, R. Jordan, *Soft Matter* **2011**, *7*, 4861-4867.

[114] Advincula, R. C. *Polymer brushes synthesis, characterization, applications*; Wiley-VCH: Weinheim, 2004.

[115] M.A. White, J.A. Johnson, J.T. Koberstein, N.J. Turro, *J. Am. Chem. Soc.* **2006**, *128*, 11356-11357.

[116] R. Ranjan, W.J. Brittain, *Macromolecules* **2007**, *40*, 6217-6223.

[117] P.L. Golas, K. Matyjaszewski, *Chem. Soc. Rev.* **2010**, *39*, 1338-1354.

[118] R. Ranjan, W.J. Brittain, *Macromol. Rapid Comm.* **2008**, *29*, 1104-1110.

[119] T. Zhang, Z. Zheng, X. Ding, Y. Peng, *Macromol. Rapid Comm.* **2008**, *29*, 1716-1720.

[120] O. Prucker, J. Rühe, *Macromolecules* **1998**, *31*, 592-601.

[121] M. Husseman, E.E. Malmström, M. McNamara, M. Mate, D. Mecerreyes, D.G. Benoit, J.L. Hedrick, P. Mansky, E. Huang, T.P. Russell, C.J. Hawker, *Macromolecules* **1999**, *32*, 1424-1431.

[122] M. Husemann, M. Morrison, D. Benoit, J. Frommer, C.M. Mate, W.D. Hinsberg, J.L. Hedrick, C.J. Hawker, *J. Am. Chem. Soc.* **2000**, *122*, 1844-1845.

[123] B. Zhao, W.J. Brittain, *J. Am. Chem. Soc.* **1999**, *121*, 3557-3558.

[124] R. Jordan, A. Ulman, *J. Am. Chem. Soc.* **1998**, *120*, 243-247.

[125] R. Jordan, A. Ulman, J.F. Kang, M.H. Rafailovich, J. Sokolov, *J. Am. Chem. Soc.* **1999**, *121*, 1016-1022.

[126] B. Kong, J.K. Lee, I.S. Choi, *Langmuir* **2007**, *23*, 6761-6765.

[127] N. Zhang, S. Salzinger, F. Deubel, R. Jordan, B. Rieger, *J. Am. Chem. Soc.* **2012**, *134*, 7333-7336.

[128] N. Marshall, S.K. Sontag, J. Locklin, *Acta Crystall. B-Stru.* **2011**, *47*, 5681-5689.

[129] W. Yang, B. R□nby, *J. Appl. Polym. Sci.* **1996**, *62*, 533-543.

[130] W. Yang, B. R□nby, *J. Appl. Polym. Sci.* **1996**, *62*, 545-555.

[131] H. Ma, R.H. Davis, C.N. Bowman, *Macromolecules* **1999**, *33*, 331-335.

[132] Y.H. Ma, L.Y. Liu, W.T. Yang, *Polymer* **2011**, *52*, 4159-4173.

[133] J.-P. Deng, W.-T. Yang, B. Rånby, *Macromol. Rapid Comm.* **2001**, *22*, 535-538.

[134] H.L. Wang, H.R. Brown, *Macromol. Rapid Comm.* **2004**, *25*, 1095-1099.

[135] W.-H. Fang, R.-Z. Liu, *J. Am. Chem. Soc.* **2000**, *122*, 10886-10894.

[136] J. Wan, H. Nakatsuji, *Chemical Physics* **2004**, *302*, 125 - 134.

[137] N. Zhang, M. Steenackers, R. Luxenhofer, R. Jordan, *Macromolecules* **2009**, *42*, 5345-5351.

[138] S. Gupta, M. Agrawal, M. Conrad, N.A. Hutter, P. Olk, F. Simon, L.M. Eng, M. Stamm, R. Jordan, *Adv. Funct. Mater.* **2010**, *20*, 1756-1761.

[139] N. Zhang, T. Pompe, I. Amin, R. Luxenhofer, C. Werner, R. Jordan, *Macromol. Biosci.* **2012**, *12*, 926-936.

[140] Korfmann, T.; Ph. D. Thesis, München, 2012.

[141] M. Steenackers, S.Q. Lud, M. Niedermeier, P. Bruno, D.M. Gruen, P. Feulner, M. Stutzmann, J.A. Garrido, R. Jordan, *J. Am. Chem. Soc.* **2007**, *129*, 15655-15661.

[142] N.A. Hutter, A. Reitinger, N. Zhang, M. Steenackers, O.A. Williams, J.A. Garrido, R. Jordan, *Phys. Chem. Chem. Phys.* **2010**, *12*, 4360-4366.

[143] M. Steenackers, A.M. Gigler, N. Zhang, F. Deubel, M. Seifert, L.H. Hess, C.H.Y.X. Lim, K.P. Loh, J.A. Garrido, R. Jordan, M. Stutzmann, I.D. Sharp, *J. Am. Chem. Soc.* **2011**, *133*, 10490-10498.

[144] I. Amin, M. Steenackers, N. Zhang, R. Schubel, A. Beyer, A. Gölzhäuser, R. Jordan, *Small* **2011**, *7*, 683-687.

[145] M. Steenackers, R. Jordan, A. Küller, M. Grunze, *Adv. Mater.* **2009**, *21*, 2921-2925.

[146] K. Matyjaszewski, J. Xia, *Chem. Rev.* **2001**, *101*, 2921-2990.

[147] Elias, H. G. *Makromoleküle*; Wiley-VCH: 2009.

[148] B. Radhakrishnan, R. Ranjan, W.J. Brittain, *Soft Matter* **2006**, *2*, 386-396.

[149] S.J. Teertstra, M. Gauthier, *Prog. Polym. Sci.* **2004**, *29*, 277 - 327.

[150] M. Steenackers, A. Küller, S. Stoycheva, M. Grunze, R. Jordan, *Langmuir* **2009**, *25*, 2225-2231.

[151] Y. Liu, V. Klep, B. Zdyrko, I. Luzinov, *Langmuir* **2004**, *20*, 6710-6718.

[152] V. Senkovskyy, N. Khanduyeva, H. Komber, U. Oertel, M. Stamm, D. Kuckling, A. Kiriy, *J. Am. Chem. Soc.* **2007**, *129*, 6626-6632.

[153] K. Matyjaszewski, P.J. Miller, N. Shukla, B. Immaraporn, A. Gelman, B.B. Luokala, T.M. Siclovan, G. Kickelbick, T. Vallant, H. Hoffmann, T. Pakula, *Macromolecules* **1999**, *32*, 8716-8724.

[154] X. Kong, T. Kawai, J. Abe, T. Iyoda, *Macromolecules* **2001**, *34*, 1837-1844.

[155] W.H. Yu, E.T. Kang, K.G. Neoh, S. Zhu, *J. Phys. Chem. B* **2003**, *107*, 10198-10205.

[156] W.H. Yu, E.T. Kang, K.G. Neoh, *Langmuir* **2004**, *20*, 8294-8300.

[157] F.J. Xu, E.T. Kang, K.G. Neoh, *Macromolecules* **2005**, *38*, 1573-1580.

[158] F.J. Xu, D. Xu, E.T. Kang, K.G. Neoh, *J. Mater. Chem.* **2004**, *14*, 2674-2682.

[159] I.W. Moran, K.R. Carter, *Langmuir* **2009**, *25*, 9232-9239.

[160] .Y. Kwok, C.N.C. Lam, A. Li, K. Zhu, R. Wu, .W. Neumann, *Polym. Eng. Sci.* **1998**, *38*, 1675-1684.

[161] Steenackers, M; Ph. D. Thesis, München, 2007.

[162] O. Prucker, J. Habicht, I.-J. Park, J. Rühe, *Mat. Sci. Eng. C* **1999**, *8–9*, 291 - 297.

[163] A. Andrade, M. Ma, K. King, G. Gregonis, *J. Colloid Interf. Sci.* **1979**, *72*, 488 - 494.

[164] J. Lalevée, X. Allonas, J.P. Fouassier, *J. Org. Chem.* **2007**, *72*, 6434-6439.

[165] L.J. Webb, N.S. Lewis, *J. Phys. Chem. B* **2003**, *107*, 5404-5412.

[166] E.J. Nemanick, P.T. Hurley, L.J. Webb, D.W. Knapp, D.J. Michalak, B.S. Brunschwig, N.S. Lewis, *J. Phys. Chem. B* **2006**, *110*, 14770-14778.

[167] Y. Lv, N. Wang, C. Zhuang, P. Li, B. Han, H. Gong, *Semicond. sci. tech.* **2006**, *21*, 771.

[168] K.E. Plass, X.L. Liu, B.S. Brunschwig, N.S. Lewis, *Chem. Mater.* **2008**, *20*, 2228-2233.

[169] N.S. Lewis, *Appl. Phys. Lett.* **2000**, *77*, 1988-1990.

[170] M. Seifert, A.H. Koch, F. Deubel, T. Simmet, L.H. Hess, M. Stutzmann, R. Jordan, J.A. Garrido, I.D. Sharp, *Chem. Mater.* **2013***, 25,* 466-470

[171] K. Liang, M. Dossi, D. Moscatelli, R.A. Hutchinson, *Macromolecules* **2009**, *42*, 7736-7744.

[172] A.P. Francis, D.H. Solomon, T.H. Spurling, *J. Macromol. Sci. Chem.* **2006**, *8*, 469-476.

[173] .M. Dibona, .F. Fibiger, .F. Gurnee, .E. Shuetz, *J. Appl. Polym. Sci.* **1986**, *31*, 1509-1514.

[174] F.J. Xu, E.T. Kang, K.G. Neoh, *J. Mater. Chem.* **2006**, *16*, 2948-2952.

[175] S.J. Blanksby, G.B. Ellison, *Acc. Chem. Res.* **2003**, *36*, 255-263.

[176] H. Bai, Z. Huang, W. Yang, *J. Polym. Sci. A1* **2009**, *47*, 6852-6862.

[177] M.Z. Hossain, H.S. Kato, M. Kawai, *J. Am. Chem. Soc.* **2008**, *130*, 11518-11523.

[178] R.J. Clark, M.K.M. Dang, J.G.C. Veinot, *Langmuir* **2010**, *26*, 15657-15664.

[179] E. Ruckenstein, Z.F. Li, *Polym. Degrad. Stabil.* **2005**, *113*, 43-63.

[180] Z. Xu, D. Wang, M. Guan, X. Liu, Y. Yang, D. Wei, C. Zhao, H. Zhang, *ACS Appl. Mater. Interfaces* **2012**, .

[181] Tieke, B. *Makromolekulare Chemie*; Wiley-VCH: 2012.

[182] E.V. Rogozhina, D.A. Eckhoff, E. Gratton, P.V. Braun, *J. Mater. Chem.* **2006**, *16*, 1421-1430.

[183] B. Bulgakova, M. Mazanova, S. Semenov, Y.D. Semchikov, *Eur. Polym. J.* **2007**, *43*, 644 - 651.

[184] D.J. Dyer, J. Feng, R. Schmidt, V.N. Wong, T. Zhao, Y. Yagci, *Macromolecules* **2004**, *37*, 7072-7074.

[185] S. Malynych, I. Luzinov, G. Chumanov, *J. Phys. Chem. B* **2002**, *106*, 1280-1285.

[186] F. Wen, W. Zhang, G. Wei, Y. Wang, J. Zhang, M. Zhang, L. Shi, *Chem. Mater.* **2008**, *20*, 2144-2150.

[187] C. Evangelisti, N. Panziera, P. Pertici, G. Vitulli, P. Salvadori, C. Battocchio, G. Polzonetti, *J. catal.* **2009**, *262*, 287-293.

[188] J.M. Campelo, D. Luna, R. Luque, J.M. Marinas, A.A. Romero, *ChemSusChem* **2009**, *2*, 18-45.

[189] S. Pathak, M.T. Greci, R.C. Kwong, K. Mercado, G.K.S. Prakash, G.A. Olah, M.E. Thompson, *Chem. Mater.* **2000**, *12*, 1985-1989.

[190] H. Zhuang, V.V.S.S. Srikanth, X. Jiang, I. Aronov, B.W. Wenclawiak, J. Luo, H. Ihmels, *Chem. Mater.* **2010**, .

[191] Odian, G. *Principles of polymerization*; Wiley-Interscience: 2004.

[192] M. Perring, S. Dutta, S. Arafat, M. Mitchell, P.J.A. Kenis, N.B. Bowden, *Langmuir* **2005**, *21*, 10537-10544.

[193] S.N. Arafat, S. Dutta, M. Perring, M. Mitchell, P.J.A. Kenis, N.B. Bowden, N.B. Bowden, *Chem. Commun.* **2005**, 3198-3200.

[194] A.A. Lebedev, *Semicond. sci. tech.* **2006**, *21*, R17.

[195] L. Manna, D. Dorfs, K. Miszta, S. Deka, A. Genovese, G. Bertoni, R. Brescia, S. Marras, Y. Zhang, R. Krahne, *US Patent 20,130,032,767,* **2013.**

[196] P.T.B. Shaffer, *Acta Crystallogr. B* **1969**, *25*, 477-488.

[197] S. Beuermann, M. Buback, *Prog. Polym. Sci.* **2002**, *27*, 191-254.

[198] K. Liang, R.A. Hutchinson, *Macromol. Rapid Comm.* **2011**, *32*, 1090-1095.

[199] C.E. Hoyle, C.N. Bowman, *Angew. Chem. Int. Ed. Engl.* **2010**, *49*, 1540-1573.

[200] C.E. Hoyle, A.B. Lowe, C.N. Bowman, *Chem. Soc. Rev.* **2010**, *39*, 1355-1387.

[201] C.R. Becer, R. Hoogenboom, U.S. Schubert, *Angew. Chem. Int. Ed. Engl.* **2009**, *48*, 4900-4908.

[202] T. Posner, *Ber. dtsch. chem. Ges.* **1905**, *38*, 646-657.

[203] M.J. Kade, D.J. Burke, C.J. Hawker, *J. Polym. Sci A* **2010**, *48*, 743-750.

[204] L.M. Campos, I. Meinel, R.G. Guino, M. Schierhorn, N. Gupta, G.D. Stucky, C.J. Hawker, *Adv. Mater.* **2008**, *20*, 3728-3733.

[205] J. von Braun, R. Murjahn, *Ber. dtsch. chem. Ges.* **1926**, *59*, 1202-1209.

[206] J. von Braun, T. Plate, *Ber. dtsch. chem. Ges.* **1934**, *67*, 281-285.

[207] A.A. Oswald, K. Griesbaum, D.N. Hall, *J. Polym. Sci. C* **1968**, *24*, 113-123.

[208] O. Nuyken, M. Hofinger, R. Kerber, *Polym. Bull.* **1980**, *2*, 21-24.

[209] O. Nuyken, M. Hofinger, *Polym. Bull.* **1981**, *4*, 343-350.

[210] O. Nuyken, M. Hofinger, *Polym. Bull.* **1981**, *4*, 335-341.

[211] O. Nuyken, M. Hofinger, *Polym. Bull.* **1981**, *4*, 75-82.

[212] O. Nuyken, M. Hofinger, *Polym. Bull.* **1984**, *11*, 165-170.

[213] O. Nuyken, G. Reuschel, F. Siebzehnrübl, *Makromol. Chem-M Symp.* **1989**, *26*, 313-331.

[214] M. Kharash, A.T. Read, F. Mayo, *Chem. Ind.* **1938**, *57*, 752.

[215] C.R. Morgan, F. Magnotta, A.D. Ketley, *J. Polym. Sci. A* **1977**, *15*, 627-645.

[216] B.D. Fairbanks, T.F. Scott, C.J. Kloxin, K.S. Anseth, C.N. Bowman, *Macromolecules* **2009**, *42*, 211-217.

[217] N.B. Cramer, J.P. Scott, C.N. Bowman, *Macromolecules* **2002**, *35*, 5361-5365.

[218] N.B. Cramer, C.N. Bowman, *J. Polym. Sci. A* **2001**, *39*, 3311-3319.

[219] Y. Yamanoi, N. Shirahata, T. Yonezawa, N. Terasaki, N. Yamamoto, Y. Matsui, K. Nishio, H. Masuda, Y. Ikuhara, H. Nishihara, *Chem. Eur. J.* **2006**, *12*, 314-323.

[220] R.A. Fisher, R.B. Nielsen, W.M. Davis, S.L. Buchwald, *J. Am. Chem. Soc.* **1991**, *113*, 165-171.

[221] M.L. Hallensleben, *Makromol. Chem.* **1976**, *177*, 3207-3212.

[222] M.L. Hallensleben, *Makromol. Chem.* **1976**, *177*, 3213-3219.

[223] D. Witt, *Synthesis* **2008**, *16*, 2491-2509.

[224] J. Hornung, D. Fankhauser, L.D. Shirtcliff, A. Praetorius, W.B. Schweizer, F. Diederich, *Chem. Eur. J.* **2011**, *17*, 12362-12371.

[225] Launer, P. J. *Silicone Compounds Register and Review*; Petrarch Systems Bristol, PA: 1987.]

9 Appendix

Table S 1: Absorption bands of different silicon compounds[225]

vibration	wavenumbers (cm^{-1})
ν(Si-OH)	950-810
ν(Si-OR)	1000-1100
ν(Si-H)	2280-2080
δ(Si-H_2)	800-900
δ(Si-H)	600-650

Table S 2: Band assignment of DRIFT spectrum of nc-Si irradiated for 16 h in styrene (0.05/0.025 wt%) with intensities

wavenumbers (cm^{-1})	vibration	intensity
3062, 3027	ν(Aryl-H)	strong
2924, 2848	ν(CH_n)	strong
2325, 2343	ν(Si-H_n)	weak
2095	ν(Si-H)	strong
1947, 1870, 1813	Aryl-H combination and overtones	weak
1703, 1599, 1493	ν(C=C)	medium
1425	δ(CH_n)	strong
1195	Aryl fingerprint bands/ ν(Si-O)	strong, broad
887, 707	δ(CH), *out of plane*	weak to medium

Table S 3: Band assignment of DRIFT spectrum of nc-Si irradiated for 16 h in styrene with HF ('one-pot') with intensities

wavenumbers (cm^{-1})	vibration	intensity
3085, 3067, 3028	ν(aryl-H)	medium
2925, 2851	ν(CH_n)	medium
2095	ν(Si-H)	strong
1942, 1881, 1800	Aryl-H combination and overtones	weak
1603, 1495	ν(C=C)	medium
1423	δ(CH_n)	strong
1135	Aryl fingerprint bands/ ν(Si-O)	Strong, broad
721	δ(CH), *out of plane*	medium

Table S 4: Band assignment of DRIFT spectrum of nc-Si irradiated for 16 h in MMA with HF ('one-pot') with intensities

wavenumbers (cm^{-1})	vibration	intensity
2958, 2923, 2848	ν(CH_n)	weak
2513	ν($Si-H_n$)	weak
2086	ν(Si-H)	strong
1737	ν(C=O)	medium
1428	δ(CH_n)	strong
1203	ν(C-O)/ν(Si-O)	strong, broad

Table S 5: Band assignment of DRIFT spectrum of nc-Si irradiated for 16 h in tBMA with HF ('one-pot') with intensities

wavenumbers (cm^{-1})	vibration	intensity
2978, 2853	$\nu(CH_n)$	weak
2093	ν(Si-H)	strong
1726	ν(C=O)	strong
1422	$\delta(CH_n)$	medium
1252, 1150	ν(C-O)/ν(Si-O)	weak

Table S 6: Band assignment of DRIFT spectrum of nc-Si irradiated for 16 h in allyl amine with HF ('one-pot') with intensities

wavenumbers (cm^{-1})	vibration	intensity
3280	$\nu(NH_2)$	strong, broad
2989	$\nu(CH_2)$	strong, superposed
2242	ν(Si-O-Si-H)	very weak
1625	$\delta(NH_2)$	medium
1515, 1454, 1430	$\delta(CH_n)$	weak

Table S 7: Band assignment of DRIFT spectrum of TEMPO nc-Si reacted for 4 h in styrene at 120 °C with intensities

wavenumbers (cm^{-1})	vibration	intensity
3072, 3026	ν(Aryl-H)	weak
2966, 2916, 2854	$\nu(CH_n)$	medium
2382	$\nu(Si\text{-}H_n)$	weak

2106	ν(Si-H)	medium
1984, 1872	Aryl-H combination and overtones	weak
1629	ν(C=C)	medium
1421	$\delta(CH_n)$	strong
1249	Aryl fingerprint bands/ ν(Si-O)	strong, broad
804, 719	δ(CH), *out of plane*	weak to medium

Table S 8: Band assignment of DRIFT spectrum of nc-Si reacted for 4 h in styrene at 120 °C with intensities

wavenumbers (cm^{-1})	vibration	intensity
3062, 3028	ν(Aryl-H)	strong
2925, 2850	$\nu(CH_n)$	strong
2365, 2339, 2313	$\nu(Si-H_n)$	very weak
2086	ν(Si-H)	strong
1945, 1872, 1862, 1740	Aryl-H combination and overtones	medium
1602, 1495	ν(C=C)	strong
1421	$\delta(CH_n)$	strong
1113, 904	Aryl fingerprint bands/ ν(Si-O)	strong, broad
723, 103	δ(CH), *out of plane*	strong

Table S 9: Band assignment of DRIFT spectrum of BP-grafted nc-Si irradiated for 16 h in styrene with intensities

wavenumbers (cm^{-1})	vibration	intensity
3084, 3066, 3028	ν(Aryl-H)	medium
2926, 2850	ν(CH_n)	medium
2362	ν(Si-H_n)	weak
2097	ν(Si-H)	strong
1944, 1865, 1795	Aryl-H combination and overtones	weak
1603	ν(C=C)	medium, several superposed
1603	δ(CH_n)	strong
1216	Aryl fingerprint bands/ ν(Si-O)	strong, broad
730	δ(CH), *out of plane*	strong

Table S 10: Band assignment of DRIFT spectrum of nc-SiC irradiated for 16 h in styrene with HF ('one-pot') with intensities

wavenumbers (cm^{-1})	vibration	intensity
3093	ν(Aryl-H)	weak
2971, 2840	ν(CH_n)	medium
2524	ν(Si-H_n)	very weak
2327, 2244	ν(Si-O-Si-H)	very weak

2071	ν(Si-H)	medium
1891, 1803, 1733	Aryl-H combination and overtones	weak
1611, 1542, 1508	ν(C=C)	strong
1456	$\delta(CH_n)$	strong
1108	Aryl fingerprint bands/ ν(Si-O)	strong, broad
802, 711	δ(CH), *out of plane*	medium

Table S 11: Band assignment of DRIFT spectrum of nc-Si_3N_4 irradiated for 16 h in styrene with HF ('one-pot') with intensities

wavenumbers (cm^{-1})	vibration	intensity
3409	ν(N-H)	strong, broad
3078, 3026	ν(Aryl-H)	weak
2971, 2840	$\nu(CH_n)$	medium
2524	$\nu(Si\text{-}H_n)$	very weak
2327, 2244	ν(Si-O-Si-H)	very weak
2071	ν(Si-H)	medium
1891, 1803, 1733	Aryl-H combination and overtones	weak
1611, 1542, 1508	ν(C=C)	strong
1456	$\delta(CH_n)$	strong
1108	Aryl fingerprint	strong, broad

	bands/ ν(Si-O)	
802, 711	δ(CH), *out of plane*	medium

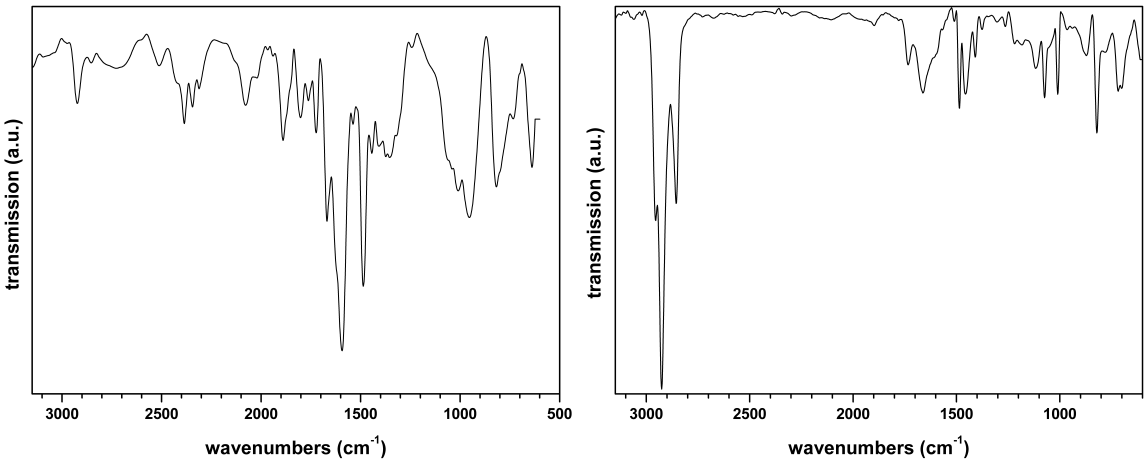

Figure S 1: IR spectra of P4BS-grafted and P4BS-g-P3HT-grafted graphene

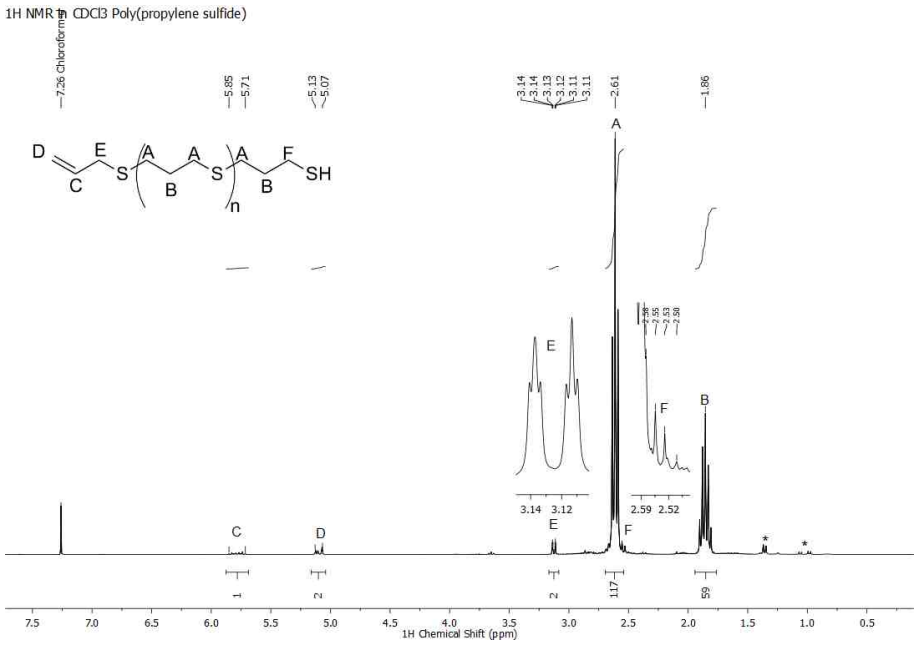

Figure S 2: ^{1}H NMR spectrum of poly(propylene sulfide) in chloroform measured at 25°C. A and B are assigned to proton signals of the saturated backbone. C and D refer to allylic end group, E refers to CH_2 protons between allylic end group and the thioether. Signal F overlaps with backbone signal A and belongs to CH_2 group next to the SH end group. Impurities are indicated by *.

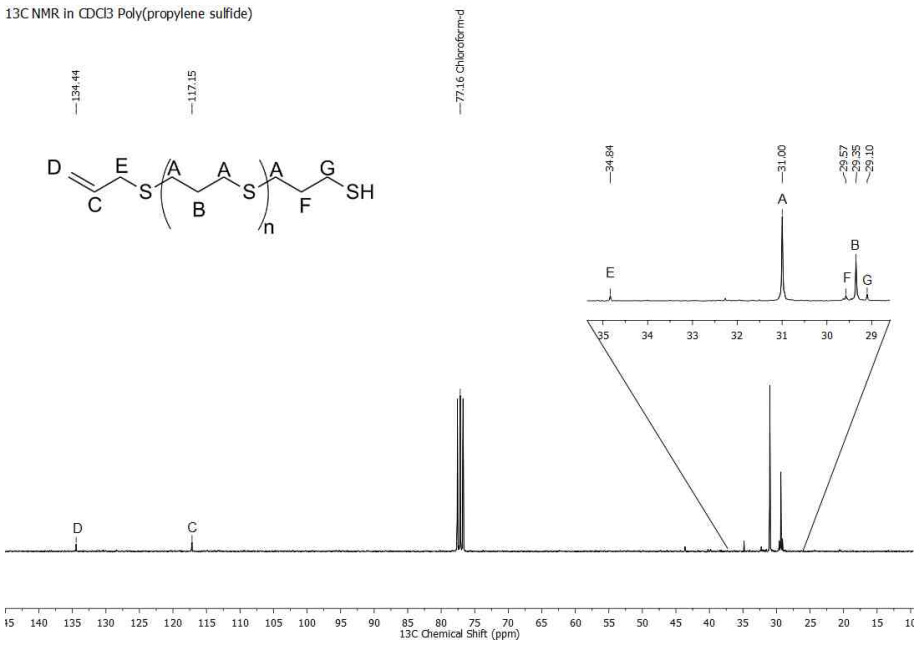

Figure S 2: ^{13}C NMR spectrum of poly(propylene sulfide) in chloroform measured at 25°C. A and B are assigned to proton signals of the saturated backbone. D and C refer to allylic end group, E refers to the signal of CH_2 carbon between allylic endgroup and first thioether. Signals F and G are assigned to CH_2 carbons next to the SH end group.

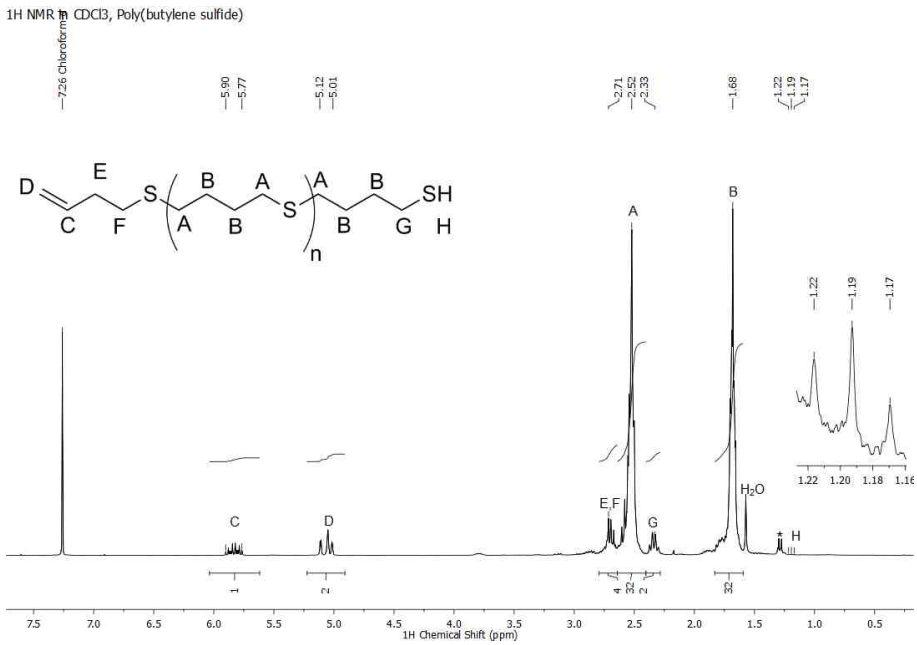

Figure S 3: ^{1}H NMR spectrum of poly(butylene sulfide) in chloroform measured at 25°C. A and B are assigned to proton signals of the saturated backbone. C and D refer to unsaturated end group, signals E and F overlap and are assigned to CH_2 protons between unsaturated end group and first thioether. Signal G can be assigned to CH_2 protons next to SH end group. Signal H is assigned to SH protons and shows a coupling

constant of 7.0 Hz which is typical for CH_2-SH couplings. However, integral of signal H is smaller than expected. This might be attributed to an H-D exchange. Impurities are indicated by *.

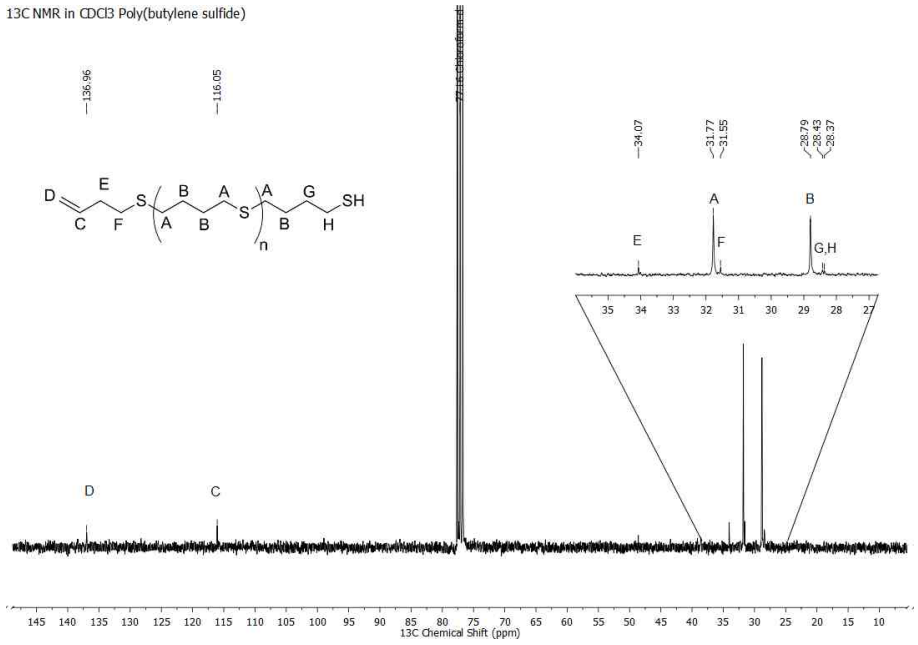

Figure S 4: ^{13}C NMR spectrum of poly(butylene sulfide) in chloroform measured at 25°C. A and B are assigned to proton signals of the saturated backbone. C and D refer to unsaturated end group, signals E and F are assigned to CH_2 carbons between unsaturated end group and first thioether. Signals G and H refer to CH_2 carbons next to SH endgroup.

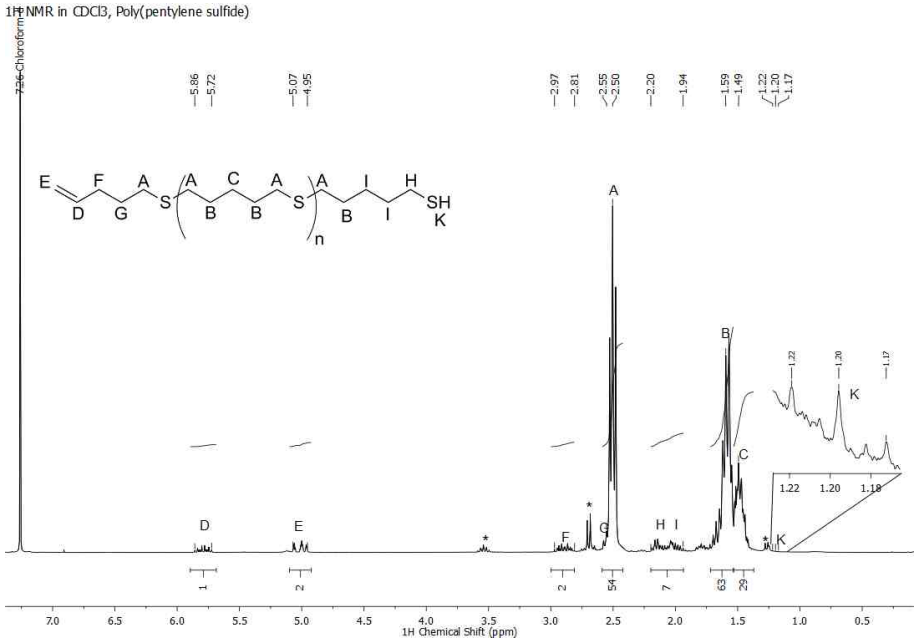

Figure S 5: ^{1}H NMR spectrum of poly(pentylene sulfide) in chloroform measured at 25°C. Signal A is assigned to CH_2 protons next to thioether groups. B and C are assigned to proton signals of the saturated backbone. D and E refer to unsaturated end group, F and G are assigned to protons of CH_2 units next to the unsaturated end group. Proton signals of the three CH_2 groups next to SH end group are indicated with H and I. Signal K is assigned to SH protons and shows a coupling constant of 7.0 Hz which is typical for CH_2-SH couplings. However, integral of signal H is smaller than expected. This might be attributed to an H-D exchange. Impurities are indicated by *.

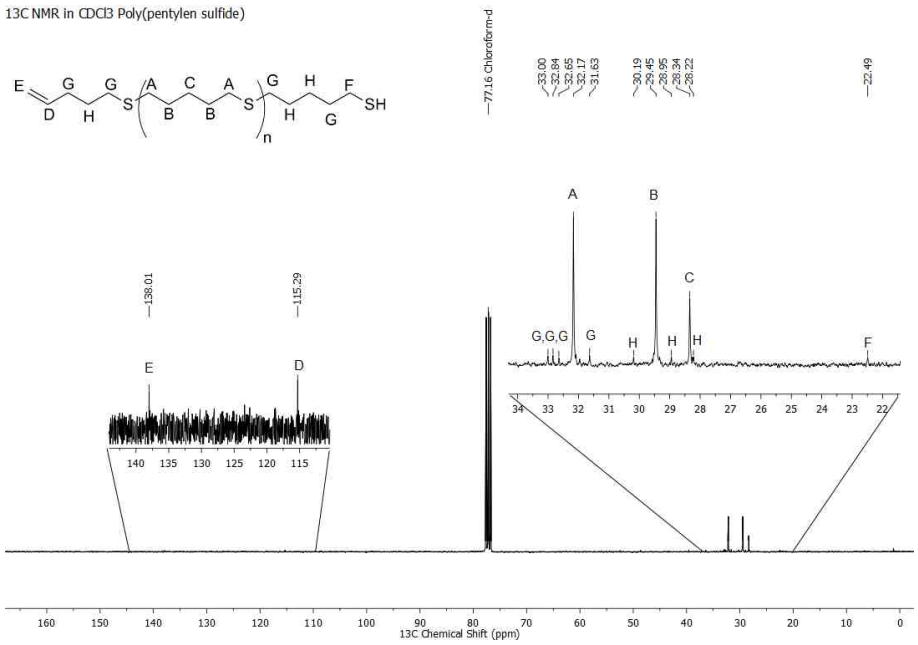

Figure S 6: ^{13}C NMR spectrum of poly(pentylene sulfide) in chloroform measured at 25°C. A, B and C are assigned to carbon signals of the saturated backbone. D and E refer to the unsaturated end group. CH_2 signal H is from carbon atom in a position to SH end group. Four signals G are assigned to CH_2 carbons next to unsaturated end group, next to fist and last thioether linkages and to CH_2 carbon in b position to SH end group. Three signals H are assigned to CH_2 carbons in between these refered to with G.

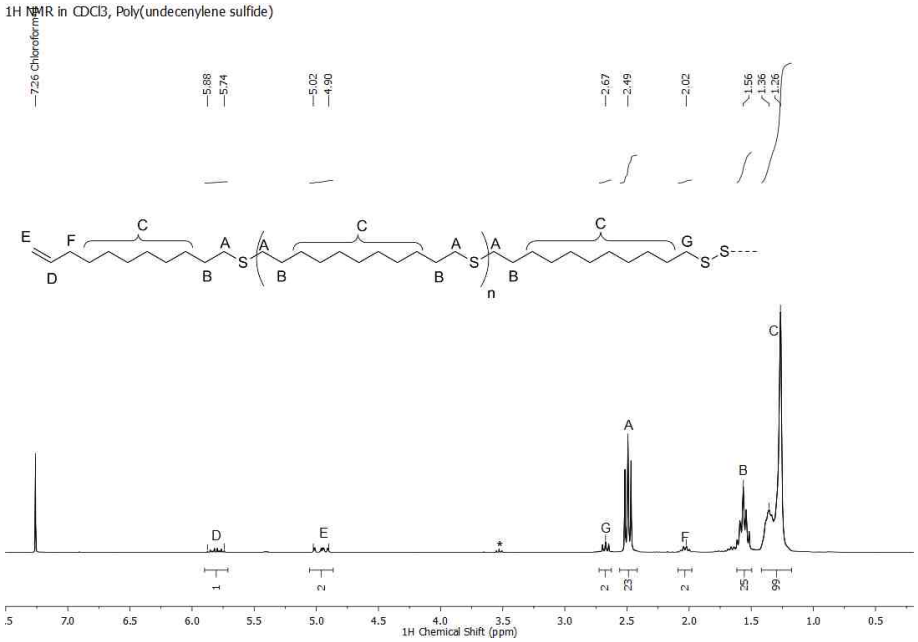

Figure S 7: ^{1}H NMR spectrum of poly(undecenylene sulfide) in chloroform measured at 25°C. Signal A is assigned to CH_2 protons next to thioether groups. Signal B is assigned to CH_2 protons in b position to thioether units. Signal C refers to protons of the

saturated backbone. D and E refer to unsaturated end group, Signal F is assigned to protons of CH_2 units next to the unsaturated end group. Signal G probably belongs to a CH_2 group in a position to a disulfide. However, a possible signal of SH protons cannot be found due to the overlap with signal C. Impurities are indicated by *.

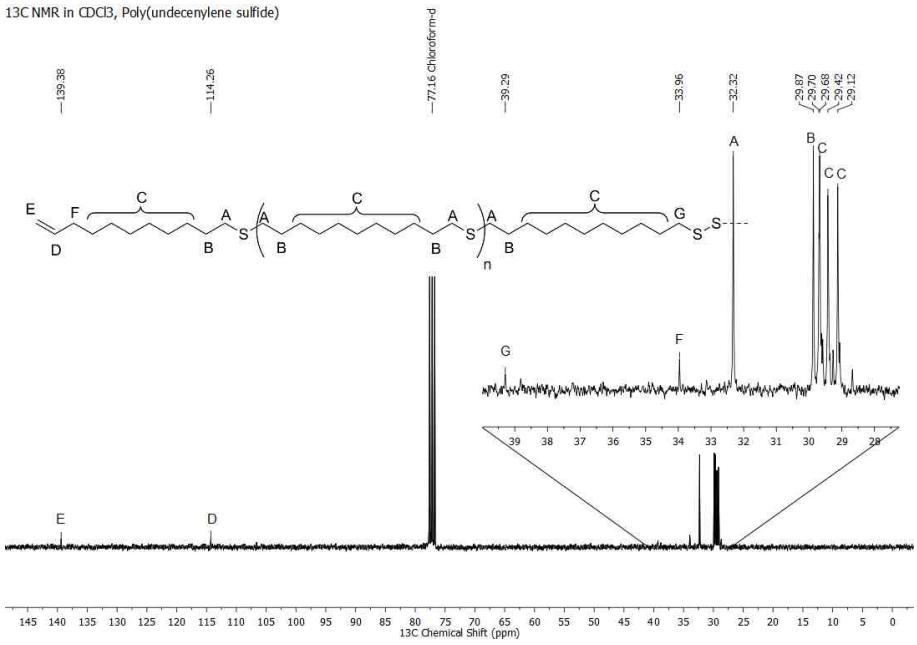

Figure S 8: ^{13}C NMR spectrum of poly(undecenylene sulfide) in chloroform measured at 25°C. Signal A is assigned to CH_2 carbons next to thioether groups. Signal B is assigned to CH_2 carbons in b position to thioether units. Signals indicated with C refer to carbons of the saturated backbone and (together with small signals where indication was omitted for reasons of clarity) saturated parts of end groups. D and E refer to the unsaturated end group. CH_2 signal F is assigned to carbon atom next to unsaturated end group. Signal G most probably refers to a CH_2 carbon in a position to a disulfide bond.

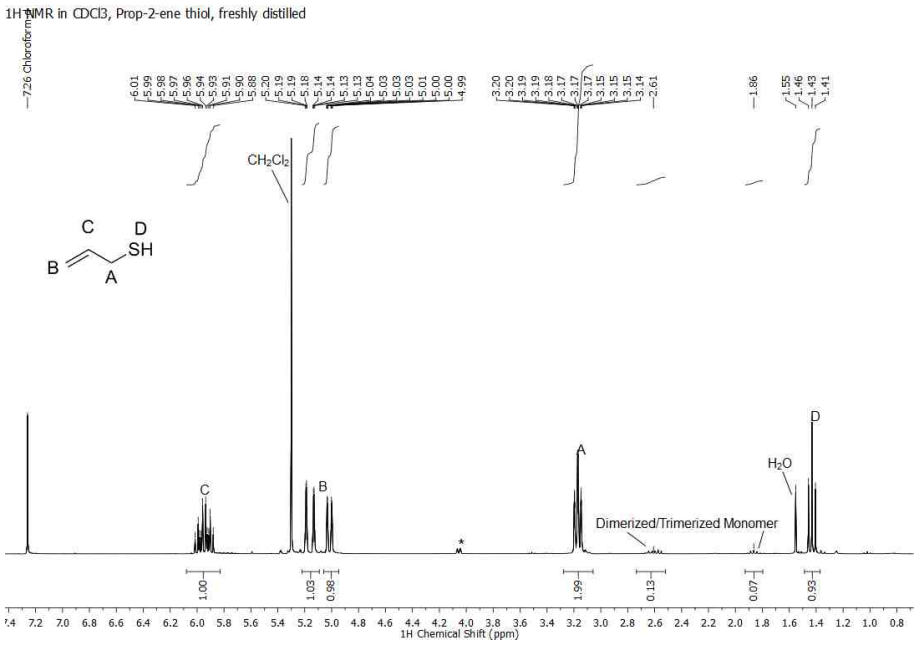

Figure S 9: [1]H NMR spectrum of freshly distilled prop-2-ene thiol in chloroform measured at 25°C. Signal A is aligned to CH2 group, Signals B and C to olefinic protons and D to the SH functionality. Small quantities of addition products from thiol-ene reaction appear at 2.61 ppm and 1.86 ppm. Impurities are indicated by *. ([1]H-NMR spectrum of prop-2-ene thiol used for kinetic measurement depicted in Figure 113)